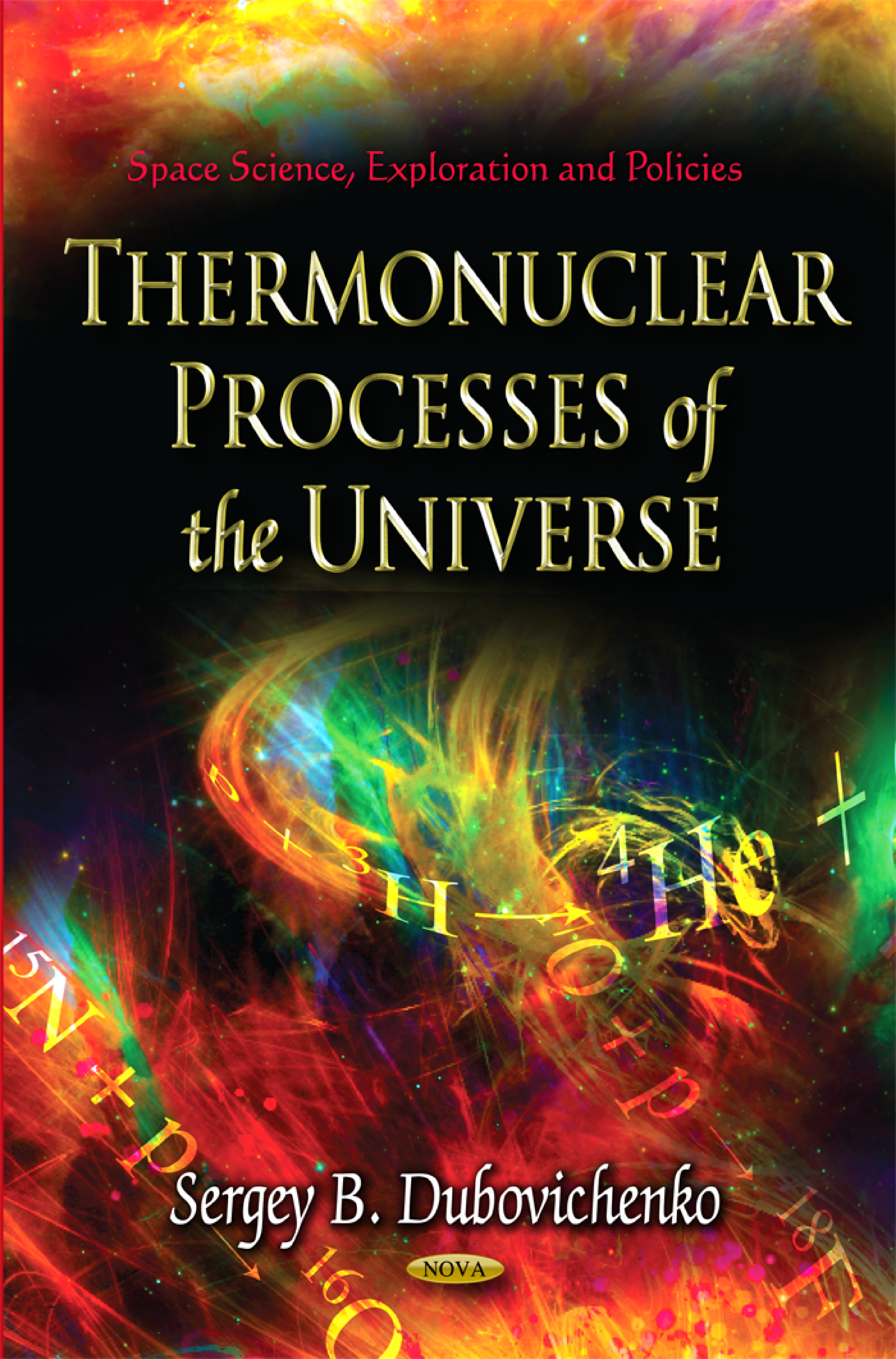

Space Science, Exploration and Policies

THERMONUCLEAR PROCESSES *of the* UNIVERSE

Sergey B. Dubovichenko

NOVA

SPACE SCIENCE, EXPLORATION AND POLICIES

THERMONUCLEAR PROCESSES OF THE UNIVERSE

No part of this digital document may be reproduced, stored in a retrieval system or transmitted in any form or by any means. The publisher has taken reasonable care in the preparation of this digital document, but makes no expressed or implied warranty of any kind and assumes no responsibility for any errors or omissions. No liability is assumed for incidental or consequential damages in connection with or arising out of information contained herein. This digital document is sold with the clear understanding that the publisher is not engaged in rendering legal, medical or any other professional services.

SPACE SCIENCE, EXPLORATION AND POLICIES

Additional books in this series can be found on Nova's website under the Series tab.

Additional e-books in this series can be found on Nova's website under the e-book tab.

SPACE SCIENCE, EXPLORATION AND POLICIES

THERMONUCLEAR PROCESSES OF THE UNIVERSE

SERGEY B. DUBOVICHENKO

Nova Science Publishers, Inc.
New York

Copyright © 2012 by Nova Science Publishers, Inc.

All rights reserved. No part of this book may be reproduced, stored in a retrieval system or transmitted in any form or by any means: electronic, electrostatic, magnetic, tape, mechanical photocopying, recording or otherwise without the written permission of the Publisher.

For permission to use material from this book please contact us:
Telephone 631-231-7269; Fax 631-231-8175
Web Site: http://www.novapublishers.com

NOTICE TO THE READER

The Publisher has taken reasonable care in the preparation of this book, but makes no expressed or implied warranty of any kind and assumes no responsibility for any errors or omissions. No liability is assumed for incidental or consequential damages in connection with or arising out of information contained in this book. The Publisher shall not be liable for any special, consequential, or exemplary damages resulting, in whole or in part, from the readers' use of, or reliance upon, this material. Any parts of this book based on government reports are so indicated and copyright is claimed for those parts to the extent applicable to compilations of such works.

Independent verification should be sought for any data, advice or recommendations contained in this book. In addition, no responsibility is assumed by the publisher for any injury and/or damage to persons or property arising from any methods, products, instructions, ideas or otherwise contained in this publication.

This publication is designed to provide accurate and authoritative information with regard to the subject matter covered herein. It is sold with the clear understanding that the Publisher is not engaged in rendering legal or any other professional services. If legal or any other expert assistance is required, the services of a competent person should be sought. FROM A DECLARATION OF PARTICIPANTS JOINTLY ADOPTED BY A COMMITTEE OF THE AMERICAN BAR ASSOCIATION AND A COMMITTEE OF PUBLISHERS.

Additional color graphics may be available in the e-book version of this book.

LIBRARY OF CONGRESS CATALOGING-IN-PUBLICATION DATA

Dubovichenko, S. B. (Sergei Borisovich), 1953-
[Termoiadernye protsessy vselennoi. English]
Thermonuclear processes of the universe / Sergey Borisovich Dubovichenko.
p. cm.
Includes bibliographical references and index.
ISBN: 978-1-61942-579-8 (eBook)
1. Radiative capture. 2. Thermodynamic equilibrium. 3. Astrophysics. I. Title.
QB464.4.D8313 2011
523.01'975--dc23
2011050470

Published by Nova Science Publishers, Inc. ✢ New York

CONTENTS

Foreword vii

Preface ix

Acknowledgments xi

Summary xiii

Introduction 1

Chapter 1 Thermonuclear Processes 5

Chapter 2 The Model and Calculation Methods 25

Chapter 3 Astrophysical S-Factor of the p^2H Radiative Capture 41

Chapter 4 Process of the p^3H Radiative Capture 53

Chapter 5 Process of the p^6Li Radiative Capture 63

Chapter 6 S-Factor of the p^7Li Radiative Capture 77

Chapter 7 Radiative Capture in the p^9Be System 87

Chapter 8 Radiative $p^{12}C$ Capture 95

Chapter 9 Astrophysical S-Factors of the Radiative Capture in the $^3He^4He$, $^3H^4He$ and $^2H^4He$ Systems 111

Chapter 10 Reaction of the $^4He^{12}C$ Radiative Capture 127

Conclusion 143

Appendix 1 Calculation Methods for Coulomb and Whittaker Functions 145

Appendix 2 Basic Astrophysical Terms and Concepts (For Beginners) 155

References 165

Reviewers and Scientific Editors of the Book 173

Index 175

FOREWORD

The monograph of Dubovichenko S.B. is the treatise covering a wide range of problems applying to the nuclear structure and mechanisms of nuclear reactions, as well as application of nuclear methods for the analysis of astrophysical processes in the stars. The exposition bears on the numerous original works of the author published in the prestige science journals. The wide set of nuclear systems containing from three (p + ^{2}H) to sixteen (^{4}He + ^{12}C) nucleons was discussed in this book.

The uniqueness of the book material consists in the fact that the theoretical description of all these systems is based on the unified approach, which can be named as the two-body potential cluster model with the classification of the states according to Young schemes. In spite of the comparative simplicity (in comparison with the other known methods), this approach allowed author to obtain a good description, both for states of discrete spectrum (bound states) and for continuous spectrum states (scattering states).

In a great measure, the actuality of the book matter is determined by the application of the developed approach to problems of nuclear astrophysics that is one of the most violently developing fields of science at the present time. The author calculates the astrophysical *S*-factor of the radiative capture $b(c,y)a$ process, where a is a bound state of b and c, for each considered two-cluster b+c systems. The astrophysical *S*-factor is proportional to the cross section of this process and determines its rate in the inner star regions (including our Sun).

At the same time, it should be noted the good agreement of the author theoretical results with the experimental values of the astrophysical *S*-factors, that have been measured under laboratory conditions at energies which are available for experimenters. The fact is that, in spite of the progress in the experimental technology, for the majority of astrophysical nuclear reactions going in the stars and specifying the abundance of the elements and isotopes in the Universe, the direct measurement of cross sections and astrophysical *S*-factors at star energies is impossible, because of smallness of the cross sections caused by the Coulomb repulsion. Therefore, there are two possible ways for obtaining the information about rates of similar reactions:

1) The extrapolation of the data on the astrophysical *S*-factors, measured at higher energies, to the astrophysical energy region (of the order of units to tens of keV).
2) The calculation of the *S*-factors at the required energies in the frame of some theoretical models.

The second way, which was chosen by the author, seems to be more perspective and reasonable at the present time. The reached agreement with the experimental results at higher energies is the essential condition of adequacy of the used approach. It allows one to hope for the reliability of the obtained results at low (stellar) energies, which are interesting for astrophysicists. In some cases the author calculation results coincide to a good accuracy with the experimental data obtained much later than these calculations (for example for p + ^{2}H and p + ^{3}H systems). The book of Dubovichenko S.B. profitably differs from other monographs in the field of nuclear physics and nuclear astrophysics by unusually wide combination of different types of materials. The physical approaches and the results obtained on their basis, the mathematical and numerical calculation methods and certain computer program listings are stated in it thoroughly. The obvious advantage of the book is in the availability of the Introduction and Chapter 1, where the fundamentals of physics of thermonuclear processes in the stars (nuclear star cycles, stellar evolution etc) are stated in a condensed form.

The book “Thermonuclear processes of the Universe” will be useful undoubtedly for advanced students, postgraduate students (PhD doctoral candidates) and researchers specializing in the field of atomic nuclear physics and nuclear astrophysics.

L. D. Blokhintsev
Doctor of Physical and Mathematical sciences,
Professor of the Moscow State University
blokh@srd.sinp.msu.ru

PREFACE

> Nuclear astrophysics is one of the youngest branches of the modern astrophysics, which practically represents the sphere of application of the results obtained in experimental and theoretical physics to the astronomical objects with a view to explain their nature, energy sources, age and chemical composition peculiarities [1].

Owing to the modern development of astronomy and astrophysics, we have a general understanding of the Universe – of its evolution and structure within the distances of the order 14 billions light years. The observations of the Universe reveal the areas of very compact matter concentration and extremely large distances between them, which seem to be “empty”. However, all this “empty” space is filled with gas and dust matter, atoms and various kinds of radiation including neutrino. Furthermore, the modern theories about the Universe involve such concepts as dark matter and dark energy, which determine its mass and characterize its mode of Expansion.

The matter which concentrates in the stars and planets of the visible Universe and which forms the gas and dust clouds consists of nuclides, i.e. the atoms of ninety two chemical elements having different numbers of protons and neutrons in their nuclei and ranging from hydrogen to uranium. All the diversity of nuclear composition of the Universe is made up of several hundreds of nuclides and the current level of science – nuclear astrophysics – allows explaining in general the history of their formation and their relative occurrence.

The world around us also consists of various chemical elements and, presently, it is generally recognized that all the elements forming the Earth, the Sun and the whole solar system were produced in the course of the stellar evolution. Our Earth is one of the eight planets of the solar system and our Sun is a common stable star of our galaxy – the Milky Way. According to the current estimates the Milky Way only comprises several hundred billion stars and even at present time, i.e. 14 billions years after the formation of the visible Universe, which may contain hundred billions of similar galaxies, new stars can be born [2].

ACKNOWLEDGMENTS

I would like to express a profound gratitude to Prof. Neudatchin V.G. (Institute of Nuclear Physics, Moscow State University, Moscow, Russia), Prof. Strakovsky I.I. (GWU, Washington, USA), Prof. Bagrov V.G. (Tomsk State University, Tomsk, Russia), Doctor Uzikov Yu.N. (Joint Institute of Nuclear Research, Dubna, Russia), Academician of the National Academy of Sciences of the Republic of Kazakhstan Boos E.G. (Physical-technical Institute, Almaty, Republic of Kazakhstan), Prof. Duisebaev A.D. and Prof. Burtebaev N.T. (Institute of nuclear physics of the National Nuclear Centre of the Republic of Kazakhstan, Almaty), Prof. Danaev N.T. (Al-Farabi Kazakh National University, Almaty, Republic of Kazakhstan) for the very important discussions of some questions which where considered in the book.

In addition, I would like to express my particular gratefulness to Prof. Ishkhanov B.S. (Institute of Nuclear Physics, Moscow State University, Moscow, Russia) for the possibility to use in the Internet his lectures on thermonuclear physics for students of the Moscow State University and his book “Nucleosynthesis in the Universe”. A part of these materials was used in the Foreword, Introduction and First Chapter of this book.

I am also grateful to Dzhazairov-Kakhramanov A.V. (Fessenkov Astrophysical Institute, Almaty, Republic of Kazakhstan) and Zazulin D.M. (Institute of Nuclear Physics of the National Nuclear Centre of the Republic of Kazakhstan, Almaty) for searching and selecting the experimental material. I also express great thanks to Dzhazairov-Kakhramanov A.V. for the translation of the book into English.

I want to mention a special contribution made by science editors Prof. Burkova N.A. (Al-Farabi Kazakh National University, Almaty, Republic of Kazakhstan) and Prof. Chechin L.M. (Fessenkov Astrophysical Institute, Almaty, Republic of Kazakhstan) who wrote a number of useful comments, introduced corrections and amendments while editing the book.

Finally, I would like to express my deepest gratitude to Prof. Blokhintsev L.D. (Institute of Nuclear Physics, Moscow State University, Moscow, Russia). He was more than just a scientific reviewer who made some fundamental comments with regard to the contents of the book, he also read thoroughly the manuscript and as a technical editor introduced significant corrections to the initial text.

The work has been partly supported by the MES RK (the Ministry of Education and Science of the Republic of Kazakhstan) Program of Fundamental Research via the Fessenkov Astrophysical Institute "NCSRT" NSA RK.

I would like to express a particular gratitude to the President of "NCSRT" NSA RK Prof. Zhantaev Zh.Sh. for the assistance and the permanent support of the work with this book and the whole Nuclear Astrophysics themes.

SUMMARY

> The progress in studies about the Universe is substantially associated with the achievements in the nuclear and elementary particle physics. It turned out that the laws of microcosm allow understanding what is going on in the Universe. This unity of micro- and macrocosm is a remarkable and edifying example of the unity of Nature [2].

Before proceeding to the main results, we would like to present a summary of the book. In the first chapter, we will consider briefly and simply all the major thermonuclear reactions that may take place in the stars at different stages of their formation and evolution. Then, we will expand on the analysis of the main thermonuclear processes involving radiative capture – processes in which two colliding particles fuse together to form one particle and emit γ-quantum. They are mediated by electromagnetic interactions, which somewhat simplifies their consideration from the theoretical point of view. Further, in addition to the properties of bound states of light atomic nuclei participating in thermonuclear reactions, we will consider the principal characteristics, in particular *S*-factors, of radiative capture of protons and other particles by such nuclei at astrophysical energies.

Now, we are going to give an overview of possible reactions in three major thermonuclear cycles for stable stars of the Main Sequence and then indicate which processes will be considered in this book and which ones will be analyzed in the nearest future.

The first cycle is the proton-proton chain, which includes five two-particle processes (according to the initial channel) mediated by strong or electromagnetic interactions, three of which belong to radiative capture processes. Two such processes will be considered in the present book and the results will be given in chapters 3 and 9. The other five reactions of this cycle (in total there are 10 of them as it is shown in Figure 1.4) are mediated by weak interactions and we will not consider them either in this book or in the nearest future.

The stellar CNO cycle consists of nine similar reactions (13 in total, see table 1.2÷1.4, four of which are mediated by weak forces), six of which involve radiative capture. The first of these reactions ($p^{12}C \rightarrow {}^{13}N\gamma$) is considered in chapter 8 and the two last reactions (see table 1.2÷1.4) lead to a formation of ${}^{17,18}F$ nuclei which are not 1*p*-shell nuclei and the applicability of the potential cluster model (PCM), which was used for all further calculations, has never been tested for such cases. Therefore, only three of remaining CNO cycle reactions will be consider in future.

The triple alpha process represents two reactions, one of which involves a two-particle radiative capture. They are analyzed basing on the potential cluster model in chapter 10.

As a result, we have 15 basic thermonuclear reactions with two-particle initial channels mediated by strong and electromagnetic forces, 10 of which are the radiative capture processes, with 4 being considered in this book, the next 4 to be considered in future and two, seemingly, out of consideration within the PCM.

In addition to the mentioned above processes, there are some other radiative capture reactions that supposedly took place at the prestellar stage of evolution of the Universe, i.e. within the first seconds of its existence. They include, for instance [1,2]:

$$p + {}^{3}H \rightarrow {}^{4}He + \gamma$$

or

$${}^{2}H + {}^{4}He \rightarrow {}^{6}Li + \gamma\ ,$$

$${}^{3}H + {}^{4}He \rightarrow {}^{7}Li + \gamma\ ,$$

which could take place during the primordial nucleosynthesis [3,4] and the astrophysical *S*-factors of which are considered in chapters 4 and 9.

In conclusion, we would like to note that the general title of the book “Thermonuclear processes of the Universe” is chosen for the future expansion of the book. In the nearest future, we are planning to finish the consideration of all possible thermonuclear reactions of radiative capture type on light nuclei, and first of all the four reactions directly associated with the thermonuclear cycles. The obtained results will be published in the second edition of the book that presently deals with nine capture reactions.

In total, there are 16 basic radiative capture processes, which lead to *p*-shell nuclei and may be consider within the PCM, including the primordial nucleosynthesis reactions and reactions of the type

$$p^{6,7}Li \rightarrow {}^{7,8}Be\gamma,$$

or

$$p^{9}Be \rightarrow {}^{10}B\gamma$$

considered in chapters 5, 6 and 7, and

$$p^{10,11}B \rightarrow {}^{11,12}C\gamma$$

– the proton capture reaction for the two stable boron isotopes, which will be considered in the future.

They are all out of the standard thermonuclear cycles of proton-proton *(pp)* chain or CNO cycle. Then we will consider the remaining thermonuclear processes of *pp*-chain and CNO cycle which are associated with the rearrangement of channels (in total there are 5 such reactions), for example

$^3He + {}^3He \rightarrow {}^4He + 2p$,

and

$^7Li + p \rightarrow {}^4He + {}^4He$

or

$^{15}N + p \rightarrow {}^{12}C + {}^4He$,

and only three, given above, ending in the nuclei 1*p*-shell.

Actually, it is supposed to carry out the analysis of all these processes based on the potential cluster model for light nuclei and classification of orbital states according to Young schemes in case of states forbidden by the Pauli principle in some cluster systems.

INTRODUCTION

> The application of the achievements of modern nuclear physics to the study of cosmic phenomena and thermonuclear reactions has allowed to develop a theory of the formation, structure and evolution of stars, a theory of supernova explosion and pulsar production, which are concordant, in qualitative terms, with observations, and to explain the abundance of chemical elements in the Universe [2].

First, we will consider the background of and conditions required for the initiation of thermonuclear reactions in astronomical objects, specifically in stars with different masses. Explanation of the processes of the star formation and their evolution is one of the most important task of the modern astrophysics on the whole and nuclear astrophysics in particular, since in the known region of the Universe a considerable part of the observable matter is contained exactly in stars at different stages of their progress or in the objects that have already overcame the star stage.

According to the most popular point of view, stars, at the initial stage of their formation, condense under gravity forces from giant gas molecular clouds [3]. These gas clouds mainly consist of molecular hydrogen with a small admixture of deuterium and helium that form, as a result, of primordial nucleosynthesis at the prestellar development stage of the Universe. Stars are formed in this giant gas molecular cloud from separate irregularities or star formation zones [5]. An example of such nebula is given in Figure B1 [6].

The compression of this zone begins from the collapse in its initial part, i.e. from free fall of the matter to the zone centre because of gravity. The compression area gradually moves from the centre to the periphery including completely the whole zone. This is how star formation process begins. The generating cluster in the centre of the collapsing cloud is a protostar or a star at the early stage of its formation [2].

Generally, the protostar evolution occurs in several stages. The first stage is isolation of a cloud fragment and its densification, which can take place, for example, a result of random fluctuation or under external gravity force. Because of growing weight and gravity, more matter is attracted to the centre of the protostar. The process of the matter falling to protostar from the surrounded external cloud is known as accretion.

The next stage is rapid compression. At this moment, a protostar is practically non-transparent for visible light but transparent for infrared radiation that carries away excess heat generated during the compression so that the interior temperature does not rise considerably and the gas pressure does not prevent further collapse. However, the protostar becomes less transparent during compression, because of the growing density of the matter, and this impedes escape of radiation and leads to an increase in gas temperature. At a certain moment, the protostar becomes practically non-transparent for its heat radiation. Temperature increases rapidly along with gas pressure and, together, they can partially compensate gravity and then the protostar compression slows down.

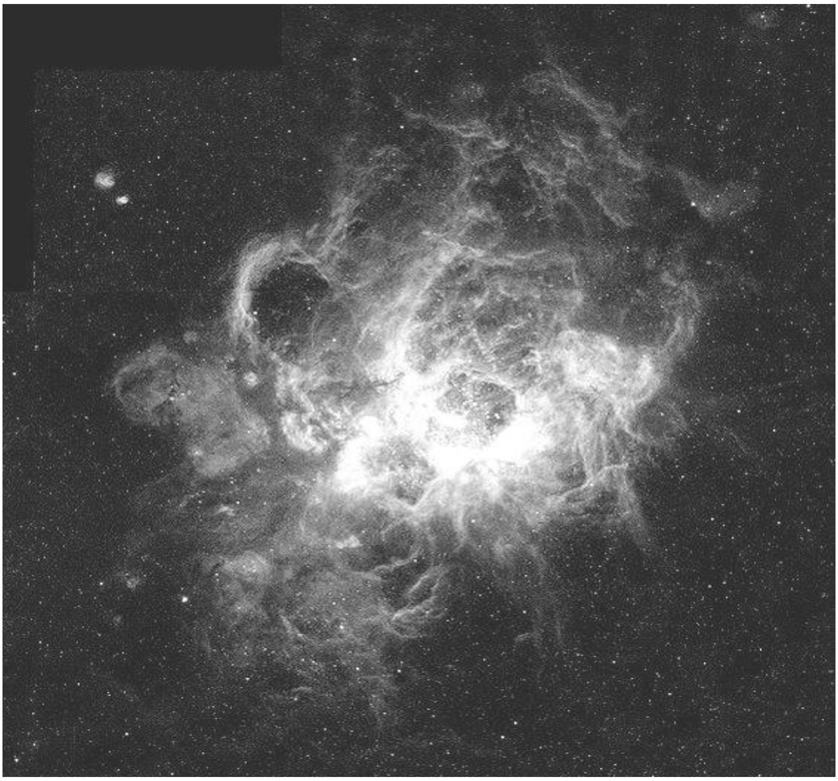

Figure B1. Star formation nebula in Triangulum Galaxy.
(from http://en.wikipedia.org/wiki/H_II_region). (Many size of the pictures here and further have been changed).

Then the stage of slow compression begins. Further rise of temperature causes significant changes of the properties of the matter. Molecules decay to form single atoms at a temperature of several thousands degrees and atoms are ionized at a temperature of about 10,000 Kelvin (K), i.e. their electronic shells break down. These power-intensive processes, as a result, of which the matter turns into plasma, delay the temperature increase for some time, but after all the matter transforms into plasma it recommences. The protostar gradually achieves the state when gravity is practically balanced by internal gas pressure. However, since heat continues to go away and the protostar does not have another energy sources yet, except compression, its compression gradually continues and its interior temperature continues to grow.

How things develop further depends on the sizes and masses of the forming celestial body when the protostar temperature reaches a certain limit. If its mass is not great and equals less than 8% of the mass of the Sun (M_0) then there are no conditions for a stable thermonuclear reaction to begin, which would support its balance. This protostar cannot become a real star but acquires a state known as Brown Dwarf and then cools with time and can become a planet-like object [6].

If the mass of the compressing matter is more than 8% of M_0, this is enough for stable thermonuclear reactions to begin to take place inside the protostar under compression and a stable Main Sequence star will form from such cloud (see Appendix 2).

The temperature in the star centre approximates 1 million K and the new stage in the protostar life (the earliest thermonuclear fusion reactions) can begin, when the mass of the most compact part of the cloud approximates, due to accretion, 0.1 of the solar mass. However, these thermonuclear reactions differ, to a significant extent, from reactions taking place in sun-like stationary stars [2]. The point is that the first solar fusion reaction is hydrogen burning

$$p + p \rightarrow {}^{2}H + e^{+} + \nu_e .$$

It requires higher temperature (approximately 10 million K), while the temperature in the protostar centre equals 1 million K. Only the deuterium fusion reaction can occur effectively at this temperature:

$${}^{2}H + {}^{2}H \rightarrow {}^{3}He + n .$$

Deuterium (the same as ^{4}He) is formed at the prestellar evolution stage of the Universe [7] and its content in the protostellar substance approximates 10^{-5} of the proton content. However, even such a small amount is enough for the appearance of an effective energy source in the protostar centre, which leads to future temperature increases [2].

According to Hayashi [5], convection gas flows begin to appear because of non-transparency of the protostellar matter. Heated gas regions go from the star centre to the periphery and the cold matter goes down from the surface to the protostar centre, supplying additional deuterium. However, the thermonuclear fusion reactions of deuterium nuclei that have begun produce comparatively low quantities of energy and cannot resist gravitational compression, which still continues at this stage.

Further compression of the stellar matter due to gravity causes a greater temperature rise in the centre of the star, thus creating conditions for the beginning of the helium burning thermonuclear reaction. At this moment, the protostar becomes a stable star since the release of thermonuclear energy can now balance gravity and the star, depending on its mass, takes a certain place in the Hertzsprung-Russell diagram [5] (see Appendix 2). The scheme of the mechanism of formation, development and death of massive star, which can turn into a supernova [2] in the course of its evolution, is shown in Figure B2.

Star evolution, i.e. the process of its formation, life and transformation into the White Dwarf, is shown in Figure B3. This is a star with a mass close to the solar mass (http://en.wikipedia.org/wiki/Stellar_evolution) [6]. It gradually turns into the Red Giant and the remaining core turns into the White Dwarf after the ejection of the planet nebula (see Appendix 2).

We have described in brief the process of the protostar evolution into an ordinary star, whose stable state is maintained because of the thermonuclear reactions in it. Obviously, this description is not rigorous and has a quality nature. A rigorous solving of the problem of the star formation from interstellar matter (i.e. molecular gas) and the stellar evolution as a whole is hardly possible. It is only possible to develop separate parts of the star formation theory and control them in a continuous fashion through new astronomical observations [5].

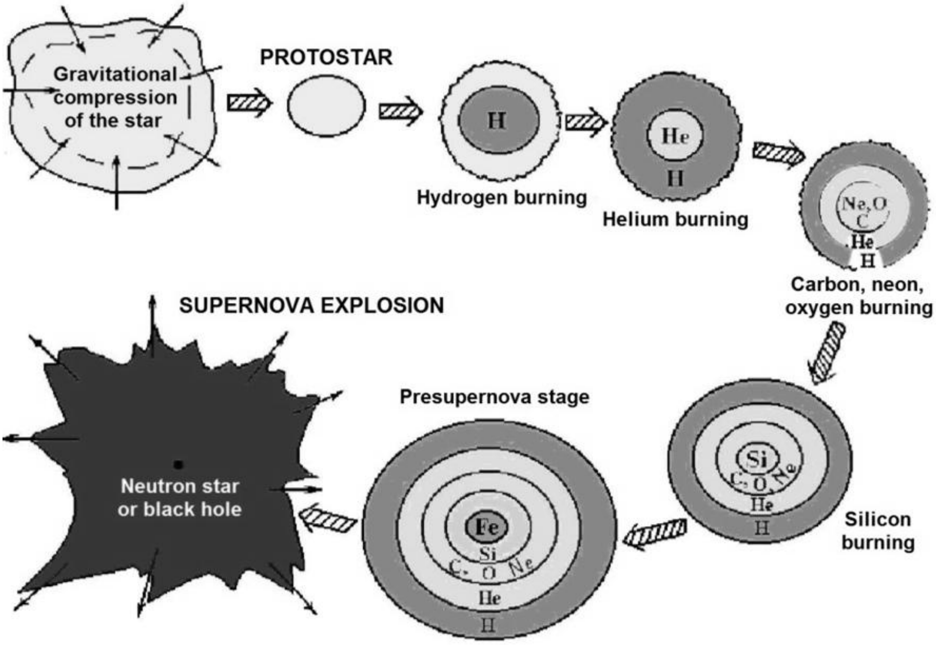

Figure B2. Basic stages of massive star evolution with the mass M > 25 $\mathfrak{M}_\odot$ ($\mathfrak{M}_\odot$ – mass of the Sun) [2]. (from: http://nuclphys.sinp.msu.ru/nuclsynt/n01.htm).

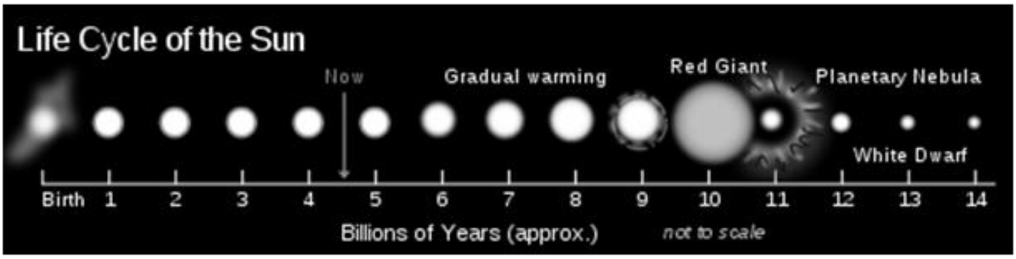

Figure B3. Development stages of the star like our Sun (M ~ $\mathfrak{M}_\odot$). Numerals show the lifetime in billions of years.(from: http://en.wikipedia.org/wiki/Stellar_evolution).

We have shown that an astrophysical object turns into a star when stable thermonuclear reactions begin to occur in it and, because of them, the star, depending on its mass, takes a certain place in the Main Sequence. Now let us consider different types of thermonuclear reactions that are a part of three main cycles: proton-proton chain, CNO cycle, and helium cycle. Then, we will consider the causes of reactions caused by interaction of atomic nuclei in the stars of different masses at various stages of their development.

Chapter 1

THERMONUCLEAR PROCESSES

INTRODUCTION

Slightly coming back in study of the stellar evolution, we would remind that, when the temperature in the star centre rise up to 10÷15 mln K because of the gravity compression, the value of kinetic energy of scattering hydrogen nuclei is enough for overcoming Coulomb repulsion. The nuclear reaction of hydrogen burning, which is the first reaction of the proton-proton chain [2], begins. Strictly speaking, such explanation of the reaction is not exact, but it is most clear for the followers of classic (not quantum) physics. However, from the modern point of view, it is more correct to say that the increasing of the kinetic energy leads to the increase in probability of the particles penetration through the potential barrier. In a certain period, it appears that this is enough for initiation of stable thermonuclear reaction of hydrogen fusion. This reaction begins in the bounded central part of the star, but the resulting energy output stops its further gravity compression.

The qualitative change of the energy release mechanism begins at this stage of star development. If the star warming is a result of gravitational compression before the beginning of the nuclear reaction of hydrogen burning, but now the other mechanism is opened – the energy output goes at the expense of nuclear fusion reactions and that is enough for counteraction against the gravitational forces. As a result, the star acquires stable dimensions and luminosity, which are not changed during billions of years for stars near the solar mass, i.e. all time when the hydrogen burning going in its centre.

The small value of the cross section of this reaction explains the fact that the stage of hydrogen burning is the most long-continued stage in the stellar evolution. The value proportional to the probability of certain interaction process of nuclear particles between each other is named as a cross section in quantum physics; the small value of the cross section means the small probability of given process. Thermonuclear reactions, in the stars with various masses, go differentially, with different speed and approximately continue from tens of millions to tens of billions of years [2].

1.1. THERMONUCLEAR REACTIONS IN THE STARS

Thermonuclear reaction (fusion reaction, nucleosynthesis or fusion of atomic nuclei) is a variety of nuclear reaction which, as generally regarded, proceeds in stars at energies about

0.1÷100 keV (1 keV approximately corresponds to the temperature 10^7 K according to the $E = kT$ relation) and leads to the fusion of light atomic nuclei into heavier nuclei [6].

Now, before going to the description of the star thermonuclear processes, we briefly stop on the mechanism of thermonuclear reaction, i.e. on the reason why it is going in plasma (evacuated and ionized gas, generally consisting in atomic nuclei having positive electric charge, and electrons with negative charge). The process of nuclear fusion or thermonuclear reaction goes on if the atomic nuclei, having positive charge, will approach each other at the distance where the strong attractive interaction affects. This distance has the nuclei size order, that is approximately equals 10^{-13} cm or 1 fm (Fermi) and considerably less than atomic size in ordinary, non-ionized state, which has the order of 10^{-8} cm or 1 A (angstrom).

The charges of nuclei and electrons compensate each other at low temperatures and energies if non-ionized atoms exist. But electron shell radii already not exist within distances of the order of 1 fm and can not shade nuclear charges, so they experience strong electrostatic repulsion. The force of this repulsion, in accordance with Coulomb law, varies inversely as the square between the charge distances. The value of the strong interaction, which trend to attract them, begins to rise quickly and becomes more than Coulomb repulsion at the distances of the order of nuclear size.

Thereby, atomic nuclei have to take the potential Coulomb barrier for enter into a reaction or, be more exact, have enough probability to penetrate this barrier. For example, the value of this barrier approximately equals 0.1 MeV = 100 keV = 10^5 eV (electronvolt) for the radiative capture reaction of deuterium by tritium $^2\text{H} + {}^3\text{H} \rightarrow {}^5\text{He} + \gamma$. Let us provide, for comparison, the required energy for ionization of hydrogen atom, which equals 13 eV only. If to convert the energy equals 0.1 MeV to the temperature, we obtain approximately 10^9 K. Such temperature can not be in the majority of stars, for example in the Sun, and it seems that thermonuclear processes are impossible there.

However, at least there are two known nature effects, which are reducing the temperature required for initiation of the thermonuclear reaction. Examine them into detail:

1. Firstly, the temperature characterizes the average kinetic energy of particles in the centre of the star only. There are particles with low and high energy, because it is defined by the Maxwell distribution for gas and plasma. Only a small quantity of nuclei really takes part in thermonuclear reaction. They have energy much more than average – so-called “tail” of the Maxwell distribution [6].

This distribution can be written in the form of velocity distribution (see Figure 1.1)

$$F(v) = 4\pi v^2 \left(\frac{m}{2\pi kT} \right)^{3/2} \exp\left(-\frac{mv^2}{2kT} \right)$$

or by energies

$$F(E) = 2\left(\frac{E}{\pi (kT)^3} \right)^{1/2} \exp\left(-\frac{E}{kT} \right) .$$

The form of velocity distribution function, which is absolutely analogous to the energy distribution, is shown in Figure 1.1.

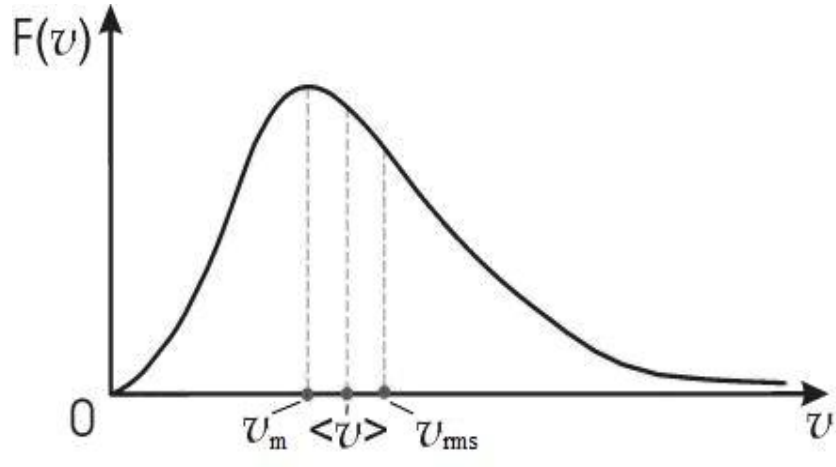

Figure 1.1. The Maxwell velocity distribution.
(from:(http://fn.bmstu.ru/phys/bib/physbook/tom2/ch5/texthtml/ch5_4.htm)

This distribution has the most probable velocity and energy

$$v_{\mathrm{m}} = \left(\frac{2kT}{m}\right)^{1/2}, \quad E_{\mathrm{m}} = \frac{mv_{\mathrm{m}}^2}{2} = kT \ ,$$

noticed above and mean square velocity v_{rms} expressing through the average velocity $\langle v \rangle$ and average energy of the particles

$$v_{\mathrm{rms}} = \left\langle v^2 \right\rangle^{1/2} = \left(\frac{3kT}{m}\right)^{1/2}, \ E_{\mathrm{rms}} = \frac{mv_{\mathrm{rms}}^2}{2} = \frac{3}{2}kT \ .$$

Only small parts of the hydrogen nuclei with a maximum kinetic energy enter into a thermonuclear reaction while the star compression process, because of it the considerable quantity of additional energy emits. The part of this energy is expended to the increasing of the kinetic energy of some other part of hydrogen nuclei, preparing them to the participation in further nuclear processes. Thereby, the low-energy nuclei, forming the basic star mass, are the energy source for thermonuclear reactions.

2. Secondly, because of effects of quantum physics, atomic nuclei do not need to have the energy more than the value of Coulomb barrier as it was in classic mechanics. These particles can to penetrate through the barrier with certain probability, even through their energy less than this barrier. This phenomenon is called as quantum tunneling effect and is shown graphically below in Figure 1.2 [8].

It is shown in Figure 1.2 that quantum particle can penetrate through the barrier. This particle has the oscillating wave function (WF) Ψ outside the barrier ($r > r_1$) determining probability of its existence in the certain point of space, with the energy less than barrier's height. The WF Ψ of particle inside the barrier ($r < r_1$) is not equal to zero and represents itself the function of position with exponentially drooping dependence [8]. In other words, there is certain and completely nonzero probability of particle penetration through the potential Coulomb barrier and its penetration into the region of strong interaction, which leads to the beginning of nuclear or thermonuclear reactions.

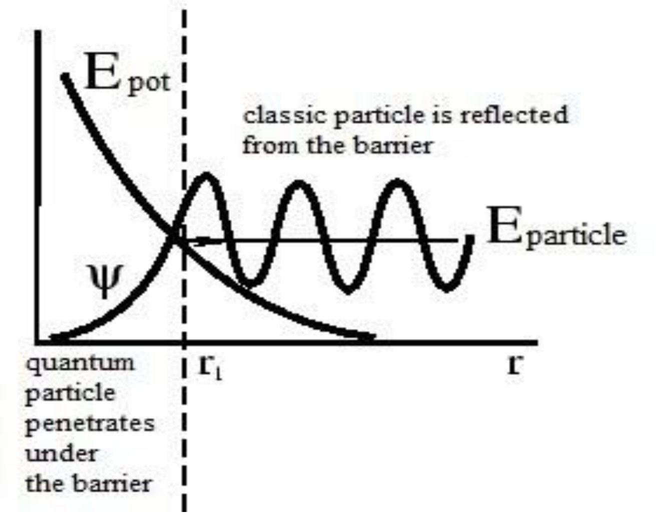
E pot
classic particle is reflected from the barrier
E particle
ψ
quantum particle penetrates under the barrier
r_1
r

Figure 1.2. Quantum particle penetration trough the potential barrier [8].
(from: http://astronet.ru/db/msg/1169513/node36.html).

Now we will have detailed consideration of fusion processes of light atomic nuclei, which are possible because of thermonuclear reactions in the centre of the star. At the main part of its existence, the star is in the balance stage and it means, on the one hand, that the gravitation force tends to compress and decrease it, but, on the other hand, the energy release of thermonuclear reactions forces the star to expand and increase. The star stays in balance until these two forces, which act on the star, are equivalent and opposite in direction and this star stays in the stationary state in Main Sequence (see Appendix 2).

1.2. PROTON-PROTON CHAIN

Proton-proton or *pp*-chain is a set of thermonuclear reactions for the stars of Main Sequence when hydrogen (or more exactly, hydrogen atomic nucleus – proton "p") turns to helium (helium atomic nucleus ^{4}He). This cycle can go at lowest energies and it is the main alternative to the CNO cycle, which will be considered next. Evidently, the proton-proton chain dominates in stars with the masses on the order of solar mass, in stable stage of their development. At the same time, the CNO cycle dominates in more massive and hot stars.

The total result of these *pp*-reactions is the fusion of four protons with the formation of the atomic nucleus ^{4}He, with the energy output equivalent to 0.7% of the mass of these protons.

Such reaction chain in simplified form goes through the three stages. At first, two protons, having enough energy for penetration through the Coulomb barrier, merge forming of deuteron, positron and electron neutrino. Then the deuteron merges with the positron forming ^{3}He nucleus and γ-quantum and, then, two nuclei of ^{3}He atom merge forming the atomic nucleus ^{4}He; in this case two protons are disengaged.

Schematically it is usually identified as [6]:

1. $p + p \rightarrow {}^2H + e^+ + \nu_e$, $Q = 0.42$ MeV,
2. ${}^2H + p \rightarrow {}^3He + \gamma$, $Q = 5.49$ MeV,
3. ${}^3He + {}^3He \rightarrow {}^4He + 2p$, $Q = 12.86$ MeV.

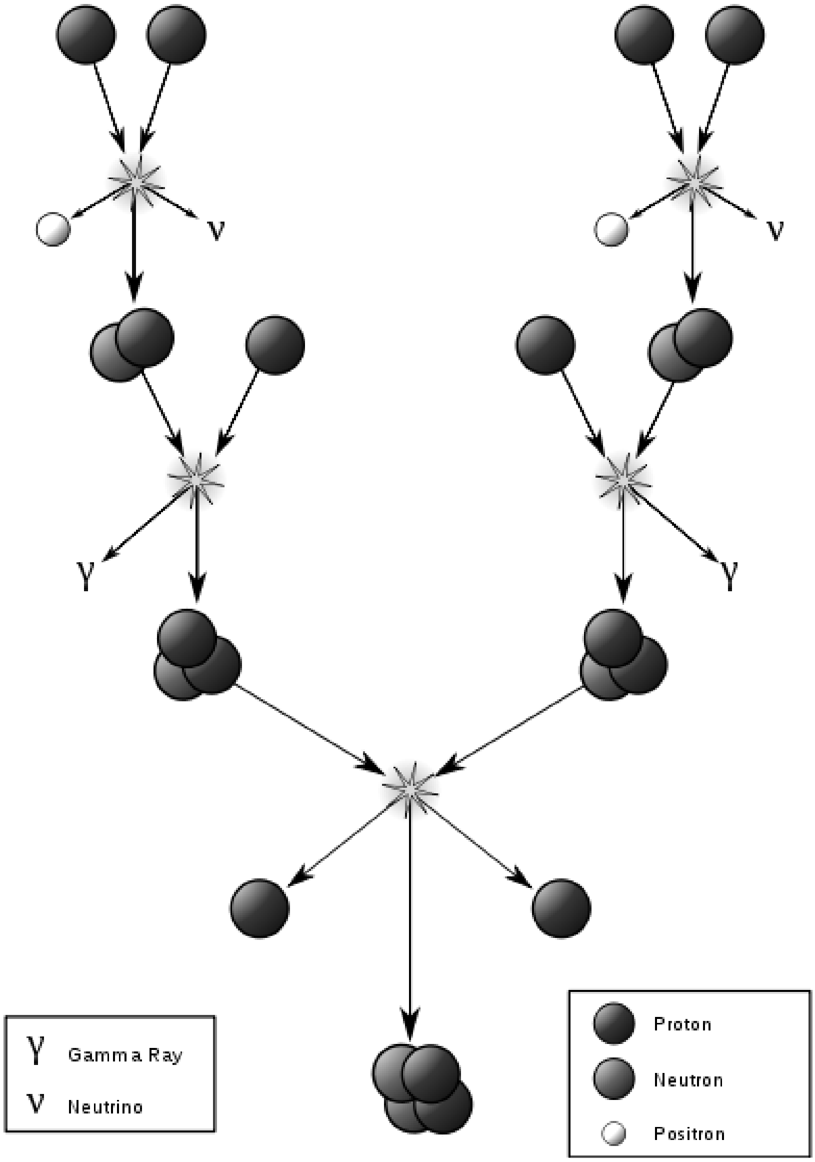

Figure 1.3. Simplified scheme of the proton-proton chain [6].
(from: http://en.wikipedia.org/wiki/File:FusionintheSun.svg).

Here the Q value is the energy releasing in the reaction process, which is expressed in the energy units called megaelectronvolt (MeV). Such reaction chain is shown graphically in Figure 1.3 [6].

These are only the main reactions of the proton-proton chain, but all other reactions with the designation of channel relative contributions and reaction rates are shown in Figure 1.4 [2] and Table 1.1 [8].

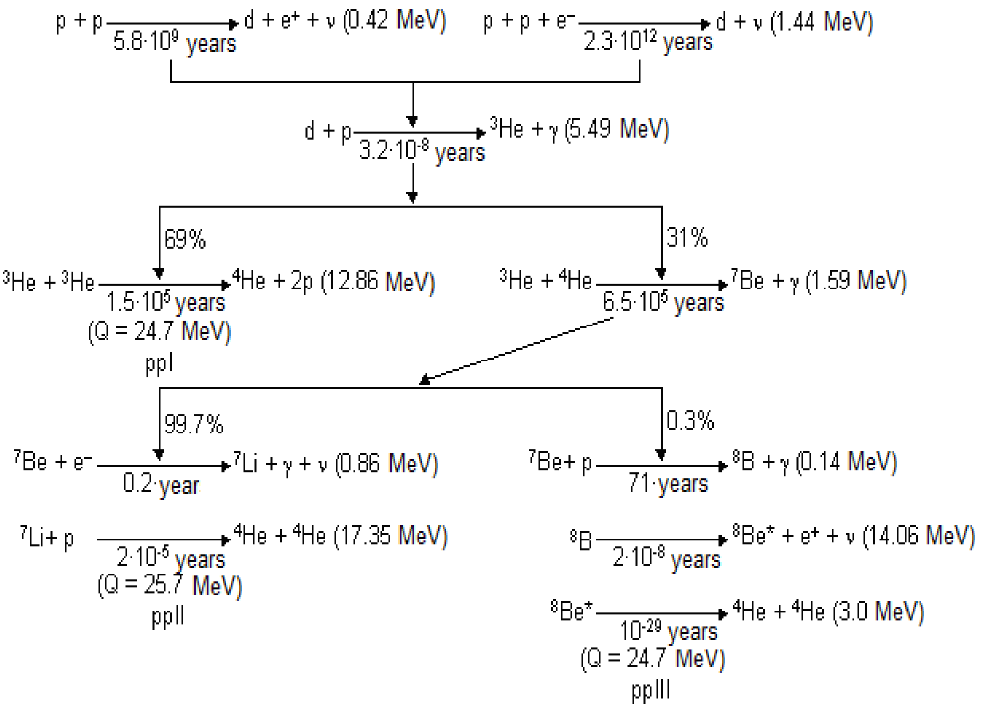
p + p → d + e⁺ + ν (0.42 MeV)
5.8·10⁹ years
p + p + e⁻ → d + ν (1.44 MeV)
2.3·10¹² years
d + p → ³He + γ (5.49 MeV)
3.2·10⁻⁸ years
69%
31%
³He + ³He → ⁴He + 2p (12.86 MeV)
1.5·10⁵ years
(Q = 24.7 MeV)
ppI
³He + ⁴He → ⁷Be + γ (1.59 MeV)
6.5·10⁵ years
99.7%
0.3%
⁷Be + e⁻ → ⁷Li + γ + ν (0.86 MeV)
0.2·year
⁷Be+ p → ⁸B + γ (0.14 MeV)
71·years
⁷Li+ p → ⁴He + ⁴He (17.35 MeV)
2·10⁻⁵ years
(Q = 25.7 MeV)
ppII
⁸B → ⁸Be* + e⁺ + ν (14.06 MeV)
2·10⁻⁸ years
⁸Be* → ⁴He + ⁴He (3.0 MeV)
10⁻²⁹ years
(Q = 24.7 MeV)
ppIII

Figure 1.4. All reactions of proton-proton chain [2]. (from: http://nuclphys.sinp.msu.ru/nuclsynt/ n04. htm#docref1)

Table 1.1. Reactions of proton-proton chain with the designation of energy output Q and characteristic reaction time τ for each process [8] (from: http://astronet.ru/db/msg/1190731)

No	Reaction	Q (MeV)	τ (years)	ε_ν (MeV); X
I	$p(p,e^+\nu)^2H$	0.42	$8.2{\cdot}10^9$	$\bar{\varepsilon}_\nu = 0.26$; $\varepsilon_{\nu,\,max} = 0.42$
	$^2H(p,\gamma)^3He$	5.49	$4.4{\cdot}10^{-8}$	$X(^2H) = 2.7{\cdot}10^{-18}$
	$^3He(^3He,2p)^4He$	12.86	$2.4{\cdot}10^5$	$X(^3He) = 1.6{\cdot}10^{-5}$
II	$^3He(^4He,\gamma)^7Be$	1.59	$9.5{\cdot}10^5$	$X(^7Be) = 1.2{\cdot}10^{-11}$
	$^7Be(e^-,\gamma\ \nu)^7Li$	0.86	0.30	$\varepsilon_\nu = 0.86$ (90%); 0.38 (10%); $\bar{\varepsilon}_\nu = 0.8$
	$^7Li(p,^4He)^4He$	17.35	$3.8{\cdot}10^{-5}$	$X(^7Li) = 1.5{\cdot}10^{-15}$
III	$^7Be(p,\gamma)^8B$	0.14	$1.0{\cdot}10^2$	$X(^8B) = 4{\cdot}10^{-21}$
	$^8B(e^+\nu)^8Be^*$	14.06	$3.0{\cdot}10^{-8}$	$\bar{\varepsilon}_\nu = 7.3$; $\varepsilon_{\nu,\,max} = 14.06$
	$^8Be^* \rightarrow 2^4He$	3.0	–	–

As it is seen from Table 1.1, this circle can be finished in three different paths. The first two reactions have to be realized twice for finishing of the I branch, which was shown above and gives maximal energy contribution, because of the fact that two ^{3}He nuclei are needed for the third reaction. Here, it seems, that it is possible to neglect reaction $p + p + e^- \to {}^2H + \nu$ (see Figure 1.4), which, like the main process $p + p \to {}^2H + e^- + \nu$, goes at the expense of weak interactions, but with the probability near three orders less.

Rates and probabilities of the intermediate reactions in the proton-proton chain are great and the characteristic time is low in comparison with the rate of first reaction of the branch I, which occurs very slowly, so ^{2}H, ^{3}He, ^{7}Be, ^{7}Li and ^{8}B nuclei are not accumulated in the stars in noticeable amounts.

Neutrinos are emitted with the extremely high energy for the *pp*-chain in III branch at the atomic nucleus decay process of ^{8}B nucleus with the forming of the unstable beryllium nucleus in the excited state ($^8Be^*$), which almost instantly decays into two ^{4}He nuclei. These neutrinos from solar thermonuclear reaction products are registered with the different indicators in the Earth [8]. The chain is finished by the I branch in the 70% cases, 30%-the II branch and only the few tenth of percent [2] are related to the III branch, as it is shown in Figure 1.4.

The certain main parameters of the proton-proton chain reactions are listed in Table 1.1. Particularly, ε_v is the energy of emitted neutrinos, $\bar{\varepsilon}_v$ and $\varepsilon_{v,\,max}$ are their average and maximum values when neutrinos are emitted in the energy range $0 < \varepsilon_v < \varepsilon_{v,\,max}$, also X is the mass concentration of the intermediate atomic nuclei. The τ and X values are rated for physical conditions closed to expecting in the inner part of the Sun, i.e. for the temperature $1.5 \cdot 10^7$ K, for the density 100 g/cm^3 and for equal concentrations of hydrogen and helium by mass ($X_H = X_{He} = 0.5$). Let us see that the data of characteristic time τ, which is given in Figure 1.4 [2] and in Table 1.1 [8], slightly differ because it is taken from different sources.

Let us note that the hydrogen store in the Sun could be enough for 100 billions of years at the up-to-date rate of its burning by proton-proton chain. However, certain circumstance considerably reduces the hydrogen burning stage.

The problem is that hydrogen practically burns only in the inner part of the Sun where the hydrogen stores are enough for 5÷6 billions of years, i.e. after this time the Sun, as it follows from the modern star development model, ought to turn into the Red Giant. At this stage, the solar radius approximately will rise in 200 times and the solar outer shell firstly will reach Mercury, then Venus and will come nearer to the Sun, but, it seems, will not affect to its orbit [2].

The core of the star, more massive than the Sun, begins gradually compress under gravity while hydrogen burning-out. It leads to the pressure and temperature rising and along with proton-proton chain the other thermonuclear process, called CNO cycle, comes into force.

1.3. THE STELLAR CNO CYCLE

The CNO cycle is the collection of three linked or, more exactly, partly overlapped cycles. The first and most simple of them is the CN cycle (Bethe-cycle or carbon cycle) was suggested by Hans Bethe and, regardless of him, by Carl von Weizsäcker in 1939 year. The main reaction path of the CN cycle is shown in Figure 1.5 and Table 1.2 [6].

Table 1.2. CN cycle reactions with the designation of energy output and characteristic reaction time [6]

Fusion	**→**	**Result**	**Q (MeV)**	**τ (years)**
$^{12}C + p$	→	$^{13}N + \gamma$	1.95	$1.3\ 10^7$
^{13}N	→	$^{13}C + e^+ + \nu_e$	1.37	7 min
$^{13}C + p$	→	$^{14}N + \gamma$	7.54	$2.7\ 10^6$
$^{14}N + p$	→	$^{15}O + \gamma$	7.29	$3.2\ 10^8$
^{15}O	→	$^{15}N + e^+ + \nu_e$	2.76	82 sec
$^{15}N + p$	→	$^{12}C + {}^4He$	4.96	$1.1\ 10^5$

The initial nuclei taking part in the reaction are listed in the first column of this and other tables given below. The third column reproduces the issue nuclei obtaining in the reaction, in the next – the energy release and in the last – the reaction time.

The alternative final channel in the reaction of proton capture by ^{15}N nucleus is the formation of ^{16}O nucleus with γ-quantum emission. This is initial reaction for the new CNO-I cycle, which has exactly the same structure as the CN cycle and its reactions are represented in Table 1.3 [6]. The CNO-I cycle raises up the energy-release rate of the CN cycle increasing the number of ^{14}N nuclei-catalytic agents for this cycle.

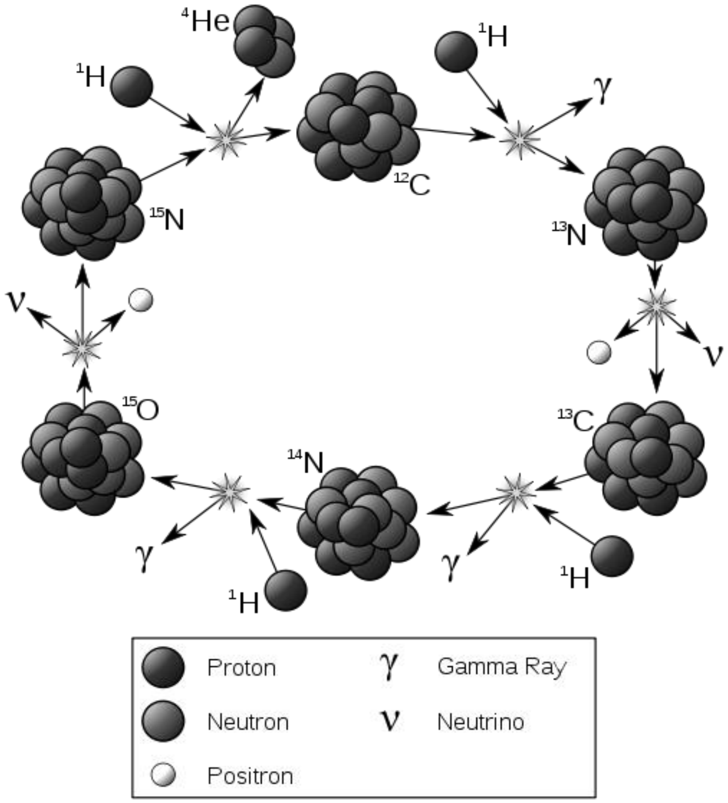

Figure 1.5. CN cycle reactions [6]. (from: http://en.wikipedia.org/wiki/CNO_cycle).

Table 1.3. CNO-I cycle reactions with designation of energy output [6]

Fusion	→	**Result**	**Q (MeV)**
$^{15}N + p$	→	$^{16}O + \gamma$	12.13
$^{16}O + p$	→	$^{17}F + \gamma$	0.60
^{17}F	→	$^{17}O + e^{+} + \nu_e$	2.76
$^{17}O + p$	→	$^{14}N + {}^{4}He$	1.19

The last reaction, given here, is the interaction of the proton with ^{17}O nucleus, which is also able to have another final channel creating new, so called, CNO-II cycle listed in Table 1.4 [6]. Thereby, all these CN, CNO-I and CNO-II cycles are formed CNO cycle, which supports the star burning at the next stage after the hydrogen burning cycle.

Table 1.4. CNO-II cycle reactions with designation of energy output [6]

Fusion	→	**Result**	**Q (MeV)**
$^{17}O + p$	→	$^{18}F + \gamma$	5.61
^{18}F	→	$^{18}O + e^{+} + \nu_e$	1.66
$^{18}O + p$	→	$^{15}N + {}^{4}He$	3.98

Let us note that there is another and very slow cycle, called OF cycle, but its role in the energy production is negligibly small. However, this cycle is essential for explanation of ^{19}F nuclei origin in stars. The cycle follows from the last reaction of the previous cycle going through another channel, and it is shown in Table 1.5 [6].

Table 1.5. OF cycle reactions with designation of energy output [6]

Fusion	→	**Result**	**Q (MeV)**
$^{18}O + p$	→	$^{19}F + \gamma$	7.99
$^{19}F + p$	→	$^{16}O + {}^{4}He$	8.11
$^{16}O + p$	→	$^{17}F + \gamma$	0.60
^{17}F	→	$^{17}O + e^{+} + \nu_e$	2.76

All of main reactions of the triple CNO cycle can be represent in Figure 1.6, which was taken from another source [2] and where energy values and reaction time ($T_{1/2}$ half-life) are slightly differed. The proton-proton chain dominates apparently in the stars with masses comparable with the solar mass or less. The CNO cycle is the main source of energy in more massive stars having higher core temperature.

So, the initial stage of fusion reactions consists in the forming of helium nuclei from four hydrogen nuclei, as it was listed in Table 1.1. In addition, the helium nuclei along with ^{12}C, ^{14}N and ^{15}N nuclei are the final products of all three CNO cycles as it was demonstrated in Tables 1.2÷1.4. During the time when hydrogen burning is going in the star's central part the *pp*-chain and CNO cycle going because of hydrogen burning and its reserves are exhausted but helium accumulation is taken place. So-called helium core is formed in the centre of the star.

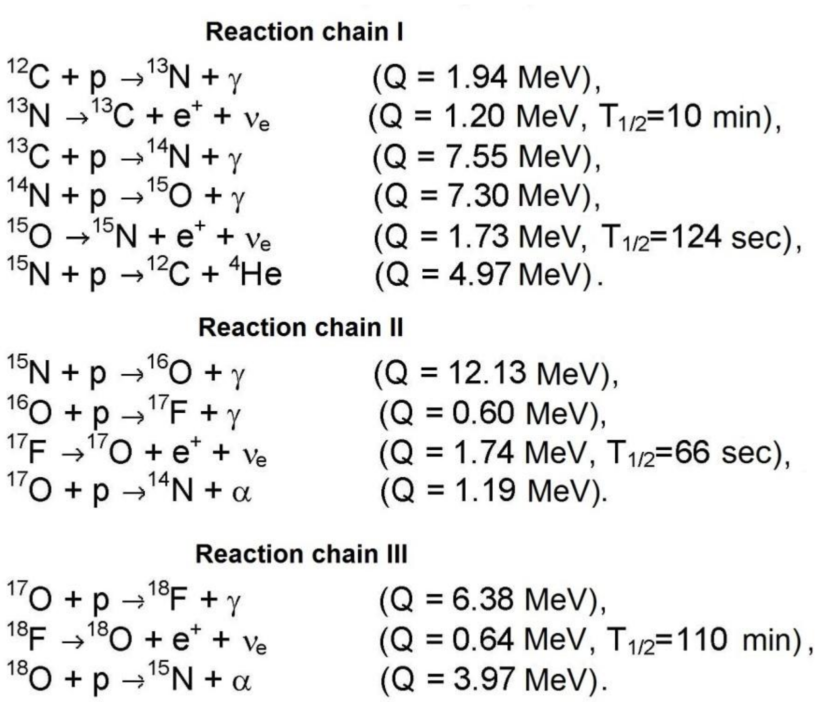

Reaction chain I

$^{12}C + p \rightarrow {}^{13}N + \gamma$ (Q = 1.94 MeV),

$^{13}N \rightarrow {}^{13}C + e^+ + \nu_e$ (Q = 1.20 MeV, $T_{1/2}$=10 min),

$^{13}C + p \rightarrow {}^{14}N + \gamma$ (Q = 7.55 MeV),

$^{14}N + p \rightarrow {}^{15}O + \gamma$ (Q = 7.30 MeV),

$^{15}O \rightarrow {}^{15}N + e^+ + \nu_e$ (Q = 1.73 MeV, $T_{1/2}$=124 sec),

$^{15}N + p \rightarrow {}^{12}C + {}^4He$ (Q = 4.97 MeV).

Reaction chain II

$^{15}N + p \rightarrow {}^{16}O + \gamma$ (Q = 12.13 MeV),

$^{16}O + p \rightarrow {}^{17}F + \gamma$ (Q = 0.60 MeV),

$^{17}F \rightarrow {}^{17}O + e^+ + \nu_e$ (Q = 1.74 MeV, $T_{1/2}$=66 sec),

$^{17}O + p \rightarrow {}^{14}N + \alpha$ (Q = 1.19 MeV).

Reaction chain III

$^{17}O + p \rightarrow {}^{18}F + \gamma$ (Q = 6.38 MeV),

$^{18}F \rightarrow {}^{18}O + e^+ + \nu_e$ (Q = 0.64 MeV, $T_{1/2}$=110 min),

$^{18}O + p \rightarrow {}^{15}N + \alpha$ (Q = 3.97 MeV).

Figure 1.6. Reactions of CNO cycle [2]. (from: http://nuclphys.sinp.msu.ru/nuclsynt/n04.htm#docref2).

The energy release at the expense of the above considered thermonuclear reactions is reduced, when the hydrogen in the centre of the star has burned and the gravitational forces come into force again. In this case, the additional heating will be the result of the compression beginning of the formed helium core of the star. The kinetic energy of the colliding helium nuclei rises up and reaches the sufficient value of probability for overcoming the Coulomb barrier. The next stage of thermonuclear reactions begins – helium burning.

1.4. TRIPLE ALPHA PROCESS

When the hydrogen in the centre of the star is finished, the stars with the mass less than 40% of solar mass are dying turning into the dim and compact White Dwarfs consisting from the helium [8]. The gravity compression force, it means the temperature in stars with this mass too, is not enough for the helium reaction ignition.

The central region of more massive stars is so compressed under the gravity, that the temperature in it comes up to hundreds of millions K. The interaction of helium nuclei is possible at this temperature and the high density of stellar interiors gives the collision of three or even four helium nuclei with the production reaction of carbon or oxygen [8] quite probable

$$^4He + {}^4He + {}^4He \rightarrow {}^{12}C + \gamma,$$

and

$^4He + ^{12}C \rightarrow ^{16}O + \gamma$.

The first of these reactions is named as “Triple helium reaction” (Triple alpha process) and represents fusion nuclear reaction of three ^4He atomic nuclei in stellar interiors. It starts at the temperature about $1.5 \cdot 10^8$ K and at the density of the order of $5 \cdot 10^7$ kg/m^3. It is possible that this reaction goes in two stages [8]:

1. Forming of the unstable ^8Be nucleus (the half-life is equal to 10^{-16} sec)

$^4He + ^4He \rightarrow ^8Be + \gamma$.

2. Forming of ^{12}C nucleus in one of the excited states

$^4He + ^8Be \rightarrow ^{12}C^* + \gamma$.

This reaction is shown in Figure 1.7 schematically and leads to the energy output equals 7.28 MeV [6].

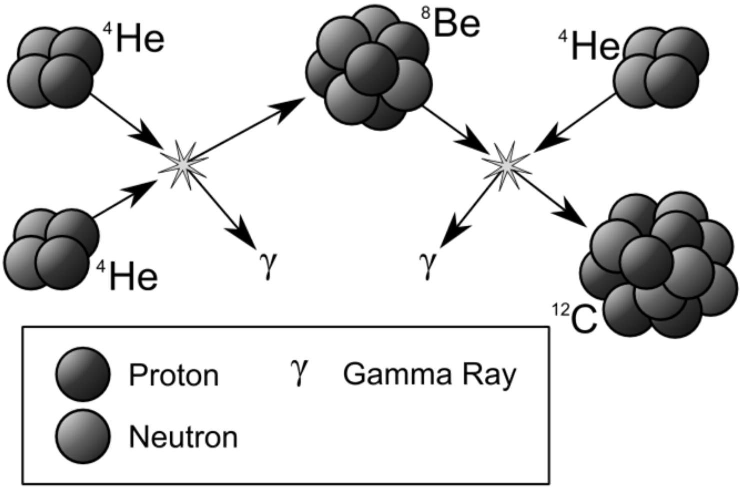

Figure 1.7. Triple alpha process [6].(from: http://en.wikipedia.org/wiki/Triple-alpha_process)

The second reaction, given above, is alpha particle capture by carbon nucleus, which can go practically simultaneously with triple ^4He-process. This reaction leads to the energy output equals 7.16 MeV [8] and, along with the two-particle $^4He^{12}C$ capture, it can go, apparently, as the reaction of consistent fusion of four helium nuclei with the formation of ^{16}O.

The stars, with the mass less than 6÷8 solar mass, have the stage of helium flashing or helium burning (continuing only few percent of hydrogen burning time) de facto is the last period in their life. The certain part of helium and nitrogen forming in the CNO cycle, carbon and oxygen are carried to the star surface.

The stellar brightness is increasing; it is blowing and releasing the shell in the form of planet nebula, replenishing the interstellar medium by these elements. The core of this star survives in the form of carbon-oxygen White Dwarf [8].

Thus, one can see from the given reactions that carbon and oxygen are the products of helium burning in the centre of the star, which are formed approximately in equal amounts.

1.5. ANOTHER THERMONUCLEAR PROCESSES IN THE STARS

The central part of the star, generally consisting from carbon and oxygen, loses stability once more and begins compression, which leads to the temperature rising, when the whole helium exhausts (burns) in massive stars, with masses more than 6÷8 solar mass. The temperature also rises in the layer, which adjacent to the star core, consisting of helium. It rises in the external star layers too, which consist of hydrogen. Therefore, the next script could be real: the helium and hydrogen burning in the quite thin shell around the already inactive carbon-oxygen core. At the same time, the temperature in the core itself is not enough high and, probably, the nuclear reactions with the formation of heavier elements do not take place yet [9].

But, the continuing compression of the star core with such mass and the temperature rising in it stimulate future nuclear reactions, bearing a wide gamma of new chemical elements. At the beginning, the carbon burns first generally producing neon and sodium. Then the neon burns producing in another elements magnesium and aluminum. After that, the oxygen burns producing silicon and sulfur. Finally, the silicon burns turns into iron or elements that close to it. These reactions are going at the temperature about 1 billion K and pass several thousands of years of over one million of years of massive star life [8].

The temperature and pressure in the centre of the star are increased with rising rate while burning of the elements with large nucleus charge Z, and it increases, by-turn, the nuclear reaction rate. This dependence is shown schematically in Figure 1.8 [2]. If the hydrogen burning reaction goes about several millions of years for the massive star (the star mass is about 25 solar masses), then the helium burning goes tenfold rapidly. The oxygen burning process lasts about 6 months and silicon burning passes during one day.

Nuclear fusion reactions for elements that heavier than ^{12}C or ^{16}O can go on till the energy output is possible. The nuclei in the iron zone are formed, as a result, of silicon burning at the final stage of thermonuclear reactions. This is the final stage of all processes of the stellar thermonuclear fusion because the nuclei in the iron zone have the maximal specific binding energy; its diagram is shown in Figure 1.9 [2].

The thermonuclear reactions with the formation of elements heavier than nuclei in the iron zone cannot occur with the energy output. The energy has to be absorbed in the synthesis of such elements in the reaction process; therefore these processes do not make a contribution to the general energy output of star thermonuclear reactions.

They lose their stability and begin compression to their centre with the rising rate after exhaustion of the material for thermonuclear processes in the massive stars, i.e. after the passing of all possible fusion reactions. If the increasing of internal pressure stops gravity compression, the star central part turns into the superdense neutron star and it can be accompanied by shell ejection and be observed as supernova outburst.

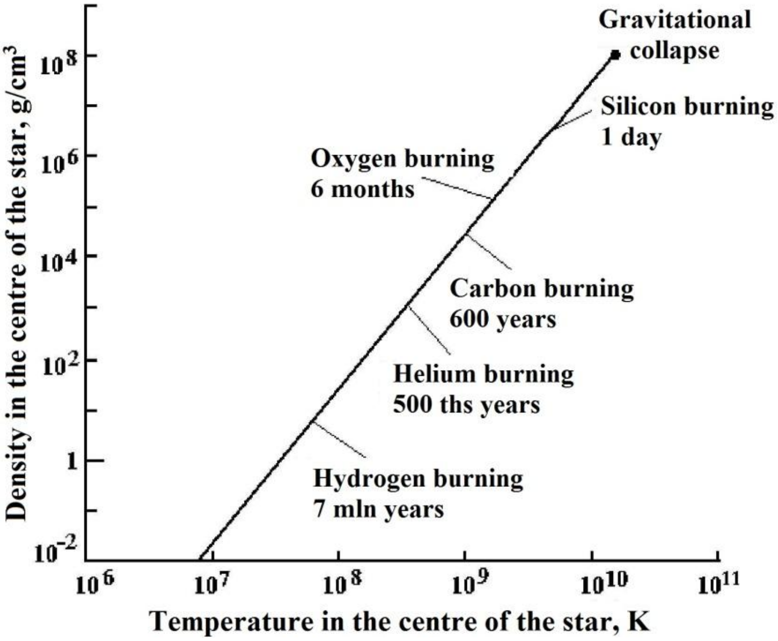

Figure 1.8. Evolution of the massive star [2]. (from: http://nuclphys.sinp.msu.ru/lect/index.html).

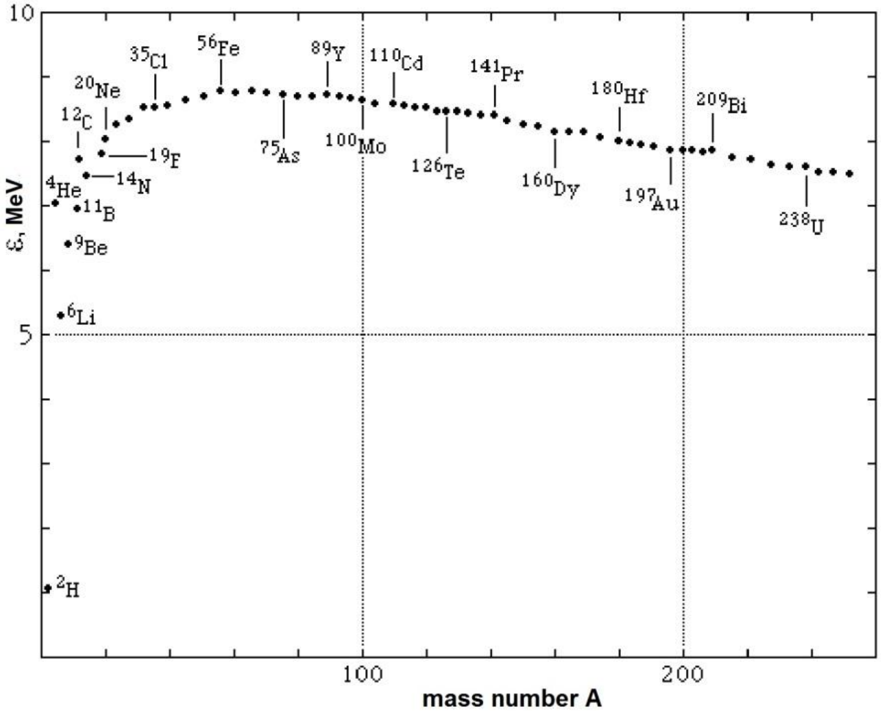

Figure 1.9. Dependence of the specific binding energy ε from the nucleus mass number A [2]. (from: http://nuclphys.sinp.msu.ru/lect/index.html)

However, if the mass of the neutron star, formed in the previous process after supernova explosion, exceeds the certain limit (Oppenheimer-Volkoff limit which equals 2÷3 $\mathfrak{M}_{\odot}$ [5-7]), then the gravitational collapse goes on till its complete transformation to the black hole [6]. Such process with the final star collapse at temperatures more than 10^{10} K and densities above 10^{8} g/cm^{3} is shown in Figure 1.8.

1.6. THE DEPENDENCE OF THERMONUCLEAR REACTIONS FROM THE STAR MASS

As we have already seen, the nuclear reactions taken place in the thermodynamic equilibrium conditions considerably depend on the star mass. It takes place because the star mass determines the value of the compression gravitational forces that finally determines the maximum temperature, accessible in the star core, where the main thermonuclear reactions occur.

The theoretical calculations results of possible fusion nuclear reactions for stars with different masses [2] are listed in Table 1.6. One can see from the table that the full sequence of fusion nuclear reactions is possible in the massive stars only. The gravitational energy is not enough for compression and heating of the stellar material to the temperatures that are necessary to the hydrogen burning reactions in the stars with the masses about $M < 0.08\ \mathfrak{M}_{\odot}$.

As we said before, the star is in the Main Sequence, which is shown in Figure 1.10 (see also Appendix 2), till the hydrogen burning reaction occurs in the stars with masses in the order of solar mass or more.

Table 1.6. Theoretical calculation of possible nuclear reactions in stars with different masses [2]

Stellar mass in $\mathfrak{M}_{\odot}$ units	**Possible nuclear reactions**
<0.08	No
0.3	Hydrogen burning
0.7	Hydrogen and helium burning
5.0	Hydrogen, helium and carbon burning
25.0	All fusion reactions with energy output

In the course of time, its central part begins to compress and star temperature rises while the helium nuclei accumulate in this star. The star layers with ever more distant from the centre can be involved into the process of thermonuclear burning. Expansion and cooling of external star shell is a result of heating, related with this process. Its size increases, and the red color prevails in the radiation spectrum. The star leaves the Main Sequence and moves more to the right, into the Red Giants and Subgiants zone.

Each of described up to now nuclear reaction maintains stellar radiation at different stages of stellar development. But the iron nuclei are bound strongly than all other atomic nuclei at the last stage, therefore their future transformations can not give the energy output. However, the energy continues to release from its shell at these moments of star life. So such sort of situation can be possible: in the issue of silicon burning the iron core of a star is forming and that is too massive for resistance to action of its own gravity.

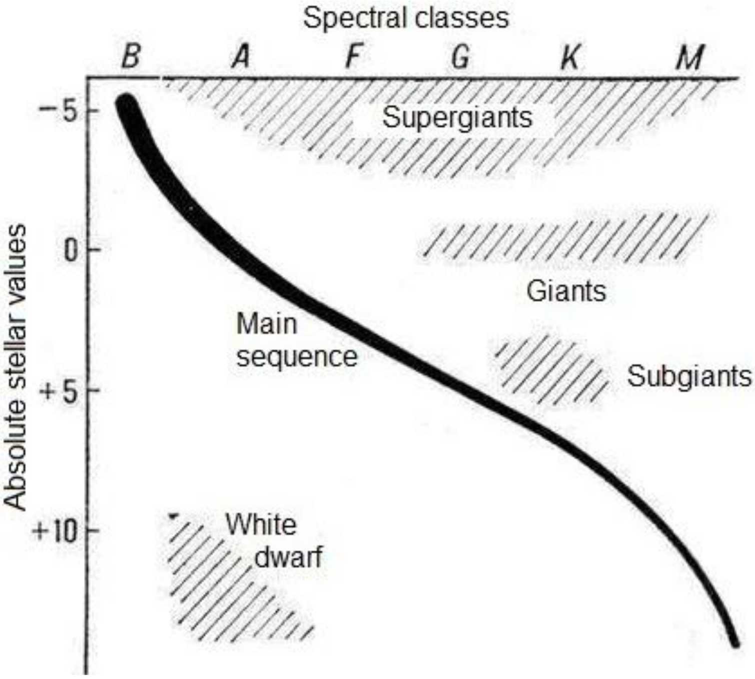

Figure 1.10. Stellar evolution diagram [8]. (from: http://www.astronet.ru/db/msg/eid/FK86/stars).

Its limit mass has been calculated first by S. Chandrasekhar in the range from 1.38 to 1.44 solar masses [6,8] and defines the upper mass limit whereby the star can exists as a White Dwarf. If the star mass is more than this limit, it can turn into neutron star.

Few different processes begin simultaneously when the star mass approaches to the Chandrasekhar limit. These processes cool the star core as much as its inner pressure can not resist to the gravity and it begins catastrophically compress. Such collapse goes on within calculate seconds, but at that energy output is more than the star has released during the whole period of its existence. The main part of this energy releases in the neutrino and gravitational wave forms, but about 1% goes to the heating of external layer of the star and their ejection. For a short time the star becomes comparable in brightness with the whole galaxy, it calls supernova [8] and, as we said, its core can turn into the neutron star. If the mass of the remain core of such star exceeds the Oppenheimer-Volkoff limit, which estimates as 2÷3 solar mass on the modern stage of development of our astrophysical conceptions, then it turns into the black hole [6] and hereon the process of its evolution as astronomical or astrophysical object called the star is finishing.

In the conclusion of our popular review on thermonuclear reactions we represent the scheme of the cycle of matter in the Nature in Figure 1.11. It is shown how the protostar is formed in the course of compression of the interstellar gas nebula and then the ordinary star is formed, which meets with a number of transformations depending on its mass and leads to the production and explosion of supernova and formation of the new nebula. The new protostar, by-turn, can be formed from it and the whole process will repeat again and again.

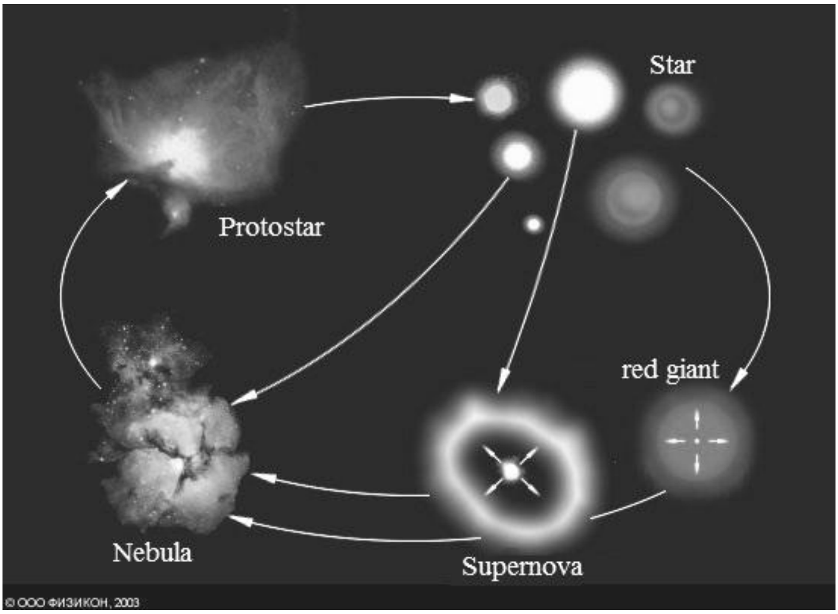

Figure 1.11. Cycle of matter in the Nature. (from: http://www.gomulina.orc.ru/reterats/nebul_5.html).

In the above review, we did not aspire to the detailed description of the formation process of stars with different masses. The aim of this popular description of the stellar evolution is to demonstrate that all star formation stages, independently on their masses, are determined by thermonuclear (per se nuclear) reactions going at ultralow or astrophysical energies and symbolically combined to the different cycles. The possibility of one or another thermonuclear cycle depends on the star mass and wholly determines the stellar evolution process.

1.7. ADVANCES AND PROBLEMS OF NUCLEAR ASTROPHYSICS

The explanation of ways in the chemical element formation in the stars is one of the significant components of modern nuclear astrophysics. The nuclear doctrine of origin of elements describes the prevalence of different elements in the Universe on the basis of characteristics of these elements, taking into account physical conditions in which they can be formed. In addition, the set of considering nuclear astrophysics processes allows us to interpret, for example, the star luminosity on the different stages of its evolution and to describe, generally, the process of stellar evolution itself. Hereby, the nucleosynthesis questions are closely coupled on the one part with the questions of structure and evolution of the stars and the Universe and on the other part with the nuclear particle interaction properties [2,8].

However, there are a number of complicated and till unsolved problems, which does not allow to formulate the complete theory of formation and evolution of the objects in the Universe now. Let us give some examples of these up-to-date unsolved problems directly connected with nuclear astrophysics and nuclear interactions, which are followed from the existing to date nuclear physics problems [2]:

1. The insufficiency of experimental data of the nuclear reaction cross sections at low and ultralow (astrophysical energies).
2. The difficulty of the correct accounting of the reactions going at the expense of weak interactions in describing of the whole set of nuclear reactions, which responsible for element formation in the zone of iron maximum and heavier elements.
3. The absence of accurate data for the experimental cross sections of nuclear reactions by the action of neutrons on radioactive nuclei. This problem occurs at the correct description of the prevalence of the elements generated in the r-process, which is the successive neutron capture in the (n,γ) reactions.

Further, in this book, we will consider only the questions concerning the first item listed above. This problem consists in the impossibility, at the modern stage of the development of experimental methods, to carry out direct measurements of the cross sections of thermonuclear reactions in the earth's conditions for energies at which they are proceeding in the stars. Further, we will stay at this problem more particularly, but now we will illustrate the main conceptions and representations generally using for the description of the thermonuclear reactions.

The astrophysical *S*-factor, which determines the reaction cross section, is the main characteristic of any thermonuclear reaction, i.e. the probability of reaction behavior at vanishing energies. It can be define experimentally, but it is possible for the majority of interacting nuclei taking place in thermonuclear processes at the energy range above 100 keV÷1 MeV, but for real astrophysical calculations, for example, for the developing of star evolution model, the values of astrophysical *S*-factor are required at the energy range about 0.1÷100 keV, which corresponds to the temperatures in the star core about 10^6 K÷10^9 K.

One of the methods for obtaining the astrophysical *S*-factor at zero energy, i.e. the energy of the order of 1 keV and less, is the extrapolation of its values to lower energy range, where it can be determined experimentally. It is the general way which is used, first of all, after carrying out the experimental measurements of cross sections of certain thermonuclear reaction at low energy range.

The second and evidently *most preferable method* consists in theoretical calculations of the *S*-factor of some thermonuclear reaction on the basis of certain nuclear models [1; sec. 2]. However, the analysis of all thermonuclear reactions in the frame of unified theoretical point of view is quite labor-consuming problem and further we will consider only photonuclear processes with γ-quanta, namely the radiative capture for certain light nuclei.

As for the model choice, one of these models, which we use in present calculations, is the potential cluster model of the light atomic nuclei with the classification according to the Young schemes. The model, in the certain cases, contains the forbidden states (FS) for intercluster interactions and, in the simplest form, gives a lot of possibilities for carrying out the similar calculations.

We will consider these possibilities more thoroughly in the future, but now we emphasize the general way that leads to the real results in the calculations of the astrophysical *S*-factor of certain thermonuclear reaction with γ-quanta; in this case, it is the radiative capture reaction. For carrying out such calculations, it is necessary to have the certain data and execute following steps:

1. Have at one's own disposal the experimental data of the differential cross sections or excitation functions σ_{exp} for the elastic scattering of the considering nuclear particles (for example – p^2H) at lowest energies known at the present moment.
2. Carry out the phase shift analysis of this data or have the results of the phase shift analysis of the similar data that were done earlier, i.e. know the phase shifts $\delta_L(E)$ of the elastic scattering depended on the energy E. It is one of the major parts of the whole calculation procedure of the astrophysical *S*-factors in the PCM with FS, since it allows obtaining the potentials of the intercluster interaction on the next step.
3. Construct the interaction potentials V(r) (for example for p^2H system) according to the discovered phase shifts of scattering. This procedure is called as the potential description of the phase shifts of the elastic scattering in the PCM with FS and it is necessary to carry out it at lowest energies.
4. It is possible to calculate the total cross sections of the photodecay process (for example $^3He + \gamma \rightarrow p + {}^2H$) and the total cross sections of the radiative capture ($p + {}^2H \rightarrow {}^3He + \gamma$) process connected with the previous by the principle of detailed balancing, if we have the intercluster potentials obtained in such a way. As a result one can calculate the total theoretical cross sections $\sigma(E)$ of the photonuclear reactions.
5. Then, it is possible to calculate the astrophysical *S*-factor of the thermonuclear reaction, for example $p + {}^2H \rightarrow {}^3He + \gamma$, if you have the total cross sections of the radiative capture only, i.e. the *S*(E) value as the function of energy E, at any lowest energies.

Let us note that, as of today, the experimental measurements were done only for the astrophysical *S*-factor of the radiative p^2H capture down to 2.5 keV, i.e. in the energy range which can be named as astrophysical. For all other nuclear systems taking part in the thermonuclear processes such measurements were thoroughly done only down to 50 keV at the best, as it was done, for example, for the p^3H system.

All of these steps can be schematically represented in the next form:

$$\sigma_{exp}(\text{elastic}, E) \rightarrow \delta_L(E) \rightarrow V(r) \rightarrow \sigma_c(E) \rightarrow S(E).$$

The path, stated above, is identical for all photonuclear reactions and is independent of, for example, reaction energy or some other factors; it is the general under the consideration of any thermonuclear reaction with γ-quanta, if it is analyzed in the frame of potential cluster model with FS.

The general sense or goal of using nuclear models and theoretical methods for calculation of thermonuclear reaction characteristics consists in the following: if the certain nuclear model correctly describes the experimental data of the astrophysical *S*-factor in that energy range where this data exists, for example 100 keV÷1 MeV, then it is reasonably assume that this model will describe the form of the *S*-factor correctly at the most low energies (about 1 keV) too.

This is the certain advantage of the approach stated above over the simple data extrapolation to zero energy, because the using model has, as a rule, the certain microscopic justification with a view to the general principles of nuclear physics and quantum mechanics.

Then, we are going over to the immediate description of the concrete results obtained for the astrophysical *S*-factors of the radiative capture reactions at the lowest energies in the frame of potential cluster model of light atomic nuclei with the classification of the cluster states according to the Young schemes, which we will consider more thoroughly in the next chapter.

CONCLUSION

Further in this book the processes of radiative capture for p^2H, p^3H, p^6Li, p^7Li, p^9Be and $p^{12}C$, as well as $^2H^4He$, $^3H^4He$, $^3He^4He$ and $^4He^{12}C$ systems will be considered and it will be shown that this approach gives the possibility to describe the experimental data in the range of ultralow energies comparatively well, when the errors of extracted experimental phase shifts of the elastic scattering have the minimal values. In addition, in cases of certain systems, it is even possible to predict the behavior of the astrophysical *S*-factors at the energies lower than 100÷200 keV.

The model representations, i.e. physical models of the atomic nuclear and mathematical calculation methods including numerical methods and algorithms, will be described in detail in the beginning of the next chapter. The certain justification of the cluster model in terms of nuclear shell model will be done; it allows one to obtain good results during the description of the properties of certain light nuclei and gives the mathematical apparatus further used in part in the PCM with FS.

Chapter 2

THE MODEL AND CALCULATION METHODS

INTRODUCTION

The experimental data on cross sections of nuclear reactions is the main source of information on the cluster structure of the nucleus and the properties and mechanisms of interaction between nuclei and their fragments. However, the nuclear astrophysical experimental studies of reactions are complicated by the fact that the energy of matter interaction in stars is very low, from tenths to tens of keV. In laboratory conditions, it is practically impossible to perform direct measurements of cross sections of nuclear reactions necessary for astrophysical calculations at such energies, with rare exceptions. Usually cross sections are measured at higher energies and then the obtained results are extrapolated to the energy range of interest for nuclear astrophysics [1].

However, as a rule, the real measurements are related to rather high energy (0.2÷1 MeV) as compared to stellar energy; therefore, simple linear extrapolation of experimental data to the astrophysical energy range is not always justified. Moreover, the interval of experimental errors in measured total radiative capture cross sections or astrophysical S-factor at 3÷300 keV in different systems reaches 100%, which highly depreciates results of such an extrapolation of experimental data.

Therefore, in many cases only theoretical predictions can fill a gap in experimental information on characteristics of astrophysical fusion reactions [1]. During recent years, due to essential progress in the chiral effective theory of hadron interactions, strict microscopic calculations with realistic nucleon interaction potentials have become possible. At low energies the chiral perturbation theory makes it possible to take into account in a unified way both two-nucleon and multinucleon interactions with controlled accuracy [10], which provides true microscopic calculations of characteristics of few-nucleon systems.

However, due to technical complexity of such calculations the scattering problem is mainly limited by three-nucleon systems, which are considered based on solution of the Faddeev equations [11]. Four-nucleon calculations in the continuous spectrum at low energies based on the Faddeev–Yakubovsky equations [12] in the AGS form [13] with the realistic NN potentials and account of Coulomb interaction were published just in the last years [14,15]. It is expected, in these articles, that the calculation accuracy is as high as for three-nucleon systems, so that the deviation of the theory from experiment can be considered as a critical test for two- and multi-nucleon forces.

In practice, systems with a large number of nucleons in the continuous spectrum are examined based on different microscopic methods, such as the resonating group method (RGM) [16], no-core shell-model [17], and their combinations [18], as well as variational methods (VM) with different bases [19]. Most of these methods are reduced to very cumbersome multichannel calculations, which have an accuracy that cannot always be reliably determined.

In this situation, upon investigation of the astrophysical aspects of nuclear physics, the application of realistic – and relatively simple from the practical point of view – models is quite justified. Usually calculations performed based on model ideas are compared with available low-energy experimental data, and as a result, those approaches that result in the best agreement with experiment are selected.

Then, calculations for astrophysical energies are performed based on the selected approaches and conceptions. Results on astrophysical *S*-factors – for example, for reactions of radiative capture – obtained in this case, can be considered as an estimate of corresponding values that is more realistic than simple extrapolation of experimental data. Since, the applied theoretical model, as a rule, has a quite reasonable microscopic justification in terms of nuclear physics.

The knowledge of the wave function of relative motion of nuclear particles taking parts in collisions (scattering processes, reactions) or determines the bound state (BS) of nucleus in two-particle channel is needed in such calculations. These functions can be obtained from the solutions of the Schrödinger equation for each concrete physical problem in discrete or continuous spectrum, if the interaction potential of these particles is known.

The nuclear interaction potential of particles (in problems of scattering i.e. continuous spectrum or bound states – discrete spectrum) is wittingly unknown and, in principle, its directly determination by currently familiar methods is not seemed to be possible. Therefore, the certain form of its dependence from the distance is chosen (for example Gaussian or exponential), and, by certain nuclear characteristics (usually these are phase shifts of nuclear scattering or binding energy and charge radius for bound states), the parameters of the potential are fixed so that to describe these characteristics. In future, such potential can be used for the calculations of any other nuclear properties, for example, formfactors of the bound states or cross sections of different reactions [20].

Thus, practically all range of nuclear physics problems requires the ability to solve the Schrödinger equation with the specified potential and with certain initial and asymptotic conditions. In principle, this is purely mathematical problem in the field of mathematical modeling of physical processes and physical systems.

One can solve the Schrödinger equations for bound and scattering states using the Runge-Kutt method or finite-difference method [21,22]. Such methods quite allow us to find eigen wave functions and self-energies of quantum system. The obtaining of the wave function is appreciably simplified if one use the combination, suggested by us, of numerical and variational methods with the accuracy control of equation solution with the help of residuals [23] or use the alternative solution method of the integrated matrix eigenvalue problem. These methods will be briefly stated bellow and more detailed description can be found in the book [24].

Consequently, numerous nuclear characteristics are calculated on the basis of obtained solutions, i.e. wave functions of the nucleus, which are the solutions of the initial equations, including phase shifts of scattering and binding energies of atomic nuclei in cluster channels, different characteristics of nuclear and thermonuclear reactions, for example, astrophysical *S*-factors etc.

The model, using here, is constructed based on the assumption that the considered nuclei have a two-cluster structure. The choice of this model is determined by the fact that, in many light atomic nuclei, the probability of formation of nucleon associations (clusters) and the degree of separation from each other are rather high. This is proved by multiple experimental data and theoretical calculations obtained during the last 50 years [25].

For construction of phenomenological potentials of intercluster interaction, the results of phase shift analysis of experimental data on differential cross sections of elastic scattering of corresponding free nuclei are used [26,27]. As a rule, the main contribution in expansion over orbital angular moments for energies below 1 MeV is made by the *S*-wave only; therefore, the data on differential cross sections measured at $8 \div 10$ scattering angles, i.e. angular distribution, provides rather complete and accurate phase shift analysis.

The interaction potentials in the framework of the formally two-body scattering problem are chosen from the condition of the best description of obtained phase shifts. In this case, for the considered nucleon system, the many-body character of the problem is taken into account by separation of the single-particle levels of this potential into Pauli-allowed and Pauli-forbidden states. For the lightest atomic nuclei ($A<4$), the potential cluster model in which the orbital states are split according to Young schemes is used. The extended description of this approach you can see in [28,29] and in this section of the book.

In the applied model, due to its formally two-body character and potentials obtained on the basis of phase shifts of elastic scattering, it is possible to rather easily calculate the required nuclear characteristics, for example, total cross sections of photonuclear reactions and astrophysical *S*-factors practically for any, even the lowest, energies.

2.1. CLUSTER MODEL

The considered potential cluster model is very simple in application, since technically it comes to solution of the two-body problem, or, which is equivalent, to the problem of one body in the field of a force center. Therefore, an objection can be put forward that this model is absolutely inadequate to the many-body problem to which the problem of description of properties of the system consisting of *A* nucleons is related.

In this regard, it should be noted that one of the successful models in the theory of atomic nucleus is the model of nuclear shells (SM) that mathematically represents the problem of one body in the field of a force center. The physical grounds of the potential cluster model considered here trace to the shell model or, more precisely, in a surprising connection between the shell model and the cluster model, which is mentioned in the literature as the nucleon association model (NAM) [25].

In the nucleon association model and PCM, the wave function of the nucleus consisting of two clusters with the numbers of nucleons A_1 and A_2 ($A = A_1 + A_2$) has the form of antisymmetrized product of totally antisymmetric internal wave functions of clusters $\Psi(1, \ldots, A_1) = \Psi(R_1)$ and $\Psi(A_1 + 1, \ldots, A) = \Psi(R_2)$ multiplied by the wave function of their relative motion $\Phi(R = R_1 - R_2)$,

$$\Psi = \hat{A}\ \{\Psi(R_1)\ \Psi(R_2)\ \Phi(R)\}, \tag{2.1}$$

where $\hat{A}$ is the operator of antisymmetrization under permutations of nucleons belonging to different clusters, R is the intercluster distance, R_1 and R_2 are the radius vectors of the position center mass of clusters.

Usually cluster wave functions are chosen in such a way that they correspond to ground states of nuclei consisting of A_1 and A_2 nucleons. These shell wave functions are characterized by specific quantum numbers, including Young schemes $\{f\}$, which determine the permutation symmetry of the orbital part of cluster relative motion WF.

The most important thing, in the model considered in this study, is the rule of calculation of the number of nodes of the wave function of cluster relative motion in the ground state of the nucleus. In the oscillatory shell model for nuclei of 1*p*-shell in the system of $A \leq 16$ nucleons there are $A - 4$ oscillatory excitation quanta [25]. In the total wave function of the nucleus, these oscillatory quanta can be relocated in a random order between states of internal cluster motion (forming excited clusters) and the state of their relative motion.

For ground states of clusters in the nucleus interior with the minimal number of excitation quanta compatible with the Pauli principle for the given number of nucleons A_1 or A_2 the number of excitation quanta N per relative motion is maximal and is determined by the following relation, named as oscillatory rule:

$$N = (A - 4) - N_1 - N_2\ . \tag{2.2}$$

Here, $N_1 = A_1 - 4$, if $A_1 > 4$, $N_1 = 0$, if $A_1 \leq 4$, and similar $N_2 = A_2 - 4$, if $A_2 > 4$, $N_2 = 0$, if $A_2 \leq 4$. The value N determines the number of nodes in relative cluster function and depends on the orbital angular moment of relative motion L [25].

The next step is that this oscillatory rule is transferred to the realistic cluster model of the nucleus in which clusters are isolated, i.e., the oscillatory parameters of the clusters $\hbar\omega_1$ and $\hbar\omega_2$ are not agree with the oscillatory parameter of the wave function of relative motion $\hbar\omega_3$. However, the cluster isolation that takes place in real cluster nuclei makes it possible to neglect the action of the operator of antisymmetrization in Eq. (2.1) in the first approximation, without rejecting oscillatory rule (2.2) for ground states of clusters.

Assuming this rule for nonoscillatory wave functions, we find that the realistic (nonoscillatory) cluster interaction potential in the corresponding partial wave L should be sufficiently deep to contain, along with the “ground” (energy lowest) nodeless state and the given state with the number of nodes ν, all levels with a smaller number of nodes upon solution of the Schrödinger equation.

This conclusion suggests the idea of Pauli-forbidden states in the cluster model: all levels with a number of nodes less than ν that occur in the two-body problem describing cluster relative motion correspond to the number of oscillatory quanta which is less than the minimal Pauli-allowed number N.

Therefore, the total wave functions (2.1) with these relative motion functions vanish in case of antisymmetrization over all A nucleons. The ground state of this cluster system, i.e. really existed bound state in this potential, is described by wave function with nonzero; in the general case, the number of nodes determined from the relation (2.2). But to this effect, in this book, we will use the Young scheme technique, which we will state latter and which will apply at the consideration of different cluster systems, as more general, against (2.2), cluster state classification method.

For preliminary example of utilization of this method, let us consider the classical two-cluster system of ^{6}Li nucleus, where ^{4}He and ^{2}H clusters are in the states with Young schemes {4} and {2}, respectively. The outer product of these Young schemes yields {4} × {2} = {6} + {51} + {42}.

The Young schemes {6} and {51} correspond to the shell configurations s^6 and s^5p^1 with orbital moments 0 and 1 are Pauli-forbidden, because it is impossible to be more than four nucleons at the *s*-shell [25]. The Young scheme {42} with $L = 0{,}2$ corresponds to the ground state of the nucleus and the allowed configuration s^4p^2. It contains one forbidden state in the *S*-wave, which means that there is one node in the wave function of cluster relative motion at $L = 0$.

Thus, the idea of Pauli-forbidden states makes it possible to take into account the many-body character of the problem in terms of interaction potential between clusters. In this case, in practice, the interaction potential is chosen in order to describe the experimental data (scattering phase shifts) on elastic cluster scattering in the corresponding *L* partial wave and preferably in the state with one particular Young scheme {*f*} for the spatial part of the wave function of *A* nucleons.

Since the results of phase shift analysis in the limited energy range, as a rule, prevent unambiguous reconstruction of the interaction potential, the additional restriction on the potential is the requirement of reproduction of the binding energy of the nucleus in the corresponding cluster channel and some other static nuclear properties. In this case, cluster masses are identified with masses of corresponding free nuclei. This additional requirement, obviously, is an idealization, since it assumes that, in the ground state, the nucleus is 100% clusterized. Actually, the success of this potential model, in description of a system of *A* nucleons in the bound state, is determined by the actual degree of clusterization of the nucleus in the ground state.

It is remarkable that the model does not require the knowledge of details of *NN* interaction. In this model, *NN* interaction is manifested, similarly to the shell model, in creation of the mean nuclear field, and provides clusterization of the nucleus. The remaining "work" on formation of the necessary number of nodes of the wave function of cluster relative motion is executed by the Pauli principle. Therefore, it should be expected that the domain of applicability of the considered model is limited by nuclei with pronounced cluster properties.

However, some nuclear characteristics of particular, even non-cluster, nuclei can be mainly determined by one specific cluster channel and the small contribution of other possible cluster configurations. In this case, the applied single-channel cluster model makes it possible to identify the dominating cluster channel and separate those properties of the cluster system that are determined by this channel [30].

2.2. ASTROPHYSICAL S-FACTORS

Astrophysical *S*-factors characterize the behavior of a cross section of nuclear reactions at an energy tending to zero and are determined as follows [31]:

$$S(NJ,J_\mathrm{f}) = \sigma(NJ,J_\mathrm{f}) E_\mathrm{cm} \exp\left(\frac{31.335 Z_1 Z_2 \sqrt{\mu}}{\sqrt{E_\mathrm{cm}}} \right), \tag{2.3}$$

where σ is the total cross section of the radiative capture process in barn, E_cm is the particle energy in the center of mass system in keV, μ is the reduced mass of particles in the initial channel in atomic mass units, $Z_{1,2}$ are the particle charges in units of elementary charge, and N are E or M transitions with J multipolarity to the final J_f state of the nucleus. The numerical coefficient 31.335 was obtained basing on the modern values of the fundamental constants [32].

The rapidly variable exponential factor specified by the Coulomb barrier is evidently segregated in the given expression for the reaction S-factor. Thus, the changing of S-factor value is too slow comparing the cross section, in the case of nonresonance reactions. Such cross section for binary process

$$\sigma(NJ,J_\mathrm{f}) = S(NJ,J_\mathrm{f}) P(E)$$

substantially simplifies the analysis of the behavior of astrophysical S-factor in dependence of energy, even in the resonance region, and usually applies in the range of low and ultralow energies.

The total radiative capture cross sections in the cluster model are given, for example, in [33] or [20] and are written as

$$\sigma(N) = \sum_{\mathrm{J},\mathrm{J_f}} \sigma(NJ,J_\mathrm{f}), \tag{2.4}$$

$$\sigma_c(EJ,J_\mathrm{f}) = \frac{8\pi K e^2}{\hbar^2 q^3} \frac{\mu}{(2S_1+1)(2S_2+1)} \frac{J+1}{J[(2J+1)!!]^2} A_\mathrm{J}^2(EJ,K) \sum_{\mathrm{L_i},\mathrm{J_i}} |P_\mathrm{J}(EJ,J_\mathrm{f},J_\mathrm{i}) I_\mathrm{J}(J_\mathrm{f},J_\mathrm{i})|^2$$

where for electric convective $EJ(L)$ transitions of J multipolarity the next simple expressions are known [20,33] ($S_\mathrm{i} = S_\mathrm{f} = S$)

$$A_\mathrm{J}(EJ,K) = K^\mathrm{J} \mu^\mathrm{J} \left[\frac{Z_1}{m^\mathrm{J}_1} + (-1)^\mathrm{J} \frac{Z_2}{m^\mathrm{J}_2} \right], \tag{2.5}$$

$$I_\mathrm{J}(J_\mathrm{f},J_\mathrm{i}) = \langle L_\mathrm{f} J_\mathrm{f} | R^\mathrm{J} | L_\mathrm{i} J_\mathrm{i} \rangle ,$$

$$P_\mathrm{J}^2(EJ,J_\mathrm{f},J_i) = \delta_{\mathrm{S_i S_f}} \left[(2J+1)(2L_\mathrm{i}+1)(2J_\mathrm{i}+1)(2J_\mathrm{f}+1) \right] (L_\mathrm{i} 0 J 0 | L_\mathrm{f} 0)^2 \begin{Bmatrix} L_\mathrm{i} & S & J_\mathrm{i} \\ J_\mathrm{f} & J & L_\mathrm{f} \end{Bmatrix}^2$$

Here, q is the wave number of particles in the initial channel; L_f, L_i, J_f, and J_i are the angular moments of particles in the initial (i) and final (f) channels; S_1 and S_2 are the spins; m_1, m_2, Z_1, Z_2 are the masses and charges of the particles in the initial channel, respectively; K and J are the wave number and angular moment of γ-quantum in the final channel; and I_J is the integral over wave functions of the initial χ_i and final χ_f states as a function of relative cluster motion with the intercluster distance R.

The above expressions for total cross sections sometimes include the spectroscopic factor S of the final state of the nucleus; however, in the potential cluster model we used it equal to unity, similarly to [33].

For examination of the magnetic $M1(S)$ transition caused by the spin part of the magnetic operator using expressions from [34], one can obtain ($S_i = S_f = S$, $L_i = L_f = L$),

$$P_1^2(M1, J_f, J_i) = \delta_{S_iS_f}\,\delta_{L_iL_f}\,\left[S(S+1)(2S+1)(2J_i+1)(2J_f+1)\right]\begin{Bmatrix} S & L & J_i \\ J_f & 1 & S \end{Bmatrix}^2$$

$$A_1(M1, K) = i\frac{e\hbar}{m_0c}K\sqrt{3}\left[\mu_1\frac{m_2}{m} - \mu_2\frac{m_1}{m}\right], \qquad (2.6)$$

$$I_J(J_f, J_i) = \langle \chi_f | R^{J-1} | \chi_i \rangle \ , \quad J = 1 \ .$$

where m is the mass of the nucleus; μ_1 and μ_2 are the magnetic moments of the clusters taken from [35], and, for example, for $\mu_{^2H}$ = $0.857\mu_0$ and $\mu_p = 2.793\mu_0$; μ_0 is the nuclear magneton.

The expression in square brackets in (2.6) for $A_1(M1,K)$ has been obtained on the assumption that, in the general form, for the spin part of the magnetic operator [36],

$$W_{Jm}(S) = i\frac{e\hbar}{m_0c}K^J\sum_i \mu_i\,\hat{\vec{S}}_i \cdot \vec{\nabla}_i\left(r_i^J Y_{Jm}(\Omega_i)\right)$$

summation by r_i, i.e. by coordinates of center of mass of clusters, relative to common centre of mass of nucleus, is held before the action of the ∇-nabla operator which acts on the expression in brackets $(r_i^J Y_{Jm}(\Omega_i))$ and leads to decrease of r_i degree [34],

$$\vec{\nabla}_i\left(r_i^J Y_{Jm}(\Omega_i)\right) = \sqrt{J(2J+1)}\,r_i^{J-1}\,\vec{Y}_{Jm}^{J-1}(\Omega_i) \ .$$

In this case the coordinates r_i are $R_1 = m_2/mR$ and $R_2 = -m_1/mR$, where R is the relative intercluster distance and R_1 and R_2 are the distances from the common center of mass to the centers of mass of each cluster. The operator of electromagnetic transitions for radiation interaction with matter, in electromagnetic processes like radiative capture or photodecay, is well-known [36].

Therefore, there is a fine possibility for clearing the form of two-particle strong interaction in the initial channel, when they are in continuous spectrum and in bound states of the same particles in the final channel, i.e. in discrete spectrum.

2.3. POTENTIALS AND WAVE FUNCTIONS

The intercluster interaction potentials for each partial wave, i.e., for the given orbital angular moment L, and point-like Coulomb term, were represented as (further, the only nuclear part of potential is given)

$$V(R)=V_0\exp(-\alpha R^2)+V_1\exp(-\gamma R) \tag{2.7}$$

or

$$V(R)=V_0\exp(-\alpha R^2)\ . \tag{2.8}$$

Here, parameters V_1 and V_0 (dim.: MeV), α and γ (dim.: fm^{-2} and fm^{-1}, correspondingly) are the potential parameters found from experimental data under the constraint of best description of elastic scattering phase shifts extracted in the course of phase shift analysis from the experimental data on the differential cross sections, i.e. angular distributions or excitation functions.

In some cases, the Coulomb potential includes the Coulomb radius R_{Coul} and then the Coulomb potential takes the form

$$V_{\text{Coul}}(r) = \frac{2\mu}{\hbar^2}\begin{cases} \dfrac{Z_1Z_2}{r} & r > R_{\text{Coul}} \\ Z_1Z_2\left(3-\dfrac{r^2}{R^2_{\text{Coul}}}\right)\Big/ 2R_{\text{Coul}} & r < R_{\text{Coul}} \end{cases} .$$

In the variational method, the expansion of cluster relative motion WF in non-orthogonal Gaussian basis was used, and independent parameter variation was performed. The wave function itself has the form [20]

$$\Phi_{\text{L}}(R)=\frac{\chi_{\text{L}}(R)}{R}=R^{\text{L}}\sum_{\text{i}} C_{\text{i}}\exp(-\beta_{\text{i}}R^2)\ , \tag{2.9}$$

where β are the variational parameters and C are the expansion coefficients [24].

The behavior of the wave function of bound states (BS), including ground states (GS) of nuclei in cluster channels at large distances, is characterized by the asymptotic constant C_{W} determining by the Whittaker constant of the form [37]

$$\chi_{\text{L}}(R)=\sqrt{2k_0}\,C_{\text{W}}W_{-\eta\text{L}+1/2}(2k_0R)\ , \tag{2.10}$$

where $\chi_{\text{L}}(R)$ is the numerical wave function of the bound state obtained from the solution of the radial Schrödinger equation and normalized to unity; $W_{-\eta\text{L}+1/2}$ is the Whittaker function of the bound state determining the asymptotic behavior of the wave function which is the solution to the same equation without the nuclear potential; i.e., at large distances R having the form [24] (see Appendix 1); k_0 is the wave number determined by the channel binding energy; η is the Coulomb parameter; and L is the orbital angular moment of the bound state.

Asymptotic constant (or asymptotic normalization coefficient) is an important nuclear characteristic. In many cases the knowledge of its value for the a nucleus in the $b + c$ channel determines the value of the astrophysical *S*-factor of the radiative $b(c,\gamma)a$ capture process [38]. The asymptotic constant is proportional to the nuclear vertex constant for the virtual $a \rightarrow b + c$, which is the matrix element of this process at the mass surface [39].

The mean square mass radius of the nucleus in the cluster model for the system of two correctly sized clusters is determined as

$$R_{\mathrm{m}}^2 = \frac{m_1}{m}\left\langle r_{\mathrm{m}}^2\right\rangle_1 + \frac{m_2}{m}\left\langle r_{\mathrm{m}}^2\right\rangle_2 + \frac{m_1 m_2}{m^2} I_2 \,,$$

where $\left\langle r_m^2\right\rangle_{1,2}$ are the mean squared mass radii of clusters, which are taken equal to the radii of corresponding nuclei in the free state and I_2 is the integral of the form

$$I_2 = \left\langle \chi_{\mathrm{L}}(R) \right| R^2 \left| \chi_{\mathrm{L}}(R) \right\rangle$$

for the intercluster distance *R* over radial wave functions $\chi_L(R)$ of relative cluster motion normalized to unity in the ground state of the nucleus with the orbital angular moment *L*.

The mean square charge radius is written as

$$R_{\mathrm{z}}^2 = \frac{Z_1}{Z}\left\langle r_{\mathrm{z}}^2\right\rangle_1 + \frac{Z_2}{Z}\left\langle r_{\mathrm{z}}^2\right\rangle_2 + \frac{(Z_2 m_1^2 + Z_1 m_2^2)}{Z m^2} I_2 \,,$$

where $\left\langle r_z^2\right\rangle_{1,2}$ are the mean squared charge radii of clusters which are also taken equal to the radii of corresponding nuclei in the free state, $Z = Z_1 + Z_2$, and I_2 is the above integral.

The wave function $\chi_{\mathrm{L}}(R)$ of the relative cluster motion is the solution of the radial Schrödinger equation

$$\chi_{\mathrm{L}}''(R) + [k^2 - V(R) - V_{\mathrm{Coul}}(R) - L(L+1)/R^2]\chi_{\mathrm{L}}(R) = 0 \,,$$

where $V(R)$ is intercluster potential (2.7) or (2.8) with dimension fm^{-2}; $V_{\mathrm{Coul}}(R)$ is the Coulomb potential; and *k* is the wave number determined as $k^2 = \frac{2\mu E}{\hbar^2}$.

2.4. NUMERICAL METHODS

Finite-difference methods (FDM), which are the modification of methods [40] and take into account Coulomb interactions; variational methods for solution of the Schrödinger equation; and other numerical methods used in these calculations of nuclear characteristics were described in detail in [24]. Therefore, here we mention briefly the main issues connected with general and numerical methods of calculation.

In all calculations using finite-difference and variational methods [20] at the boundary of the region in which the asymptotic constant becomes steady, i.e., approximately 10–20 fm, the numerical or variational wave function was replaced by Whittaker function (2.10) taking into account the asymptotic constant found earlier. Numerical integration in any matrix elements was performed from 0 to 25–30 fm. Simpson's method [41] was used; this method yields good results for smooth and weakly oscillating functions provided that several hundred steps per period are given [24].

Computer programs based on the finite-difference method [20,24] were rewritten for these calculations; for calculation of total radiative capture cross sections and characteristics of bound states of nuclei programs were rewritten from TurboBasic to Fortran-90, a more advanced computer language that possesses much broader capabilities. This made it possible to essentially increase the accuracy of all calculations, including the nuclear binding energy in the two-body channel.

Now, for example, the accuracy of calculating Coulomb wave functions for scattering processes controlled by the value of Wronskian (see Attachment 1) and the accuracy of finding the root of the determinant in finite-difference method [24] that determines the accuracy of finding the binding energy are of the order of $10^{-14}\div10^{-20}$ and the real absolute accuracy of determination of binding energy in the finite-difference method for different two-body systems was $10^{-6}\div10^{-8}$ MeV.

The rapidly converging continued fraction representation [42], described in Attachment 1, has been used for calculation of Coulomb scattering functions; this representation makes it possible to obtain the values of the functions with high accuracy in a wide range of variables taking modest computing time [43].

The variational program for finding variational wave functions and binding energies of nuclei in cluster channels has been rewritten in Fortran, which made it possible to essentially increase the rate of seeking the minimum of the multiparametric functional determining the binding energy of two-body systems in all considered nuclei [24]. This program, as before, applies the multiparametric variational method with expansion of WF in non-orthogonal Gaussian basis and independent parameter variation. Similar programs, based on multiparametric variational method, were also modified for phase shift analysis in which differential cross sections of elastic scattering of nuclear particles have been used.

Exact values of particle masses [35] were determined in all calculations, if there are no special reserves, and the constant $\hbar^2/m_0$ was taken equal to 41.4686 MeV fm^2. The Coulomb parameter $\eta = \mu\cdot Z_1\cdot Z_2\cdot e^2/(q\cdot\hbar^2)$ was represented as $\eta = 3.44476\cdot10^{-2}\cdot Z_1\cdot Z_2\cdot\mu/q$, where q is the wave number determined by the energy of interacting particles in the initial channel in fm^{-1}. The Coulomb potential for $R_{\text{Coul}} = 0$ was written as $V_{\text{Coul}}(\text{MeV}) = 1.439975\cdot Z_1\cdot Z_2/R$, where R is the distance between particles in the initial channel in fermi.

2.5. CLASSIFICATION OF CLUSTER STATES

States with minimal spin in the processes of scattering of some light atomic nuclei turn out to be mixed according to Young orbital schemes, for example, the doublet state p^{2}H [28] is mixed according to schemes {3} and {21}. On the other hand, these states considered as bound ones, for example, the doublet p^{2}H channel of ^{3}He nucleus is pure with scheme {3} [28].

Let us put the classification of states of, for example, p^{2}H system according to orbital and spin-isospin Young schemes and demonstrate how to obtain these results. In the general case, the possible orbital Young scheme {*f*} of some nucleus *A*({*f*}) consisting of two parts $A_1(\{f_1\})$ + $A_2(\{f_2\})$ is the direct outer product of orbital Young schemes of these parts $\{f\}_L = \{f_1\}_L \times \{f_2\}_L$ and is determined using the Littlewood's theorem [28]. Therefore, the possible orbital Young schemes of p^2H system, in which scheme {2} is used for ^2H nucleus, are the symmetries $\{3\}_L$ and $\{21\}_L$.

Spin-isospin schemes are the direct inner product of spin and isospin Young schemes of the nucleus of *A* nucleons $\{f\}_{ST} = \{f\}_S \otimes \{f\}_T$ and for the system with the number of particles not larger than eight are given in [44]. For any of these moments (spin and isospin), the corresponding scheme of the nucleus consisting of *A* nucleons, each of which has an angular moment equals 1/2, is constructed as follows: in the cells of the first row, the number of nucleons with the moments pointing in one direction, for example, upward, is indicated. In cells of the second row, if it is required, the number of nucleons with the moments directed in the opposite direction, for example, downward, is indicated. The total number of cells in both rows is equal to the number of nucleons in the nucleus. Moments of nucleons in the first row which have a pair in the second row with the oppositely directed moment are compensated and yield zero total moment. The sum of moments of nucleons of the first row, which are not compensated by moments of nucleons of the second row, yields the total moment of the whole system.

In this case for p^2H system and the isospin $T = 1/2$, we have $\{21\}_T$; for the spin state with $S = 1/2$, we also obtain $\{21\}_S$; and for *S* or $T = 3/2$, the scheme of the form $\{3\}_{ST}$. Upon construction of the spin-isospin Young scheme for the quartet spin state of p^2H system with $T = 1/2$, we have $\{3\}_S \otimes \{21\}_T = \{21\}_{ST}$, and for the doublet state $\{21\}_S \otimes \{21\}_T = \{111\}_{ST} + \{21\}_{ST} + \{3\}_{ST}$ [44].

The total Young scheme of the nucleus is determined in a similar way as the direct inner product of the orbital and spin-isospin scheme $\{f\} = \{f\}_L \otimes \{f\}_{ST}$. The total wave function of the system in the case of antisymmetrization does not identically vanish only if it does not contain the antisymmetric component $\{1^N\}$, which is realized upon multiplication of conjugated $\{f\}_L$ and $\{f\}_{ST}$. Therefore, the schemes $\{f\}_L$ conjugated to $\{f\}_{ST}$ are allowed in this channel and all other symmetries are forbidden, since they result in zero total wave function of the system of particles after its antisymmetrization.

This yields that, for the p^2H system in the quartet channel, only the orbital wave function with the symmetry $\{21\}_L$ is allowed and the function with $\{3\}_L$ turns out to be forbidden, since the product $\{21\}_{ST} \otimes \{3\}_L$ does not result in an antisymmetric component of the wave function. At the same time, in the doublet channel, we have $\{111\}_{ST} \otimes \{3\}_L = \{111\}$ and $\{21\}_{ST} \otimes \{21\}_L \sim \{111\}$ [44], and in both cases we obtain the antisymmetric scheme. Therefore, the doublet spin state turns out mixed according to Young orbital schemes.

In [28] the method for separation of such states according to Young schemes was proposed and it was shown that the mixed scattering phase shifts can be represented in the form of the half-sum of pure phase shifts $\{f_1\}$ and $\{f_2\}$,

$$\delta^{\{f_1\}+\{f_2\}} = 1/2(\delta^{\{f_1\}} + \delta^{\{f_2\}}). \qquad (2.11)$$

In this case it is assumed that $\{f_1\} = \{21\}$ and $\{f_2\} = \{3\}$ and the doublet phase shifts extracted from the experiment are mixed according to these two schemes. Then it is assumed that the quartet scattering phase shifts, pure according to orbital Young scheme {21}, can be identified with the pure doublet scattering phase shift p^{2}H corresponding to the same Young scheme. Then Eq. (2.11) allows to find the pure doublet p^{2}H phase shift with scheme {3} and then construct the pure interaction potential according to Young schemes that can be used for description of characteristics of the bound state.

Similar relations exist for a number of other lightest nuclear systems, for example, p^{3}H, ^{2}H^{2}H, ^{2}H^{3}He, p^{6}Li, etc. which are mixed according to Young schemes and (or) isospin [20], and some of them will be considered in this book later.

2.6. METHODS OF PHASE SHIFT ANALYSIS

If the experimental differential cross sections of elastic scattering are known, certain set of parameters called the scattering phase shifts $\delta^{J}_{S,L}$ can be found, which makes it possible to describe the behavior of these cross sections with a reasonable accuracy. The quality of description of experimental data based on certain theoretical function (functional of several variables) can be estimated using the χ^2 method represented in [45]

$$\chi^2 = \frac{1}{N}\sum_{i=1}^{N}\left[\frac{\sigma^{t}_{i}(\theta)-\sigma^{e}_{i}(\theta)}{\Delta\sigma^{e}_{i}(\theta)}\right]^2 = \frac{1}{N}\sum_{i=1}^{N}\chi^2_i \;, \qquad (2.12)$$

where σ^e and σ^t are the experimental and theoretical, i.e., calculated for some given values of scattering phase shifts $\delta^{J}_{S,L}$, elastic scattering cross sections of nuclear particles for the i^{th} scattering angle; $\Delta\sigma^e$ is the error of the experimental cross sections for this angle; and N is the number of measurements.

The expressions describing differential cross sections are the expansion of some functional $d\sigma(\theta)/d\Omega$ in a numerical series containing variational parameters. The expansion parameters $\delta^{J}_{S,L}$ have to be found from the constraint of the best description of the expansion. Since, the expressions for differential cross sections are usually accurate [45], then, if the number of expansion terms L increases to infinity, the value of χ^2 should tends to zero. This criterion was used for choosing the specified set of phase shifts resulting in the minimum of χ^2, which may be the global minimum of the given multiparametric variational problem [46].

Thus, for example, in the p^{6}Li system, the procedure of minimization of the functional χ^2 as a function of $2L + 2$ variables, each being the phase shift δ_L of the particular partial wave without spin-orbital splitting, was performed for searching of scattering phase shifts using experimental cross sections. To solve this problem, the minimum of χ^2 in certain bounded range of values of the variables is sought. However, even in this range, many local minima of χ^2 with a magnitude of the order of unity can be found. The choice of the lowest of them makes it possible to hope that it will correspond to the global minimum that is the solution to the variational problem under given orbital moment L. Moreover, the value of this minimum should relatively smoothly decrease with increasing number of partial waves L.

We used the criteria and methods presented above for phase shift analysis in p^{6}Li, p^{12}C, and ^{4}He^{12}C systems at low energies, which are important for astrophysical calculations. The expressions for finding differential cross sections require for carrying out phase shift analysis for the systems mentioned above are presented in the corresponding sections below.

2.7. GENERALIZED MATRIX EIGENVALUE PROBLEM

Let us consider, at first, the standard method for solution of the generalized matrix problem for the Schrödinger equation, which occurs if the non-orthogonal variational method is used in nuclear physics or nuclear astrophysics, and then examine its modification appropriate for solution of this problem in numerical calculations at the up-to-date computer [24,47].

For determination of the energy eigenvalue spectrum and eigenwave functions in the variational method upon expansion of wave function in the non-orthogonal Gaussian basis [48], the generalized matrix eigenvalue problem [49] is solved,

$$\left(H - EL\right)C = 0 \ , \tag{2.13}$$

where H is the symmetric Hamiltonian matrix; L is the matrix of overlapping integrals, which is transformed into the identity matrix I in the case of using orthogonal basis; E are the energy eigenvalues; and C are the eigenvectors of the problem.

Representing the matrix L in the form of the product of the lower N and upper V triangular matrices [49], after simple transformations, we obtain the common eigenvalue problem

$$H'C' = EIC' \ , \tag{2.14}$$

where

$$H' = N^{-1}HV^{-1} \ ,$$

$$C' = VC \ ,$$

where V^{-1} and N^{-1} are inverse to the V and N matrices, respectively.

Furthermore, we find the matrices N and V, performing triangularization of the symmetric matrix L [50], for example, using the Khaletskii method [49]. Then we determine the inverse matrices N^{-1} and V^{-1}, for example, using the Gauss method, and calculate the elements of the matrix $H' = N^{-1}HV^{-1}$. We find the complete diagonal with respect to the E matrix $(H' - EI)$ and calculate its determinant $\det(H' - EI)$ for some energy E. The energy resulting in the zero determinant is the eigenenergy of the problem, and the corresponding vectors C' are the eigenvectors (2.14). If C' are known, it is easy to find the eigenvectors of the initial problem C (2.13), since the matrix V^{-1} is already known. The described method of reduction of the generalized matrix problem to the common matrix problem is called the Schmidt orthogonalization method [51].

In two-body problems for light atomic nuclei with one variational parameter β_i in variational wave function (2.9), this method is rather stable and makes it possible to obtain reasonable results. However, in the three-body nuclear system, when the variational wave function is represented in the form [20]

$$\Phi_{l,\lambda}(r,R) = r^{\lambda}R^{l}\sum_{i} C_i \exp(-\delta_i r^2 - \beta_i R^2) = \sum_{i} C_i \Phi_i \ , \tag{2.15}$$

for some values of two variational parameters δ_i and β_i, the method for finding inverse matrices sometimes results in instability and overflow upon running the computer program [52], which is a certain trouble for solution of tasks of this type.

Therefore, an alternative method for numerical solution of the generalized matrix eigenvalue problem free from the difficulties indicated above with enhanced computer performance can be proposed. That is to say that initial matrix Eq. (2.13) is the homogeneous system of linear equations and has nontrivial solutions only if its determinant det($H – EL$) is equal to zero. For computer numerical methods, it is not necessary to expand the matrix L into triangular matrices and find the new matrix H' and new vectors C' by determining inverse matrices, as was described above using the standard method.

It is possible to expand the nondiagonal symmetric matrix ($H – EL$) into triangular matrices and seek energies resulting in zero determinant, i.e. eigen energies, using numerical methods in the given domain. In the real physical problem it is not necessary to seek all eigenvalues and eigen energies, but only one or two eigenvalues for the system energy and corresponding wave functions have to be found.

Therefore, the initial matrix ($H – EL$) can be expanded into two triangular matrices using, for example, the Khaletskii method, in such a way that the main diagonal of the upper triangular matrix V contains units,

$$A = H - EL = NV$$

the determinant of this matrix for det(V) = 1 [49] is calculated,

$$D(E) = \det(A) = \det(N)\det(V) = \det(N) = \prod_{i=1}^{m} n_{ii}$$

and the zero of this determinant is used to find the required energy eigenvalue. Here, m is the order of the matrices and the determinant of the triangular matrix N is equal to the product of its diagonal elements.

Thus, we obtain a rather simple problem of finding the zero of a functional of one variable,

$$D(E) = 0 \ ,$$

the solution of this problem does not present great difficulty and can be found to any accuracy, for example, using dichotomy method (method of division in halves).

As a result we eliminate the necessity of finding both inverse to *V* and *N* matrices, and performing several matrix multiplications in order to first obtain the new matrix *H'* and then the finite matrix of eigenvectors *C*. The absence of such operations, especially inverse matrices searching, appreciably increase the computer count rate, independently of program language [53].

For estimation of the accuracy of solution, i.e., the accuracy of expansion of the initial matrix into two triangular matrices, residuals [54] for matrix elements can be used. After expansion the matrix *A* into two triangular matrices *NV*, the residue matrix is calculated,

$$T = A - S \quad ,$$

i.e., the difference over all elements of the initial matrix *A* and the approximate matrix

$$S = NV \quad ,$$

where *V* and *N* are the preliminarily found numerical triangular matrices.

As a result, the residue matrix *T* yields the deviation of the approximate quantity *S* found numerically from the true value of each element of the initial matrix *A*. The method described in this book is used practically in all variational calculations presented below, and the maximal value of any element of the matrix *T* does not exceed 10^{-10}.

This method, which seems quite obvious in numerical implementation, made it possible to obtain good stability of the algorithm for solution of the considered problem; it does not result in overflow in the course of running the computer program, since it does not require determination of inverse to *V* and *N* matrices [55].

Hereby, the introduced alternative method of finding eigenvalues of the generalized matrix problem, considered on the basis of the Schrödinger equation solution using the non-orthogonal variational basis, delivers us from the instabilities appearing during the use of normal solution methods of such mathematical problem, i.e., usual Schmidt orthogonalization method.

Chapter 3

ASTROPHYSICAL S-FACTOR OF THE P^{2}H RADIATIVE CAPTURE

INTRODUCTION

Let us start the consider of thermonuclear reactions from the radiative capture process

$p + {}^2H \rightarrow {}^3He + \gamma$,

which is the first nuclear reaction of the proton-proton or *pp*-chain mediating due to the electromagnetic interactions, since γ-quantum takes a part in it. This reaction process makes essential contribution into the energy yield of the fusion reactions [57] that, as usually considered, determine the burning of the Sun and stars of our Universe.

Since, interacting nuclear particles of the proton-proton chain have a minimal potential barrier. The *pp*-chain is the first chain of nuclear reactions which can take place at lowest energies and, consequently, at stellar temperatures, and there is in all stable stars of the Main Sequence.

As we already say in the first section: the process of radiative p^{2}H capture in the *pp*-chain is the basic one for the transition from the primary proton fusion

$p + p \rightarrow {}^2H + e^+ + \nu_e$,

which takes place due to the weak interactions with the participation of electron neutrino ν_e, to one of the final in *pp*-chain reaction of capture of two nuclei ^{3}He [58],

${}^3He + {}^3He \rightarrow {}^4He + 2p$,

which occurs due to the strong nuclear interactions [56].

A detailed study of the reaction of radiative p^{2}H capture from the theoretical and experimental points of view is of fundamental interest not only for nuclear astrophysics, but for the whole nuclear physics of ultralow energies and the lightest atomic nuclei [59].

Therefore, experimental studies of this process are continuing and already at the beginning of 2000th year, due to the European project LUNA, new experimental data of radiative p^{2}H capture at energies down to 2.5 keV has appeared. These energies may take place in fusion reactions in the Sun and many stable stars [5]. These experimental results, along with earlier results at greater energies will be used by us in future and will examine more thoroughly in the next paragraphs of this section.

It should be noted that the lightest nuclei with A≤4, strictly speaking, are neither shell nor cluster ones. This follows from microscopic calculations of these nuclei with realistic *NN* potentials [60]. For example, in an ^{3}He nucleus along with the p^{2}H cluster configuration, the configuration p^{2}H* is also present, where ^{2}H* is the spin-singlet deuteron (np pair in $^1S_0$ state), and spectroscopic factors for common and singlet deuterons are approximately equal to S = 1.5 [61,62]. The channel with singlet deuteron is clearly manifested in the elastic p^{3}He backward scattering both in purely nucleon scattering mechanism [61] and in processes with production of virtual π meson [62].

However, at low energies and low momentum transfers, it is reasonable to apply the considered two-cluster approach to few-nucleon systems with A = 3 and 4, at least to compare results obtained in the frame of the PCM with multiparticle calculations and the PCM results for systems with A>4. In this regard, the using of this approach to such systems, especially for low-energy process analysis, seems quite reasonable.

3.1. SCATTERING POTENTIALS AND PHASE SHIFTS

Total cross sections of photoprocesses for the lightest ^{3}He and ^{3}H nuclei in the potential cluster model with FS were considered earlier in [29]. In these calculations for photodisintegration of ^{3}He and ^{3}H in the p^{2}H and n^{2}H channels, $E1$ transitions due to the orbital part of the electric operator $Q_{Jm}(L)$ [20] were taken into account. Cross sections of $E2$ processes and cross sections depending on the spin part of electric operator turned out to be lower by several orders of magnitude. Then it was assumed that electric $E1$ transitions in N^{2}H system are possible between ground pure according to Young scheme {3} doublet ^2S state of ^{3}H nuclei and ^{3}He and doublet ^2P scattering states mixed according to Young schemes {3} + {21}. Such transition is quite possible since the quantum number, connected with Young schemes, evidently is not saved in electromagnetic processes [28].

For calculation of photonuclear processes in p^{2}H and n^{2}H systems, the nuclear part of the intercluster interaction potential was represented in form (2.7) with the point-like Coulomb term, Gaussian attractive V_0, and exponential repulsive V_1 parts. The potential of each partial wave was constructed in order to correctly describe the corresponding partial elastic scattering phase [63].

Using these representations the potentials of p^{2}H interaction for scattering processes were obtained; the parameters of these potentials are given in [20,29,64] and Table 3.1. Then in the doublet channel, mixed according to Young schemes {3} and {21} [28], pure phase shifts (2.11) were separated, and based on these phase shifts the pure ^2S potential of the bound state with Young scheme {3} for ^{3}He in p^{2}H channel was constructed [20,29,64].

Calculations of $E1$ transition showed [29] that best results for description of total photodisintegration cross sections for ^{3}He nucleus in the region of γ-quantum energies 6÷28 MeV, including the maximum at E_γ = 10÷13 MeV, can be obtained if the potential of the ^2P wave for p^{2}H scattering with peripheral repulsion given in Table 3.1 is used. In this case it is assumed that ^2S interaction in the bound state is pure according to Young scheme {3} and has a Gaussian form with the parameters V_0 = –34.75 MeV, α = 0.15 fm^{-2} obtained based on a correct description of the binding energy (with an accuracy of several keV) and charge radius of ^{3}He nucleus. These potentials were used to calculate total radiative cross sections for p^{2}H and astrophysical *S*-factor at energies down to 10 keV [20,29], although at that time experimental data on *S*-factor for energies above 150÷200 keV only was known [65].

New experimental data on the *S*-factor of p^{2}H capture at energies down to 2.5 keV appeared not long ago [66-68]. Therefore, it is interesting to elucidate whether the potential cluster model based on *E*1 and *M*1 transitions is capable of describing new data using the ^2P scattering interaction obtained earlier, the mixed ^2S potential of the bound p^{2}H state from Table 3.1 and the pure, according Young schemes, ^2S potential of the bound p^{2}H state specified here in Table 3.1.

Our preliminary results [69] showed that the accuracy of calculation of the binding energy of the p^{2}H system in ^{3}He nucleus, which was at a level 1÷2 keV [29], should be substantially increased for calculating the *S*-factor at energies about 1 keV. More stringent control of the behavior of the “tail” of the wave function of the bound state at large distances is needed. Moreover, it is necessary to increase the accuracy of calculation of the Coulomb wave functions [24] determining the behavior of asymptotics of the scattering wave function in the ^2P wave.

Using the capabilities of improved computer programs for more correct description of experimental binding energy of ^{3}He nucleus in p^{2}H channel, the parameters of a pure with Young scheme {3} doublet ^2S potential were specified. This potential (see Table 3.1) became somewhat deeper than that used in [29]; now it results in complete agreement of the experimental (–5.4934230 MeV) binding energy and calculated (–5.4934230 MeV) binding energy obtained with exact values of particle masses [35].

The difference between the potentials given in [29] and Table 3.1 is, first of all, due to the application of the exact masses of particles and more accurate description of binding energy of ^{3}He nucleus in p^{2}H channel. For all of these calculations, the absolute accuracy of calculation of the binding energy in our computer program using the finite-difference method was set on a level 10^{-8} MeV [24].

The charge radius of ^{3}He with this potential turns out to be equal to 2.28 fm, which is somewhat larger than experimental data given in Table 3.2 [35,70,71]. It follows from this data that the radius of deuteron cluster is larger than the radius of ^{3}He nucleus. Therefore, if the deuteron is inside ^{3}He as a cluster, for correct description of ^{3}He radius, it should be compressed by approximately 20÷30% of its size in the free state [20,48,72].

Table 3.1. Potentials of p^{2}H [29] interaction for $S = 1/2$

^{2S+1}L, {*f*}	V_0 (MeV)	α (fm^{-2})	V_1 (MeV)	γ (fm^{-1})
^2S, {3}	–34.76170133	0.15	–	–
^2S, {3} + {21}	–55.0	0.2	–	–
^2P, {3} + {21}	–10.0	0.16	+0.6	0.1

With kind permission of the European Physical Journal (EPJ)

Table 3.2. Experimental masses and charge radii of light nuclei used in these calculations [35,70,71]

Nucleus	Radius (fm)	Mass (amu)
^{1}H	0.8768(69)	1.00727646677
^{2}H	2.1402(28)	2.013553212724
^{3}H	1.63(3); 1.76(4); 1.81(5) Average 1.73	3.0155007134
^{3}He	1.976(15); 1.93(3); 1.877(19); 1.935(30) Average 1.93	3.0149322473
^{4}He	1.671(14)	4.001506179127

In order to control the behavior of wave functions of bound states at large distances, the asymptotic constant C_W with the asymptotics of the wave function in the form of Whittaker function (2.10) [59] was calculated; the value of this constant in an interval 5÷20 fm is C_W = 2.333(3). The error shown here is determined by averaging the constant over the interval indicated above.

The determination of this constant from experimental data yields values in an interval 1.76÷1.97 [73-75], which is somewhat lower than the value obtained here. The results of three-body calculations [76] should also be mentioned; in these calculations, good agreement with experiment [77] for the ratio of asymptotic constants of ^2S and ^2D waves was obtained and the following value was found for the constant C_W = 1.878.

However, in [37], which was published later than [73-75], a value 2.26(9) was given for C_W, which agrees well with our calculations. It can be seen from the data presented in these works that experimental results on asymptotic constants obtained at different times and by different authors scatter considerably. This data is in the range from 1.76 to 2.35 with a mean value 2.06.

In the cluster two-cluster model, the value of C_W and charge radius strongly depends on the width of the potential well. Other parameters of ^2S potential of ground states can always be found, for example,

$$V_0 = -48.04680730 \text{ MeV}, \alpha = 0.25 \text{ fm}^{-2}, \tag{3.1}$$

$$V_0 = -41.55562462 \text{ MeV}, \alpha = 0.2 \text{ fm}^{-2}, \tag{3.2}$$

$$V_0 = -31.20426327 \text{ MeV}, \alpha = 0.125 \text{ fm}^{-2}, \tag{3.3}$$

which yield the same binding energy for ^{3}He in the p^{2}H channel. The first of them at an interval 5÷20 fm results in the asymptotic constant C_W = 1.945(3) and the charge radius R_{ch} = 2.18 fm, the second yields the constant C_W = 2.095(5) and R_{ch} = 2.22 fm, and the third C_W = 2.519(3) and R_{ch} = 2.33 fm. The cluster radii from Table 3.2 are used in the calculations of charge radii.

It can be seen from these results that potential (3.1) makes it possible to obtain the charge radius that is the closest to experiment value. Further reduction of the potential width may result in correct description of its value; however, it will be shown below that it will not make it possible to reproduce the *S*-factor of radiative p^2H capture. In this sense potential (3.2), which is characterized by somewhat larger width, has the minimal admissible width of the potential well for which it is possible to obtain an asymptotic constant practically equal to its experimental average value 2.06 and acceptably describe the behavior of the astrophysical *S*-factor in the broadest energy region.

For a complementary check of the determination of the binding energy in two-body channels, the variational method has been used; this method already made it possible to obtain a binding energy of –5.4934228 MeV for a grid with a dimensionality 10 and independent parameter variation [24] for the pure, according Young schemes, potential from Table 3.1. The asymptotic constant C_W of the variational wave function at distances 5÷20 fm in these calculations was on a level 2.34(1), and the residual did not exceed 10^{-12} [24]. The parameters and coefficients of expansion of the radial wave function for this potential of form (2.9) are given in Table 3.3.

The variant of potential (3.2) was also considered in the framework of the variational method; the same binding energy, –5.4934228 MeV, has been obtained for this potential. The variational parameters and coefficients of expansion of the radial wave function are given in Table 3.4. The asymptotic constant in a range 5÷20 fm turned out to be equal to 2.09(1), and the residual was of the order of 10^{-13}.

Since the variational energy decreases with increasing dimensionality of the basis and yields the upper boundary of the true binding energy [78], and the finite-difference energy increases with decreasing step and increasing number of steps [24], an average value of –5.4934229(1) MeV can be taken as a realistic estimate of the binding energy in this potential.

Thus, it may be considered that the error of determination of the binding energy of the p^2H system in ^3He nucleus using two methods based on two different computer programs is ±0.1 eV in the given potential.

Table 3.3. Variational parameters and expansion coefficients of radial wave function of the p^2H bound state system for potential from Table 3.1. Normalization of function with these coefficients on an interval 0÷25 fm is N = 0.999999997

i	β_i	C_i
1	2.682914012452794E–001	–1.139939646617903E–001
2	1.506898472480031E–002	–3.928173077162038E–003
3	8.150892061325998E–003	–2.596386495718163E–004
4	4.699184204753572E–002	–5.359449556198755E–002
5	2.664477374725231E–002	–1.863994304088623E–002
6	4.4687619986542310E+001	1.098799639286601E–003
7	8.482112461789261E–002	–1.172712856304303E–001
8	1.541789664414691E–001	–1.925839668633162E–001
9	1.527248552219977E–000	3.969648696293301E–003
10	6.691341326208045E–000	2.097266548250023E–003

With kind permission of the European Physical Journal (EPJ).

Table 3.4. Variational parameters and expansion coefficients of radial wave function of the p^2H bound state system for potential (3.2). Normalization of function with these coefficients on an interval 0÷25 fm is N= 0.999999998

i	β_i	C_i
1	3.485070088054969E–001	–1.178894628072507E–001
2	1.739943603152822E–002	–6.168137382276252E–003
3	8.973931554450264E–003	–4.319325351926516E–004
4	5.977571392609325E–002	–7.078243409099880E–002
5	3.245586616581442E–002	–2.743665993408441E–002
6	5.8379917320454490E+001	1.102401456221556E–003
7	1.100441373510820E–001	–1.384847981550261E–001
8	2.005318455817479E–001	–2.114723533577409E–001
9	1.995655373133832E–000	3.955231655325594E–003
10	8.741651544040529E–000	2.101576342365150E–003

With kind permission of the European Physical Journal (EPJ).

3.2. ASTROPHYSICAL S-FACTOR

In our calculations of the astrophysical S-factor, the region of energies of radiative p^2H capture from 1 keV to 10 MeV was considered and also $E1$ transition from ^2P wave of scattering to the ground ^2S state with {3} and potential parameters listed in Table 3.1.

For the $S(E1)$ factor for 1 keV, a value 0.165 eV b was obtained, which is in a quite agreement with the known data including the separation of $S(0)$-factor into S_s and S_p parts due to $M1$ and $E1$ transitions. This separation was made in [67], where it was obtained that $S_s(0) = 0.109(10)$ and $S_p(0) = 0.073(7)$ eV b, which for the total S-factor should yield 0.182(17) eV b. On the other hand, in the expression for linear interpolation of the total S-factor, the authors give the following values [67]: $S_0 = 0.166(5)$ and $S_1 = 0.0071(4)$ eV b keV^{-1},

$$S(E_{cm}) = S_0 + E_{cm}{\cdot}S_1 \,, \tag{3.4}$$

and for $S(0)$ a value 0.166(14) keV b was given; this value is determined with all possible errors taken into account.

The results obtained with separation of the S-factor into $M1$ and $E1$ parts were given in one of the first papers [65] devoted to astrophysical factors, wherein it was obtained that $S_s(0) = 0.12(3)$ and $S_p(0) = 0.127(13)$ eV b for a total S-factor 0.25(4) eV b. This data of $S_s(0)$ value quite coordinate with data given in [67].

Experimental data [68] yield the total astrophysical factor $S(0) = 0.216(10)$ eV b; this means that the contributions of $M1$ and $E1$ differ from the above values [67]. In this paper the following parameters of linear extrapolation (3.4) are given: $S_0 = 0.216(6)$ eV b and $S_1 = 0.0059(4)$ eV b keV^{-1}, which noticeably differ from the data of [67]. The other known results for the S-factor obtained from experimental data without separation into $M1$ and $E1$ parts yield for zero energy 0.165(14) eV b [79]. Previous results of the same authors yield 0.121(12) eV b [80], and in theoretical calculations [81] the following values were obtained for different models: $S_s(0) = 0.105$ and $S_p(0) = 0.08{\div}0.0865$ eV b and the total S-factor equals to 0.185÷0.192 eV b. It follows from these results that there exists a great ambiguity in the data obtained during the last 10÷15 years. These results make it possible to conclude that, most probably, the value of the total *S*-factor at zero energy is in an interval 0.109÷0.226 eV b. The average of these values yields an *S*-factor equal to 0.167(59) eV b, which quite agrees with that obtained here based on *E*1 transition.

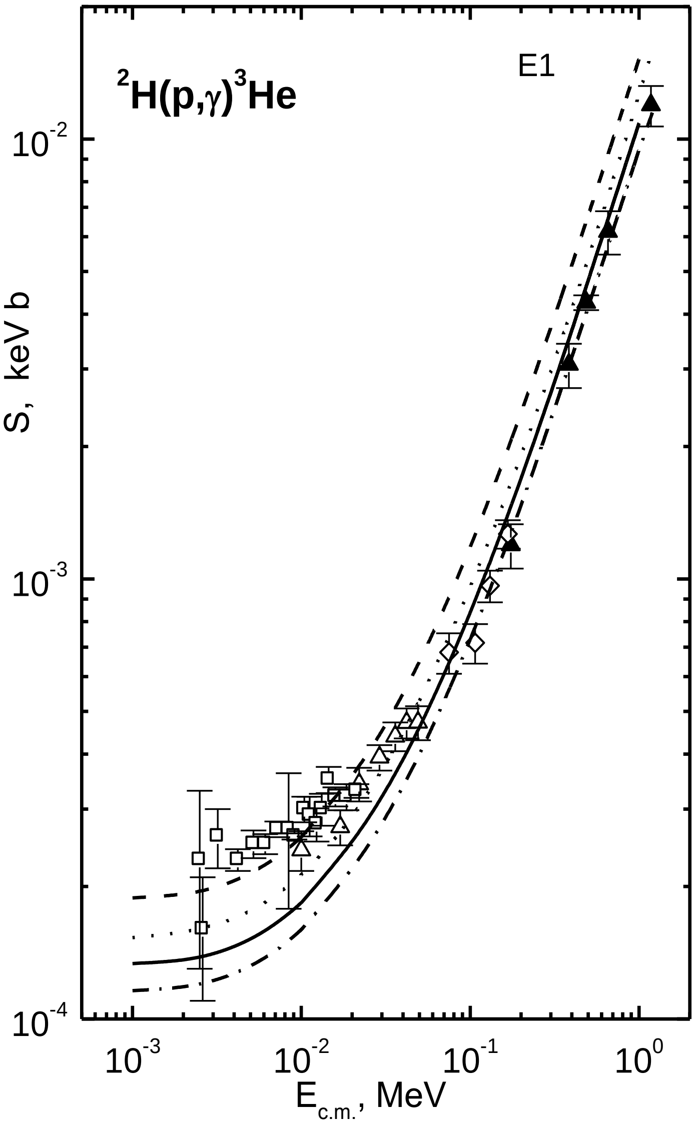

With kind permission of the European Physical Journal (EPJ).

Figure 3.1. Astrophysical *S*-factor of p^{2}H radiative capture in a range 1 keV÷1 MeV for *E*1 transition. Curves show calculations with potentials given in the text. Triangles show experiment [65], open rhombs [66], open triangles [67], and open squares [68].

Our calculations of the *S*-factor of radiative p^{2}H capture for the potential given in Table 3.1 at energies from 1 keV to 10 MeV are shown in Figs. 3.1 and 3.2 with dotted lines. The obtained *S*-factor rather well reproduces new experimental data at energies 10÷50 keV [67], and at lower energies the calculated curve is within the interval of experimental errors of [68].

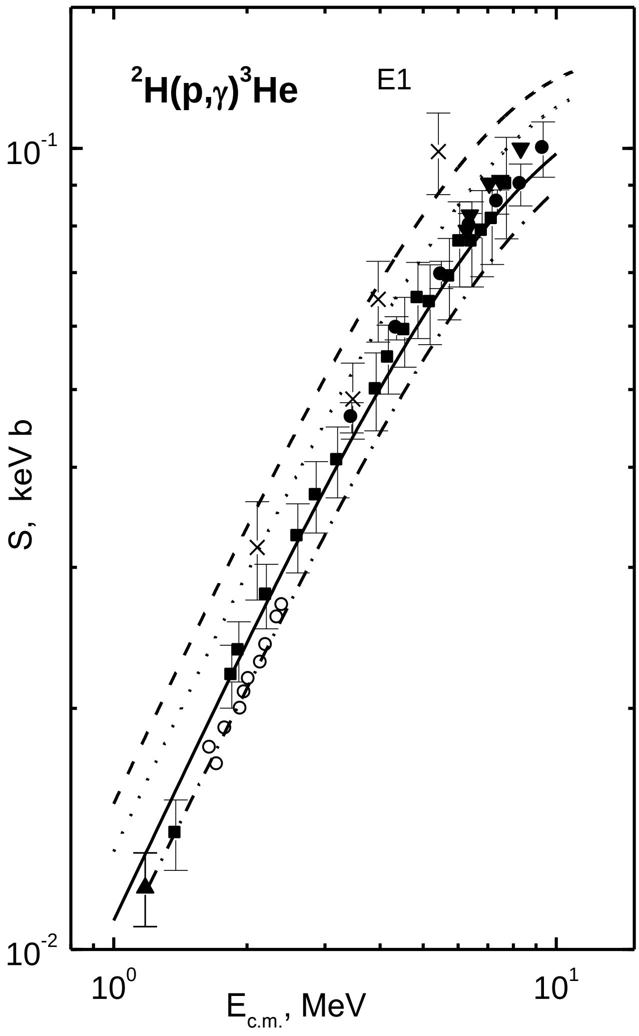

With kind permission of the European Physical Journal (EPJ).

Figure 3.2. Astrophysical *S*-factor of p^{2}H radiative capture in a range 1÷10 MeV for *E*1 transition. Curves show calculations with potentials given in the text. Upward triangles show experiment [65], squares [82], points [83], crosses [84], downward triangles [85], and circles [86].

The solid lines in Figures 3.1 and 3.2 show the results for potential (3.2), which reproduces the behavior of *S*-factor at energies 50 keV÷10 MeV somewhat better and for 1 keV yields S_p = 0.135 eV b. For 20÷50 keV, the calculated curve follows the lower boundary of errors [67], and below 10 keV it falls into the interval of experimental errors of the project LUNA obtained most recently [68]. The value of the *S*-factor obtained at zero energy with this potential agrees well with data [65] for electric *E*1 transition S_p.

The dashed lines in Figures 3.1 and 3.2 show the results for potential (3.3), and the dash-dotted line, for potential (3.1). It can be assumed based on these calculations that the best results are obtained for bound state potential (3.2), which describes experimental data in the broadest energy interval. It provides a certain compromise in description of the asymptotic constant, charge radius, and astrophysical *S*-factor of radiative p^{2}H capture.

It can be seen in Figure 3.1 that, at low energies of about 1÷3 keV, the S_p-factor is practically independent of the energy; thus, the determination of this factor at zero energy yields approximately the same value as at 1 keV. Therefore, the difference of *S*-factor at 0 and 1 keV probably comes to no more than 0.005 eV b; this quantity can be assumed for the error of determination of the calculated *S*-factor for zero energy and accept that it equals 0.135(5) eV b.

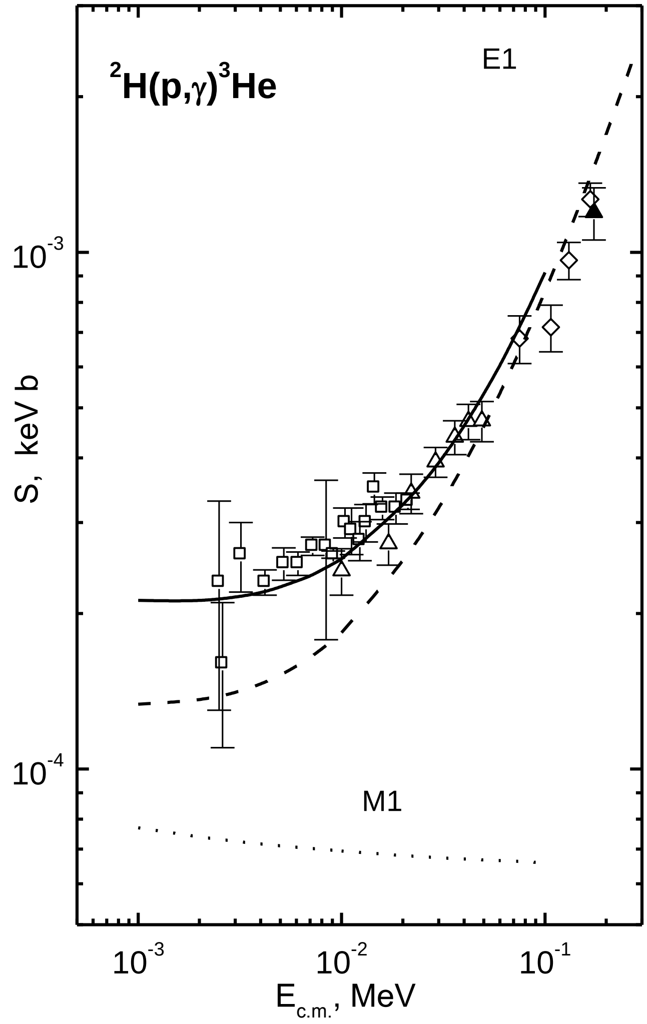

Figure 3.3. Astrophysical *S*-factor of p^{2}H radiative capture in a range 1 keV÷0.3 MeV for *E*1 and *M*1 transitions. Curves show calculations with potentials given in the text. Triangles show experiment [65], open rhombs [66], open triangles [67], and open squares [68].

At low energies, the *M*1 transition from the ^2S scattering state mixed according to Young schemes to the bound ^2S state of a ^{3}He nucleus pure for orbital symmetry can give contribution to the total astrophysical *S*-factor. For these calculations we used expressions (2.4,2.6), the doublet ^2S potential of scattering states with parameters given in Table 3.1 [20,64,87] and ground state ^2S potential (3.2).

The results of calculations of the *M*1 process at 1÷100 keV are shown in Figure 3.3 by the dotted line at the bottom of the figure and the results of *E*1 transition for the GS potential with the parameters (3.2) are shown by the dashed curve.

The dashed curve in Figure 3.3 is shown the calculation results of the *E*1 transition for the GS potential (3.2), which shown in Figure 3.1 by the solid line. The total *S*-factor is shown by the solid line, which demonstrates a small contribution of *M*1 S_s-factor at the energies above 100 keV and its significant influence to the energy range of the order of 1÷10 keV [88].

The total *S*-factor dependence on energy in the range 2.5÷50 keV is in complete accordance with the findings of works [67,68] and for the S_s-factor of the *M*1 transition at 1 keV we obtained the value 0.077 eV b, which leads to the value 0.212(5) eV b for the total *S*-factor and which is in a good agreement with the new measurements data from LUNA project [68]. And as it can be seen from Figure 3.3, at the energies 1÷3 keV the value of the total *S*-factor is more stable than it was for the *E*1 transition and we consider it to be absolutely reasonable to write the result as 0.212 eV b with the error 0.005.

However, it is necessary to note that we are unable to build the scattering ^2S potential uniquely because of the ambiguities in the results of phase shift analysis of p^{2}H scattering. The other variant of potential with parameters V_0 = –35.0 MeV, α = 0.1 fm^{-2} [20,64,87], which also describes well the doublet *S* phase shift of scattering, leads at these energies to *S*-factor of the *M*1 process several times lower than in the previous case.

Such a big ambiguity in parameters of the ^2S potential of scattering, associated with errors of phase shifts extracted from the experimental data of phase shifts of scattering, does not allow us to make certain conclusions about the contribution of the *M*1 process in the p^{2}H radiative capture, probably because of neglecting of spin-orbital splitting in such analysis, which can influence to the value of the ^2S phase shift. But the first of described variants conforms to the latest measurements [67,68].

If the GS potentials are defined by the bound energy, asymptotic constant and charge radius quite uniquely and by an additional criterion – usage of the scattering phase shifts which are "pure" in accordance with Young scheme, but the situation with the construction of scattering potentials is not so unambiguous. Then, in the case of scattering, it is necessary to carry out a more accurate phase shift analysis for the ^2S wave and to take into account the spin-orbital splitting of ^2P phase shifts at low energies, as it was done for the elastic p^{12}C scattering at energies 0.2÷1.2 MeV [89]. Carrying out of this additional analysis will allow us to adjust the potential parameters used in the calculations of the p^{2}H capture in the potential cluster model, thereby increasing the accuracy of the calculation results.

CONCLUSION

Thus, the S-factor calculations of the p^{2}H radiative capture for the $E1$ transition at the energy range down to 10 keV, which we carried out about 15 years ago [29], when the experimental data above 150÷200 keV was only known, are in a good agreement with the new data of works [66,67] in the energy range from 10÷20 to 150÷200 keV. Moreover, this is true about the GS potential from Table 3.1 and the interaction with parameters from (3.2). The results of S_p-factors for the two considered potentials at the energies lower than 10 keV (Figure 3.1) practically fall within the error band of work [68] and show that the S-factor tends to remain constant at energies 1÷3 keV.

In spite of the uncertainty of the $M1$ contribution to the process, which results from the errors and ambiguity of ^2S phases of scattering, the scattering potential (set forth in Table 3.1) with mixed Young schemes in the ^2S wave allows obtaining a reasonable value for the astrophysical S_s-factor of the magnetic transition in the range of low energies. At the same time, the value of the total S-factor is in a good agreement with all known experimental measurements at energies from 2.5 keV to 10 MeV.

As a result, the PCM based on the intercluster potentials adjusted for the elastic scattering phase shifts and GS characteristics, for which the FS structure is determined by the classification of BS according to Young orbital schemes and parameters suggested as early as 15 years ago [29], allows describing correctly the astrophysical S-factor for the whole range of energies under consideration.

Chapter 4

PROCESS OF THE P^{3}H RADIATIVE CAPTURE

INTRODUCTION

In a continuation of the investigation of fusion reactions [59] based on the potential cluster model with separation of orbital states according to Young schemes [90], we consider the possibility of description of the astrophysical *S*-factor of radiative p^{3}H capture at energies as low as 1 keV. This reaction is of certain interest from the theoretical and experimental points of view for understanding the dynamics of photonuclear processes with the lightest atomic nuclei at low energies. Therefore, experimental studies of this reaction continue, and new data for the total radiative p^{3}H capture cross section and astrophysical *S*-factor in the energy range from 50 keV to 5 MeV and at 12 and 39 keV (center of mass system) has been obtained.

Probably, this reaction took a certain role at the prestellar stage of evolution of the Universe [2], when at the temperature about 10^9 K the next reactions (primordial nucleosynthesis) became possible

1. $p + n \rightarrow {}^2H + \gamma$,
2. ${}^2H + p \rightarrow {}^3He + \gamma$,
3. ${}^2H + n \rightarrow {}^3H + \gamma$,
4. ${}^2H + {}^2H \rightarrow {}^3He + n$,
5. ${}^2H + {}^2H \rightarrow {}^3H + p$,
6. ${}^2H + {}^2H \rightarrow {}^4He + \gamma$,
7. ${}^3H + p \rightarrow {}^3He + n$,
8. ${}^3He + n \rightarrow {}^3H + p$,
9. ${}^3H + p \rightarrow {}^4He + \gamma$,
10. ${}^3He + n \rightarrow {}^4He + \gamma$,
11. ${}^2H + {}^3H \rightarrow {}^4He + n$.

This situation could realize at the live time of the Universe about 10^2 sec, when the number of protons and neutrons was comparable – approximately 0.2 neutrons from the proton number [2,3,7,8]. The last reaction No.10 mediates with comparatively small probability, since the *E*1 process is forbidden by the isospin selection rules, which leads to the factor $\left(\frac{Z_1}{m_1^J}+(-1)^J\frac{Z_2}{m_2^J}\right)$ at J = 1 that evaluated expressions (2.5), and, in general, the probability of $E2$ transitions is near 1.5÷2.0 orders less [36].

The epoch of primordial nucleosynthesis [3] is finished approximately at 200 sec; practically all neutrons are bound into ^{4}He nuclei, the number of which is about 25% from ^{1}H nuclei. The relative content of ^{2}H and ^{3}He is about at the level 10^{-5} from ^{1}H [3].

Let us go now to the direct consideration of the astrophysical S-factor of the p^{3}H radiative capture in the potential cluster model at lowest energies. At the beginning we will construct the intercluster interaction potentials for the elastic scattering and bound states and will carry out their classification according to Young schemes.

4.1. SCATTERING POTENTIALS AND PHASE SHIFTS

The system p^{3}H is mixed with respect to isospin, since for T_z = 0 the following values are possible: T = 0 and 1. Hence, both triplet and singlet phase shifts and, therefore, potentials effectively depend on two isospin values. Due to the Pauli exclusion principle, mixing with respect to isospin results in mixing according to Young schemes. In particular, in the singlet spin state, two orbital Young schemes, {31} and {4}, are allowed [90]. Then it was shown in [90,92] that singlet phase shifts of p^{3}H scattering mixed with respect to isospin can be represented in the form of the half-sum of pure with respect to isospin singlet phase shifts,

$$\delta^{\{T=1\}+\{T=0\}}=1/2\delta^{\{T=1\}}+1/2\delta^{\{T=0\}}, \tag{4.1}$$

which is equivalent to the following expression for the scattering phase shifts in terms of Young schemes:

$$\delta^{\{4\}+\{31\}}=1/2\delta^{\{31\}}+1/2\delta^{\{4\}}.$$

Pure phases correspond to Young schemes {31} and T = 1 for the p^{3}He system and {4} and T = 0 for p^{3}H system. Since p^{3}He system at T_z = 1 is pure according to isospin, then from the equation (4.1) based on known pure scattering phases with T = 1 in the p^{3}He system [93-95] and mixed phases in the p^{3}H system with isospin T = 0 and 1 [99-101] yields pure with respect to isospin phases of p^{3}H scattering with T = 0 and corresponding pure potentials of p^{3}H interaction are constructed based on these scattering phases [92]. It is supposed in this approach that pure phase shifts with isospin T = 1 in p^{3}H system can be compared to phase shifts with T = 1 in p^{3}He channel.

The nuclear part of the intercluster potential of the p^{3}H and p^{3}He interactions is represented in the form (2.7) with the point-like Coulomb term for performing calculations of the photonuclear processes in the considered system. The potential of the each partial wave, as for the previous p^{2}H system, is constructed for a correct description of the applicable partial wave of the elastic scattering [91].

Table 4.1. Singlet potentials of the form (2.7) for p^{3}He scattering, pure with respect to isospin of $T = 1$ [90,92]

^{2S+1}L	V_0 (MeV)	α (fm^{-2})	V_1 (MeV)	γ (fm^{-1})
^1S	–110.0	0.37	+45.0	0.67
^1P	–15.0	0.1	–	–

Consequently, the potentials of the p^{3}He interactions for the elastic scattering processes and pure with respect to isospin of $T = 1$ were obtained, their parameters are listed in Table 4.1 [90,92]. The singlet and pure with respect to isospin S phase shift of the p^{3}He elastic scattering, using in future in order to obtain singlet p^{3}H phase shifts with isospin $T = 0$, is shown by the solid line in Figure 4.1a together with the experimental data from the works [93-95].

Then, using expression (4.1), for the pure p^{3}H potential with $T = 0$ (2.8) in the ^1S wave, the following parameters have been found:

$$V_0 = -63.1 \text{ MeV}, \alpha = 0.17 \text{ fm}^{-2}. \qquad (4.2)$$

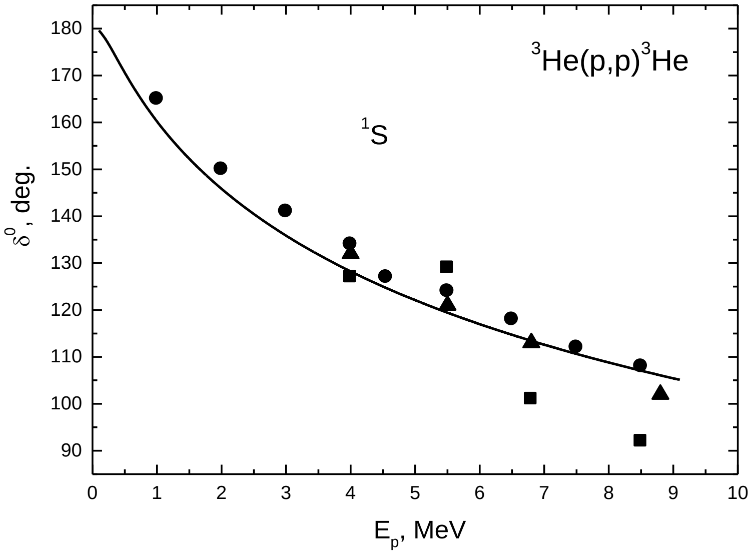

Figure 4.1a. Singlet ^1S phase shift of elastic p^{3}He scattering. Experimental data: points [93], squares [94], and triangles [95].

Parameters of the potential for singlet $^1P_1$ and triplet $^3P_1$ waves given in the Table 4.1 are chosen in order to obtain a certain compromise between different results, so far as there are few different variants of the phase shift analyses of the elastic p^{3}He scattering, for example [93-95]. The singlet $^1P_1$ phase shift of the elastic p^{3}He scattering with $T = 1$ used in our calculations of the $E1$ transition to the ground state of ^{4}He nucleus in the p^{3}H channel with $T = 0$ is shown in Figure 4.1b by solid line and the experimental data of works [93-98] is given in this figure too. The singlet and mixed according to isospin and Young schemes S phase shift of the elastic p^{3}H scattering, determining from the experimental differential cross sections and used later for the obtaining of pure p^{3}H phase shifts for potential of the form

(2.8) with parameters V_0 = -50 MeV, α = 0.2 fm^{-2}, is shown in Figure 4.2 by the solid line together with the experimental data of works [99-101].

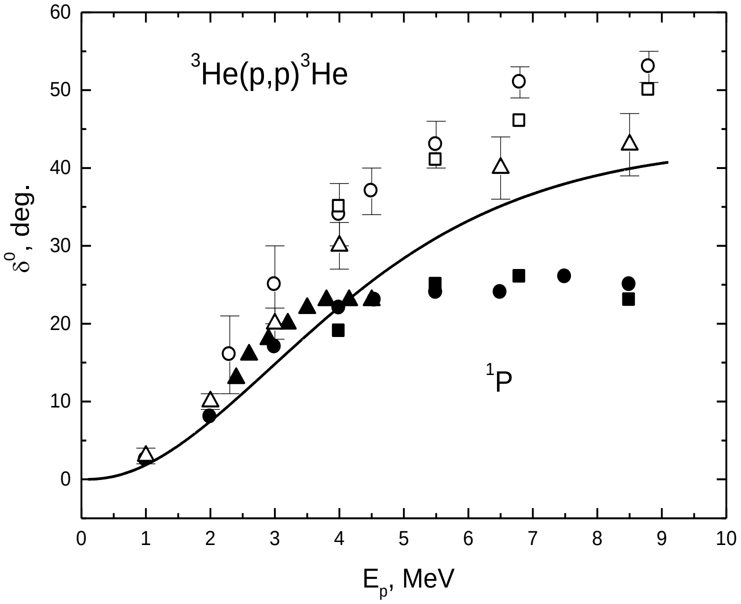

Figure 4.1b. Singlet ^1P phase shift of elastic p^{3}He scattering. Experimental data: points [93], squares [94], triangles [96], circles [97], open squares [95], and open triangles [98].

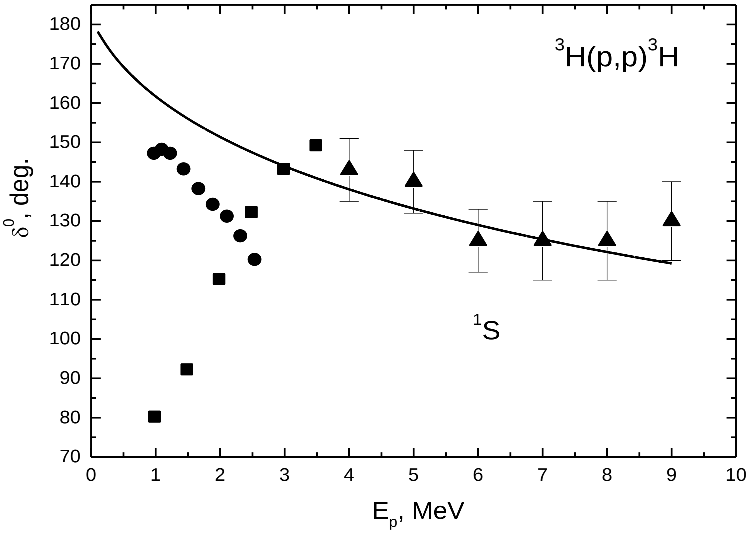

Figure 4.2. Singlet ^1S phase shift of elastic p^{3}H scattering. Experimental data: points [99], squares [100], and triangles [101].

Figure 4.3 shows the pure according to the Young scheme singlet ^1S phase of elastic p^{3}H scattering (dotted line) and the results of calculation of this phase with potential (4.2) (solid line). Thus-obtained pure (according to Young scheme) interactions can be used for calculation of different characteristics of the bound ground state ^{4}He in p^{3}H channel. The degree of agreement of the results obtained in this case with experiment now depends on the degree of clusterization of this nucleus in the considered channel only.

The interaction potential (4.2) obtained in [92] on the whole correctly describe the channel binding energy of the p^3H system (to several keV) and the mean square radius of ^4He nucleus [92]. These potentials were used to calculate differential [90] and total cross sections of radiative p^3H capture and astrophysical *S*-factors at energies as low as 10 keV [92]. It should be noted that, at that time, experimental data for the *S*-factor only was known in the energy region above 700÷800 keV [86].

New experimental data at energies from 50 keV to 5 MeV [103] and at 12 and 36 keV [104] was obtained not long ago. Therefore, it is of interest to elucidate whether the potential cluster model with the singlet ^1P potential obtained earlier and refined interaction of the ground ^1S state of ^4He nucleus is capable of describing this new, more accurate, data.

Our preliminary results [105] have shown that, for calculation of the *S*-factor at energies of the order of 1 keV, the same conditions as in the p^2H system [69] discussed in the previous section should be satisfied – first of all, the accuracy of finding ^4He binding energy in a p^3H channel should be increased. New modified programs were used in order to refine parameters of the potential of the ground state of the p^3H system in ^4He nucleus (see Table 4.2), which differ from those presented in [92] by approximately 0.2 MeV.

This difference is mainly connected with the application in new calculations of more accurate values of masses of p and ^3H particles [35] and more accurate description of the binding energy of ^4He nucleus in the p^3H channel. For this energy based on more accurate values of particle masses [35], a value of –19.813810 MeV was obtained; the calculation with the potential considered here yields –19.81381000 MeV. The accuracy of determination of the energy value in this potential using our program based on the finite-difference method [24] is 10^{-8} MeV.

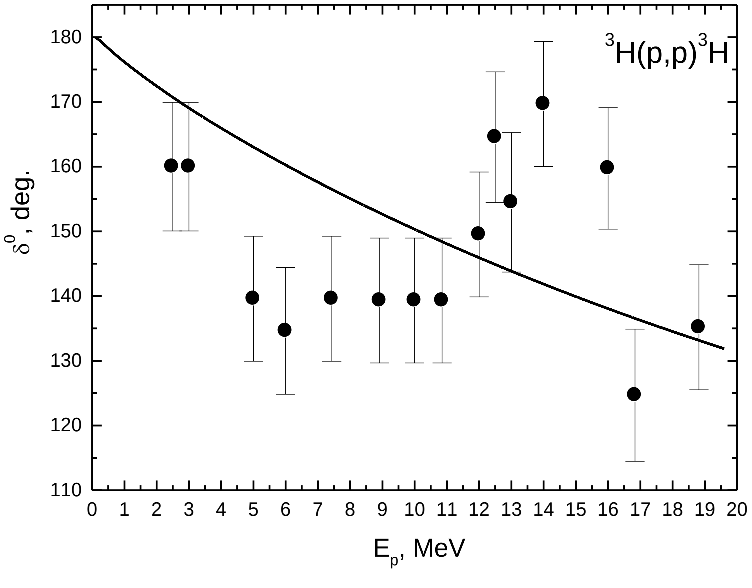

Figure 4.3. Singlet pure according to Young scheme ^1S phase shift of elastic p^3H scattering.

Table 4.2. Pure with respect to isospin of $T = 0$ potentials of the form (2.8) for p^{3}H interactions [92] in a singlet channel. Here, E_{BS} is the calculated bound state energy and E_{exp} is the experimental value of this energy [71]

^{2S+1}L	V_0 (MeV)	α (fm^{-2})	E_{BS} (MeV)	E_{exp} (MeV)
^1S	–62.906841138	0.17	–19.81381000	–19.813810
^1P	+8.0	0.03	–	–

The behavior of the "tail" of the wave function of the bound state of p^{3}H system at large distances was verified using asymptotic constant (2.10) [37,106], which turned out to be equal to $C_W = 4.52(1)$ at an interval 5÷10 fm. As before, the given error of the asymptotic constant becomes clear by its averaging over the range referred above. Known results on extraction of the asymptotic constant from experimental data yield a value 5.16(13) for the p^{3}H channel [37]. For the asymptotic constant of the n^{3}He system in [37], a value 5.1(4) has been obtained that is very close to the parameter of the p^{3}H channel.

On the other hand, in [106] a value 4.1 was given for the constant of n^{3}He system, a value 4.0 – for p^{3}H. The average value between these constants is in a quite agreement with our results. Again, a considerable difference between the data on asymptotic constants can be seen. For the n^{3}He system, the constant is in the interval 4.1÷5.5, whereas for the p^{3}H channel it may assume values from 4.2÷4.4 to 5.3.

For the charge radius of ^{4}He nucleus, a value 1.73 fm has been obtained by taking the tritium radius as 1.63 fm [70] and the proton radius as 0.877 fm [35]. Note that the experimental value of ^{4}He radius is 1.671(14) fm [71] (see Table 3.2).

For complementary control of the accuracy in determining the binding energy in the S potential from Table 4.2, the variational method with expansion of the wave function over a non-orthogonal Gaussian basis has been used; this method for a dimensionality 10 and independent parameter variation [24] made it possible to increase the binding energy to 19.81380998 MeV. Asymptotic constant C_W (2.10) of the variational wave function at distances 5÷10 fm was on the level 4.52(2), and the residual did not exceed 10^{-11} [24]. The variational parameters and coefficients of expansion of the radial wave function of form (2.9) are given in Table 4.3.

It has been mentioned in the previous section that the variational energy decreases with increasing dimensionality of the basis and yields the upper limit for the true binding energy, while the finite-difference energy increases with decreasing step and increasing number of steps [24]. Therefore, for the actual binding energy in this potential, an average value of –19.81380999(1) MeV can be taken. In this case the error of determination of the binding energy using the two methods presented above and based on two different computer programs is ±0.01 eV.

It can be seen from these results that the simple two-cluster p^{3}H model with classification of orbital states according to Young schemes makes it possible to obtain a quite reasonable value for such characteristics of the bound state of ^{4}He nucleus as charge radii and asymptotic constants.

Table 4.3. Variational parameters and expansion coefficients of radial wave function of the p^{3}H bound state system for the ^1S potential given in Table 4.2. Normalization of the function with these coefficients in an interval 0÷25 fm is N = 0.9999999998

i	β_i	C_i
1	3.775399682294165E–002	–3.553662130779118E–003
2	7.390030511120065E–002	–4.689092850709087E–002
3	1.377393687979590E–001	–1.893147614352133E–001
4	2.427238748079469E–001	–3.619752356073335E–001
5	4.021993911220914E–001	–1.988757841748206E–001
6	1.780153251456691E+000	5.556224701527299E–003
7	5.459871888661887E+000	3.092889292994009E–003
8	1.921317723809205E+001	1.819890982631486E–003
9	8.416117121198026E+001	1.040709526875803E–003
10	5.603939880318445E+002	5.559240350868498E–004

These results can testify in favor of a relatively high degree of clusterization of this nucleus in the p^{3}H channel. Therefore, such model is completely able to bring us to reasonable results at the calculations of the astrophysical *S*-factors at low energy range, and now we are going over to their consideration.

4.2. ASTROPHYSICAL S-FACTOR

Earlier in [92], based on the potential cluster model, the total cross sections and astrophysical *S*-factor of the process of radiative p^{3}H capture were calculated and it was assumed that the main contribution into the cross sections of *E*1 photodisintegration of ^{4}He nucleus in the p^{3}H channel, or radiative p^{3}H capture, was due to the isospin-flip transitions for which $\Delta T = 1$ [107]. Therefore, the $^1P_1$ potential for p^{3}He scattering in the pure with respect to isospin ($T = 1$) singlet state of this system and the ^1S potential for the ground pure with respect to the isospin $T = 0$ bound state of ^{4}He nucleus in the p^{3}H channel [92] should be used in calculations.

These ideas were used to calculate anew the *E*1 transition with refined potential of the ground state of ^{4}He (see Table 4.2) [108]. The results of calculation of the astrophysical *S*-factor at energies as low as 1 keV are shown in Figures 4.4a and 4.4b with a solid line. At energies as low as 10 keV, the obtained results practically do not differ from our previous results given in [92].

New experimental data was taken from [103,104], and additional data from [109] not known to us earlier was also used. It can be seen from these figures that the calculations we carried out about 15 years ago well reproduce the new data on the *S*-factor obtained in [103] at energies from 50 keV to 5 MeV (center of mass system).

This data possess noticeably lower ambiguity at energies above 1 MeV than do earlier results [102,110-112] and more accurately determine the general behavior of the *S*-factor at low energies, practically coinciding with early data [109] in an energy range 80÷600 keV.

The energy region above 1÷2 MeV has been studied in many papers; therefore, for comparison, we are shown these earlier results in Figure 4.4b, demonstrated a large ambiguity of experimental measurements which was done in different time and works: circles [110], open squares [111], crosses (×) [112], and downward open triangles [102].

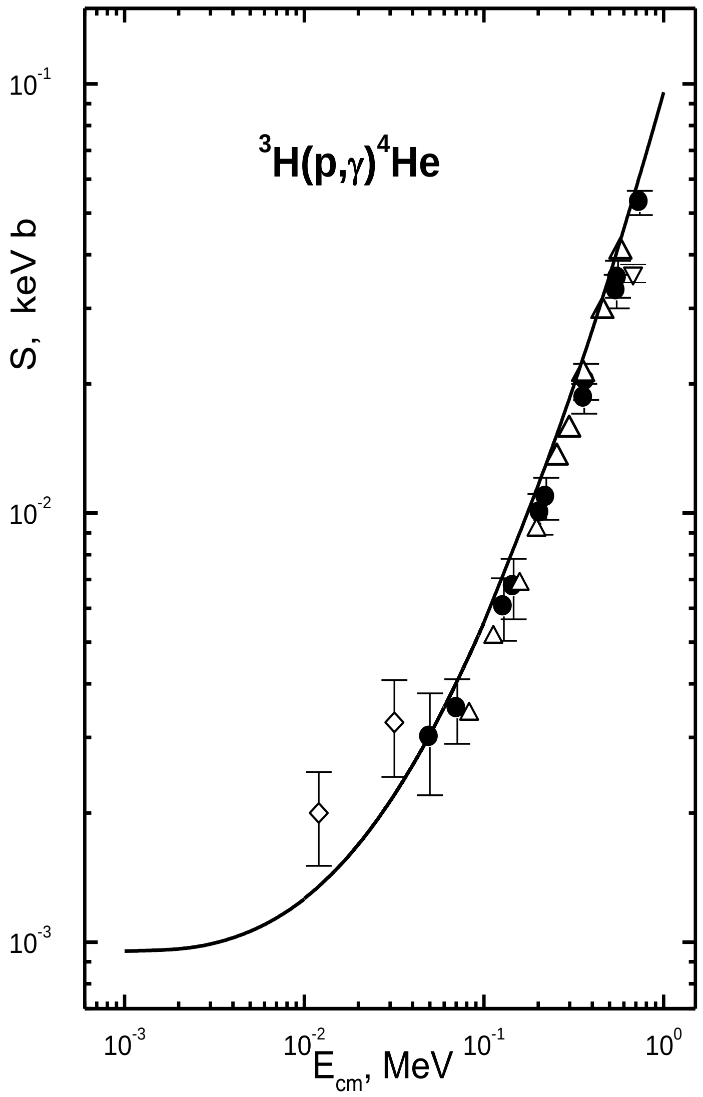

Figure 4.4a. Astrophysical *S*-factor of radiative p^{3}H capture in a range 1 keV÷1 MeV. Solid line shows calculation with the potential given in the text. Points show recalculation of total capture cross sections [103] from [104], upward open triangles [109], rhombs [104], downward open triangles [102].

At energy 1 keV, the value of the *S*-factor turned out to be equal to 0.96 eV b, and the results of calculation at energies below 50 keV are somewhat lower than the data of [104], where a value 2.0(2) eV b was obtained for *S*(0). Note that simple extrapolation of the available experimental data to 1 keV over the last three points of [103,109] results in a value of approximately 0.6(3) eV b, i.e., that is lower by a factor 3 than the value obtained in [104]. The data of work [104] has the large error and, it seems, ought to be improved in future.

It can be seen from Figure 6a that, at the lowest energies, approximately in a range 1÷3 keV, the *S*-factor is almost independent of energy. This gives grounds to assume that its value at zero energy practically does not differ from the value at 1 keV. Therefore, the difference of the *S*-factor at 0 and 1 keV probably is not more than 0.05 eV b, and this value may be considered as the error in determining the calculated *S*-factor at zero energy.

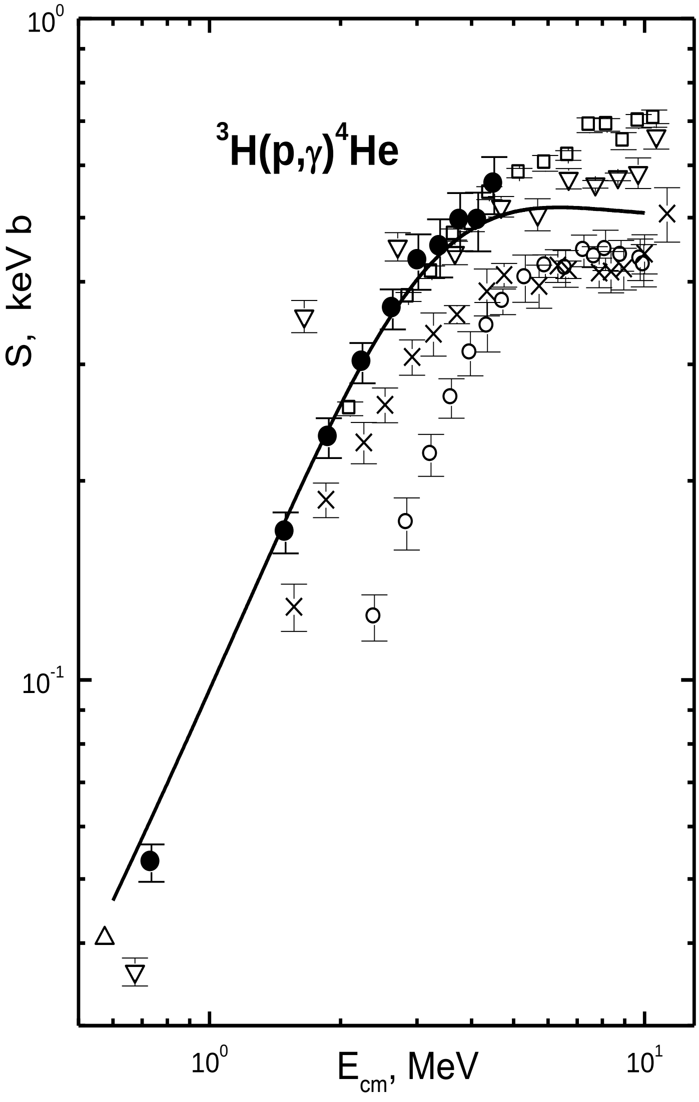

Figure 4.4b Astrophysical *S*-factor of radiative p^{3}H capture in a range 1÷10 MeV. Solid line shows calculation with the potential given in the text. Points show recalculation of total capture cross sections [103] from [104], upward open triangles [109], circles [110], open squares [111], crosses [112], and downward open triangles [102].

CONCLUSION

Thus, in the framework of the considered cluster model based on *E*1 transition only, it was possible to predict the general behavior of the *S*-factor of p^{3}H capture at energies from 50 to 700 keV. Indeed, based on the analysis of experimental data above 700 keV about 15 years ago, we made predictions of the behavior of the *S*-factor for energies as low as 10 keV [92].

It can be seen now that the results of these calculations well reproduce new data on *S*-factor obtained in [103] (points in Figures 4.4a, 4.4b) at energies from 50 keV to 5 MeV.

So, the using two-particle model, which are based on intercluster potentials describing phase shifts of elastic scattering and characteristics of the bound state, with parameters suggested about 15 years ago [87], allows correctly describe the astrophysical *S*-factor on the base of *E*1 transition in the whole energy range. The structure of FS of such potentials is defined on the base of cluster state classification according to Young scheme.

Chapter 5

PROCESS OF THE P^{6}LI RADIATIVE CAPTURE

INTRODUCTION

For refinement of the available experimental data in [26,113], the new measurement of differential cross sections of elastic p^{6}Li scattering at energies from 350 keV to 1.15 MeV (laboratory system) with 10% error has been performed. The data [26] considered in this section was obtained for five energies: 593 keV for 13 scattering angles in the interval 57°÷172°, 746.7 and 866.8 keV for 11 scattering angles in the interval 45°÷170°, and 976.5 and 1136.6 keV for 15 scattering angles in the interval 30°÷170°.

Based on measurements [26,113] and differential cross sections of elastic scattering at 500 keV from an earlier paper [114], we performed phase shift analysis and obtained $^{2,4}S$ and ^2P scattering phase shifts. The found phase shifts were used to construct the potentials for L = 0 and 1 of p^{6}Li interaction at low energies without taking into account spin-orbital splitting, and then the astrophysical S-factor was calculated for energies beginning with 10 keV.

Though, it seems, that the reaction of the p^{6}Li radiative capture may be of certain interest for nuclear astrophysics [115], it has not been experimentally studied sufficiently well. There are comparatively few works devoted to measurements of the total cross sections and determination of the astrophysical S-factor [33] performed in the energy range from 35 keV to 1.2 MeV. However, it seems to us that it is of interest to consider the possibility of description of the S-factor in the astrophysical energy region where experimental data is available using the potential cluster model with classification of bound states according to orbital Young's schemes [116,117].

5.1. DIFFERENTIAL CROSS SECTIONS

Upon examination of scattering processes in the system of particles with spins 1/2 and 1 without taking into account spin-orbital splitting of phase shifts, the cross section of elastic scattering is presented in the simplest form [45]

$$\frac{d\sigma(\theta)}{d\Omega} = \frac{2}{6}\frac{d\sigma_{\mathrm{d}}(\theta)}{d\Omega} + \frac{4}{6}\frac{d\sigma_{\mathrm{k}}(\theta)}{d\Omega}, \qquad (5.1)$$

where the indices d and k are related to the doublet (with a total spin 1/2) and quartet (with a total spin 3/2) states of p^{6}Li scattering. The corresponding cross sections are expressed in terms of scattering amplitudes

$$\frac{d\sigma_{\mathrm{d}}(\theta)}{d\Omega} = |\, f_{\mathrm{d}}(\theta)|^2 ,$$

$$\frac{d\sigma_{\mathrm{k}}(\theta)}{d\Omega} = |\, f_{\mathrm{k}}(\theta)|^2 , \tag{5.2}$$

which are written in the form

$$f_{\mathrm{d,k}}(\theta) = f_{\mathrm{c}}(\theta) + f^{\mathrm{N}}_{\mathrm{d,k}}(\theta), \tag{5.3}$$

where

$$f_{\mathrm{c}}(\theta) = -\left(\frac{\eta}{2k\sin^2(\theta/2)}\right)\exp\{i\eta\ln[\sin^{-2}(\theta/2)] + 2i\sigma_0\} \;,$$

$$f^{\mathrm{N}}_{\mathrm{d}}(\theta) = \frac{1}{2ik}\sum_{\mathrm{L}}(2L+1)\exp(2i\sigma_{\mathrm{L}})[S^{\mathrm{d}}_{\mathrm{L}} - 1]P_{\mathrm{L}}(\cos\theta) \;, \tag{5.4}$$

$$f^{\mathrm{N}}_{\mathrm{k}}(\theta) = \frac{1}{2ik}\sum_{\mathrm{L}}(2L+1)\exp(2i\sigma_{\mathrm{L}})[S^{\mathrm{k}}_{\mathrm{L}} - 1]P_{\mathrm{L}}(\cos\theta) \;.$$

Here $S^{\mathrm{d,k}}_{\mathrm{L}} = \eta^{\mathrm{d,k}}_{\mathrm{L}}\exp[2i\delta^{\mathrm{d,k}}_{\mathrm{L}}(k)]$ is the scattering matrix in the doublet or quartet spin state [45].

The possibility of application of simple expressions (5.1)÷(5.4) for calculation of elastic scattering cross sections is valid due to the fact that, in the low-energy region, spin-orbital splitting of phase shifts is relatively small, what is proved by the results of phase shift analysis performed in [118], where spin-orbital splitting of scattering phase shifts was taken into account.

5.2. PHASE SHIFT ANALYSIS

Earlier phase shift analysis of differential cross sections and excitation functions for elastic p^{6}Li scattering without taking into account the doublet ^2P wave has been performed in [118]. Our phase shift analysis is done at lower energies important for nuclear astrophysics and takes into account all lower partial waves, including the doublet ^2P wave. The analysis is based on differential cross sections given in [26,113] and [114].

At the energy 500 keV, based on data from [114], we found ^2S and ^4S scattering phase shifts given in Table 5.1 numbered 1. The obtained results of calculated cross sections quite agree with experimental data for the averaged over all points χ^2 = 0.15. The error of differential cross sections for this data was assumed equal to 10%. The account of the doublet ^2P and quartet ^4P phase shifts showed that their numerical values are smaller than 0.1°.

The next five energies correspond to the new results of measurement of differential cross sections performed in [26,113]. The first of them, 593 keV, provides the possibility of finding $^{2,4}S$ phase shifts, which slightly differ from phase shifts at the previous energy, possess the same χ^2, and are given in Table 5.1 numbered 2; the phase shifts for $^{2,4}P$ waves also tend toward zero.

At the energy 746.7 keV, we find $^{2,4}S$ phase shifts (Table 5.1, No. 3-1), which make possible to describe the cross sections with the accuracy $\chi^2 = 0.23$. In spite of the smallness of χ^2, the attempt to take into account $^{2,4}P$ phase shifts has been made. First it was assumed that the quartet ^4P phase shift is negligible, which follows from the results of [118], in which the account began from 1.0÷1.5 MeV. The results of our analysis taking into account the ^2P phase shift only are shown in Figure 5.1a and Table 5.1 numbered 3-2. It can be seen that taking into account the small doublet ^2P phase shift somewhat changes the value of the doublet ^2S phase shift, increasing its value, and decrising $\chi^2 = 0.16$. Taking into account the quartet ^4P phase shift yielded a negligible value, smaller than 0.1°, which completely agrees with the results of [118] and our results for energy 866.8 keV.

The result of a phase shift search for the energy 866.8 keV taking into account $^{2,4}S$ waves only is given in Table 5.1 No.4-1 for $\chi^2 = 0.39$. It can be seen that the value of the ^2S phase shift sharply drops comparing to the previous energy. The account of ^2P wave noticeably increases its value (Figure 5.1b and Table 5.1 No.4-2) and decreases the value of χ^2 by practically a factor 2. The attempt to take into account the quartet ^4P phase shift resulted in a value no higher than 0.1° (Table 5.1 No.4-3), which indicates a small contribution of this phase shift at this energy. Any increase of the ^4P wave, including for other values of the other phase shifts, resulted in the growth of χ^2. For this energy, as well as all other considered energies from [26,113], it is impossible to find any variant for nonzero quartet phase shift if χ^2 tends to minimum.

Table 5.1. Results of phase shift analysis of elastic p^{6}Li scattering

No	***E* (keV)**	**^2S (deg)**	**^4S (deg)**	**^2P (deg)**	**^4P (deg)**	**χ^2**
1	500	176.2	178.7	–	–	0.15
2	593.0	174.2	178.8	–	–	0.15
3-1	746.4	170.1	180.0	–	–	0.23
3-2	746.4	172.5	179.9	1.7	–	0.16
4-1	866.8	157.8	180.0	–	–	0.39
4-2	866.8	170.2	174.9	3.9	–	0.22
4-3	866.8	169.6	175.0	3.5	0.1	0.23
5-1	976.5	160.0	178.5	–	–	0.12
5-2	976.5	167.0	174.5	1.1	–	0.12
6-1	1136.3	144.9	180.0	–	–	0.58
6-2	1136.3	164.7	171.1	5.8	–	0.32
6-3	1136.3	166.4	169.9	5.5	0.1	0.32

For the next energy 976.5 keV, the values of the ^2S and ^4S phase shifts were found without considering $^{2,4}P$ waves (see Table 5.1 No.5-1). The subsequent account of ^2P wave noticeably increases the value of the ^2S phase shift if ^4P wave is neglected, as can be seen from Figure 5.1c and Table 5.1 No.5-2 for $\chi^2 = 0.12$. If the quartet ^4P wave is included in the analysis, it tends toward zero with decreasing χ^2.

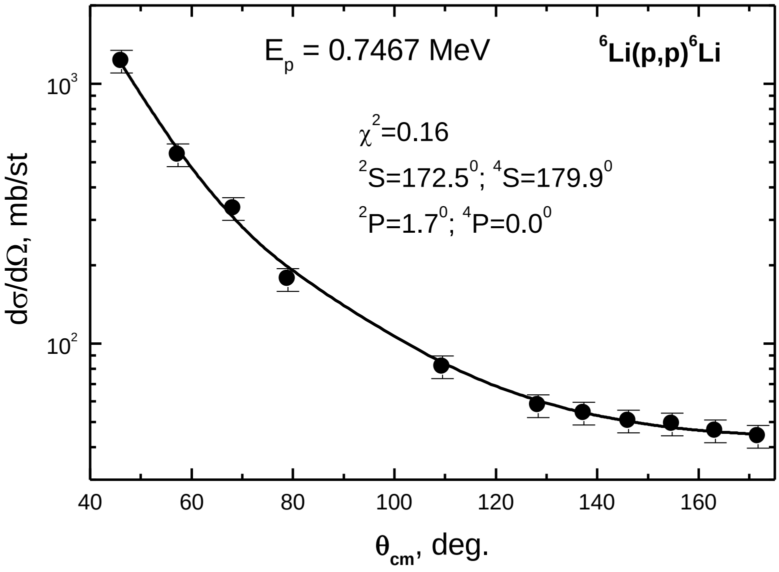

Figure 5.1a. Cross sections of elastic p^{6}Li scattering at 746.7 keV.

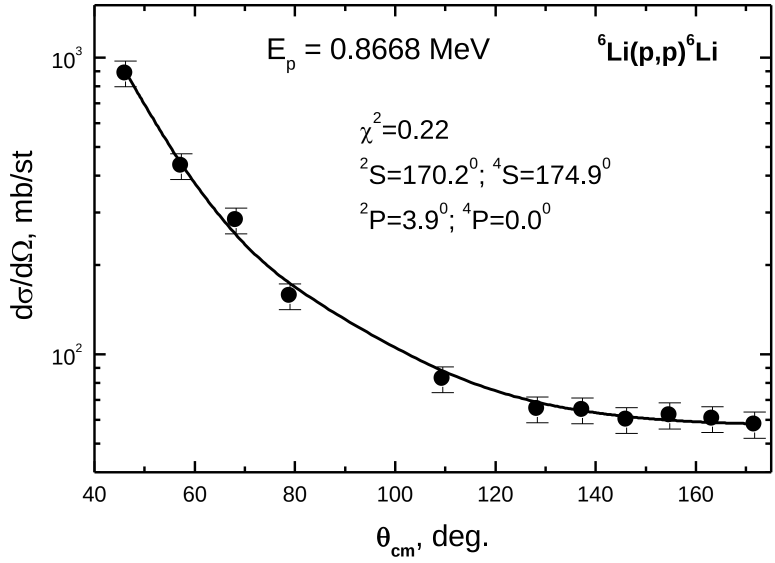

Figure 5.1b. Cross sections of elastic p^{6}Li scattering at 866.8 keV.

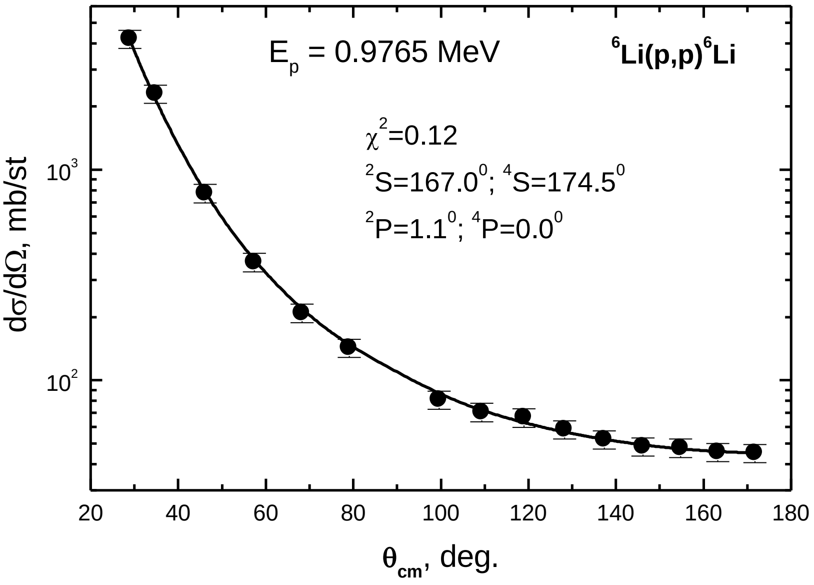

Figure 5.1c. Cross sections of elastic p^{6}Li scattering at 976.5 keV.

The last of the considered energies equal to 1.1363 MeV from [26,113], even with $^{2,4}S$ waves taken into account, only results in relatively low χ^2 equal to 0.58 (see Table 5.1 No.6-1).

In this case taking into account the ^2P wave results in a noticeable increase of the ^2S phase shift. The corresponding results for calculated cross section are shown in Figure 5.1d and in Table 5.1 No.6-2. The process of taking into account the quartet ^4P wave, at this energy too, leads to the value about 0.1°, as it is shown in Table 5.1 No.6-3.

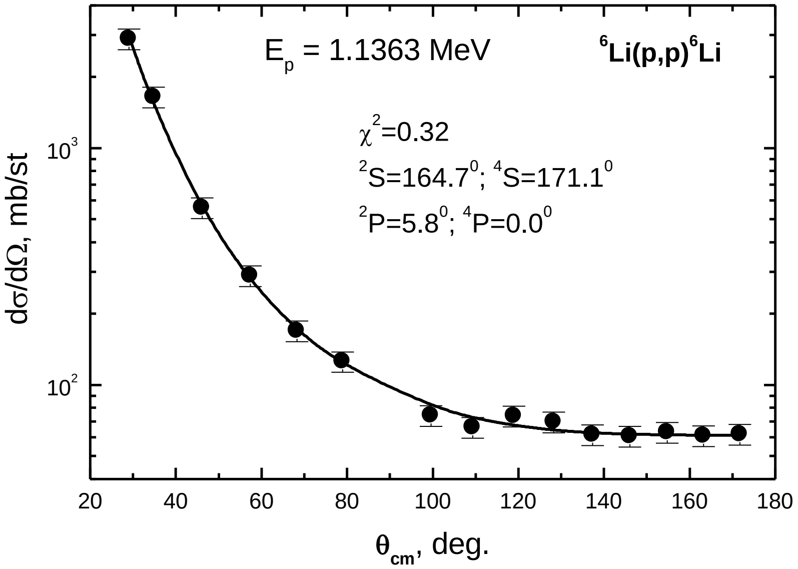

Figure 5.1d. Cross sections of elastic p^{6}Li scattering at 1136.3 keV.

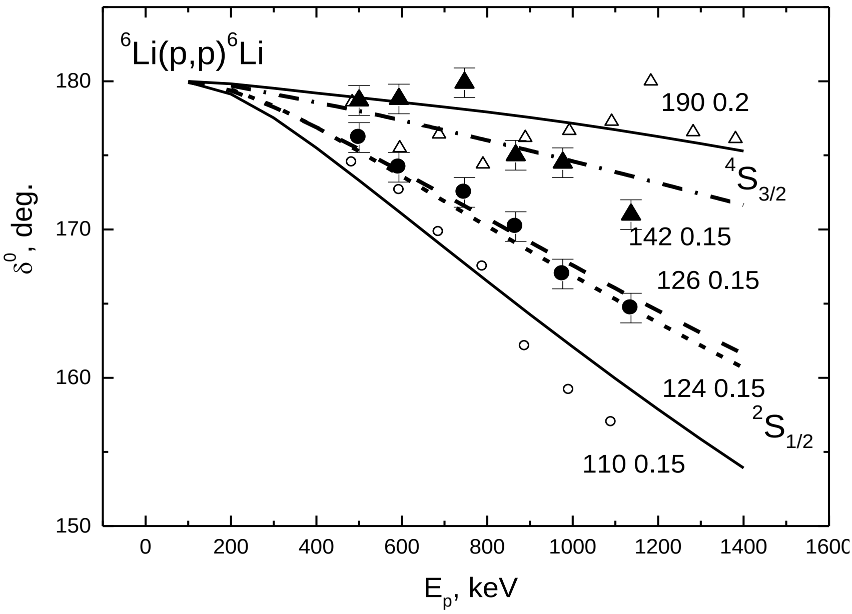

Figure 5.2a. Doublet and quartet *S* phase shifts of elastic p^{6}Li scattering at low energies. Doublet and quartet *S* phase shifts in the presence of the ^2P wave are given when the ^4P phase shift is equal to zero. ^2S (points) and ^4S (triangles) phase shifts are obtained according to data [26,113,114]. Upward open triangles and open circles show results of phase shift analysis [118] for comparison. Lines show results of calculation with different potentials.

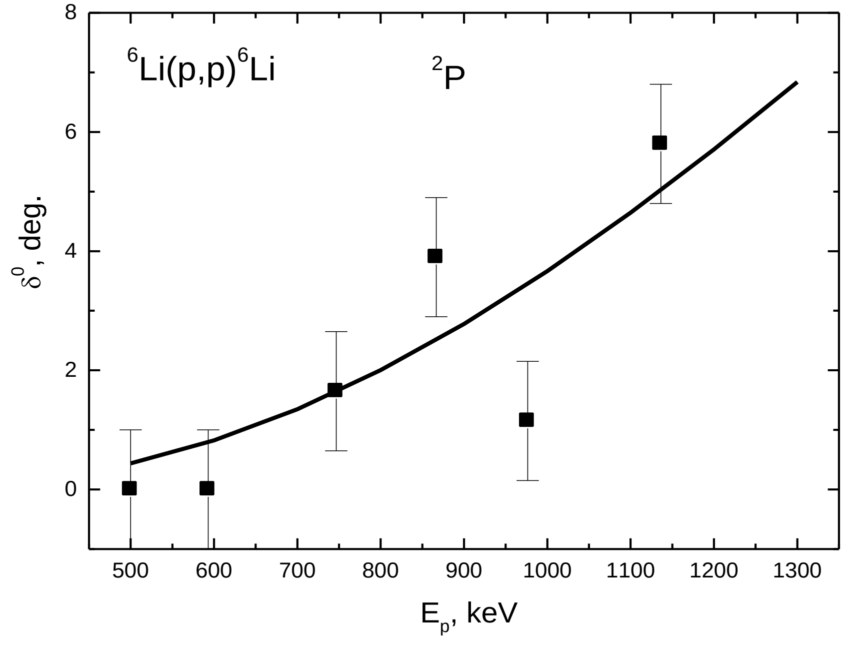

Figure 5.2b. Doublet ^2P phase shifts of elastic p^{6}Li scattering at low energies. Squares show the results of our phase shift analysis for ^4P = 0. The solid line shows the result of calculation with the found potential.

Thus, for description of all experimental data from [26,113], it is not necessary to take into account quartet ^4P waves in this energy region, i.e., their value is equal to or smaller than 0.1°. On the whole, this agrees with the results of [118]; however, the doublet ^2P phase shift reaches almost 5.5°÷6° and cannot be neglected.

The general form of the ^2S and ^4S scattering phase shifts is shown in Figure 5.2a, and that of the doublet ^2P phase shift is shown in Figure 5.2b. In spite of the rather large spread of results for ^4S phase shifts, the doublet ^2S phase shift has a certain tendency toward a smaller magnitude, but this takes place much more slowly than it follows from results of analysis [118], in which the ^2P wave was not taken into account. If the doublet ^2P wave is not taken into account in our analysis, results very close to the resulting phase shift in [118] obtained for the ^2S phase shift.

The errors of elastic scattering phase shifts are determined by the ambiguity of phase shift analysis, namely, for virtually the same value of χ^2, it is possible to obtain somewhat different magnitudes of scattering phase shifts. We estimate this ambiguity on a level 1°÷1.5°; this is shown for $^{2,4}S$ and ^2P phase shifts in Figures 5.2a and 5.2b.

5.3. CLUSTER STATES CLASSIFICATION

The possible orbital Young schemes in p^{6}Li system turn out to be forbidden, if the scheme {6} forbidden for ^{2}H^{4}He in ^{6}Li is used. They correspond to the forbidden states with {7} and {61} configurations and the relative moment L = 0 and 1, which evaluates by the Elliot rule [119]. The forbidding of such diagrams for wave functions follows from the requirement of Littlewood's theorem that it can not be more than four cells in one row of Young scheme for 1*p*-shell nuclei [119].

When the allowed scheme {42} in the ^{2}H^{4}He cluster channel of ^{6}Li is accepted, then, for the complete system p^{6}Li, for spin $S = 1/2$ there is the forbidden level with the scheme {52} and moments one and two, and there are forbidden states with {43} and {421} configurations for L = 1. Thus, the p^{6}Li potentials ought to have forbidden bound {52} state in *S* wave and allowed bound level in *P* wave with two Young schemes {43} and {421}. Only one scheme {421} is allowed in the quartet spin state of this system, as it was shown in Table 5.2.

It is possible that, for the bound states of ^{6}Li nucleus, it is more correct to consider both acceptable schemes {6} and {42}, since both of them are included to the number of forbidden and allowed states of the ^{2}He^{4}He configuration. Then the level classification will be slightly different, the number of forbidden states will increase, and additional forbidden bound level will be added in the each partial wave with L = 0 and 1.

This, more complete, scheme of states also listed in Table 5.2, and intrinsically it is the sum of first and second cases, considered above. In Table 5.2 the complete spin $\{f\}_S$ and isospin $\{f\}_T$ Young schemes of ^{7}Be nucleus in the p^{6}Li channel, their production $\{f\}_{ST}$, and all possible orbital $\{f\}_L$ symmetries of the p^{6}Li system, which are divided into allowed $\{f\}_{AS}$ and forbidden $\{f\}_{FS}$ schemes with the orbital moment L.

As it is seen from this table, there are two allowed schemes {43} and {421} in the doublet spin state of the p^{6}Li system and then scattering states are mixed according to the orbital symmetries. At the same time, one generally consider that for the doublet GS of ^{7}Be nucleus in the p^{6}Li channel with $J = 3/2^-$ и $L = 1$ corresponds only one allowed scheme {43} [116].

The considered p^{6}Li system is completely analogous to the p^{2}H channel in ^{3}He nucleus, which doublet state is also mixed according to the Young schemes {3} and {21}. Therefore, the potentials, which are constructed on the base of the phase shifts of the elastic scattering description in the p^{6}Li system can not use for the description of the GS of ^{7}Be in the p^{6}Li channel.

Table 5.2. The classification of the orbital states in p^{6}Li and n^{6}Li systems. Here: *T*, *S* and *L* are, respectively, the isospin, spin and orbital moment of particles in the p^{6}Li system; $\{f\}_S$, $\{f\}_T$, $\{f\}_{ST}$ and $\{f\}_L$ are, respectively, the spin, isospin, spin-isospin and possible orbital Young schemes; $\{f\}_{AS}$ and $\{f\}_{FS}$ are the Young schemes of allowed and forbidden states, respectively. The conjugate schemes $\{f\}_{ST}$ and $\{f\}_L$ are shown in boldface italic font

System	*T*	*S*	$\{f\}_T$	$\{f\}_S$	$\{f\}_{ST} = \{f\}_S \otimes \{f\}_T$	$\{f\}_L$	*L*	$\{f\}_{AS}$	$\{f\}_{FS}$
n^{6}Li p^{6}Li	1/2	1/2	{43}	{43}	{7}+{61}+{52}+{511}+{43}+ +{421}+{4111}+{322}+ ***{3211}***+ + ***{2221}***+{331}	{7}	0	–	{7}
						{61}	1	–	{61}
						{52}	0,2	–	{52}
						{43}	1,3	{43}	–
						{421}	1,2	{421}	–
		3/2	{43}	{52}	{61}+{52}+{511}+{43}+ +2{421}+{331}+{322}+***{3211}***	{7}	0	–	{7}
						{61}	1	–	{61}
						{52}	0,2	–	{52}
						{43}	1,3	–	{43}
						{421}	1,2	{421}	–

In this case, the phase shifts of the p^{6}Li elastic scattering as well as p^{2}H system (2.11) are represented as the half-sum of the “pure” phase shifts [20,25].

$$\delta_L^{\{43\}+\{421\}} = 1/2\delta_L^{\{43\}} + 1/2\delta_L^{\{421\}}.$$

The mixed phase shifts are determined as a result of the phase shift analysis of the experimental data, which are, generally, differential cross sections of the elastic scattering or excitation functions. Then, it is supposed [20,25] that it is possible to use the phase shifts, of the same symmetry from the quartet channel, as the {421} pure phase shifts of the doublet channel. As a result, it is possible to find the {43} pure doublet phase shifts for the p^{6}Li scattering and use these phase shifts for the construction the pure interaction, which should correspond to the potential of the bound state of the p^{6}Li system in ^{7}Be nucleus [20,25].

5.4. POTENTIAL DESCRIPTION OF THE SCATTERING PHASE SHIFTS

For obtaining partial intercluster p^{6}Li interactions using available scattering phase shifts, we use the common Gaussian potential with a point-like Coulomb term that can be represented in form (2.8). The following potential parameters were obtained upon description of results of phase shift analysis from [118]:

^2S: V_0 = –110 MeV, α = 0.15 fm^{-2},
^4S: V_0 = –190 MeV, α = 0.2 fm^{-2}.

The obtained potentials contain two forbidden bound states corresponding to Young schemes {52} and {7} [2,116]. The results of phase shift calculation for these potentials are shown in Figure 5.2a by solid lines together with the results of phase shift analysis from [118] which shown by circles and open triangles.

For description of the obtained scattering phase shifts, the potentials with the parameters

^2S: V_0 = –126 MeV, α = 0.15 fm^{-2},
^4S: V_0 = –142 MeV, α = 0.15 fm^{-2}

are preferable.

These potentials also contain two forbidden bound states each with Young schemes {52} and {7}. The phase shifts calculated with these potentials are shown in Figure 5.2a by dashed and dot-dashed lines, in comparison with the results of our phase shift analysis shown by points and triangles.

The potential for the doublet ^2P wave of the elastic p^{6}Li scattering can be represented, for example, by the following parameters:

^2P: V_0 = –68.0 MeV, α = 0.1 fm^{-2}.

The solid line in Figure 5.2b shows the results of calculation of phase shifts with this potential, which has one forbidden bound state with Young scheme {61} and allowed state with Young schemes {43} and {421}.

This potential erroneously represents the binding energy of ^{7}Be in the p^{6}Li channel because this allowed state turns out to be mixed with respect to the two above symmetries, while the ground bound state corresponds only to the scheme {43} [116,117]. Even if the methods, for obtaining the pure phase shifts presented in [116,117], are used it is impossible to obtain a potential of the ground state which is pure according to Young schemes. This is probably due to low clusterization probability of ^{7}Be nucleus in the p^{6}Li channel, which value has the essential role using the abovementioned methods.

Therefore, $^2P_{3/2}$ wave potential of the ground state of ^{7}Be that was pure according to orbital symmetries with Young scheme {43} was constructed in such a way that the channel energy, i.e., the binding energy of the ground state of the nucleus with $J = 3/2^-$ as p^{6}Li system and its mean square radius, were described well. The thus-obtained parameters of the pure $^2P_{3/2}^{\{43\}}$ potential are as follows:

$$^2P_{3/2}\text{: } V_0 = -252.914744 \text{ MeV}, \ \alpha = 0.25 \text{ fm}^{-2}. \qquad (5.5)$$

This potential in the framework of the finite-difference method yields the binding energy of an allowed state with Young scheme {43} equal to –5.605800 MeV for an experimental value of –5.6058 MeV [120] and has one forbidden state corresponding to Young scheme {61}. The mean square charge radius turns out to be equal to 2.63 fm, what in the whole agrees with the data of [120], and the constant C_W from (2.10) in an interval 5÷13 fm is equal to 2.66(1).

For the parameters of ${}^2P_{1/2}^{\{43\}}$ potential of the first excited state of ^{7}Be with $J = 1/2^-$, the following values were obtained:

$$^2P_{1/2}\text{: } V_0 = -251.029127 \text{ MeV}, \alpha = 0{,}25 \text{ fm}^{-2}. \tag{5.6}$$

This potential results in a binding energy of –5.176700 MeV for an experimental value of –5.1767 MeV [120] and contains the forbidden state with scheme {61}. Asymptotic constant (2.10) in an interval 5÷13 fm is equal to 2.53(1), and the mean square charge radius is equal to 2.64 fm. The absolute accuracy of finding the energy of bound levels of p^{6}Li system in ^{7}Be nucleus for our new programs was determined to be equal to 10^{-6} MeV.

The parameters of potentials of bound states obtained here somewhat differ from our previous results [116]. This is connected with the use of precise values of particle masses and more accurate description of the experimental values of energy levels [120].

The variational method, used for controlling of the accuracy of determination of the binding energy, yielded a value –5.605797 MeV for the energy of the ground state, and as we noted in section three, for this potential the mean binding energy obtained by two methods is –5.6057985(15) MeV. Therefore, the accuracy of calculation of the binding energy, obtained by two different methods and by two different programs, is equal to ±1.5 eV. The asymptotic constant in the interval 5÷13 fm turned out to be relatively stable and equals 2.67(2), and the mean square charge radius coincided with the results of the finite-difference method.

Table 5.3. Variational parameters and expansion coefficients of the radial wave function of the ground bound state of the p^{6}Li system in ^{7}Be for $^2P_{3/2}$ potential (5.5). Normalization of the function with these coefficients in an interval 0÷25 fm is N= 0.9999999999999895

i	β_i	C_i
1	2.477181344627947E–002	1.315463702527344E–003
2	5.874061769072439E–002	1.819913407984276E–002
3	1.277190608958812E–001	9.837541674753882E–002
4	2.556552559403827E–001	3.090018297080802E–001
5	6.962545656024610E–001	–1.195304944694753
6	87.215179556255360	3.237908749007494E–003
7	20.660304078047520	5.006096657700867E–003
8	1.037788131786810	–6.280751485496025E–001
9	2.768782138965186	1.282309968994793E–002
10	6.753591325944827	8.152343478073063E–003

The variational wave function of form (2.9) for the ground state of ^{7}Be in p^{7}Li channel with potential (5.5) is given in Table 5.3, and the residual WF value does not exceed 10^{-12}.

Table 5.4. Variational parameters and expansion coefficients of the radial wave function of the first excited bound state of the p^{6}Li system in ^{7}Be for $^2P_{1/2}$ potential (5.6). Normalization of the function with these coefficients on an interval of 0÷25 fm is N = 0.9999999999999462

i	β$_i$	C$_i$
1	2.337027900191992E–002	1.218101547601343E–003
2	5.560733180673633E–002	1.653319276756672E–002
3	1.214721917930904E–001	9.009619752334307E–002
4	2.474544878067495E–001	3.003291466882630E–001
5	7.132725465249825E–001	–1.332325501226168
6	84.896023494945160	3.273725679869025E–003
7	1.162854732120233	–5.340018423135894E–001
8	1.574203000936825	9.367648737801053E–002
9	5.779896847077723	1.033713941440747E–002
10	19.422905786572090	5.314592946045428E–003

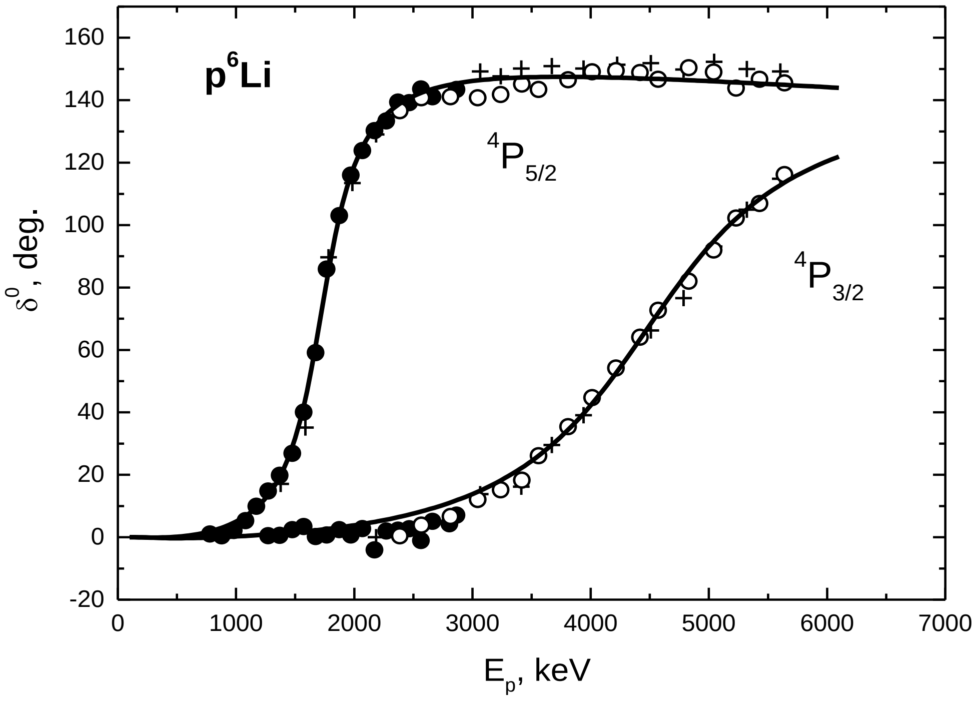

Figure 5.3a. Quartet ^4P phase shifts of elastic p^{6}Li scattering. Points, circles, and crosses show the results of phase shift analysis [118]. Solid lines show the results of calculation with the obtained potentials.

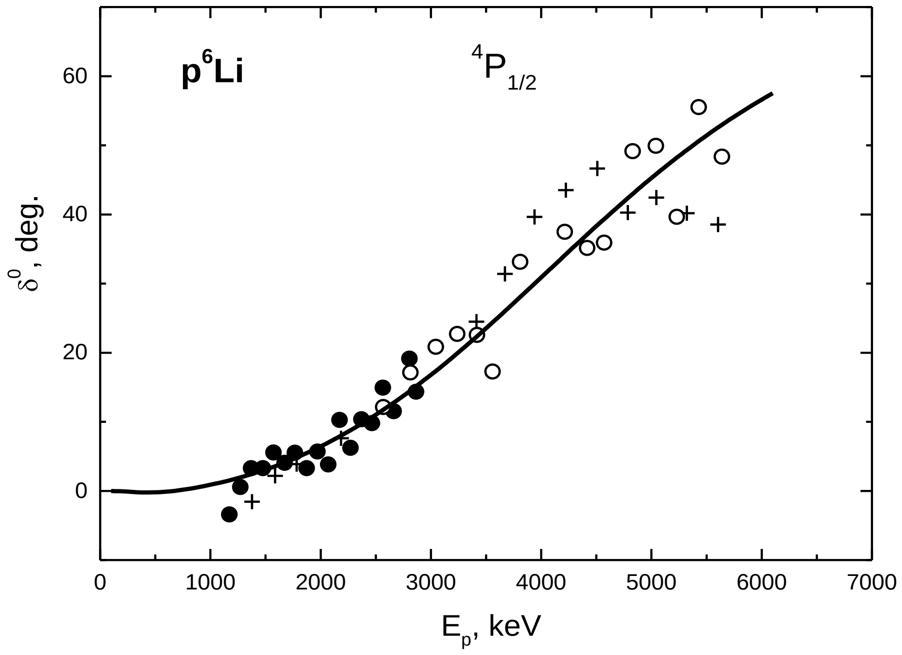

Figure 5.3b. Quartet ^4P phase shifts of elastic p^{6}Li scattering. Points, circles, and crosses show the results of phase shift analysis [118]. The solid line shows the result of calculation with the found potential.

The variational method yielded an energy –5.176697 MeV for the first excited level; therefore, the average energy is equal to –5.1766985(15) MeV with the same accuracy for both methods as for the ground state. The asymptotic constant in an interval 5÷13 fm is about 2.53(2), the residual is no larger than 10^{-12}, and the mean square charge radius almost does not differ from the corresponding value for the ground state. The parameters of the wave function (2.9) of excited state of ^{7}Be nucleus in the p^{6}Li channel for potential (5.6) are given in Table 5.4.

Let us present the parameters of potentials describing the quartet ^4P elastic scattering phase shifts from [118],

$^4P_{1/2}$: $V_0 = -802.0$ MeV, $\alpha = 0.5$ fm^{-2},
$^4P_{3/2}$: $V_0 = -4476.0$ MeV, $\alpha = 2.65$ fm^{-2},
$^4P_{5/2}$: $V_0 = -1959.0$ MeV, $\alpha = 1.15$ fm^{-2}.

The quality of phase shift description using these potentials is illustrated in Figures 5.3a and 5.3b. The potentials contain two forbidden bound states each corresponding to the forbidden, in the quartet spin channel, Young schemes {61} and {43}.

It should be noted that, based on the results for the doublet ^2P scattering phase shift shown in Figure 5.2b obtained in this phase shift analysis, it is impossible to construct an unambiguous ^2P potential. For this purpose, results of analysis at higher energies are necessary and they should be obtained taking into account the ^2P wave and spin-orbital splitting of phase shifts.

5.5. ASTROPHYSICAL S-FACTOR

Upon examination of the astrophysical *S*-factor, *E*1 transitions from the ^2S and ^2D scattering states to the ground $^2P_{3/2}$ and the first excited $^2P_{1/2}$ bound states of ^{7}Be nucleus in p^{6}Li channel have been taken into account. The wave function of the ^2D scattering state without account being taken of spin-orbital splitting has been calculated based on the ^2S potential with the orbital angular moment $L = 2$.

The results of calculations showed that the above ^2S scattering potential based on phase shift analysis [118] with a depth 110 MeV strongly underestimates the astrophysical *S*-factor. At the same time, the doublet ^2S potential with a depth 126 MeV following from our results correctly reproduces the general behavior of the experimental *S*-factor. The obtained results are shown in Figure 5.4. The dashed line shows the result for the transition from ^2S and ^2D scattering waves to the ground state of ^{7}Be nucleus, the dotted line shows the results for the transitions to the first excited state, and the solid line shows the total *S*-factor. Points, triangles, and circles show experimental data from [121] given in [122].

The calculated *S*-factor for 10 keV has the values $S(3/2^-) = 76$ eV b and $S(1/2^-) = 38$ eV b for a total value 114 eV b. The obtained $S(1/2^-)$-factor quite well describes the experimental data for transition to the first excited state of ^{7}Be at low energies (circles in Figure 5.4).

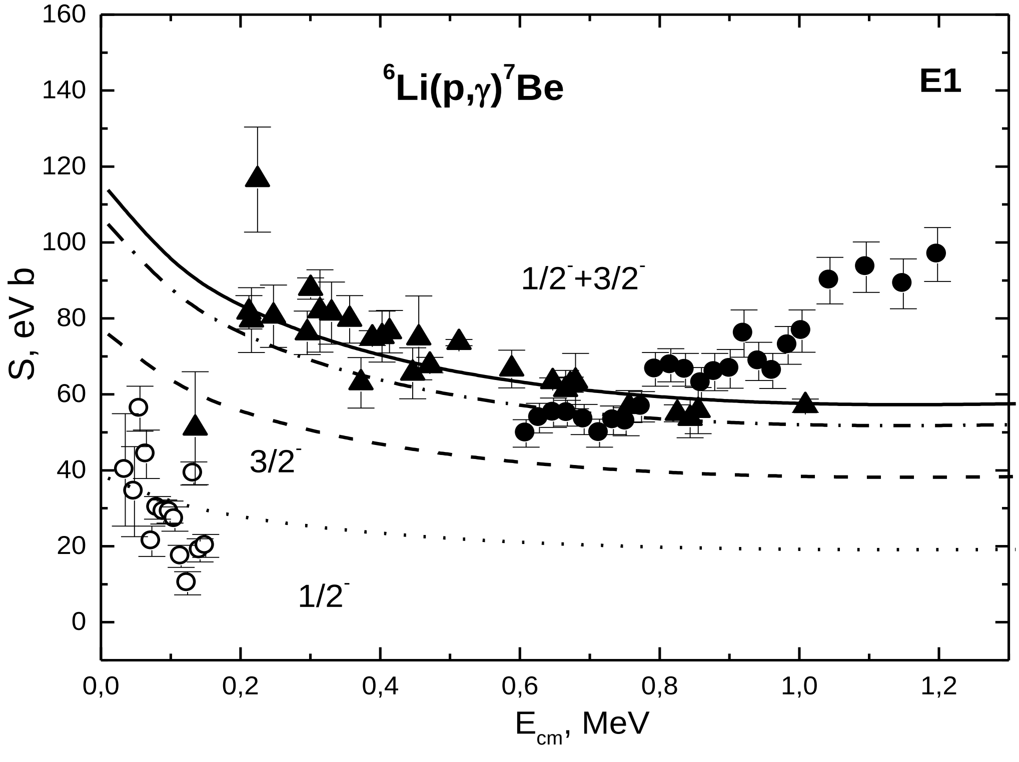

Figure 5.4. Astrophysical *S*-factor of radiative p^{6}Li capture. Points, triangles, and circles show experimental data [121] given in [122]. The dashed line shows the result for transitions from ^2S and ^2D scattering waves to the ground state of ^{7}Be nucleus and the dotted line for transitions to the first excited state. The solid line shows the total *S*-factor.

For comparison of the calculated *S*-factor at zero energy (an energy 10 keV is taken as zero), we present the known results for the total *S*(0) factor: 79(18) [123], 105 (at 10 keV) [122], and 106 eV b [124]. For the *S*-factor in the case of transition to the ground state, a value 39 eV b is given in [125], and for transition to the first excited state, 26 eV b; therefore, the total *S*-factor is equal to 65 eV b. It can be seen that there exists a rather large difference in the data and our results, on the whole, agree with the available data.

Moreover, a slight change of the depth of ^2S scattering potential, which virtually has no impact on the behavior of calculated phases, rather strongly influences the *S*-factor. For example, for the potential depth equal to 124 MeV, the phases are shown in Figure 5.2a by short-dashed lines, and for energy 10 keV we obtain 105 eV b for the *S*-factor, that is in a good agreement with the latest experimental data [122,123]. The total *S*-factor with this potential is shown in Figure 5.4 by a dash-dotted line, which agrees within error with the experimental data at energies below 1 MeV.

It should be noted that, if potentials without forbidden states or with another number of these states are used in *S* and *P* waves, the calculated value of the *S*-factor turns out to be essentially smaller than the values obtained earlier. For example, the ^2S potential with one forbidden state and the parameters 25 MeV and 0.15 fm^{-2}, which quite well describes scattering phase shifts, and the potential of the ground state presented above yield for 10 keV an *S*-factor approximately is equal to 1 eV b.

CONCLUSION

Thereby, the phase shift analysis of new experimental data of the elastic p^{6}Li scattering was done for obtaining of intercluster potentials. Then, the potentials of intercluster interaction for continuous spectrum were constructed on the base of obtained phase shifts of scattering. These potentials are mixed according to Young schemes and contain forbidden states, in what connection each partial wave is described by its own potential of the Gaussian form with certain parameters. The potentials pure according to Young schemes were used for the description of the bound states of ^{7}Be; they describe its main characteristics and, first of all, the binding energy.

Thus, the doublet ^2S phase shifts obtained in our phase shift analysis that take into account the doublet ^2P phase shift result in a potential that, unlike interaction constructed based on the results of analysis [118], provides a description of the experimental *S*-factor at the energies below 1 MeV. Similarly to the case of lighter nuclei [108], the applied potential cluster model with the above potentials makes it possible to obtain quite reasonable results for the description of the p^{6}Li radiative capture in the astrophysical energy region [126,127].

Chapter 6

S-FACTOR OF THE P^{7}LI RADIATIVE CAPTURE

INTRODUCTION

The reaction of radiative capture

$p + {}^7\mathrm{Li} \rightarrow {}^8\mathrm{Be} + \gamma$

at ultralow energies resulting in formation of unstable ^{8}Be nucleus which decays into two α-particles may take place along with the weak process

${}^7\mathrm{Be} + e^- \rightarrow {}^7\mathrm{Li} + \gamma + \nu_e$,

as one of the final reactions of the proton-proton chain [2]. Therefore the in-depth study of this reaction, in particular of the form and energy dependence of the astrophysical *S*-factor, is of a certain interest for the nuclear astrophysics.

To calculate the astrophysical *S*-factor of radiative p^{7}Li capture in the potential cluster model [20,25] which we usually use for such calculations [108,128] it is necessary to know partial potentials of p^{7}Li interaction in the continuous and discrete spectra. We will again assume that such potentials should follow the classification of cluster states by orbital symmetries [25] as it was assumed in our earlier works [47,59,127] and in previous sections of this book, for other nuclear systems.

Let us note, that in the using approach, the potentials of scattering processes are usually constructed on the basis of description of elastic scattering phase shifts obtained from experimental data while the interactions in bound states are determined by the requirement to reproduce the main characteristics of the bound state of the nucleus assuming that it is mainly due to cluster channel consisting of the input particles of the reaction under consideration.

For example, in the radiative capture process the ^{2}H^{4}He particles colliding at low energies form ^{6}Li nucleus in the ground state and the remaining energy is released as a γ-quantum. Since there is no restructuring in such reactions we can consider potentials of one and the same nuclear system of particles that is the ^{2}H^{4}He system in continuous and discrete spectra. In the latter case it is assumed that the ground state of ^{6}Li is very likely caused by the cluster ^{2}H^{4}He configuration. Such approach leads to quite reasonable results of the description of the astrophysical *S*-factors of this and some other reactions of radiative capture [129].

It seems that in this case ^{8}Be nucleus does not consist of cluster p^{7}Li system and most probably is determined by the ^{4}He^{4}He configuration into which it decays. However, one may suppose that after the radiative p^{7}Li capture ^{8}Be nucleus can stay for a time as bound p^{7}Li configuration with the following decay into unbound ^{4}He^{4}He state. Such an assumption makes it possible to consider ^{8}Be nucleus as the cluster p^{7}Li system and use the PCM methods, at least at the initial stage of its formation in the reaction p + ^{7}Li → ^{8}Be + γ [84].

6.1. CLASSIFICATION OF THE ORBITAL STATES

First, we would like to note that the p^{7}Li system has the $T_z = 0$ isospin projection and it is possible for two values of total isospin $T = 1$ and 0 [131], therefore p^{7}Li channel is mixed by isospin as p^{3}H system [108], even though as it will be shown later both of isospin states (T = 1,0), in contrast to p^{3}H system, in the triplet spin state correspond to the allowed Young scheme {431} [20]. The cluster channels p^{7}Be and n^{7}Li with $T_z = \pm 1$ and $T = 1$ are pure by isospin in a complete analogy with the p^{3}He and n^{3}H systems [108].

The spin-isospin Young schemes of ^{8}Be nucleus for the p^{7}Li channel are the product of spin and isospin parts of the WF. Particularly, under consideration of any of these moments we will have {44} scheme at the ground state of ^{8}Be nucleus with the moment equals zero, scheme {53} for a certain state with moment equals one and for the state with moment equals two – {62} symmetry form. In the first case, moments of four nucleons are directed to the opposite side to other four nucleons and the total moment of the system of eight nucleons is equal to zero.

In the second case, moments of five nucleons are directed to the one side but three nucleons to another, as a result two nucleons remain not compensated and their total moment equals one. The last variant presents moments of six nucleons directed to one side and two nucleons to other side, four nucleons are not compensated and the total moment equals two.

If the scheme {7} is used for ^{7}Li nucleus then possible Young schemes of p^{7}Li system turn out to be forbidden, because of the rule that there can not be more than four cells in a row [117,119], and they correspond to forbidden states with configurations {8} and {71} and relative motion moments (orbital angular moment) $L = 0$ and 1, which is determined by Elliot rule [119]. The p^{7}Li system, in the triplet spin state, contains forbidden states with the scheme {53} in P_1 wave and {44} in S_1 wave and allowed state with the configuration {431} at $L = 1$ when the scheme {431} is accepted for ^{7}Li [86].

Thus, the p^{7}Li potentials in the different partial waves should have the forbidden bound state {44} in the S_1 wave and forbidden and allowed bound levels in the P_1 wave with schemes {53} and {431}, respectively. The considered classification is true for any isospin state of the p^{7}Li system (T = 0 or 1) in triplet spin channel. Allowed symmetries are absent for spin $S = 2$ and all Young schemes listed above correspond to forbidden states, as it was shown in Table 6.1.

Probably, as it was in a previous case for the p^{6}Li system, it is more correctly to consider both allowed schemes {7} and {43} for bound states of ^{7}Li because of the fact that they are present in FS and AS in the ^{3}H^{4}He configuration of this nucleus [129]. Then the level classification will be slightly different, the number of forbidden states will increase and an extra forbidden state will appear in each partial wave. Such more complete scheme of FS and

AS states, per se, is a sum of the first and the second cases considered above is listed in Table 6.1.

Table 6.1. The classification of the orbital states in p^7Li (n^7Be) systems for isospin $T = 0$ and 1. Here: T, S and L are, respectively, the isospin, spin and orbital moment of p^7Li system; $\{f\}_S$, $\{f\}_T$, $\{f\}_{ST}$ and $\{f\}_L$ are, respectively, the spin, isospin, spin-isospin and possible orbital Young schemes; $\{f\}_{AS}$ and $\{f\}_{FS}$ are the Young schemes of, respectively, allowed and forbidden states.The conjugate schemes are shown in boldface italic font

System	*T*	*S*	$\{f\}_T$	$\{f\}_S$	$\{f\}_{ST} = \{f\}_S\otimes\{f\}_T$	$\{f\}_L$	*L*	$\{f\}_{AS}$	$\{f\}_{FS}$
p^7Li n^7Be	0	1	{44}	{53}	{71}+{611}+{53}+{521}+ +{431}+{4211}+{332}+***{3221}***	{8} {71} {53} {44} ***{431}***	0 1 1,3 0,2,4 1,2,3	– – – – {431}	{8} {71} {53} {44} –
		2	{44}	{62}	{62}+{521}+{44}+{431}+ +{422}+{3311}	{8} {71} {53} {44} {431}	0 1 1,3 0,2,4 1,2,3	– – – – –	{8} {71} {53} {44} {431}
p^7Be n^7Li p^7Li n^7Be	1	1	{53}	{53}	{8}+2{62}+{71}+{611}+{53}+ +{44}+2{521}+{5111}+{44}+ +{332}+2{431}+2{422}+ +{4211}+{3311}+***{3221}***	{8} {71} {53} {44} ***{431}***	0 1 1,3 0,2,4 1,2,3	– – – – {431}	{8} {71} {53} {44} –
		2	{53}	{62}	{71}+{62}+{611}+2{53}+ +2{521}+2{431}+{422}+ +{4211}+{332}	{8} {71} {53} {44} {431}	0 1 1,3 0,2,4 1,2,3	– – – – –	{8} {71} {53} {44} {431}

6.2. POTENTIAL DESCRIPTION OF THE PHASE SHIFTS OF SCATTERING

Because of the isospin mixing the phase shifts of the p^7Li elastic scattering are represented as a half-sum of the isospin pure phase shifts (4.1) [20,25]

$$\delta_L\left(T=1,0\right)=1/2\delta_L\left(T=0\right)+1/2\delta_L\left(T=1\right)$$

in complete analogy with the p^3H system. The phase shifts with $T = 1,0$ mixed by isospin are usually determined as a result of the phase shift analysis of the experimental data of differential cross sections of the elastic scattering or excitation function. The pure phase shifts with isospin $T = 1$ are determined from the phase shift analysis of the p^7Be or n^7Li elastic scattering. As a result it is possible to find pure p^7Li phase shifts of scattering with $T = 0$ and construct the interaction model using these results which have to correspond to the potential of the bound state of the p^{7}Li system in ^{8}Be nucleus [20]. Just the same method of phase shift separation was used for the p^{3}H system [25] and its absolute validity was shown [108].

However, we failed to find experimental data of differential cross sections or phase shifts of the p^{7}Be or n^{7}Li elastic scattering at astrophysical energies [132], so here we will consider only isospin-mixed potentials of the elastic scattering processes in the p^{7}Li system and pure potentials of the bound state with $T = 0$ which are constructed on the base of description BS characteristics and are chosen in the Gaussian form with point-like Coulomb term (2.8). The phase shifts of the p^{7}Li elastic scattering obtained from the phase shift analysis of the experimental data of excitation functions [133] taking into account spin-orbital splitting at the energies down to 2.5 MeV are given in the work [134]. These phases, which are shown by points and squares in Figures 6.1 and 6.2, we will use later for the intercluster potential construction for the p^{7}Li elastic scattering in S_1 and P_1 waves.

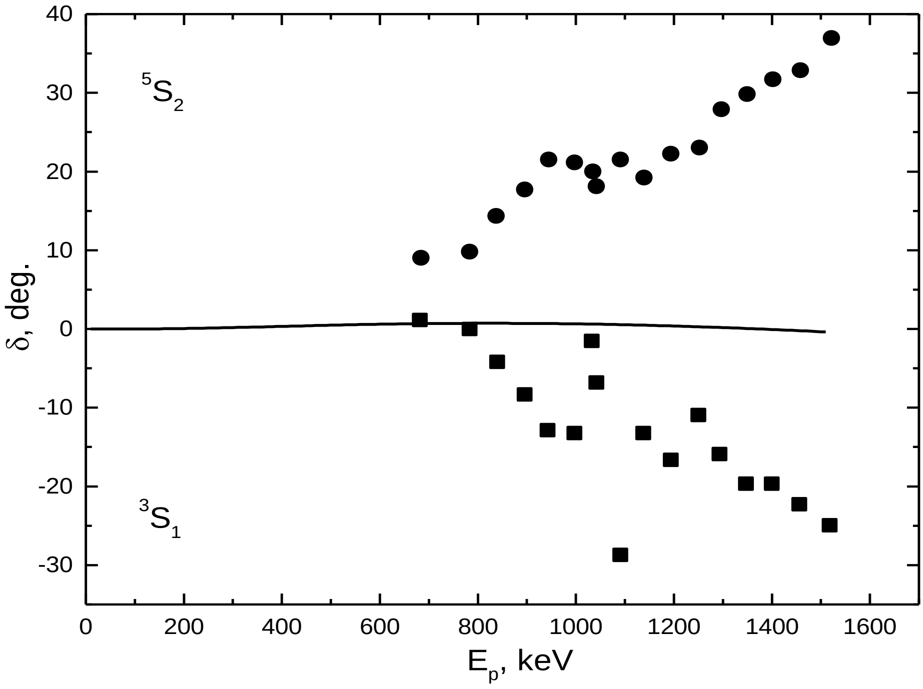

Figure 6.1. $^3S_1$ and $^5S_2$ phase shifts of the elastic p^{7}Li scattering at low energies. Points and squares – phase shifts obtained from the experimental data [134]. Line – calculations with the Gaussian potential based on parameters given in the text.

One can see in Figure 6.1 that S_1 phase shift practically equals zero in the range from 0 to 800 keV, then it rapidly drops and at 1500 keV approximately equals –25°. Since later we will consider the low and astrophysical energy range only, then we will limit the energy range from 0 keV to 800 keV. Practically zero phase shift at these energies is obtained with the potential of the form (2.8) and parameters:

$V_0 = –147.0$ MeV, $\alpha = 0.15$ fm^{-2}.

Such potential contains two FS as it follows from the state classification given in Table 6.1, and the calculation results of S_1 phase shift are shown in Figure 6.1 by the solid line. Of course, S_1 phase shift at about zero one can obtain from the other variants of potential parameters with two FS. In this regard it is not possible to fix its parameters unambiguously and the other combinations of V_0 and α are possible. However, this potential, as the above potential, should have comparatively large width, what gives small phase shift change when the energy changes in the range from 0 to 800 keV.

There is an over-threshold level in the P_1 wave with the energy 17.640 MeV and $J^\pi T = 1^+1$ or 0.441 MeV in laboratory system (lab. sys.) which is above the threshold of the cluster p^{7}Li channel in the ^{8}Be nucleus, with the bound energy of this channel being –17.2551 MeV [131]. The 0.441 MeV level has very small width of only 12.2(5) keV [131] for the p^{7}Li → ^{8}Beγ radiative capture reaction and p^{7}Li elastic scattering. Such a narrow level leads to the sharp rise of the P_1 phase shift of elastic scattering which should be mixed by spin states $^5P_1$ and $^3P_1$ [134] for the total moment $J = 1$.

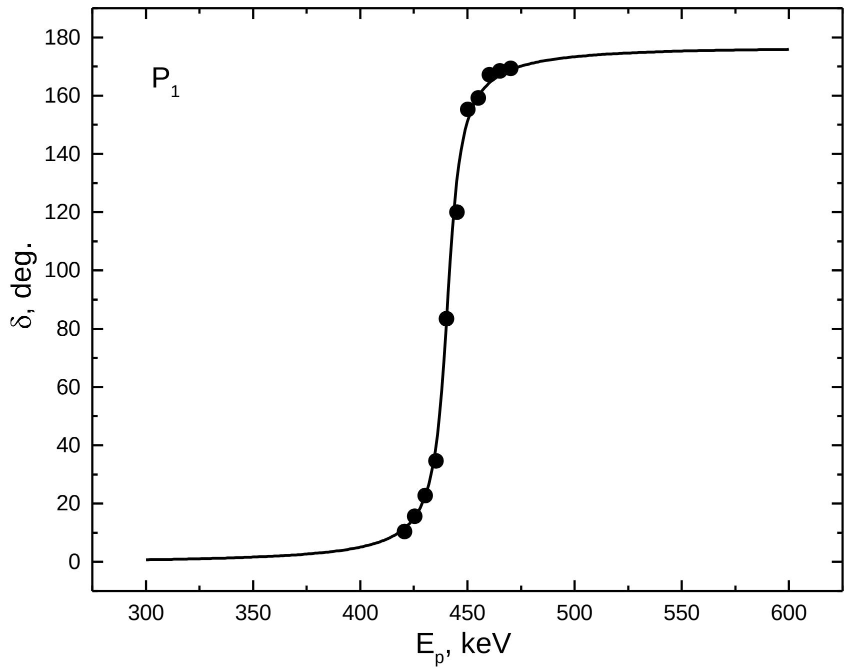

Figure 6.2. $^5P_1$ phase shift, which mixed with $^3P_1$ phase shift, for the elastic p^{7}Li scattering at low energies. Points – phase shifts obtained from the experimental data [134]. Line – calculations with the Gaussian potential based on parameters given in the text.

The phase shift, which is shown by points in Figure 6.2 [134], is described by the Gaussian potential (2.8) with parameters:

$V_0 = –5862.43$ MeV, $\alpha = 3.5$ fm^{-2}.

This potential, mixed by isospin $T = 0$ and 1, has two FS according to Table 6.1 and the calculation results of the P_1 phase shift of the elastic scattering are shown in Figure 6.2 with a solid line. The potential parameters which describe the P_1 phase shift are fixed quite unambiguously at the interval of sharp increase obtained from the experimental data and the potential itself should have very small width.

Since, later we will consider astrophysical *S*-factor only at the energies from 0 to 800 keV, it can be deemed that both of the potentials obtained above give a good description of the results of the phase shift analysis for two considered partial waves in this energy range [134].

The following parameters of the bound $^3P_0$ state potential for the p^{7}Li system corresponding to the ground state of ^{8}Be nucleus in the examined cluster channel are obtained:

$$V_0 = –433.937674 \text{ MeV}, \ \alpha = 0.2 \text{ fm}^{-2}.$$

The bound energy -17.255100 MeV with the accuracy 10^{-6} MeV, the mean square radius is equal to 2.5 fm and the asymptotic constant, calculated with the help of Whittaker functions (2.10), equals C_W = 12.4(1) were obtained with such a potential. The error of the constant is estimated by its averaging in the range 6÷10 fm where the asymptotic constant is practically stable. In addition to the allowed BS corresponding to the ground state of ^{8}Be nucleus such *P* potential has two FS in total correspondence with the classification of orbital cluster states given in Table 6.1.

It seems that the mean square radius of ^{8}Be nucleus in the p^{7}Li cluster channel should not differ a lot from ^{7}Li radius which equals 2.35(10) fm [120], since the nucleus is in a strongly bound (~ –17 MeV) i.e. compact state. Moreover, at such bound energy ^{7}Li nucleus itself can be in deformed, compressed form as it is for deuteron in ^{3}He nucleus [108]. Therefore, the value of the mean square radius for the p^{7}Li channel in the GS of ^{8}Be nucleus obtained above has quite a reasonable value.

The variational method with the expansion of the cluster wave function of the p^{7}Li system in non-orthogonal Gaussian basis [20] is used for an additional control of the accuracy of bound energy calculations and the energy –17.255098 MeV with *N* = 10 order of matrix were obtained for this potential which differ from the above finite-difference value by 2 eV only.

Residuals [24] are of the order of 10^{-11}, asymptotic constant at the range 5÷10 fm equals 12.3(2), the charge radius does not differ from previous results. Expansion parameters of the obtained variational GS radial wave function of ^{8}Be nucleus in the p^{7}Li cluster channel are listed in Table 6.2.

As it was told before, the variational energy decreases as the dimension of the basis increases and gives the upper limit of the true bound energy, but the finite-difference energy increases as the size of steps decreases and the number of steps increases [24], therefore it is possible to use the average value –17.255099(1) MeV for the real bound energy in this potential. Thus, the calculation error of the bound energy of ^{8}Be nucleus in the cluster p^{7}Li channel using two different methods is about ±1 eV.

Our computer program, based on the finite-difference method [24], was changed for carrying out these calculations, as it was in other cases, for earlier considered cluster systems. This program has been rewritten in Fortran-90, which made it possible to essentially increase the rate and accuracy of all calculations, for example, for determining the binding energy in two-body channel. Now, the absolute accuracy of finding the energy of bound states of the p^{7}Li system in the ^{8}Be nucleus is equal to 10^{-6} MeV. The accuracy of finding the root of the determinant equals 10^{-14} and the value of Wronskian of Coulomb wave functions for continuous spectrum, determined the accuracy of finding of the phase shifts of scattering, is not worse than 10^{-15}.

Table 6.2. Variational parameters and expansion coefficients of the radial wave function in the form (2.9) of the ground state of ^{8}Be nucleus in the p^{7}Li channel in non-orthogonal Gaussian basis [20]. Normalization of the function with these coefficients on an interval 0÷25 fm is N = 1.000000000000001

i	β_i	C_i
1	1.140370098659333E–001	–9.035361688615057E–002
2	5.441057961629589E–002	–5.552214961281388E–003
3	2.200385338662954E–001	–4.776382639167991E–001
4	5.657244883872561E–001	3.790054587274382
5	9.613849915820404E–001	–2.409004172680931
6	1.216602174819119	–3.280156202364487
7	4.797601726001004	2.475815245412750E–002
8	14.137444509612200	1.070215776034501E–002
9	45.160915627598030	6.119172187062497E–003
10	191.081716320368200	3.950399055271339E–003

6.3. ASTROPHYSICAL S-FACTOR

While considering electromagnetic transitions we will take into account the $E1$ process from the $^3S_1$ wave of scattering (see Figure 6.1) to the ground bound state of the ^{8}Be nucleus in the cluster p^{7}Li channel with $J^\pi T = 0^+0$ and the $M1$ transition from the P_1 wave of scattering (see Figure 6.2) also to the GS of the nucleus.

Cross sections of the $E1$ transition from the $^3D_1$ wave of scattering (with potential for the $^3S_1$ wave at $L = 2$) to the GS of the ^{8}Be nucleus are by 2÷4 orders lower than from the $^3S_1$-wave transition at the energy range 0÷800 keV. Furthermore, we will consider only S-factor for the transition to the ground state of the ^{8}Be nucleus i.e. the reaction: $^7\mathrm{Li}(p,\gamma_0)^8\mathrm{Be}$. One of the last experimental measurements of the S-factor of this reaction in the energy range from 100 keV to 1.5 MeV was made in the work [135].

The standard expressions (2.4)÷(2.6) are used for the S-factor calculations. Values: μ_p = 2.792847 [35] and $\mu(^7\mathrm{Li})$ = 3.256427 [136] are accepted for the magnetic moment of proton and ^{7}Li nucleus. The expression in square brackets (2.6) for $A_1(M1,K)$ is obtained in assumption that the summation by r_i is done in the general form for spin part of magnetic operator [36], i.e. by centre mass coordinates of clusters, before operating to the expression in parentheses $(r_i^J Y_{Jm}(\Omega_i))$ by ∇ operator, what leads to the reduction of r_i power [34]. If, at first, we use ∇ operator towards the expression in these brackets, then we obtain $A_1(M1,K)$ for $M1$

$$A(K) = \frac{e\hbar}{m_0 c} K\sqrt{3}\left[\mu_1 + \mu_2\right] \ . \tag{6.1}$$

Since the astrophysical *S*-factor of the considered reaction at the resonance energy completely depends on the value of *M*1 transition, so this reaction may be a certain test for the correctness of expressions (2.6) or (6.1).

The calculation results for the astrophysical *S*-factor with the above potentials at the energy range 5÷800 keV (lab. sys.) are shown in Figure 6.3. The *E*1 transition is shown by the dashed line, dotted line – *M*1 process, solid line – the sum of these processes. The shown results, obtained on the base of the expression (2.6), argue in favor of this approach, although the given conclusions will be absolutely correct only in the case 100% clusterization of ^{8}Be nucleus in the cluster p^{7}Li channel. In the considered reaction the *M*1 transition like the *E*1 transition in the p^{3}H system [108] goes with change of the isospin $\Delta T = 1$, since the ground state of ^{8}Be nucleus has $T = 0$ and resonance isospin in the P_1 wave of scattering equals 1.

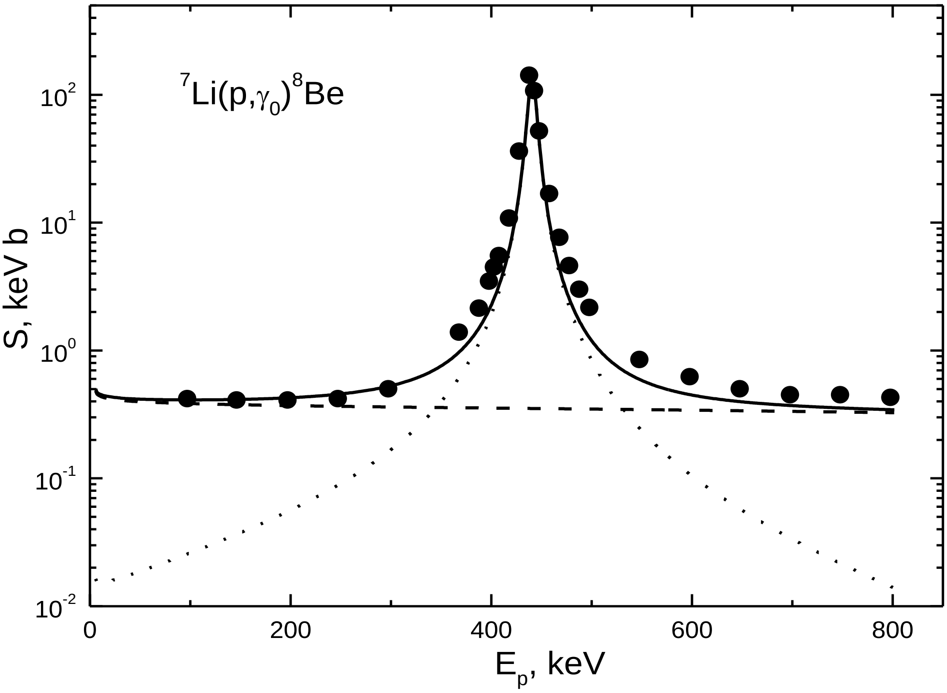

Figure 6.3. Astrophysical *S*-factor of the reaction of p^{7}Li radiative capture. Dots – experimental data [135]. Lines – calculation results for different electromagnetic transitions with the potentials mentioned in the text.

The value 0.50 keV b was obtained for the astrophysical *S*-factor at 5 keV (c.m.) for the transition to GS of ^{8}Be nucleus, where the *E*1 process gives the value 0.48 keV b, which is in a good agreement what the data from [135]. The calculated and experimental [135] *S*-factor values at the energy range 5÷300 keV (lab. sys.) are given in Table 6.3.

Table 6.3. Calculated astrophysical *S*-factor of p^{7}Li radiative capture reaction at low energies and its comparison with the experimental data [135]

E_{lab} (keV)	S_{exp} (keV b) [135]	S_{E1} (keV b)	S_{M1} (keV b)	S_{E1+M1} (keV b)
5,7	–	0,48	0,02	0,50
29,7	–	0,41	0,02	0,43
60,6	–	0,39	0,02	0,41
98,3	0,41(3)	0,39	0,03	0,42
198,3	0.40(2)	0,37	0,06	0,43
298,6	0.49(2)	0,36	0,16	0,52

As it seen from Figure 6.3 and Table 6.3, the value of the theoretical *S*-factor in the energy range 30÷200 keV is almost constant and approximately equal to 0.41÷0.43 keV b, what agrees with data [135] for the energy range 100÷200 keV practically within the experimental errors.

Let us compare some extrapolation results of different experimental data to zero energy. The value 0.25(5) keV b was obtained in work [125] and the value 0.40(3) keV b in work [137] on the basis of data [135]. Then in work [138] on the basis of new measurements of the total cross sections of ^{7}Li(p,γ_0)^{8}Be reaction in the energy range 40÷100 keV the value 0.50(7) keV b was suggested which is in a good agreement with the obtained above value at the energy 5 keV.

It is interesting to look at the chronology of different works for determination of the astrophysical *S*-factor of the ^{7}Li(p,γ_0)^{8}Be reaction. It was believed in 1992 that its value equals 0.25(5) keV b [125], the value 0.40(3) keV b [137] was obtained in 1997 on the basis of measurements made in 1995 [135] and the measurements in 1999 at lower energies led to the value 0.50(7) keV b [138]. This chronology demonstrates well the constant increase (notably double) of the value obtained for the astrophysical *S*-factor for ^{7}Li(p,γ_0)^{8}Be reaction (two fold increase) as the energy of experimental measurements decreased, and it seems that this value can undergo a visible change in the earlier future.

CONCLUSION

Thus, $E1$ and $M1$ transitions from $^3S_1$ and $^{3\text{-}5}P_1$ waves of scattering to the ground bound state in the p^{7}Li channel of ^{8}Be nucleus were considered in the potential cluster model. It is possible to completely describe present day experimental data for the astrophysical *S*-factor at the energies up to 800 keV taking into account certain assumptions concerning the channel restructuring in ^{8}Be nucleus and to obtain its value for zero (5 keV) energy, which is in a good agreement with the latest experimental measurements.

Chapter 7

RADIATIVE CAPTURE IN THE P^{9}BE SYSTEM

INTRODUCTION

Let us consider p^{9}Be → ^{10}Bγ reaction in the astrophysical energy range in the potential cluster model with splitting of orbital states according to Young schemes and, in some cases, with forbidden states. We should note that we managed to find only one work devoted to a detailed experimental measurement of cross sections and astrophysical *S*-factor for this reaction [139] at low energies. We will use the results of this work later for comparison with our model calculations.

The knowledge of p^{9}Be interaction potentials in continuous and discrete spectrum is required for the calculation of the astrophysical *S*-factor of radiative p^{9}Be capture in the PCM [20,25] which we usually used for the analysis of similar reactions [108,128]. Again we will consider that such potentials should correspond to the classification of cluster states according to orbital symmetries [20,25], as it was assumed earlier for other light nuclear systems.

7.1. CLASSIFICATION OF THE ORBITAL STATES

First, we define the orbital Young schemes of ^{9}Be nucleus considering it, for example, in the p^{8}Li or n^{8}Be channel. If we assume that it is possible to use schemes {44} + {1} in the 8 + 1 system, then two possible symmetries: {54} + {441} are obtained for this system. The first of them is forbidden because it contains five cells in one matrix row [119].

We note, promptly, that the given classification of orbital states according to Young schemes has qualitative character, because there is no table of Young schemes products for the system with A = 9,10 particles, though they exist for all systems with A < 9 [44] and they are used for the analysis of the number of allowed and forbidden states in wave functions of different cluster systems [87].

Further, if the scheme {54} is used for ^{9}Be nucleus then possible Young schemes of p^{9}Be system turn out to be forbidden, because of the rule that it can not be more than four cells in one row [119,140]. They are corresponded to forbidden states with configurations {64}, {55} and relative motion moments L = 0 and 1, which is determined by Elliot rule [119]. Another forbidden scheme {541} is present in this product as in the examined case too and correspond to L = 1.

When the scheme {441} is accepted for ^{9}Be nucleus, the p^{9}Be system contains forbidden sates with {541} scheme in the *P* wave and {442} in the *S* wave and AS with {4411} configuration with $L = 1,3$. Thus the p^{9}Be potentials in different partial waves should have forbidden bound {442} state in the *S* wave and forbidden and allowed bound levels in the *P* wave with {541} and {4411} Young schemes, respectively.

We can examine the case when for ^{9}Be nucleus both possible orbital Young schemes {54} and {441} are used. We used the same approach quite successfully earlier for consideration of the p^{6}Li [113] and p^{7}Li [130] systems. Then the level classification will be slightly different – the number of forbidden states will increase and an additional forbidden bound level will appear in every partial wave with $L = 0$ and 1.

Such a more complete scheme of states, which we will use later, equals the sum of the first and the second cases considered above and there are two FS in *S* and *P* waves with allowed states in the *P* wave. One of them – the $^5P_3$ state – can correspond to the ground state of ^{10}B nucleus in the p^{9}Be channel.

7.2. POTENTIAL DESCRIPTION OF THE SCATTERING PHASE SHIFTS

The considered p^{9}Be channel in ^{10}B nucleus has the isospin projection equal to $T_z = 0$, which is possible with two values of the total isospin $T = 1$ and 0 [131], so the p^{9}Be system, as well as p^{3}H [108], turn out to be isospin-mixed. In this case the cluster p^{9}Be and n^{9}Be channels with $T_z = \pm 1$ and $T = 1$ are isospin-pure in a complete analogy with p^{3}He and n^{3}H systems [108]. Phase shifts of the elastic p^{9}Be scattering are represented as a half-sum of pure in isospin phase shifts [20,25] because this system is isospin-mixed, as it was given above in section 4.1 (4.1).

The isospin-mixed phase shifts with $T = 1,0$ are derived from the phase shift analysis of experimental data, which is usually the differential cross sections of the elastic p^{9}Be scattering. Pure phase shifts with isospin $T = 1$ are obtained from the phase shift analysis of the p^{9}Be or n^{9}Be elastic scattering. As a result one can find pure $T = 0$ phase shifts for the p^{9}Be scattering and construct the interaction potential which should correspond to the potential of the bound state of the p^{9}Be system in ^{10}B nucleus [131]. Just the same method of splitting of phase shifts and potentials was used for the p^{3}H system [90,108] and has demonstrated its total availability.

However, we have not found the data on phase shifts for n^{9}Be, p^{9}B and p^{9}Be elastic scattering at astrophysical energies [132], so we will consider only isospin-mixed potentials of the scattering processes in the p^{9}Be system and pure potentials for bound states with $T = 0$ which are usually constructed on the basis of the description of BS characteristics – bound energy, charge radius, asymptotic constant. Exactly the same approach we used earlier for the p^{6}Li and p^{7}Li systems and the potential is selected in a simple Gaussian form with a point-like Coulomb term (2.8).

Since we don't have the phases of p^{9}Be elastic scattering obtained from the phase shift analysis of experimental data, we will only rely on the purely qualitative views about their behavior as an energy function. It is known in particular that there is $J = 1^-$ over threshold level with $T = 0+1$, energy 0.319(5) MeV (lab. sys.) and 133 keV width [131,141]. This resonance state can be formed by the $^3S_1$ configuration in the p^{9}Be channel of ^{10}B nucleus because $J(^9\text{Be}) = 3/2^-$ and $J(\text{p}) = 1/2^+$. The presence of such a level leads to the resonance of the phase shift which equals 90° at this energy.

However, the resonance of the *S*-factor measured in [139] is observed at the energy 299 keV (lab. sys.) which is listed in Table 1 and Figure 4 from work [139]. At the same time the value 0.380(30) MeV (lab. sys.) with the width 330(30) keV is given for the resonance energy in Table 2 from work [139]. Both of these values do not correspond to the well-known data [131,141]. That is why an additional analysis of the experimental results was carried out in later works [142,143] and the values 328÷329 keV (lab. sys.) with the width 155÷161 keV were obtained for the energy of this level, which slightly differs from data of [131,141].

Since there is a large difference between various data, we slightly variational parameters of this potential to obtaine the best description of the *S*-factor resonance location given in work [139]. As a result, the potential of the $^3S_1$ wave of scattering was obtained, which gives the phase shift resonance at 333 keV (lab. sys.) and has the following parameters:

$$V_0 = –69.5 \text{ MeV}, \alpha = 0.058 \text{ fm}^{-2}.$$

The triplet $^3S_1$ phase shift of this potential is shown in Figure 7.1 by a solid line and has a resonance nature, while the potential itself contains two FS in accordance with the above classification.

If we use the expression for calculation of the level width scattering δ phase shift of [78]

$$\Gamma_{\text{lab}} = 2(d\delta/dE_{\text{lab}})^{-1},$$

then the width of such resonance approximately equals 150(3) keV (lab. sys.), which is in a complete agreement with the results [142,143].

Further, we assume that the $^5S_2$ phase shift almost vanishes to zero at the energy range up to 600 keV which will be considered here because there are no such levels in ^{10}B spectra comparable to this partial wave at these energies [131,141]. Practically zero phase shift is obtained with the Gaussian potential and parameters

$$V_0 = –283.5 \text{ MeV}, \alpha = 0.3 \text{ fm}^{-2}.$$

It contains two FS as it follows from the classification of orbital states given earlier. The phase shift of scattering is shown in Figure 7.1 by the dashed line. Of course, it is possible to obtain the $^5S_2$ phase shift in the vicinity of zero by using some other variants of potential parameters with two forbidden states.

In this regard it is not possible to fix potential parameters definitely and other combinations of V_0 and α are possible. However, additional calculations of the *E*1 transition from the elastic $^5S_2$ wave to the bound $^5P_3$ state have shown the weak dependence of the *S*-factor of the radiative p^{9}Be capture on the parameters of this potential.

The following parameters of the potential of the bound $^5P_3$ state of the p^{9}Be system corresponding to the ground state of ^{10}B nucleus in the cluster channel under consideration are obtained:

$$V_0 = –719.565645 \text{ MeV}, \alpha = 0.4 \text{ fm}^{-2}.$$

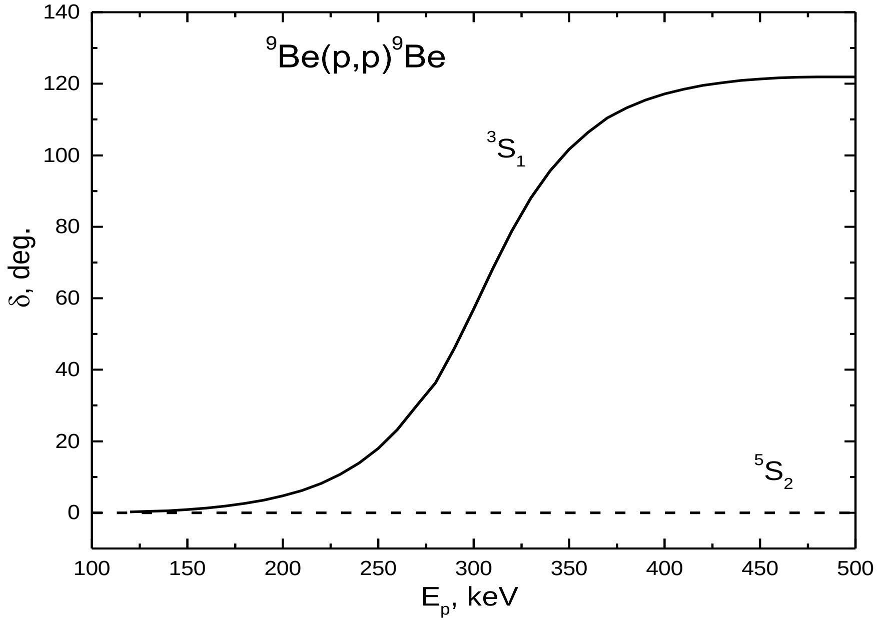

Figure 7.1. *S* phase shifts of the elastic p^{9}Be scattering at low energies. Lines – results obtained using Gaussian potentials with parameters which are given in the text.

With this potential we have obtained the bound energy –6.585900 MeV with the accuracy 10^{-6} MeV, the mean square radius is equal to 2.58 fm while the experimental value is 2.58(10) fm [131] and the asymptotic constant calculated by Whittaker functions equal to C_W = 2.94(1). Values R_p = 0.8768(69) fm [35] and R_{Be} = 2.519(12) fm [131] were used for cluster radii. The asymptotic constants C_W error is estimated by its averaging in the range 5÷15 fm where the asymptotic constant is practically stable. In addition to the allowed BS corresponding to the ground state of ^{10}B nucleus such *P* potential has two FS in complete correspondence with the classification of orbital cluster states which was given above.

For the purposes of comparison, we give the results from work [144] for AC where its value equals C_W = 2.37(2) fm$^{-1/2}$. It is necessary to note, that, in this work, we use this expression for the determination of the asymptotic constant:

$$\chi_L(R) = C_W W_{-\eta L+1/2}(2k_0 R) \ ,$$

which differs from our definition (2.10) by $\sqrt{2k_0}$ value. To bring these constants to a unified dimensionless form the results should be divided by $\sqrt{2k_0}$, where k_0 = 0.536 fm^{-1} for the p^{9}Be system. Then we obtain for AC in our definition the value 2.29, which substantially differs from the above result. However, if we take AC value obtained [144], the charge radius of ^{10}B nucleus will be somewhat underestimated because the “tail” of the wave function decreases more sharply.

The following parameters for the potentials of the first three excited states but not bound in p^{9}Be channel with $J^\pi T$ = 1^+0, 0^+1 and 1^+0 at the energies 0.71835, 1.74015 and 2.1543 MeV [131] were obtained:

$V_0(0.718350) = -715.162918$ MeV, $\alpha = 0.4$ fm^{-2},
$V_0(1.740150) = -708.661430$ MeV, $\alpha = 0.4$ fm^{-2},
$V_0(2.154300) = -705.935443$ MeV, $\alpha = 0.4$ fm^{-2}.

They describe precisely the values of energy levels given above and shown in brackets, which, relative to the p^{9}Be channel threshold, are equal to –5.867550, –4.845700 and –4.431600 MeV. They properly lead to charge radii 2.59, 2.60 and 2.61 fm, asymptotic constant 2.74(1), 2.46(1) and 2.35(1) in the range 4÷5 to 11÷13 fm and have two FS and one AS. It seems that these potentials correspond to the triplet ^3P bound levels in the p^{9}Be channels.

The variational method with the expansion of the cluster wave function of the p^{9}Be system in non-orthogonal Gaussian basis (2.9) is used for an additional control of the accuracy of bound energy calculations [24]. The GS energy of –6.585896 MeV was obtained for this potential with the order of matrix $N = 10$ which differs from the above finite-difference value [24] by 4 eV only.

Residuals have 10^{-11} order, asymptotic constant at the range 5÷10 fm equals 2.95(3), the charge radius does not differ from the previous results. Expansion parameters of the obtained variational GS radial wave function of ^{10}B nucleus in the p^{9}Be cluster channel are listed above in Table 7.1.

Table 7.1. The variational coefficients and expansion parameters of ^{10}B ground state radial WF for the p^{9}Be channel in non-orthogonal Gaussian basis [24]. The normalization coefficient of the wave function in the range 0÷25 fm equals N = 1.000000000000002

i	β_i	C_i
1	7.715930101739352E–002	–2.802002694398972E–002
2	3.224286905853033E–002	–2.092599791641983E–003
3	1.677117157858407E–001	–1.481060223206524E–001
4	3.388993785610822E–001	–5.049291144131660E–001
5	9.389553670123860E–001	4.713342588832875
6	1.999427899506135	–7.632712971301209
7	2.988529100669578	–5.267741895838846E–001
8	6.878703971128334	6.022748751134505E–002
9	23.149662023260950	2.252725100117285E–002
10	100.917699526293000	1.285655220977827E–002

As we repeatedly noted the variational energy decreases as the dimension of the basis increases and gives the upper limit of the true bound energy, but the finite-difference energy increases as the size of steps decreases and the number of steps increases [24]. Therefore, it is possible to use the average value of –6.585898(2) MeV for the real bound energy in this potential. Meanwhile, the calculation error of finding the bound energy of ^{10}B nucleus in the p^{9}Be cluster channel using two different methods is about ±2 eV.

In the frames of VM we obtained the value of energy equals –4.845692 MeV, charge radius 2.61 fm and AC is equal to 2.48(2) in the range 5÷12 fm for the potential of the second excited state. The expansion parameters of the WF in non-orthogonal Gaussian basis are listed in Table 7.2. The average energy value –4.845696(4) MeV is obtained for this level using two different methods and two different computer programs and residuals are of the order of 10^{-13}.

Table 7.2. Variational parameters and expansion coefficients of the 0^+1 state WF for ^{10}B nucleus at the energy 1.74015 MeV in non-orthogonal Gaussian basis [24]. The normalization coefficient of the wave function in the range 0÷25 fm equals *N* = 9.99999999999970E–001

i	β_i	C_i
1	6.669876139241313E–002	–2.347210794847986E–002
2	2.667656102033708E–002	–1.775040363036249E–003
3	1.517176918481825E–001	–1.283117981223353E–001
4	3.212149403864399E–001	–4.601647158129205E–001
5	9.260148198737874E–001	4.396116518097601
6	1.968143319382518	–7.091171845894630
7	2.891825315028276	–6.237051439471658E–001
8	6.205147839342107	6.217503950196968E–002
9	20.141061492467640	2.305215376077275E–002
10	86.640072856521640	1.321899076244325E–002

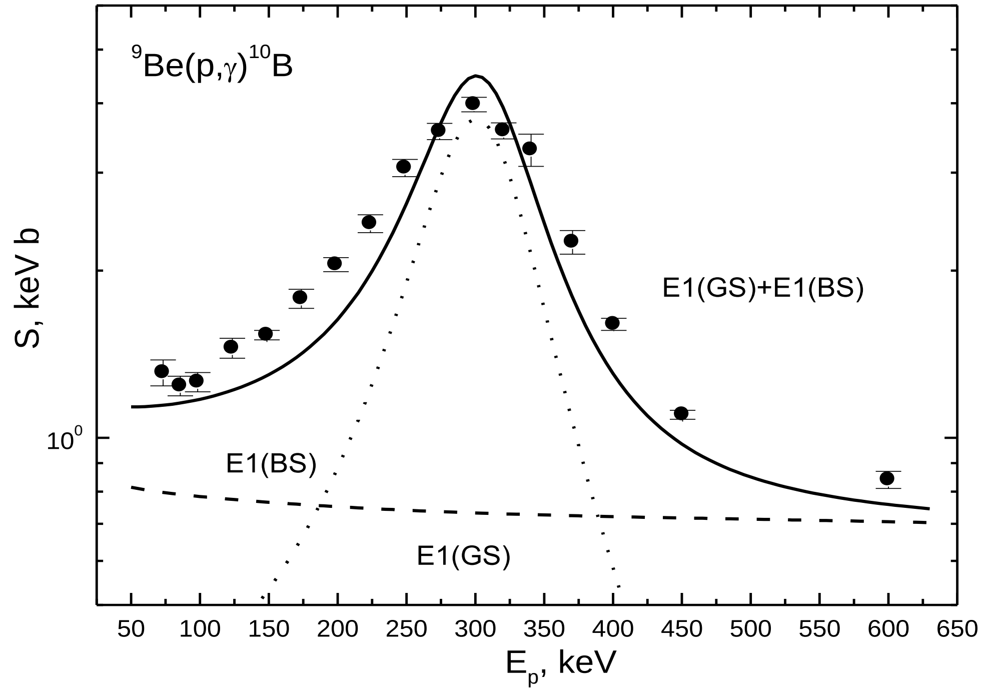

Figure 7.2. Astrophysical *S*-factor of the radiative capture p^{9}Be reaction. Dots – experimental data [139]. Lines – calculation results for different electromagnetic transitions with the potentials mentioned in the text.

7.3. ASTROPHYSICAL S-FACTOR

While considering electromagnetic transitions we will take into account the $E1$ process from the resonance $^3S_1$ wave of scattering to three bound states of the cluster p^9Be channel of ^{10}B nucleus (dotted line in Figure 7.2) with $J^\pi T = 1^+0$, 0^+1 and 1^+0 [131] denoting them as ^3P states, as well as the $E1$ transition from the $^5S_2$ wave of scattering with zero phase shift to the ground bound $^5P_3$ state of this nucleus denoting it as $E1$.

The calculation results and experimental data for the S-factor in the energy range 50÷600 keV (lab. sys.) from work [139] are shown in Figure 7.2 by the solid line. Obviously, the value of the total calculated S-factor in the energy range 50÷100 keV remains almost constant and equals 1.15(2) keV b, which is in quite a good agreement with the data from [139], where the average of the first three experimental points at the energy 70÷100 keV equals 1.27(4) keV b.

The transition to the ground $^5P_3$ state of ^{10}B nucleus from the $^5S_2$ scattering wave leads to the value 0.81 keV b for the calculated S-factor at the energy 50 keV (dashed line in Figure 7.2). Line extrapolation of the obtained result to zero energy gives 0.90÷0.95 keV b. The sum of transitions from the $^3S_1$ scattering wave to three bound ^3P levels is shown in Figure 7.2 by the dotted line.

For comparison we will give some extrapolation results to zero energy for different experimental data. For instance, for the S-factor with transition to the GS the value 0.92 keV b was obtained [125], which is in complete agreement with the value obtained here. However, the values 1.4 keV b, 1.4 keV b and 0.47 keV b are given for the transitions to the three levels considered above with $J^\pi T = 1^+0$, 0^+1 and 1^+0 respectively [125] and their sum evidently exceeds our result and data from [139].

Further, the value 0.96(2) keV b for the total S-factor was obtained in the later work [142] and the value from 0.96(6) to 1.00(6) keV b was found in one of the latest works [143] devoted to this reaction. Both of these values are in good agreement with the values obtained above.

CONCLUSION

Thus, the $E1$ transitions from $^5S_2$ and $^3S_1$ waves of scattering to the ground bound $^5P_3$ state in the p^9Be channel of ^{10}B and its three excited states 1^+0, 0^+1 and 1^+0 also bound in this channel are considered in the potential cluster model. Having made certain assumptions of common character about interactions in the p^9Be channel of ^{10}B it is possible to describe well the existing experimental data of the astrophysical S-factor at the energy range down to 600 keV and to obtain its value for zero (50 keV) energy which is in complete agreement with the latest experimental data [139]. The $S(0)$-factor for the transition to GS of ^{10}B is obtained quite correctly, too.

However, the scattering potentials are built on the basis of some qualitative conceptions because of the absence of the data for the phase shift analysis of p^9Be elastic scattering and three BS potentials are obtained only approximately because of the absence of data on the radii and AC of ^{10}B nucleus in these excited states.

Therefore, these results should be considered only as a preliminary estimate of the possibility to describe the astrophysical *S*-factor of the reaction under consideration on the basis of the PCM with FS. But it is possible to obtain quite acceptable results for the astrophysical *S*-factor in spite of approximate consideration of the $p^9Be \rightarrow {}^{10}B\gamma$ radiative capture process.

In conclusion, it should be mentioned that the available *S*-factor experimental data for this reaction differs significantly from each other and it seems that more accurate study of the $p^9Be \rightarrow {}^{10}B\gamma$ radiative capture at astrophysical energy and more precise definition of the location of the resonance and its width in ${}^3S_1$ wave are required.

Chapter 8

RADIATIVE P^{12}C CAPTURE

INTRODUCTION

In this section we will consider the p^{12}C system and the process of proton radiative capture by ^{12}C nucleus at astrophysical energies. The new measurement of differential cross sections of the elastic p^{12}C scattering at energies from 200 keV up to 1.1 MeV (center-of-mass system) within the range 10°÷170° with 10% errors was carried out in works [27].

Further, the standard phase shift analysis made and the potential of *S*-state of p^{12}C system was reconstructed in this paper on the basis of these measurements [89], and then the astrophysical *S*-factor at the energies down to 20 keV was considered in the frame of potential cluster model.

Before we start describing the results obtained, we would like to note that this process is the first thermonuclear reaction of the CNO cycle which took place at a later stage of stellar evolution when partial hydrogen burning occurred. As the hydrogen is burned the core of the star starts appreciably compressing which results in the increase in pressure and temperature in the star and triggers along with the proton-proton cycle the next chain of thermonuclear processes, called CNO-cycle.

8.1. DIFFERENTIAL CROSS SECTIONS

Upon examination of elastic scattering in the system of particles of spins 0 and 1/2 we take into account spin-orbital splitting of phase shifts that takes place in nuclear systems of the N^{4}He, ^{3}H^{4}He, and p^{12}C type. In this case elastic scattering of nuclear particles is completely described by two independent spin amplitudes (*A* and *B*) and the cross section is represented as [45]

$$\frac{d\sigma(\theta)}{d\Omega} = |A(\theta)|^2 + |B(\theta)|^2 , \qquad (8.1)$$

where

$$A(\theta) = f_c(\theta) + \frac{1}{2ik}\sum_{L=0}^{\infty}\{(L+1)S_L^+ + LS_L^- - (2L+1)\}\exp(2i\sigma_L)P_L(Cos\theta) \ , \qquad (8.2)$$

$$B(\theta) = \frac{1}{2ik}\sum_{L=0}^{\infty}(S_L^+ - S_L^-)\exp(2i\sigma_L)P_L^1(Cos\theta) \ .$$

Here, $S_L^{\pm} = \eta_L^{\pm}\exp(2i\delta_L^{\pm})$ is the scattering matrix, $\eta^{\pm}{}_L$ are the inelasticity parameters, the signs “±” correspond to the total angular moment of the system $J = L \pm 1/2$, f_c is the Coulomb amplitude represented as

$$f_c(\theta) = -\left(\frac{\eta}{2kSin^2(\theta/2)}\right)\exp\{i\eta\ln[Sin^{-2}(\theta/2)] + 2i\sigma_0\} \ ,$$

$P_n^m(x)$ are the associated Legendre polynomials, η is the Coulomb parameter, μ is the reduced mass, k is the wave number of relative particle motion, $k^2 = \frac{2\mu E}{\hbar^2}$, and E is the energy of colliding particles in the center of mass system.

Vector polarization in elastic scattering of such particles can be expressed in terms of amplitudes A and B [45],

$$P(\theta) = \frac{2\,\mathrm{Im}(AB^*)}{|A|^2 + |B|^2} \ . \qquad (8.3)$$

Developing definition for $B(\Theta)$ amplitude (8.2) we obtain the next expression

$$\mathrm{Re}\,B = \frac{1}{2k}\sum_{L=0}^{\infty}[a\sin(2\sigma_L) + b\cos(2\sigma_L)]P_L^1(x) \ ,$$

$$\mathrm{Im}\,B = \frac{1}{2k}\sum_{L=0}^{\infty}[b\sin(2\sigma_L) - a\cos(2\sigma_L)]P_L^1(x) \ ,$$

where

$$a = \eta_L^+\cos(2\delta_L^+) - \eta_L^-\cos(2\delta_L^-) \ ,$$

$$b = \eta_L^+\sin(2\delta_L^+) - \eta_L^-\sin(2\delta_L^-) \ .$$

One can find the next notation [146] for $A(\Theta)$ amplitude by the similar way

$$\mathrm{Re}\,A = \mathrm{Re}\,f_c + \frac{1}{2k}\sum_{L=0}^{\infty}[c\sin(2\sigma_L) + d\cos(2\sigma_L)]P_L(x) \ ,$$

$$\mathrm{Im}\,A = \mathrm{Im}\,f_c + \frac{1}{2k}\sum_{L=0}^{\infty}[d\sin(2\sigma_L) - c\cos(2\sigma_L)]P_L(x) \ ,$$

where

$$c = (L+1)\eta_L^+ \cos(2\delta_L^+) + L\eta_L^- \cos(2\delta_L^-) - (2L+1) \ ,$$
$$d = (L+1)\eta_L^+ \sin(2\delta_L^+) + L\eta_L^- \sin(2\delta_L^-) \ .$$

For the total elastic scattering cross section, the following expression can be obtained [45]:

$$\sigma_s = \frac{\pi}{k^2} \sum_L \left[(L+1)\left|1 - S_L^+\right|^2 + L\left|1 - S_L^-\right|^2 \right] \qquad (8.4)$$

or

$$\sigma_s = \frac{4\pi}{k^2} \sum_L \left\{ (L+1)[\eta_L^+ \sin\delta_L^+]^2 + L[\eta_L^- \sin\delta_L^-]^2 \right\} .$$

These expressions are used later for carrying out the phase shift analysis at the energy up to 1.1 MeV [147].

8.2. CONTROL OF THE COMPUTER PROGRAM

The whole text of our computer program for calculation of total and differential cross sections of elastic scattering of particles with half-integral spin, which was used for carrying out the applicable phase shift analysis, was tested using elastic scattering in the p^{4}He system.

Here we present just one variant of test calculation for p^{4}He scattering in comparison with the data of [148], in which phase shift analysis for an energy 9.89 MeV was performed, positive *D* phase shifts were obtained, and the following value averaged over all points was obtained: $\chi^2 = 0.60$.

In the analysis [148], 22 points for cross sections from [149] at an energy 9.954 MeV were used (it was not indicated in [148] which particular 22 points out of the 24 given in [149] have been used) and several points for polarizations from [148, 150]. In the latter case, it is likely that ten points for the following eight angles were used: 46.5°, 55.9°, 56.2°, 73.5°, 89.7°, 99.8°, 114.3°, and 128.3° at energies 9.89, 9.84 and 9.82 MeV.

Phase shifts from [148] are given in Table 8.1, and the average χ^2_σ for differential cross sections using our program, including 24 points from [149] (and energy 9.954 MeV) with these phase shifts, is equal to 0.586. The results of these calculations are shown in Table 8.2.

For ten experimental points for polarization from [148,150] at 9.82÷9.89 MeV and eight scattering angles with phase shifts from [148], $\chi^2_p = 0.589$ can be obtained (for an energy 9.954 MeV). These results are listed below in Table 8.3.

If χ^2 is averaged over all points (24 + 10 = 34), i.e. a more general expression is used,

$$\chi^2 = \frac{1}{(N_\sigma + N_P)}\left\{\sum_{i=1}^{N}\left[\frac{\sigma_i^{\ t} - \sigma_i^{\ e}}{\Delta\sigma_i^{\ e}}\right]^2 + \sum_{i=1}^{N}\left[\frac{P_i^t - P_i^e}{\Delta P_i^e}\right]^2\right\} = \\ = \frac{1}{(N_\sigma + N_P)}\{\chi_\sigma^2 + \chi_P^2\}, \quad (8.5)$$

we obtain $\chi^2 = 0.5875 \approx 0.59$, which is in good agreement with the results of [148]. Here, N_σ and N_P are the numbers of points for cross sections (24 points) and polarizations (10 points); σ^e, P^e, σ^t, P^t are the experimental and theoretical values of cross sections and polarizations; and $\Delta\sigma$ and ΔP are their errors.

Table 8.1. Phase shifts of elastic p^{4}He scattering from [148]

E **(MeV)**	***S*₀ (deg)**		***P*₃/₂ (deg)**		***P*₁/₂ (deg)**		***D*₅/₂ (deg)**		***D*₃/₂ (deg)**	
9.954	119.3	+2.0	112.4	+3.5	65.7	+2.7	5.3	+1.6	3.7	+1.6
		–1.8		–5.2		–3.2		–2.5		–2.8

Table 8.2. Differential cross sections of the p^{4}He scattering. Here, θ° is the scattering angle at degree; σ_e are the experimental cross sections and σ_t are the calculated cross sections at barn

θ°	**σ_e (mb/st)**	**σ_t (mb/st)**	**χ^2_i**	**θ°**	**σ_e (mb/st)**	**σ_t (mb/st)**	**χ^2_i**
25.10	371.00	366.85	0.31	109.90	21.00	20.70	0.51
30.89	339.00	331.54	1.21	120.60	23.00	22.59	0.79
35.07	305.00	308.40	0.31	122.80	24.50	24.19	0.40
49.03	232.00	230.61	0.09	130.13	31.90	31.91	0.00
54.70	205.00	199.10	2.07	130.90	33.20	32.90	0.21
60.00	176.00	170.56	2.39	134.87	37.80	38.44	0.71
70.10	124.00	120.59	1.89	140.80	47.30	47.69	0.17
80.00	82.00	79.77	1.85	145.00	54.00	54.62	0.33
90.00	49.20	48.82	0.15	149.40	61.60	61.88	0.05
94.07	39.10	39.44	0.19	154.90	70.60	70.54	0.00
102.17	26.20	26.39	0.13	160.00	78.40	77.71	0.19
106.90	22.00	22.15	0.12	164.40	83.00	82.94	0.00

If additional minimization of χ^2 is performed using our program, for χ^2_σ we obtain 0.576, for polarizations $\chi^2_P = 0.561$, and the average $\chi^2 = 0.572 \approx 0.57$ for the following phase shifts:

$S_0 = 119.01^\circ$, $P_{3/2} = 112.25^\circ$, $P_{1/2} = 65.39^\circ$, $D_{5/2} = 5.24^\circ$, $D_{3/2} = 3.63^\circ$,

which completely fall into the error range given in [148] and are given in Table 8.1.

Table 8.3. Polarizations in the p^{4}He scattering. Here, θ° is the scattering angle at degree; P_e are the experimental polarizations; ΔP_e – experimental errors for polarizations; P_t – calculated polarizations

θ°	P_e (%)	ΔP_e	P_t (%)	χ^2_i
46.50	–32.30	2.10	–33.11	0.15
55.90	–41.30	2.20	–42.50	0.30
56.20	–44.40	0.90	–42.81	3.11
73.50	–62.60	3.00	–62.84	0.01
73.50	–64.80	1.90	–62.84	1.06
89.70	–76.10	3.60	–76.33	0.01
89.70	–75.50	2.40	–76.33	0.12
99.80	–59.30	2.50	–58.55	0.09
114.30	48.20	3.20	51.03	0.78
128.30	99.40	3.30	97.66	0.28

Thus, the developed program makes it possible to obtain results that agree well with earlier analysis. The program was also tested with respect to phase shift analysis given in other papers at low energies for the p^{12}C system. Earlier phase shift analysis of excitation functions for elastic p^{12}C scattering measured in [151] at energies in a range 400÷1300 keV (center of mass system) and angles 106°÷169° was performed in [152]; in this paper it was obtained, for example, that for E_{lab} = 900 keV *S* phase shift should be in a range 153°÷154°. We obtained a value 152.7° for the same experimental data. Scattering cross sections were taken from excitation functions [152] at energies 866÷900 keV. The results of our calculations of σ_t in comparison with experimental data σ_e are given in Table 8.4. The last column of the table gives partial values of χ^2_i for each point at 10% errors of experimental cross sections, and a value 0.11 was obtained for χ^2 averaged over all experimental points.

At an energy 751 keV (laboratory system), in [152] the found value of *S* phase shift was in an interval 155°÷157°. The results we obtained for this energy are given in Table 8.5. The data for cross sections was taken from excitation functions in an energy range 749÷754 keV, and a value 156.8° was found for the *S* phase shift with the average χ^2 = 0.30. Thus, our program yielded phase shifts coinciding with the results of analysis performed based on excitation function from [152] for two energies of elastic p^{12}C scattering.

Table 8.4. Comparison of theoretical and experimental cross sections of p^{12}C elastic scattering at 900 keV

θ°	σ_e (mb/st)	σ_t (mb/st)	χ^2_i
106	341	341.5	1.90E–04
127	280	282.1	5.76E–03
148	241	251.2	1.80E–01
169	250	237.5	2.50E–01

Table 8.5. Comparison of theoretical and experimental cross sections of $p^{12}C$ elastic scattering at 750 keV

θ°	σ_e (mb/st)	σ_t (mb/st)	χ^2_i
106	428	428.3	3.44E–05
127	334	342.8	6.91E–02
148	282	299.1	3.66E–01
169	307	279.9	7.82E–01

8.3. PHASE SHIFT ANALYSIS OF $p^{12}C$ ELASTIC SCATTERING

The test results presented above agree well with each other; therefore our program was used to perform phase shift analysis [89] of new experimental data on differential cross sections of $p^{12}C$ scattering in an energy range 230÷1200 keV (laboratory system) [27]. The results of analysis are given in Table 8.6 and shown by points in Figure 8.1 in comparison with data from [152], which is shown by a dashed line.

Table 8.6. Results of phase shift analysis of $p^{12}C$ elastic scattering at low energies for *S* phase shift only

E_{cm} (keV)	$S_{1/2}$ (deg)	χ^2
213	2.0	1.35
317	2.5	0.31
371	7.2	0.51
409	36.2	0.98
422	58.2	3.69
434	107.8	0.78
478	153.3	2.56
689	156.3	2.79
900	153.6	2.55
1110	149.9	1.77

Figures 8.2a,b,c show the experimental differential cross sections in the resonance region near 457 keV in the laboratory system (data points), the results of calculation of these cross sections based on Rutherford formula (dotted curve), and cross sections obtained from our phase shift analysis (solid line), which takes into account the *S* phase shift only. It can be seen from these figures that, in the resonance region, it is impossible to describe the cross section based on *S* phase shift only

The *P* wave shown in Figure 8.3 begins to play a noticeable role, and taking this wave into account essentially improves the description of experimental data. The dashed line shows cross sections taking into account the *S* and *P* waves in phase shift analysis. In particular, at 457 keV (laboratory system), the cross sections at this energy are shown in Figure8.2b and accounting of the *P* wave reduces the value of χ^2 from 3.69 to 0.79.

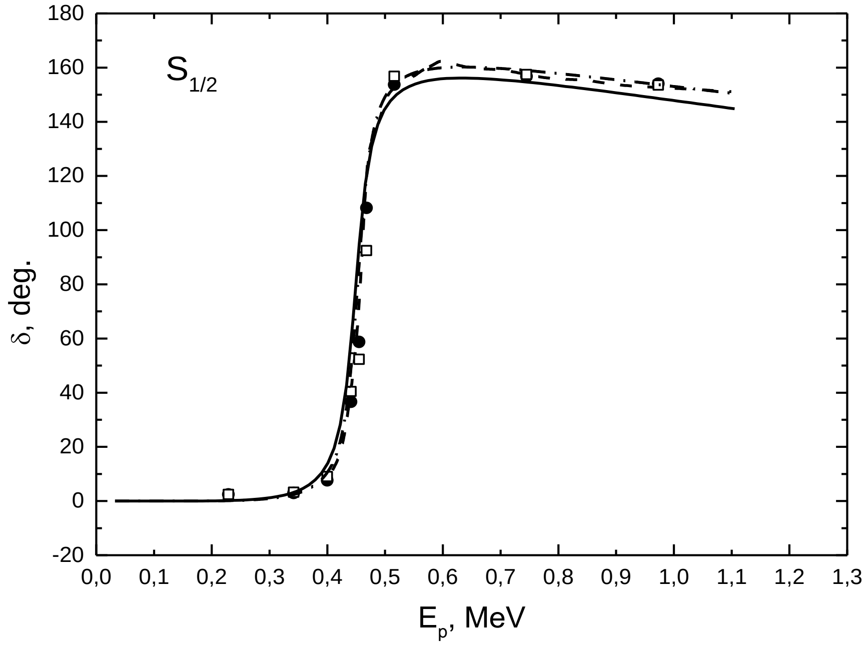

Figure 8.1. ^2S phase shift of p^{12}C scattering at low energies. Points show results of the analysis for the *S* phase shift taking into account the *S* wave only, open squares show results of the analysis for the *S* phase shift taking into account the *S* and *P* waves, and the dashed line shows the results from [152]. Curves show calculations with different potentials.

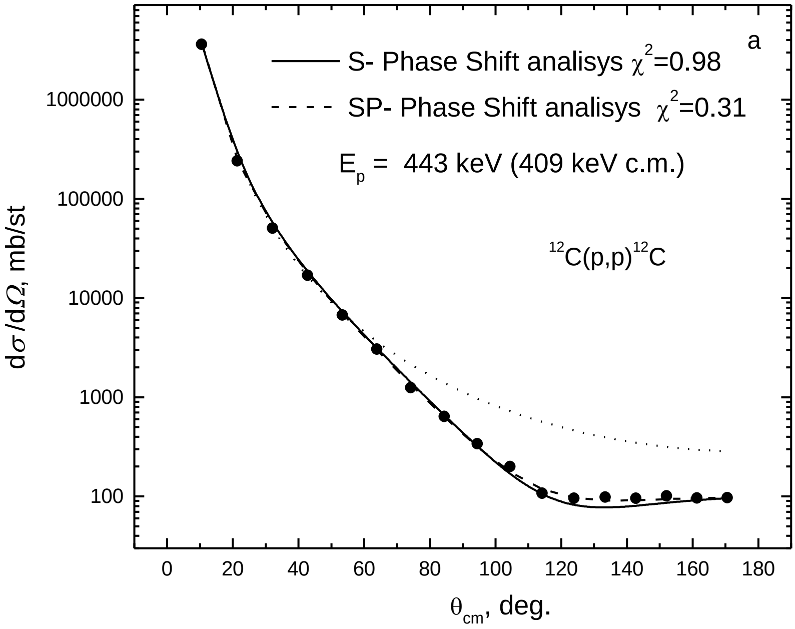

Figure 8.2a. Differential cross sections of p^{12}C scattering. The solid line – the phase shift analysis with account of *S* wave only, the dotted – Rutherford scattering, and the dashed line is phase shift analysis taking into account the *S* and *P* waves, and the data points are from experiment [27].

It can be seen from Figure 8.3 that, at low energies, the $P_{1/2}$-phase shift is higher than $P_{3/2}$, but at energies about 1.2 MeV they intersect and at higher energies $P_{3/2}$ is higher for negative angles [153,154]. The value of the S phase shift in the case in which the contribution of the P wave is taken into account practically does not change, its form being shown in Figure 8.1 by open squares.

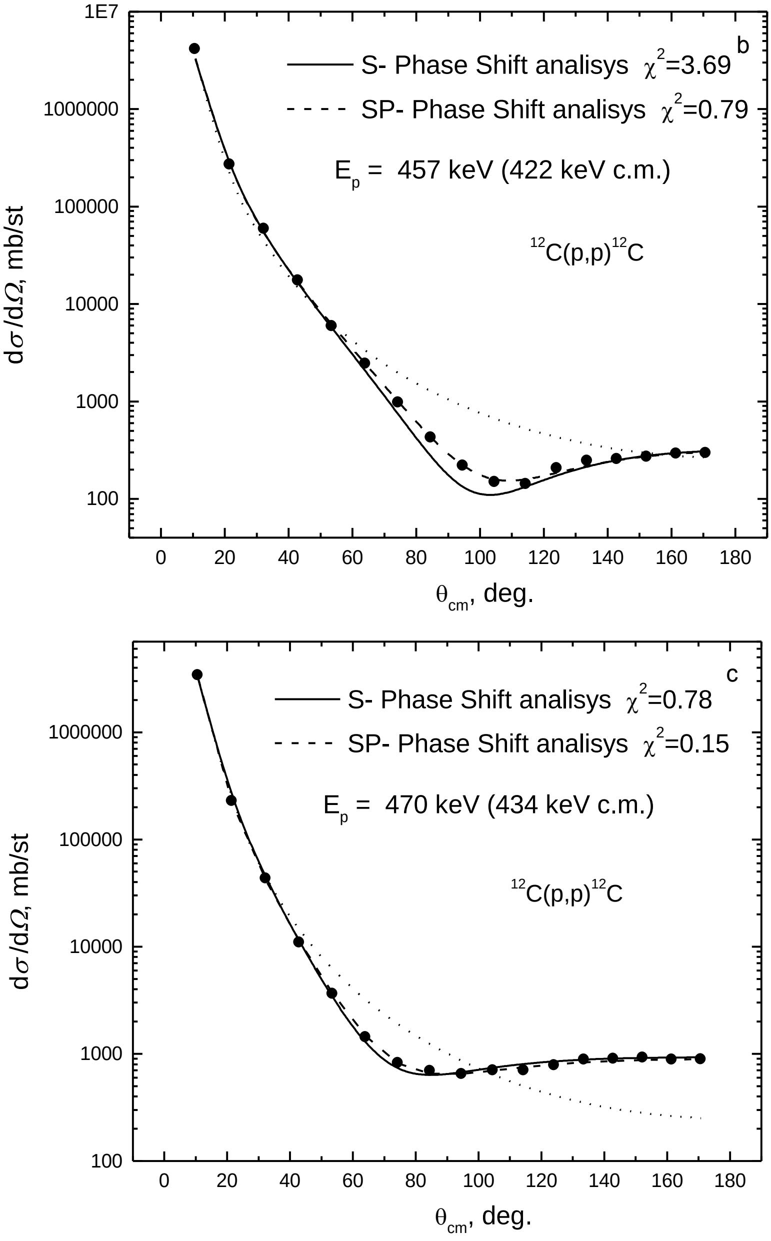

Figure 8.2b,c. Differential cross sections of $p^{12}C$ scattering. The solid line – the phase shift analysis with account of S wave only, the dotted – Rutherford scattering, and the dashed line is phase shift analysis taking into account the S and P waves, and the data points are from experiment [27].

Taking into account the *D* wave in phase shift analysis results in its value of order 1° in the resonance region and practically does not influence the behavior of calculated differential cross sections. Total elastic scattering cross sections obtained based on expression (8.4) are shown by points in Figure 8.4. They were calculated based on *S* scattering phase shifts extracted from experimental differential cross sections [27]. Open squares show total cross sections obtained from phase shift analysis in [152].

In Figure 8.4 a plateau is observed in the total cross sections in an energy range 200÷300 keV (laboratory system) and, therefore, in the *S* scattering phase shift. At present it is not clear whether this plateau is the result of experimental errors, unforeseen errors of phase shift analysis, or really exists at these energies. New measurements of angular distributions of $p^{12}C$ scattering in an energy range from 100÷150 to 300÷350 keV with a step of about 50 keV or excitation functions at different angles are required for elucidation of this question.

We ought to note, in the conclusion of this paragraph, that the value $\hbar^2/m_0$ = 41.80159 MeV fm^2, which is slightly differ than generally used, was employed in this analysis; it was obtained with more contemporary constant values.

8.4. ASTROPHYSICAL S-FACTOR

Radiative $p^{12}C$ capture at low energies is included in the CNO fusion cycle and makes a noticeable contribution to the energy gain of fusion reactions in many stars at later, than *pp*-chain, stage of their development [57,115] and whereof we stated particularly enough in the introduction. Therefore, let us go to the more detailed consideration of the based characteristics of this reaction at the astrophysical energies.

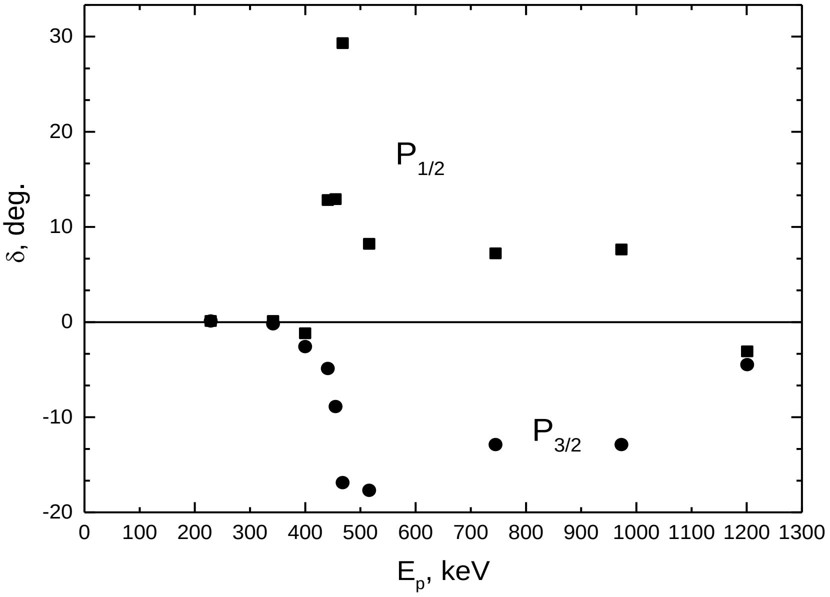

Figure 8.3. ^2P phase shifts of $p^{12}C$ scattering at low energies. Points show $P_{3/2}$ phase shifts and squares show $P_{1/2}$ phase shifts obtained as a result of phase shift analysis taking into account *S* and *P* waves.

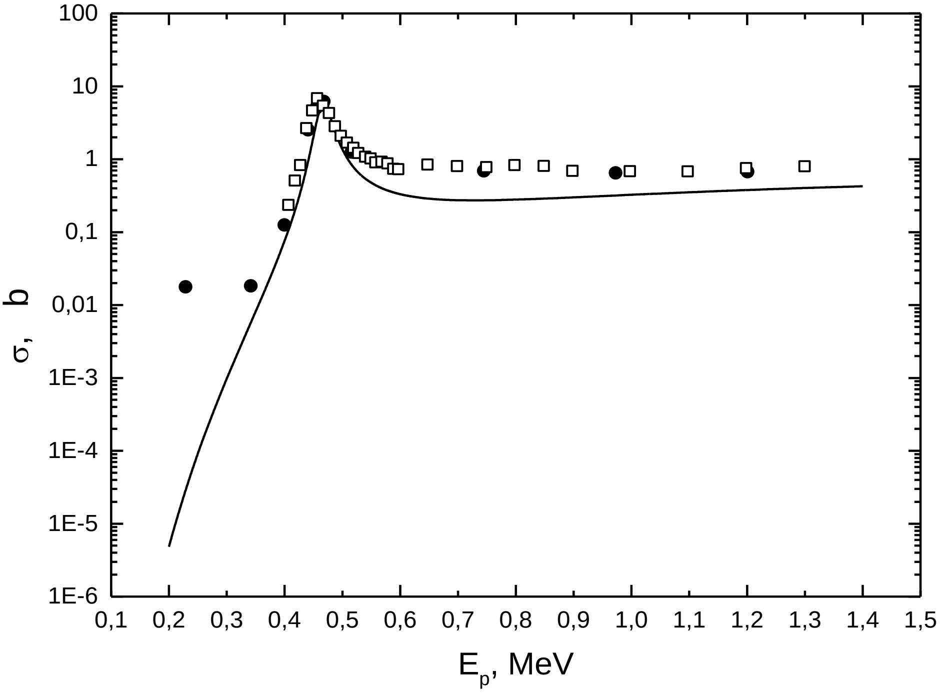

Figure 8.4. Total cross sections of elastic $p^{12}C$ scattering. Points show total cross sections found from scattering phase shifts from work [27]; squares, the same for [151,152].

The available experimental data on the *S*-factor [33] shows the presence of narrow, with a width of about 32 keV, resonance at an energy 0.422 MeV (center of mass system), which results in the increase of *S*-factor by two to three orders of magnitude. It is interesting to elucidate the possibility of description of the resonance *S*-factor of this reaction based on the potential cluster model with forbidden states. These studies are possible, since phase shift analysis of new experimental data [27] on differential cross sections of elastic $p^{12}C$ scattering at astrophysical energies [89] has been performed in previous paragraph, which makes it possible to construct potentials of $p^{12}C$ interaction using found elastic scattering phase shifts.

In the calculations of the process of radiative $p^{12}C$ capture $E1(L)$ under study, the transition due to the orbital part of the electric operator $Q_{JM}(L)$ [20,24] has been taken into account. The cross sections of $E2(L)$ and $MJ(L)$ transitions and the cross sections depending on the spin part of $EJ(S)$, $M2(S)$ turned out to be lower by several orders of magnitude. The electric $E1$ transition in the process of $p^{12}C \rightarrow {}^{13}N\gamma$ capture is possible between doublet $^2S_{1/2}$ and $2D_{3/2}$ scattering states and the ground $^2P_{1/2}$ bound state of the ^{13}N nucleus in the $p^{12}C$ channel. Therefore, we need potentials for partial waves corresponded to these states.

For construction of interaction potentials using elastic scattering phase shifts, first we consider the classification of orbital states according to Young schemes for $p^{12}C$ system. We would remind you that possible orbital Young schemes in a system of particles can be determined as the direct outer product of the orbital schemes of each subsystem, which in this case yields $\{1\} \times \{444\} = \{544\}$ and $\{4441\}$ [119,140]. The first of them is compatible with the orbital angular moment $L = 0$ only and is forbidden, since five nucleons cannot be situated in the *s*-shell. The second scheme is compatible with orbital angular moments 1 and 3 [119]; the first one corresponds to the ground bound state of ^{13}N nucleus with $J = 1/2^-$. Thus, the potential of the ^2S wave should contain the forbidden bound state, and the ^2P wave possesses an allowed state only at energy –1.9435 MeV [155].

For calculation of cross sections of photonuclear processes, the nuclear part of intercluster potential of $p^{12}C$ interaction is represented in form (2.8) with a point-like Coulomb term. The potential of the $^2S_{1/2}$ wave was constructed in such a way that the corresponding elastic scattering partial phase shift with pronounced resonance at 0.457 MeV (laboratory system) is correctly described. The results of phase shift analysis [89] presented above were used here to obtain the $^2S_{1/2}$ potential of $p^{12}C$ interaction with the forbidden state at the energy $E_{FS} = -25.5$ MeV.

The parameters of the potential are as follows:

$V_S = -67.75$ MeV, $\alpha_S = 0.125$ fm^{-2},

the results of calculation of $^2S_{1/2}$ phase shift with this potential are shown in Figure 8.1 by a solid line.

The potential of the ground $^2P_{1/2}$ state should correctly reproduce the binding energy of the ^{13}N nucleus in the $p^{12}C$ channel –1.9435 MeV [155] and reasonably describe the mean square radius. As a result, the following parameters were obtained:

$$V_{GS} = -81.698725 \text{ MeV}, \ \alpha_{GS} = 0.22 \text{ fm}^{-2}. \tag{8.6}$$

A binding energy –1.943500 MeV and the mean square radius $R = 2.54$ fm have been obtained for this potential. For the proton and ^{12}C nuclear radii the following values were used: 0.8768(69) [35] and 2.472(15) fm [156], respectively. The behavior of the wave function of bound state at large distances was controlled by using asymptotic constant C_W (2.10) with the asymptotics in the form of the Whittaker function [24], and its value in an interval 5÷20 fm turned out to be equal to 1.96(1).

The results of calculation of the S-factor of radiative $p^{12}C$ capture with $^2P_{1/2}$ and $^2S_{1/2}$ potentials obtained above for energies from 20 keV to 1.0 MeV are shown in Figure 8.5 by solid lines in comparison with the experimental data from survey [33] and work [157]. For 25 keV a value 3.0 keV b has been obtained for the S-factor, and extrapolation of experimental values of the S-factor to an energy 25 keV yields 1.45(20) and 1.54^{+15}_{-10} keV b [155].

The variant of the ^2S potential presented here is not the only possible way of describing the resonance behavior of S phase shift at energies below 1 MeV. Other combinations of bound state and scattering potentials can be found that yield close results for the $^2S_{1/2}$ phase shift and well describe the value and position of the S-factor maximum, for example,

$V_{GS} = -65.8814815$ MeV, $\alpha_{GS} = 0.17$ fm^{-2}, $R_{ch} = 2.58$ fm,
$C_W = 2.30(1)$, $E_{GS} = -1.943500$ MeV,
$V_S = -55.15$ MeV, $\alpha_S = 0.1$ fm^{-2}.

There exists a certain relationship between the parameters of the bound state and the scattering potentials that arises from the requirement of a description of the resonance S phase shift, the binding energy, and the value of resonance in the S-factor. The growth of the width of scattering and bound state potentials results in a smoother decrease of the S-factor at both sides of the resonance. For example, the value of the *S*-factor for the above potential at 25 keV is equal to 3.8 keV b.

Other combinations of potentials with a bound state potential narrower than in (8.6) can be proposed, for example, with the following parameters:

$V_{GS} = –121.788933$ MeV, $\alpha_{GS} = 0.35$ fm^{-2}, $R_{ch} = 2.49$ fm,
$C_W = 1.50(1)$, $E_{GS} = –1.943500$ MeV,
$V_S = –102.05$ MeV, $\alpha_S = 0.195$ fm^{-2}. (8.7)

These potentials result in a sharper drop of *S*-factor at energies near the resonance. The phase shift of potential (8.7) and the behavior of the corresponding *S*-factor are shown in Figs. 8.1 and 8.5 by dash-dotted lines.

The value of *S*-factor for this combination of potentials at 25 keV is equal to 1.85 keV b, which on the whole agrees with data given in survey [155].

The narrower than (8.7) bound state potential given below,

$V_{GS} = –144.492278$ MeV, $\alpha_{GS} = 0.425$ fm^{-2}, $R_{ch} = 2.47$ fm,
$C_W = 1.36(1)$, $E_{GS} = –1.943500$ MeV, (8.8)

with the same scattering V_S potential (8.7) results in slight decrease of the *S*-factor at the resonance energy, as shown in Figure 8.5 by a short-dashed line, and yields *S*(25 keV) = 1.52 keV b, which completely agrees with the data [117].

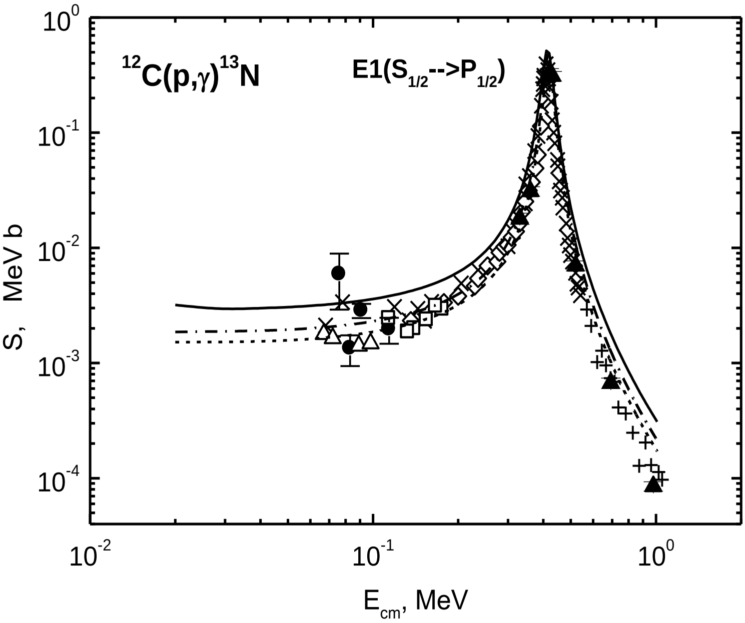

Figure 8.5. Astrophysical *S*-factor of radiative p^{12}C capture at low energies. Experimental data denoted by ×, •, □, + and Δ is taken from survey [33], triangles from [157]. Curves show calculations with different potentials.

However, it can be seen from the above results that, with decreasing width of bound state potentials, the asymptotic constant and charge radius of the nucleus also decrease. Probably, potential (8.8) yields minimum permissible values of these parameters consistent with experimental data, for example, on mean square radius. The known value of the charge radius of ^{13}C nucleus is equal to 2.46 fm [155]; it should not much differ from the radius of ^{13}N, which turn out to ^{13}C nucleus by β-transition. Thereby, the variant (8.8) of the bound state potential and the potential (8.7) for scattering states lead to the optimal *S*-factor description in the considered energy range and describing with it the resonance *S* phase shift of elastic scattering.

For complementary verification of binding energy calculation the variational method with expansion of the wave function over the non-orthogonal variational Gaussian basis [24] was used; this method yielded energy 1.943498 MeV on the grid with a dimensionality 10 in the case of independent parameter variation for first variant (8.6) of bound state potential. The asymptotic constant C_W of the variational wave function defined by parameters given in Table 8.7 reaches 1.97(2) at distances 5÷20 fm, and the residual does not exceed 10^{-13} [24]. The charge radius does not differ from the value obtained in finite-difference calculation.

Table 8.7. Variational parameters and expansion coefficients of the radial wave function in the $p^{12}C$ system for first variant (8.6) of the bound state potential

i	β_i	C_i
1	4.310731038130567E–001	–2.059674967002619E–001
2	1.110252143696502E–002	–1.539976053334172E–004
3	4.617318488940146E–003	–2.292772895754105E–006
4	5.244199809745243E–002	–1.240687319547592E–002
5	2.431248255158095E–002	–1.909626327101099E–003
6	8.481652230536312 E–000	5.823965673819461E–003
7	1.121588023402944E–001	–5.725546189065398E–002
8	2.309223399000618E–001	–1.886468874357471E–001
9	2.297327380843046 E–000	1.244238759439573E–002
10	3.756772149743554 E+001	3.435757447077250E–003

Table 8.8. Variational parameters and expansion coefficients of the radial wave function in the $p^{12}C$ system for second variant (8.7) of the bound state potential

i	β_i	C_i
1	1.393662782203888E–002	3.536427343510346E–004
2	1.041704259743847E–001	3.075071412877344E–002
3	4.068236340341411E–001	3.364496084003433E–001
4	3.517787678267637E–002	4.039427231852849E–003
5	2.074448420678197E–001	1.284484754736406E–001
6	7.360025091178769E–001	2.785322894825304E–001
7	3.551046173695889E–000	–1.636661944722212E–002
8	1.5131407009411240E+001	–9.289494991217288E–003
9	9.726024028584802E–001	–1.594107798542716E–002
10	6.634603967502104E–002	8.648073851532037E–003

Table 8.9. Variational parameters and expansion coefficients of the radial wave function in the p^{12}C system for third variant (8.8) of the bound state potential

I	β_i	C_i
1	1.271482702554672E–002	2.219877609724907E–004
2	9.284155511162226E–002	2.240043561912315E–002
3	3.485413978134982E–001	2.407314126671507E–001
4	3.088717918378341E–002	2.494885124596691E–003
5	1.815363020074388E–001	8.792233462610707E–002
6	5.918532693855678E–001	3.652121068403727E–001
7	3.909887088341156E+000	–1.906081640167417E–002
8	1.635608081209650 E+001	–1.111922033874987E–002
9	9.358886757095011E–001	2.314583156796476E–001
10	5.673177540516311E–002	5.956470542991426E–003

For variant (8.7) of the bound state potential, the same binding energy, –1.943498 MeV with a residual $3\cdot10^{-14}$, mean square radius 2.49 fm, and an asymptotic constant 1.50(2) in a range 5÷17 fm was obtained using the variational method. The variational parameters and expansion coefficients for the radial wave function of this potential are given in Table 8.8.

Third variant (8.8) of the bound state potential in the variational method results in a binding energy –1.943499 MeV with a residual $6\cdot10^{-14}$, the same mean square radius as in finite-difference calculation, and an asymptotic constant 1.36(2) in a range 5÷17 fm. Variational parameters of the radial wave function for this potential are given in Table 8.9.

We recall that the variational energy obtained in the variational method decreases with increasing basis dimensionality and, therefore, yields the upper limit of the true binding energy and the energy from the finite-difference method increases with decreasing step size and increasing number of steps. Therefore, the average value –1.943499(1) MeV for the applied methods can be taken as the actual binding energy in this potential. Thus, the accuracy of calculation of the binding energy is about ±1 eV. Let us note that in all of these calculations obtained in finite-difference and variational methods the proton mass is taken equal to unity, the mass of ^{12}C nucleus equals 12, $\hbar^2/m_0 = 41.4686$ MeV fm^2.

It should be noted that, in all calculations the cross section corresponding to electric $E1$ transition from the doublet $^2D_{3/2}$ scattering state to the ground $^2P_{1/2}$ bound state of ^{13}N nucleus turns out to be lower by four to five orders of magnitude than the cross section of transition from $^2S_{1/2}$ scattering state. Therefore, the main contribution into the calculated S-factor of the process p^{12}C → ^{13}Nγ is made by the $E1$ transition from the ^2S scattering wave to the ground state of the ^{13}N nucleus.

At the end of this paragraph it is necessary to draw attention to the interesting fact that if shallow potentials of $^2S_{1/2}$ wave without a forbidden state are used for the description of the scattering processes, for example, with the following parameters:

$$
\begin{aligned}
&V_S = -15.87 \text{ MeV}, \ \alpha_S = 0.1 \text{ fm}^{-2}, \\
&V_S = -18.95 \text{ MeV}, \ \alpha_S = 0.125 \text{ fm}^{-2}, \qquad (8.9) \\
&V_S = -21.91 \text{ MeV}, \ \alpha_S = 0.15 \text{ fm}^{-2},
\end{aligned}
$$

it is impossible to correctly reproduce the value of the maximum of *S*-factor of radiative capture. It is impossible to describe the absolute value of *S*-factor, which for any variants of scattering potentials (8.9) and bound states turns out to be higher than the experimental maximum by a factor 2÷3. For all given shallow, potentials of form (8.9) it is possible to reproduce the resonance behavior of $^2S_{1/2}$ scattering phase shift. With decreasing width of $^2S_{1/2}$ potential, i.e., with increasing α, the magnitude of *S*-factor maximum increases, and, for example, for the last variant of $^2S_{1/2}$ scattering potential in (8.9), it exceeds the experimental value by approximately a factor 3.

CONCLUSION

Thus, it is possible to combine the description of the astrophysical *S*-factor and $^2S_{1/2}$ scattering phase shift in a resonance energy region 0.457 MeV (laboratory system) and obtain reasonable values for the charge radius and asymptotic constant based on the finite-difference method and deep $^2S_{1/2}$ potential with Pauli-forbidden states. At the same time, shallow scattering potentials do not make it possible to simultaneously describe the *S*-factor and ^2S scattering phase shift for any considered combinations of p^{12}C interactions [128].

Chapter 9

ASTROPHYSICAL S-FACTORS OF THE RADIATIVE CAPTURE IN THE ^{3}HE^{4}HE, ^{3}H^{4}HE AND ^{2}H^{4}HE SYSTEMS

INTRODUCTION

In this section the astrophysical *S*-factors of radiative capture processes of ^{3}He^{4}He down to 15 keV, ^{3}H^{4}He and ^{2}H^{4}He down to 5 keV were considered in the frame of potential cluster model with classification of orbital states according to Young schemes [158] and refined potential parameters of ground states for ^{7}Be, ^{7}Li and ^{6}Li nuclei in ^{3}He^{4}He, ^{3}H^{4}He and ^{2}H^{4}He cluster models with forbidden states. Radiative capture ^{3}He^{4}He at superlow energies is of particular interest for nuclear astrophysics, since it is included in the proton-proton fusion chain, and new experimental data on the astrophysical *S*-factors of this process at energies as low as 90 keV and data on radiative ^{3}H^{4}He capture down to 50 keV appeared not long ago.

The proton-proton chain may be completed with the following process with a probability 69% [115] (according to [159] this probability is 86%):

$$^3\mathrm{He} + {}^3\mathrm{He} \to {}^4\mathrm{He} + 2\mathrm{p}$$

or the reaction, considered here, involving the prestellar ^{4}He nucleus, (for example see [7])

$$^3\mathrm{He} + {}^4\mathrm{He} \to {}^7\mathrm{Be} + \gamma,$$

the probability of which is 31% [115] (according to [159], this probability is approximately 14%). Moreover, radiative ^{3}He^{4}He and ^{2}He^{4}He capture may have played a certain role in prestellar nucleosynthesis after the Big Bang, when the temperature of the Universe decreased to $0.3T_9$ [160] ($T_9 = 10^9$ K).

9.1. SCATTERING POTENTIALS AND PHASE SHIFTS

It was shown in [158] that orbital states in the ^{3}He^{4}He, ^{3}H^{4}He and ^{2}H^{4}He systems for ^{7}Be, ^{7}Li and ^{6}Li nuclei, unlike lighter cluster systems as p^{2}H or p^{3}H [59,90,117], are pure according to Young schemes. Therefore, nuclear potentials of form (2.8) with the parameters obtained based on elastic scattering phase shifts and a spherical Coulomb term [45] can be directly used for examination of the characteristics of the bound states of these nuclei in the potential cluster model. Agreement of the obtained results with experimental data depends mainly on the degree of clusterization of such nuclei in the considered cluster channels. Since the clusterization probability for these nuclei is relatively high [158], it should be expected that the results of calculations should on the whole agree with the available experimental data [20,25].

The parameters of the Gaussian interaction potentials for cluster states in ^{7}Li, ^{7}Be and ^{6}Li nuclei that are pure according to Young schemes obtained earlier in [161,162] are given in Table 9.1, and the interactions in the ^{3}H^{4}He and ^{3}He^{4}He systems differed by the Coulomb term only. Table 9.1 also presents the energies of bound forbidden states for the ^{2}H^{4}He channel in ^{6}Li nucleus and ^{3}H^{4}He system, which slightly differ from the corresponding values for ^{3}He^{4}He interactions.

In the *S* wave for the ^{3}He^{4}He and ^{3}He^{4}He systems these bound states correspond to forbidden Young schemes {7} and {52}, in the *P* wave of scheme {61} for an allowed bound state with the Young scheme {43}, and the *D* wave has the forbidden state with scheme {52} [25,158]. For the ^{2}H^{4}He system, the *S* wave contains the forbidden bound state with scheme {6} and allowed bound state with {42}, and in the *P* wave the state with scheme {51} is forbidden [25,158]. The quality of description of scattering phase shifts is demonstrated in Figs. 9.1, 9.2 and 9.3a,b,c; these figures also show experimental data from [163,164] for ^{3}He^{4}He [164,165] for ^{3}H^{4}He and [166-169] ^{2}H^{4}He elastic scattering. The shown errors are due to inaccuracies of determination of phase shifts using figures from [163,164].

Table 9.1. Potential parameters of elastic ^{3}H^{4}He, ^{3}He^{4}He and ^{2}He^{4}He scattering and energies of corresponding forbidden bound states [161,162]. The potential width parameter for the ^{3}H^{4}He and ^{3}He^{4}He systems is $\alpha = 0.15747$ fm^{-2}, and the Coulomb radius $R_{\text{Coul}} = 3.095$ fm. It is assumed that $R_{\text{Coul}} = 0$ for scattering and bound state for the ^{2}He^{4}He system

^{7}Li and ^{7}Be			^{6}Li			
$^{2S+1}L_J$	V_0 (MeV)	E_{FS} (^{7}Li) (MeV)	$^{2S+1}L_J$	V_0 (MeV)	α (fm^{-2})	E_{FS} (MeV)
$^2S_{1/2}$	–67.5	–36.0, –7.4	$^3S_1$	–76.12	0.2	–33.2
$^2P_{1/2}$	–81.92	–27.5	$^3P_0$	–68.0	0.22	–7.0
$^2P_{3/2}$	–83.83	–28.4	$^3P_1$	–79.0	0.22	–11.7
$^2D_{3/2}$	–66.0	–2.9	$^3P_2$	–85.0	0.22	–14.5
$^2D_{5/2}$	–69.0	–4.1	$^3D_1$	–63.0 (–45.0)	0.19 (0.15)	–
$F_{5/2}$	–75.9	–	$^3D_2$	–69.0 (–52.0)	0.19 (0.15)	–
$F_{7/2}$	–84.8	–	$^3D_3$	–80.88	0.19	–

For the ^{3}He^{4}He and ^{3}H^{4}He systems, only *S* scattering phase shifts are presented, since it will be shown below that exactly transitions from *S* waves to the ground and the first excited bound states of ^{7}Be and ^{7}Li nuclei make a dominant contribution to the radiative capture *S*-factor. It can be seen from Figures 9.1, 9.2, and 9.3a that the calculated *S* phase shifts for elastic ^{3}H^{4}He, ^{3}He^{4}He and ^{2}H^{4}He scattering quite well describe the known results of phase shift analysis at low energies <10 MeV.

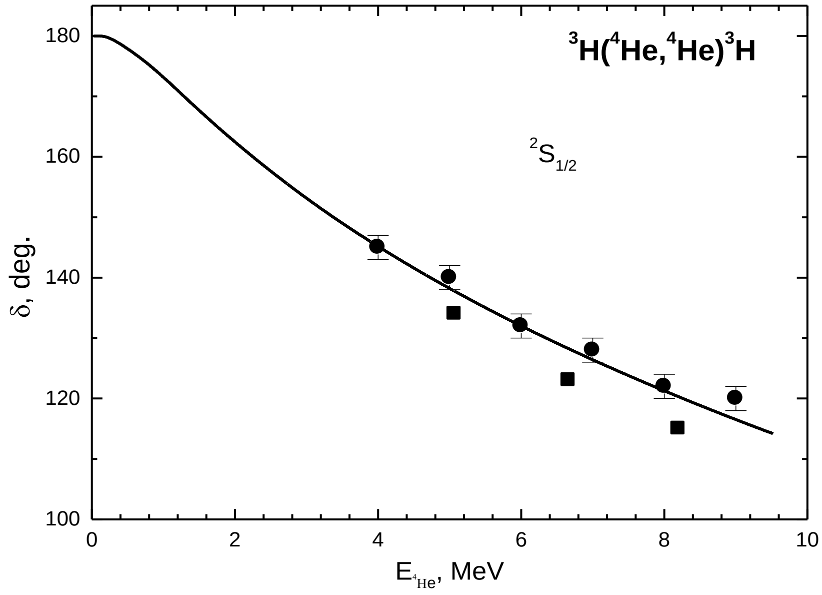

Figure 9.1. $^2S_{1/2}$ phase shift of elastic ^{3}H^{4}He scattering at low energies. Experimental data from [164] is shown by filled circles and data from [165] by filled squares. Curve is result with obtained potentials – see text.

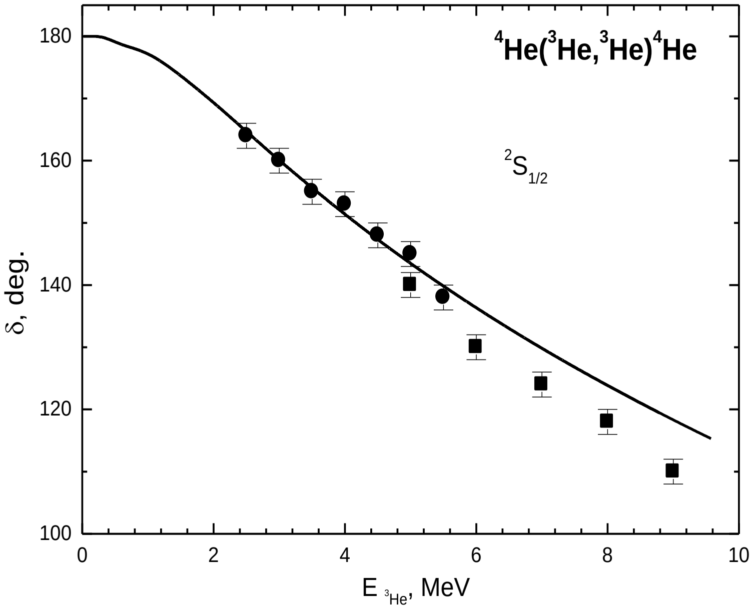

Figure 9.2. $^2S_{1/2}$ phase shift of elastic ^{3}He^{4}He scattering at low energies. Experimental data from [163] is shown by filled circles and data from [164] by filled squares. Curve is the result with obtained potentials (see text).

Figure 9.3b shows that the data on *P* phase shifts of ^{2}H^{4}He scattering from different papers strongly differs; therefore, it is possible to construct the *P* potential only approximately; however, on the whole they describe phase shifts at low energies, representing a certain compromise between the results of different phase shift analyses. For energy below 1 MeV, i.e., in the region of determination of *S*-factors, the results of calculation of all *P* phase shifts slightly differ and are close to zero.

In Figure 9.3c dashed lines show the results of calculation of $^3D_1$ and $^3D_2$ phase shifts of ^{2}H^{4}He scattering obtained using changed potentials the parameters of which are given in Table 9.1. These potentials somewhat better describe the behavior of the available experimental data, especially at the energies higher than 5 MeV.

It should be note that all *S* scattering phase shifts at zero energy are shown in Figs. 9.1, 9.2 and 9.3a beginning from a value 180°, although in the presence of two bound (allowed or forbidden) states in all systems, according to the generalized Levinson theorem [158], they should begin from 360°. Figure 9.3b shows the *P* phase shifts of ^{2}H^{4}He scattering at zero energy beginning from 0°, although, in the presence of a bound forbidden state with scheme {51}, they should be counted from 180°.

Then intercluster interactions thus matched with scattering phase shifts were used for calculation of different characteristics of ground states of ^{7}Li, ^{7}Be, and ^{6}Li and electromagnetic processes in these nuclei, and clusters were matched with corresponding properties of free nuclei [20,161].

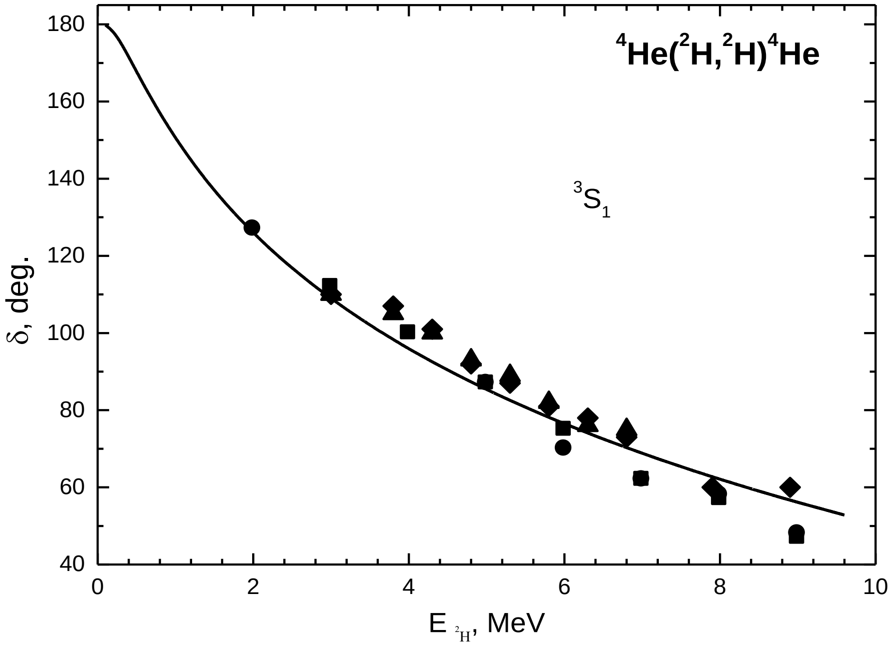

Figure 9.3a. $^3S_1$ phase shift of elastic ^{2}H^{4}He scattering at low energies. Experimental data from [166] is shown by filled circles, [167] filled squares, [168] filled triangles, and [169] filled rhombs. Curve is the result with obtained potentials (see text).

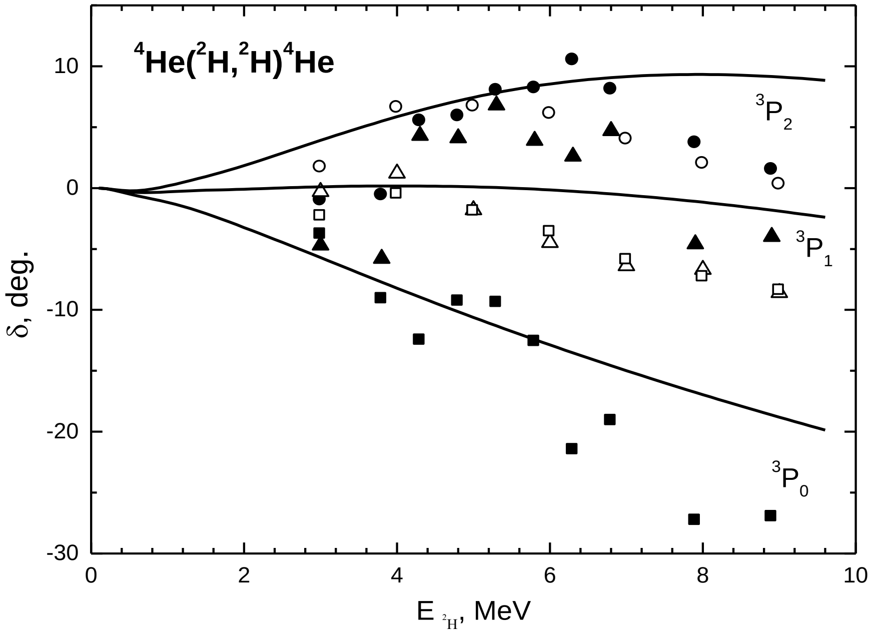

Figure 9.3b. ^3P phase shift of elastic $^2H^4He$ scattering at low energies. Experimental data from [167] is shown by open circles P_2, open triangles – P_1, and open squares – P_0; data from [169]: points – P_2, triangles – P_1, and squares – P_0. Curves are the results with obtained potentials (see text).

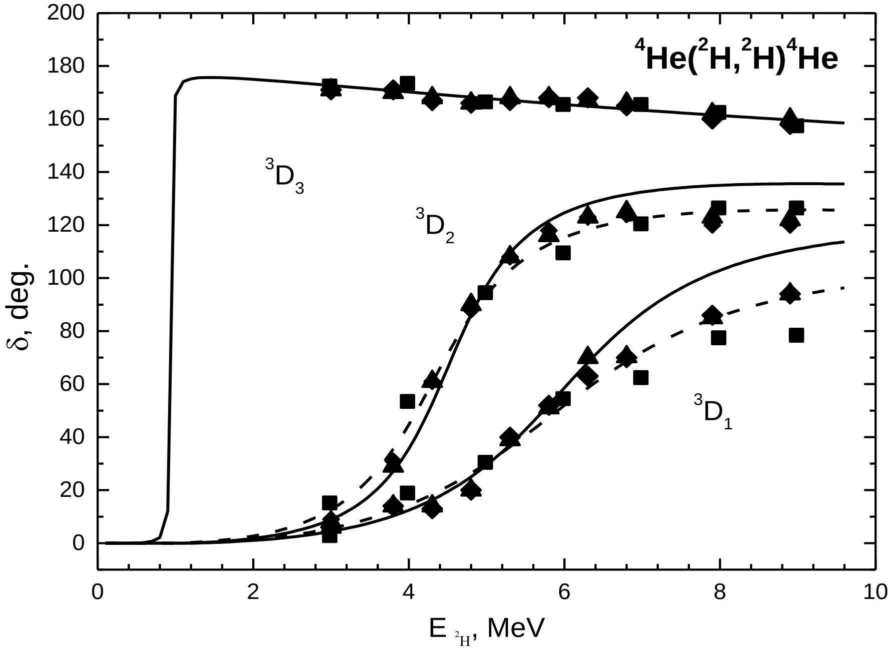

Figure 9.3c. ^3D phase shifts of elastic $^2H^4He$ scattering at low energies. Experimental data from [167] is shown by filled squares, [168] filled triangles, and [169] filled rhombs. Curves are the results with obtained potentials (see text).

The parameters of the potentials of ground states in the *P* wave for the ^{3}He^{4}He, ^{3}H^{4}He, and *S* wave for ^{2}H^{4}He were determined first of all based on correct description of binding energy [20]. In the latter case, it is possible not only to reproduce the binding energy, but also to correctly reproduce the behavior of the *S* phase shift of elastic scattering at low energies (Figure 9.3a). It should be noted that all results were obtained without taking into account tensor forces [170].

9.2. NEW VARIANTS OF POTENTIALS

In the framework of this approach, good agreement of calculations with different experimental data was obtained both for electromagnetic processes and the main characteristics of bound states of many light nuclei in cluster channels [25,158]. However, for example, the binding energy of ^{7}Li nucleus in the ^{3}H^{4}He channel with $J = 3/2^-$, as well as other systems, was really determined with an accuracy of several keV; therefore, the accuracy of calculation of the *S*-factor of radiative capture even at 10 keV turned out to be relatively low.

Therefore, in [129] the main calculated characteristics of bound states for ^{7}Li, ^{7}Be, and ^{6}Li nuclei in the ^{3}H^{4}He, ^{3}He^{4}He, and ^{2}H^{4}He channels have been refined. For this purpose the parameters of potentials for bound states have been refined, the calculated energy levels completely agreeing with the experimental values [120]. In other words, the potential parameters were chosen in such a way that experimental energy levels were described with maximal possible accuracy. If the experimental binding energy [120] was known with an accuracy to the fourth place, for example, –1.4743 MeV, it was assumed that it could be represented with six places, –1.474300 MeV.

The energies of the bound levels of the considered nuclei for the given potentials were calculated using the finite-difference method [24] with an accuracy no worse than 10^{-6} MeV. It will be shown below that the actual accuracy of determination of the binding energy in all systems using two different methods turned out to be on the order of ±1 eV and the largest error was probably introduced by the variational method of expansion of the wave function over the non-orthogonal Gaussian basis and independent parameter variation [24].

The necessary change of the parameters of the ^{3}H^{4}He and ^{3}He^{4}He potentials required for more accurate description of channel energies is given in Table 9.2. The slight change of parameters of the ^{3}H^{4}He, ^{3}He^{4}He and ^{2}H^{4}He potentials with respect to results [20,87] and Table 9.1 practically does not influence the behavior of the scattering phase shifts. However, this change makes it possible to maximally accurately reproduce energy levels in cluster channels, which plays an essential role in calculation of *S*-factors for energies of the order of 1÷10 keV.

The potential widths in Tables 9.1, 9.2 were chosen from the condition of description of charge radii and asymptotic constants [87]. Table 9.2 presents the results of calculation of the charge radii of considered nuclei in cluster channels.

For finding the charge radius of the nucleus, cluster radii given in [35,71,120] were used; the values of these radii, together with the energies of the bound states in cluster channels and cluster masses, are given in Tables 3.2 and 9.3. In the case of availability of several experimental results, the averaged value, shown in Tables 3.2, was used.

It can be seen from Table 9.2 that the mean square charge radius of ^{7}Li nucleus turns out to be somewhat larger than the experimental value (see Table 9.3). This may be due to existing experimental uncertainty of cluster radii (Table 3.2) which reaches ±5% of the average value and can change the radius of ^{7}Li nucleus by approximately 0.05 fm.

It follows from three-body and resonating-group-method calculations that the deuteron cluster in ^{6}Li nucleus is compressed by approximately a factor 1.2÷1.4, and this deformation was not taken into account in our examination of ^{6}Li nucleus in the cluster ^{2}H^{4}He model. This makes it possible to explain the somewhat overestimated ^{6}Li radius obtained in our calculations [20,87]. Thus, both for energy levels that are currently accurately reproduced and for charge radii, rather acceptable agreement with experimental data was obtained with the application of refined potentials.

Table 9.2. Refined potential parameters of ^{3}H^{4}He, ^{3}He^{4}He and ^{2}H^{4}He interactions; energy levels; and charge radii of ^{7}Li, ^{7}Be and ^{6}Li nuclei calculated with these potentials. The parameter α for ^{3}H^{4}He and ^{3}He^{4}He systems is 0.15747 fm^{-2}, and R_{Coul} = 3.095 fm. For ^{2}H^{4}He scattering, it is assumed that R_{Coul} = 0 fm

^{7}Li				**^{7}Be**		
$^{2S+1}L_J$	**V_0 (MeV)**	**E (MeV)**	**$<r^2>^{1/2}$ (fm)**	**V_0 (MeV)**	**E (MeV)**	**$<r^2>^{1/2}$ (fm)**
$^2P_{3/2}$	–83.616808	–2.467000	2.46	– 83.589554	–1.586600	2.64
$^2P_{1/2}$	–81.708413	–1.990390	2.50	– 81.815179	–1.160820	2.69
^{6}Li						
$^{2S+1}L_J$	V_0 (MeV)	α (fm^{-2})	E (MeV)		$<r^2>^{1/2}$ (fm)	
$^3S_1$	–75.8469155	0.2	–1.474300		2.65	

Table 9.3. Experimental data on charge radii and binding energies [35,71,120]

Nucleus	**Radius (fm)**	**Binding energy (MeV)**
^{6}Li	2.51(10)	$E(^4He^2H) = –1.4743$
^{7}Li	2.35(10)	$E(^4He^3H) = –2.467\ (3/2^-); –1.99039\ (1/2^-)$
^{7}Be	–	$E(^4He^3He) = –1.5866\ (3/2^-); –1.16082\ (1/2^-)$

For examination of the stability of the “tail” of the wave function of the ground and first excited bound states at large distances, the asymptotic constant C_W in form (2.10) has been used. As a result, for ground states of ^{7}Be, ^{7}Li, and ^{6}Li nuclei, in the considered channels, the following values were obtained: 5.03(1), 3.92(1), and 3.22(1), respectively. For the first excited states of ^{7}Be and ^{7}Li nuclei, in this model the following values were found: 4.64(1) and 3.43(1). The error given in brackets is determined by averaging the constant for nuclei with A = 7 obtained in calculation on an interval 6÷16 fm and for ^{6}Li at an interval 5÷19 fm.

In [48], based on a three-body np^{4}He model for the asymptotic constant of the ground S state of ^{6}Li in the ^{2}H^{4}He channel, a value 2.71 was obtained. A value 2.93(15) was found in [171] from phase shift analysis of elastic ^{2}H^{4}He scattering. In [172] interaction values from 2.09 to 3.54 were obtained for different types of NN and Nα using recalculation to the dimensionless quantity at k_0 = 0.308 fm^{-1}. In this paper references to experimental data varying from 2.29(25) to 2.96(14) are also given [172]. At the earlier work [39] the value 3.04 is given, which was obtained using recalculation to the dimensionless quantity too.

If the asymptotic $^2H^4He$ constant is determined from common exponential asymptotics, i.e., without taking into account Coulomb effects, the following value is obtained in the model used here for an interval 4÷12 fm: 1.9(2). The following values are known for this case: 2.4 [173] and 2.15(5) [37,73]. In [39] a survey of asymptotic and vertex constants, including those for the $^2H^4He$ channel, was presented and it was noted that the values of these constants, depending on the presence or absence of Coulomb effects, can differ by several times. The real change of asymptotic constant in the above results comes to approximately 1.5÷2.0.

For the ground state of the $^3H^4He$ system in ^7Li nucleus, for example in [174], with Whittaker asymptotics taking into account Coulomb (2.10), using recalculation to the dimensionless quantity with $k_0 = 0.453$ fm^{-1}, the values of asymptotic constant of the ground state in an interval 3.87(16) and asymptotic constant of the first excited state 3.22(15) were obtained. The value 3.73(26) for the GS was found in [175] after using recalculation to the dimensionless quantity, that is quite agree with our results.

The value 5.66(16), that is slightly more than our calculated value, is proposed for the ground state of ^7Be nucleus in the $^3He^4He$ channel in [176] on the base of different experimental data after using recalculation to the dimensionless quantity with $k_0 = 0.363$ fm^{-1}. The value 4.66(15) is given for the first excited state, that is in a good agreement with the value obtained here. Note that, for example in work [177], the values in an interval 3.5÷4.6 were obtained for the constant of the ground state of ^7Be nucleus in the $^3He^4He$ channel after using recalculation to the dimensionless quantity.

9.3. RESULTS OF VARIATIONAL CALCULATIONS

The variational method [24] was used to control the accuracy of determination of the binding energy in the considered cluster systems; in the $^3H^4He$ channel, this method made it possible, even for a low dimensionality of non-orthogonal Gaussian basis equal to 10 and independent parameter variation, to obtain a binding energy –2.466998 MeV. Therefore, as was mentioned earlier, for the actual binding energy in this potential, an average value –2.466999(1) MeV can be taken.

The parameters of expansion of the radial intercluster variational wave function of form (2.9) for the $^3H^4He$ system are given in Table 9.4. The asymptotic constant at distances 6÷16 fm was on a level 3.93(3), and the residual did not exceed $3 \cdot 10^{-12}$ [24]. For the first excited state in this channel, the energy –1.990374 MeV was obtained. The parameters of the corresponding wave function are also given in Table 9.4. The asymptotic constant on an interval 6÷20 fm turned out to be equal to 3.40(5), and the residual was equal to $4 \cdot 10^{-13}$.

Table 9.4. Parameters and expansion coefficients of variational wave functions of ^{7}Li nucleus in the ^{3}H^{4}He model

<table>
<tr><td colspan="3">^{7}Li (^{3}H^{4}He) $J = 3/2^-$
Normalization coefficient of wave function in an interval
0÷25 fm is equal to N = 9.99999999992E–001</td></tr>
<tr><td>i</td><td>β_i</td><td>C_i</td></tr>
<tr><td>1</td><td>6.567905679421632E–001</td><td>4.270672892119584E–001</td></tr>
<tr><td>2</td><td>1.849427298619411E–002</td><td>–6.326508826973404E–004</td></tr>
<tr><td>3</td><td>1.729324040753008E–001</td><td>–2.047665503330138E–001</td></tr>
<tr><td>4</td><td>4.173925751998056E–002</td><td>–1.032337189461229E–002</td></tr>
<tr><td>5</td><td>8.818471551829664E–002</td><td>–6.301223045259621E–002</td></tr>
<tr><td>6</td><td>4.503350223878621E–001</td><td>6.962475101962766E–001</td></tr>
<tr><td>7</td><td>9.210585557350788E–001</td><td>2.076348167318741E–002</td></tr>
<tr><td>8</td><td>2.000570770210328</td><td>1.488688664230068E–003</td></tr>
<tr><td>9</td><td>2.925234985697186</td><td>–1.124699482527892E–003</td></tr>
<tr><td>10</td><td>3.981951253509630</td><td>3.797289741762020E–004</td></tr>
<tr><td colspan="3">^{7}Li (^{3}H^{4}He) $J = 1/2^-$
Normalization coefficient of wave function in an interval
0÷25 fm is equal to N = 9.999999994E–001</td></tr>
<tr><td>i</td><td>β_i</td><td>C_i</td></tr>
<tr><td>1</td><td>3.767783843541890E–001</td><td>4.630588198830661E–001</td></tr>
<tr><td>2</td><td>3.862289845123266E–002</td><td>–1.122717538276013E–002</td></tr>
<tr><td>3</td><td>1.902467043551489E–001</td><td>–2.185424962074149E–001</td></tr>
<tr><td>4</td><td>1.465702154047247E–002</td><td>–4.355239784992325E–004</td></tr>
<tr><td>5</td><td>9.174545622012323E–002</td><td>–7.860947071320935E–002</td></tr>
<tr><td>6</td><td>8.478055592043516E–001</td><td>–5.602419628674884E–001</td></tr>
<tr><td>7</td><td>6.512974681188465E–001</td><td>1.017849119474616</td></tr>
<tr><td>8</td><td>1.401572634787409</td><td>57.704730892399640</td></tr>
<tr><td>9</td><td>1.405534176137368</td><td>–58.402969632676760</td></tr>
<tr><td>10</td><td>1.569682720436807</td><td>9.151457061882704E–001</td></tr>
</table>

For the binding energy in the ^{3}He^{4}He channel and for the same basis dimensionality, a value –1.586598 MeV was obtained; the coefficients of expansion of the wave function are given in Table 9.5.

It follows from these results that the mean binding energy in this potential can be taken equal to –1.586699(1) MeV. The asymptotic constant in a range 6÷15 fm is preserved at a level 5.01(4), and the residual does not exceed $5 \cdot 10^{-13}$.

For the first excited state, the energy –1.160801 MeV was obtained; the parameters of the wave function are also given in Table 9.5. The asymptotic constant at an interval 6÷14 fm was obtained equal to 4.64(4), and the residual did not exceed $5 \cdot 10^{-12}$.

In the ^{2}H^{4}He channel, the variational method yields the energy –1.474298 MeV and the mean binding energy for this potential is –1.474299(1) MeV. The asymptotic constant in an interval 6÷20 fm is equal to 3.23(38), the residual is no higher than $7 \cdot 10^{-13}$, and the parameters of expansion of the variational wave function are given in Table 9.6.

Table 9.5. Parameters and expansion coefficients of variational wave functions of ^{7}Be nucleusin the ^{3}He^{4}He model

<table>
<tr><th colspan="3">^{7}Be (^{3}He^{4}He) $J = 3/2^-$
Normalization coefficient of wave function in an interval
0÷25 fm is equal to N = 9.9999999995E–001</th></tr>
<tr><td><i>i</i></td><td>β_i</td><td>C_i</td></tr>
<tr><td>1</td><td>7.592678086347688E–001</td><td>4.226683168050651E–001</td></tr>
<tr><td>2</td><td>1.764646518442939E–002</td><td>–9.297447488403448E–004</td></tr>
<tr><td>3</td><td>1.713620418679277E–001</td><td>–1.913577297864284E–001</td></tr>
<tr><td>4</td><td>4.166190335743666E–002</td><td>–1.157464906616252E–002</td></tr>
<tr><td>5</td><td>8.829356096205253E–002</td><td>–6.210954724479718E–002</td></tr>
<tr><td>6</td><td>4.566882349965201E–001</td><td>7.725352747968277E–001</td></tr>
<tr><td>7</td><td>1.263871984172901</td><td>–7.575809619184885E–001</td></tr>
<tr><td>8</td><td>1.358053110884124</td><td>7.836457309371079E–001</td></tr>
<tr><td>9</td><td>1.741955980844547</td><td>–1.277551712466414E–001</td></tr>
<tr><td>10</td><td>2.379459759640717</td><td>1.446300395173141E–002</td></tr>
<tr><th colspan="3">^{7}Be (^{3}He^{4}He) $J = 1/2^-$
Normalization coefficient of wave function in an interval
0÷25 fm is equal to N = 9.99999998E–001</th></tr>
<tr><td><i>i</i></td><td>β_i</td><td>C_i</td></tr>
<tr><td>1</td><td>3.857719633413334E–001</td><td>4.891511738383773E–001</td></tr>
<tr><td>2</td><td>3.862289845123266E–002</td><td>–1.229249560611409E–002</td></tr>
<tr><td>3</td><td>1.881845128735454E–001</td><td>–2.002401467853206E–001</td></tr>
<tr><td>4</td><td>1.465702154047247E–002</td><td>–7.752125472489987E–004</td></tr>
<tr><td>5</td><td>9.174545622012323E–002</td><td>–7.680363457361430E–002</td></tr>
<tr><td>6</td><td>8.478055592043516E–001</td><td>–3.264723437643782E–001</td></tr>
<tr><td>7</td><td>6.512974681188465E–001</td><td>8.230628856230295E–001</td></tr>
<tr><td>8</td><td>1.401572634787409</td><td>21.258288548024340</td></tr>
<tr><td>9</td><td>1.405534176137368</td><td>–21.437482795337960</td></tr>
<tr><td>10</td><td>1.569682720436807</td><td>2.883954334066227E–001</td></tr>
</table>

Thus, the difference in the binding energy of ground states of all systems found using two methods does not exceed ±1 eV and the asymptotic constants in these ranges of distances and error margins completely coincide. For all the considered systems, the values of charge radii obtained using two different methods also coincide within two digits.

These results demonstrate good agreement of wave functions of bound states of all considered nuclei obtained using two different methods in an interval from 5÷6 to 16÷20 fm.

Table 9.6. Parameters and expansion coefficients of variational wave functions of ^{7}Be nucleus in the ^{2}H^{4}He model

^{6}Li (^{2}H^{4}He) $J = 1^+$ **Normalization coefficient of wave function in an interval** **0÷25 fm is equal to N = 9.99999865E–001**		
i	**β_i**	**C_i**
1	9.437818606389059E–003	5.095342831090755E–003
2	2.339033265895747E–002	3.991949900002217E–002
3	5.360473343158653E–002	1.164934149242748E–001
4	1.140512295822141E–001	2.165501771045687E–001
5	2.076705835662333E–001	1.831336962855912E–001
6	3.702254820081791E–001	–6.350857624465279E–001
7	2.848601430685521	2.165544802826948E–002
8	5.859924777191484E–001	–7.358532868463539E–001
9	82.336677993239830	5.086893578426774E–003
10	12.344385769445580	1.002621348014230E–002

9.4. ASTROPHYSICAL S-FACTOR

Earlier total cross sections of photoprocesses and astrophysical S-factors for the ^{2}H^{4}He, ^{3}H^{4}He and ^{3}He^{4}He systems were calculated in a cluster model [178] similar to that applied here and using the resonating group method [179]. For interaction potentials with forbidden states total photodisintegration cross sections in ^{2}H^{4}He cluster channel of ^{6}Li nucleus were calculated based on three-body wave functions of the ground state [180]. Total cross sections of photoprocesses for ^{6}Li and ^{7}Li nuclei in two-cluster models with forbidden states were calculated in [161] based on Gaussian potentials matched with elastic scattering phase shifts of corresponded particles.

In relation with publication of new experimental data, we consider the astrophysical S-factors of ^{3}H^{4}He, ^{3}He^{4}He, and ^{2}H^{4}He radiative capture at energies as low as possible in the framework of the potential cluster model [161,162] and specified potentials of ground states of ^{7}Li, ^{7}Be, and ^{6}Li nuclei (Table 9.2). Only $E1$ transitions were taken into account in calculations for ^{3}H^{4}He and ^{3}He^{4}He systems, since the contributions of $E2$ and $M1$ transitions are lower by two to three orders of magnitude [67]. In these systems only the $E1$ transition between the ground $P_{3/2}$ state of ^{7}Li, ^{7}Be, and $S_{1/2}$, $D_{3/2}$, $D_{5/2}$ scattering states and between the first excited bound $P_{1/2}$ state and $S_{1/2}$, $D_{3/2}$ scattering states is possible.

For radiative capture in ^{2}H^{4}He channel of ^{6}Li nucleus $E1$ transitions from ^3P scattering phase shifts to the ground bound ^3S state of ^{6}Li nucleus and $E2$ transitions from ^3D scattering waves to the ground state are possible. The main contribution to $E2$ transition at low energies is made by $^3D_3$ wave with a resonance at 0.71 MeV and $E1$ transition turns out to be strongly suppressed due to the cluster factor $A_J(K)$ given in (2.5); therefore, the cross section of the radiative capture process is mainly determined by $E2$ transition. It was shown earlier [87] that, at the lowest energies of the order 100÷150 keV, the contribution of $E1$ transition becomes prevailing; therefore, it will be shown below that it is the *E*1 process that determines the behavior of the astrophysical *S*-factor in this energy region.

The results of calculation of the astrophysical *S*-factor of radiative ^{3}H^{4}He capture at energies down to 5 keV are shown in Figure 9.4 by a solid line. Experimental data is taken from [181,182]; in the first of them the results for energies down to 55 keV are presented. The value of *S*-factor at 10 keV turned out to be equal to 111.0 eV b; the value extracted from experiment for zero energy was equal to 106.7(4) eV b [181]. Earlier results [182] yield 64 eV b; however, this data contains such large errors that they are extrapolated by a straight line.

There exist other data, which result in the following values at zero energy: 140(20) [183] and 100(20) eV b [33]. Note that results of [183] shown in Figure 9.4 by squares disagree with later measurements [181] and have relatively large errors. Among theoretical calculations, results of cluster model [178] can be noted; in this model the value of *S*-factor equals 100 eV b was obtained at zero energy, in the resonating group method, 98(6) eV b [179], and in recent paper [174] *S*(0) = 97.4(10) eV b.

If only transitions from *S* scattering wave to the ground and first excited bound *P* states are taken into account, at 10 keV we obtain 110.8 eV b, which practically does not differ from that presented above. The results of calculation of the *S*-factor in this case are shown in Figure 9.4 by a dashed line; they differ from the previous results only at energies above 0.3 MeV.

Thus, the results of our calculation of the *S*-factor of radiative ^{3}H^{4}He capture quite well describe experimental data [181] at energies below 0.5 MeV and result in the *S*-factor at 10 keV, which is in reasonable agreement with extrapolation of this experiment to zero energy. It should be noted that our previous calculations for this *S*-factor resulted in 87 eV b [87]. This difference may be related with the properties of the bound state potential used in calculations that yielded the binding energy with accuracy to several keV [87].

The results of calculation of the astrophysical *S*-factor of ^{3}He^{4}He capture at energies down to 15 keV are shown in Figure 9.5 by a solid line. Experimental data has been taken from [184-188]. The calculated curve at energy below 200 keV best agrees with results [185,186] obtained recently, and partially with data [188] at energies below 0.5 MeV. For energy 20 keV, our calculation yields an *S*-factor 0.593 keV b.

For comparison we present the results of extrapolation of experimental data to zero energy: 0.54(9) [33], 0.550(12) [189], 0.595(18) [184], 0.560(17) [185], 0.550(17) [186], and 0.567(18) keV b [190]. In the cluster model [178], the following value was obtained for this *S*-factor: 0.56 keV b, and in the resonating group method [179] 0.5(3) keV b.

Recently, it was obtained, in [176] based on analysis of different experimental data, that *S*(0) = 0.610(37) and *S*(23 keV) = 0.599(36) keV b, which well agrees with the value found here.

If transitions from *S* scattering waves to the ground and first excited bound states only are considered, similarly to the previous nuclear system, at 20 keV we obtain 0.587 keV b, which slightly differs from the above value. The calculated *S*-factor for this case is shown in Figure 9.5 by a dashed line, which slightly differs from the previous results obtained taking into account transitions from *S* and *D* waves.

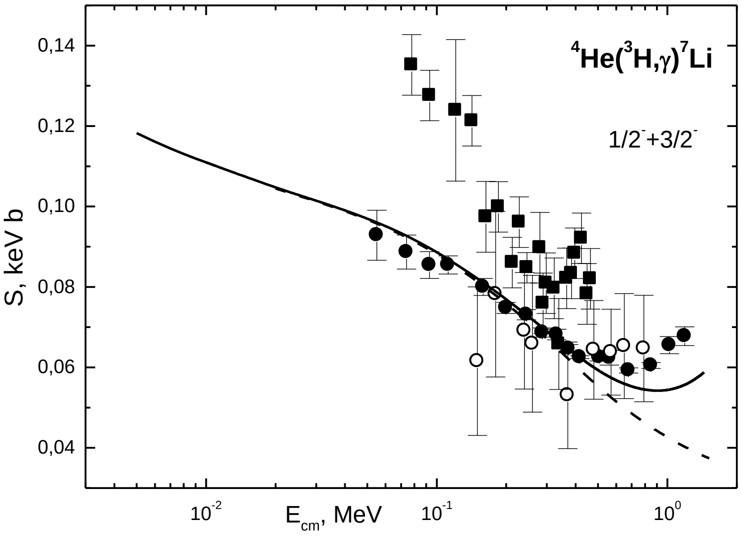

Figure 9.4. Astrophysical *S*-factor of ^{3}H^{4}He radiative capture. Filled circles show experimental data [181], open circles [182], and filled squares [183]. Lines show results of calculation with parameters of ground state potentials from Table 9.2.

It can be seen from results obtained not long ago that the value of the *S*-factor at zero energy can be in the range 0.45÷0.65 keV b and our calculated value falls in this interval. The form of the *S*-factor at energies below 0.5 MeV agrees well with data [188], and at lower energies it describes new data [185,186]. Note that our previous calculations of the ^{3}H^{4}He *S*-factor yielded 0.47 keV b [87]. The difference of this value from the new results can also be connected with the imperfection of the ground state potential used in [87].

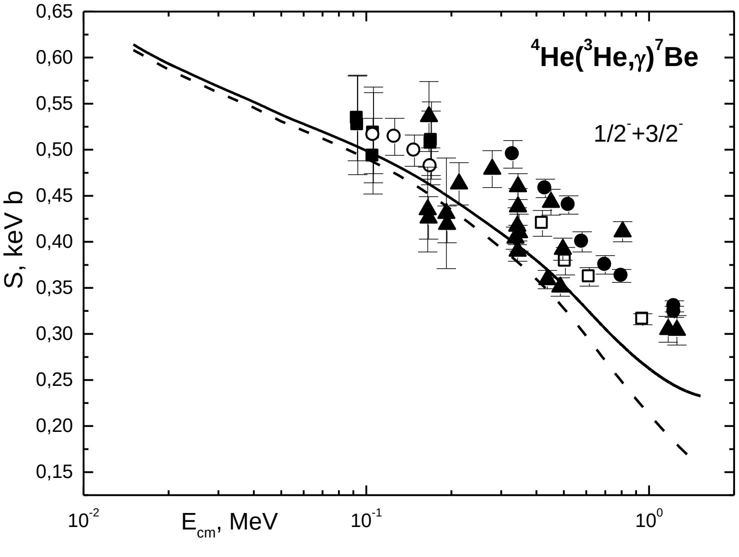

Figure 9.5. Astrophysical *S*-factor of ^{3}He^{4}He radiative capture. Filled circles show experimental data [184], filled squares [185], open circles [186], open squares [187], and filled triangles [188]. Lines show results of calculation with parameters of ground state potentials from Table 9.2.

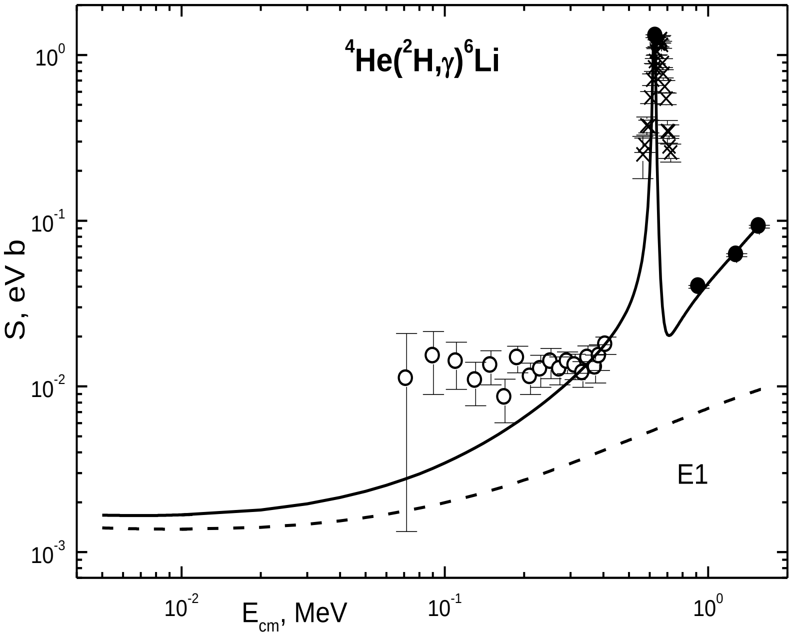

Figure 9.6. Astrophysical *S*-factor of ^{2}H^{4}He radiative capture. Filled circles show experimental data [191], crosses [192], and open circles [193]. The dashed line shows contribution of *E*1 process for transition to the ground state from *P* scattering wave. The solid line shows the total *S*(*E*1+*E*2) – factor.

The results of calculation of the *S*-factor of ^{2}H^{4}He capture are shown in Figure 9.6 by a solid line, and the contribution of the *E*1 transition is shown by a dashed line. Experimental data is taken from [191-193]; the results of the last paper were determined from figures presented in [33]. In a range 5÷10 keV for the total calculated *S*-factor determined by *E*1 and *E*2 transitions, a value $1.67(1)\cdot10^{-3}$ eV b or 1.67(1) eV mb was obtained.

The contribution of the *E*1 transition in this energy region is defining and comes to 1.39(1) eV mb. Obviously, it is the *E*1 transition that makes the main contribution to the astrophysical *S*-factor at low energies. The mentioned errors of the *S*-factor are determined by averaging over this energy interval. Unlike the systems considered above, this *S*-factor is practically constant in this energy region.

The results of extrapolation of experimental data given in [33] at 10 keV yield 1.6(1) eV mb, which well agrees with the value we obtained. However, if data from [193] that allows linear extrapolation are so extrapolated, an average value 13 eV mb can be obtained, which is higher by almost one order of magnitude.

Note that our previous calculations of *S*-factor of radiative ^{2}H^{4}He capture resulted in 1.5 eV mb [20]. The slight difference of the value 1.67(1) eV mb obtained here is also due to the approximate character of the bound state potential, which was capable of determining the binding energy with accuracy up to several keV [87].

The following value was obtained in theoretical calculations of [172] for the *S*-factor at zero energy: 1.2(1) eV mb, which corresponds to an asymptotic constant 3.06, and the constant extracted from experimental data [171,194] is equal to 2.96(14). However, the asymptotic constant obtained in calculations in which the *S*-factor is determined varies in a range 2.1÷3.5 and, therefore, the *S*-factor can have values that differ by a factor 2.

As a result, the uncertainty of experimental data and theoretical results does not make it possible to arrive at a final conclusion on the value of the *S*-factor of radiative ^{2}H^{4}He capture at zero energy and its behavior in the region below the resonance.

CONCLUSION

Thus, based on classification of orbital states according to Young schemes, it is possible to construct cluster interaction potentials that directly describe the elastic scattering phase shifts and basic characteristics of bound states of nuclei in corresponding cluster channels. Unlike lighter systems [59,105], this is possible due to the absence of mixing of Young schemes in bound states and high degree of clusterization of these nuclei in cluster ^{3}He^{4}He, ^{3}H^{4}He, and ^{2}H^{4}He channels [20,158].

As a result, the considered potential cluster model provides the description of the latest experimental data on the astrophysical *S*-factors of radiative ^{3}He^{4}He and ^{3}H^{4}He capture at low energies and yields values for them at zero energy that quite agree with the available experimental data within experimental errors.

Concerning the ^{2}H^{4}He system in ^{6}Li nucleus, at present precise experimental data at low energies is insufficient for determination of the astrophysical *S*-factor of radiative ^{2}H^{4}He capture. This data are required at least in the range 70÷500 keV, but with errors smaller than in [193]. If this data are obtained, it will be possible to draw more accurate conclusions on the form and value of the *S*-factor at low and zero energies [129].

Chapter 10

REACTION OF THE ^{4}HE^{12}C RADIATIVE CAPTURE

INTRODUCTION

Now let us consider the process of $^{12}C(^{4}He,\gamma)^{16}O$ radiative capture which, along with triple helium capture, is present in the chain of fusion reactions at the hot stage of star formation when the temperature inside the star is hundreds of millions of Kelvin [195]. At such a high temperature, the interacting particles have sufficient energy to considerably increase the probability of penetration of the Coulomb barrier to the region of strong interaction and, therefore, for increasing the contribution of this reaction to the total energy balance of the star.

The considered reaction results in the formation of the stable ^{16}O nucleus, which is an intermediate link in the process of formation of heavier elements, for example, in the reactions $^{16}O(^{4}He,\gamma)^{20}Ne$ and $^{20}Ne(^{4}He,\gamma)^{24}Mg$, etc. [2,115]. Therefore, knowledge of the cross section of this reaction and its energy dependence is important for nuclear astrophysics. However, great uncertainties in accurate determination of reaction rate for $^{12}C(^{4}He,\gamma)^{16}O$ existed for a long time, and a relatively short time ago new experimental data in an energy range 1.9÷4.9 MeV [196] appeared that possess high precision and probably eliminate most of these uncertainties.

In this section we present the results of phase shift analysis of elastic $^{4}He^{12}C$ scattering at low energies that we performed. Note that in different nuclear systems, depending on the energy of colliding particles, the number of parameters of the multiparametric variational problem formulated for the search of scattering phase shifts can vary from 1÷2 to 20÷40 [89,197].

Then the found elastic scattering phase shifts will be used to construct potentials of $^{4}He^{12}C$ interaction in continuous spectrum, which provide a correct description of the obtained scattering phase shifts and energies of bound states of ^{16}O nucleus under the assumption of $^{4}He^{12}C$ cluster configuration. Finally, the potential cluster model will be used to study the possibility of description of the astrophysical *S*-factor of $^{4}He^{12}C$ radiative capture reaction at low energies.

10.1. DIFFERENTIAL CROSS SECTIONS

In the case of elastic scattering of nonidentity particles of spin zero, the expression for the cross section takes the simplest form [45],

$$\frac{d\sigma(\theta)}{d\Omega} = |f(\theta)|^2 , \qquad (10.1)$$

where the total scattering amplitude $f(\theta)$ is represented as the sum of Coulomb $f_c(\theta)$ and nuclear $f_N(\theta)$ amplitudes,

$$f(\theta) = f_c(\theta) + f_N(\theta) ,$$

which are expressed in terms of nuclear (($\delta_L \rightarrow \delta_L + i\Delta_L$) and Coulomb ($\sigma_L$) scattering phase shifts; the form of these amplitudes is given in Section 5. We have the next form for the total cross section of the elastic scattering at $f_c = 0$:

$$\sigma_s = \frac{\pi}{k^2}\sum_L \left[(2L+1)\left(|1-S_L|^2\right)\right] = \frac{4\pi}{k^2}\sum_L (2L+1)\eta_L^2 Sin^2\delta_L \ .$$

Summation in this expression carries out over all possible L and carries till the certain L_{max}, which can be equal to the values from 1÷3 to 5÷6 due to the energy of α-particles.

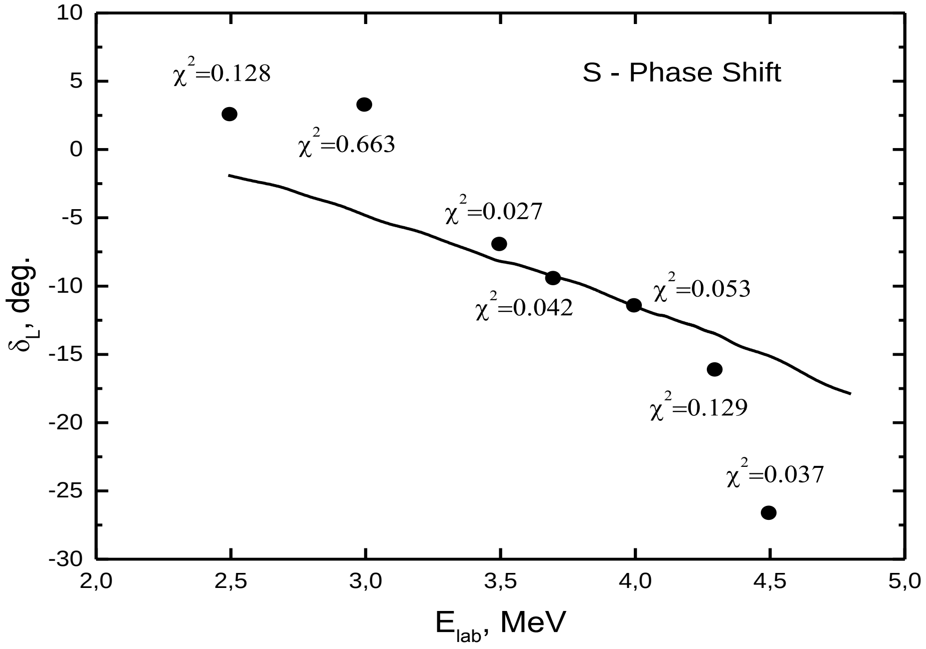

Figure 10.1. S phase shift of elastic ^{4}He^{12}C scattering. Curves show data of [198]. Points show our results obtained by using data from [198].

10.2. PHASE SHIFT ANALYSIS

Let us present the results of phase shift analysis obtained for $^4He^{12}C$ elastic scattering in the region from 1.5 to 6.5 MeV. Earlier phase shift analysis of differential cross sections at energies 2.5÷5 MeV was performed in [198]. The potential description of such scattering phase shifts based on potentials with forbidden states was performed in [199]. In this study we repeat phase shift analysis [198] in an energy range 2.5÷4.5 MeV using experimental data on excitation functions at seven angles from [198]. It can be considered as the control test of our computer program and applied calculation methods.

Note that measurement of excitation functions for such a small number of angular points is insufficient for reproduction of the form of angular distributions with good accuracy even at low energies. Therefore, phase shift analysis does not make it possible to obtain completely unambiguous values of scattering phase shifts, especially in the *S* wave, in spite of the fact that the known results of phase shift analysis from [198] were used as initial phase shifts by variation [24].

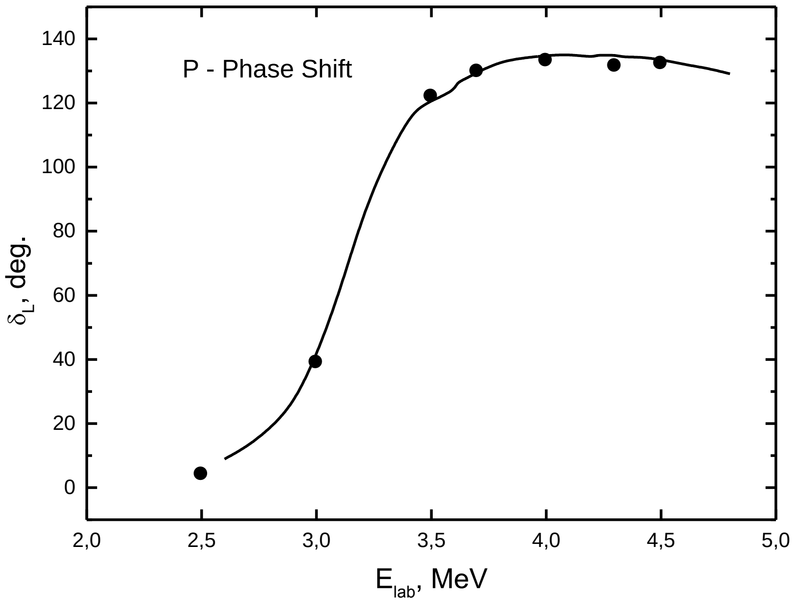

Figure 10.2. *P* phase shift of elastic $^4He^{12}C$ scattering. Conventional signs are the same as in Figure 10.1.

The results of our analysis are shown in Figs. 10.1÷ 10.5. Figure 10.1 shows the values of the average χ^2 obtained for different scattering energies. It can be seen from these figures that the *S* phase shift somewhat differs from the results of [198] and the phase shifts in all other partial waves quite agree with these results. Since, the data on excitation functions was taken from figures presented in [198], the possible error in our phase shift analysis may come to 2°÷3°, which is quite capable of explaining the deviation in the *S* phase shift values. In [200] very thorough phase shift analysis of experimental data for 49 energies from 1.5 to 6.5 MeV was performed. We used this data to perform our phase shift analysis at energies 1.466, 1.973, 2.073, 2.870, 3.371, 4.851, 5.799 and 6.458 MeV. The results of our analysis are given in Tables 10.1÷10.8, together with the average values of χ^2, in comparison with tabulated data from [200]. Table 10.9 gives the spectrum of resonance levels observed in elastic ^{4}He^{12}C scattering [201].

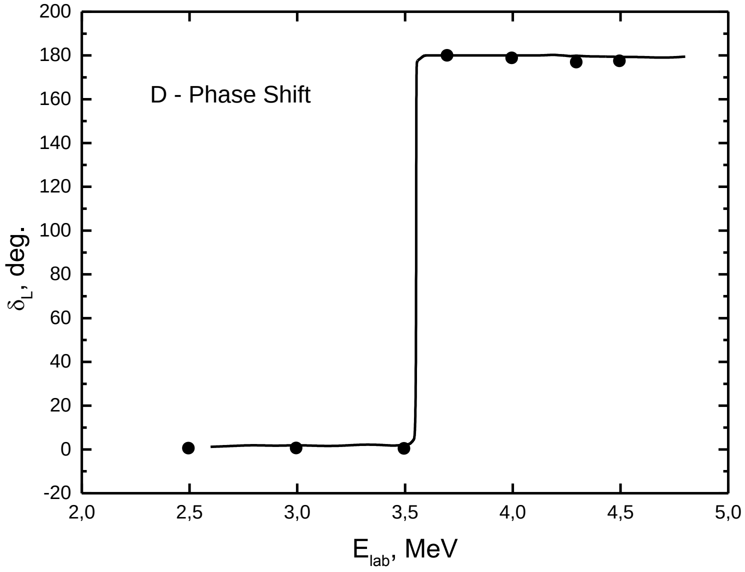

Figure 10.3. *D* phase shift of elastic ^{4}He^{12}C scattering. Conventional signs are the same as in Figure 10.1.

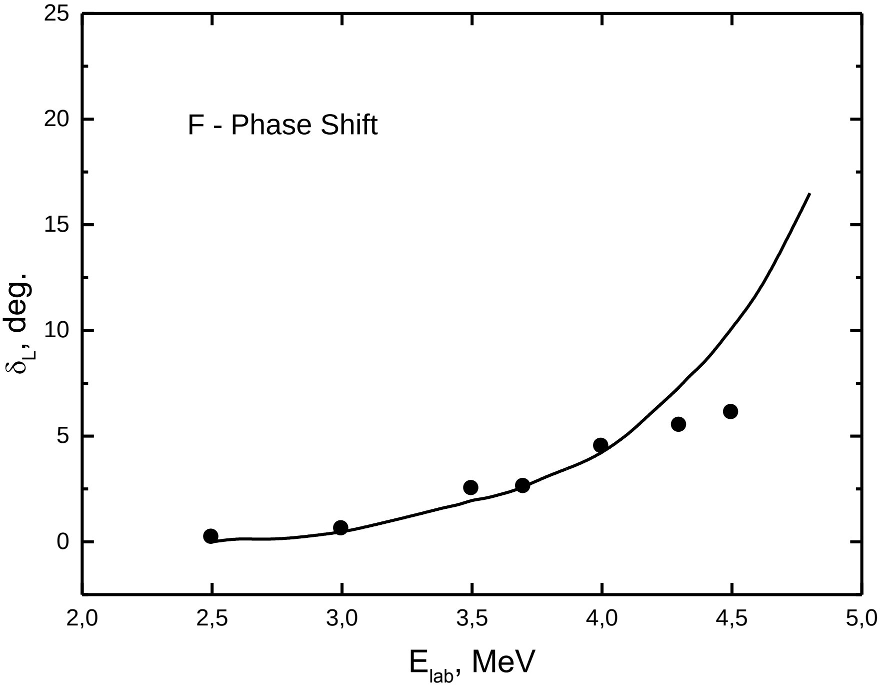

Figure 10.4. *F* phase shift of elastic ^{4}He^{12}C scattering. Conventional signs are the same as in Figure 10.1.

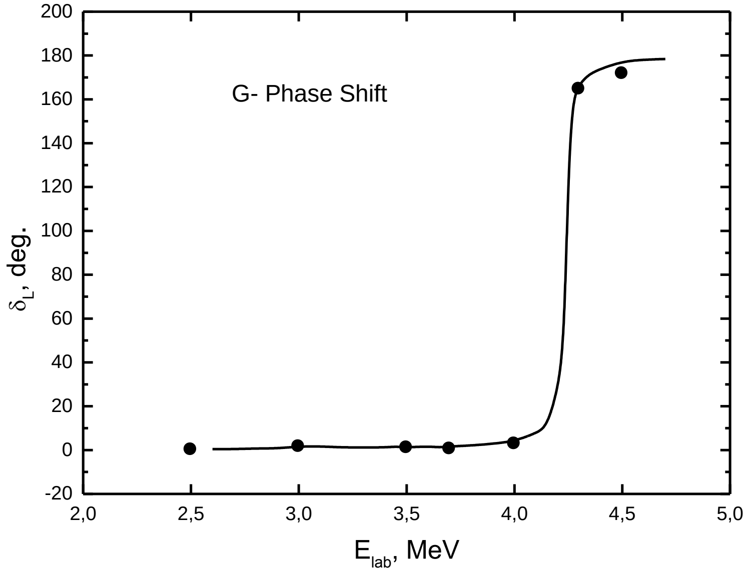

Figure 10.5. *G* phase shift of elastic ^{4}He^{12}C scattering. Conventional signs are the same as in Figure 10.1.

Table 10.1. Results of phase shift analysis of ^{4}He^{12}C elastic scattering and their comparison with data [200] at 1.466 MeV

E_{lab} = 1.466 MeV (χ^2 = 0.055)		
L	δ° (our)	δ° [200]
0	–0.2	0.5±1.0
1	–0.4	–0.1±1.0
2	–1.1	–0.8±1.0

Table 10.2. Results of phase shift analysis of ^{4}He^{12}C elastic scattering and their comparison with data [200] at 1.973 MeV

E_{lab} = 1.973 MeV (χ^2 = 0.077)		
L	δ° (our)	δ° [200]
0	–2.6	–0.5±1.0
1	0.0	0.9±1.7
2	–1.2	–0.1±1.3

Table 10.3. Results of phase shift analysis of ^{4}He^{12}C elastic scattering and their comparison with data [200] at 2.073 MeV

E_{lab} = 2.073 MeV (χ^2 = 0.029)		
L	δ° (our)	δ° [200]
0	–1.2	0±0.8
1	–0.1	0.1±1.2
2	–1.1	–0.6±0.9

Table 10.4. Results of phase shift analysis of $^4He^{12}C$ elastic scattering and their comparison with data [200] at 2.870 MeV

E_{lab} = 2.87 MeV (χ^2 = 0.038)		
L	δ° (our)	δ° [200]
0	–3.1	–2.1±1.1
1	21.3	22.0±2.1
2	0.0	0.4±0.9
3	0.5	1.0±0.5

It can be seen from these tables that energy of $^4He^{12}C$ scattering 3.371 MeV corresponds to a level 3.324 MeV with a width 480 ± 20 keV. Although in tables from [200] the phase shift for the *S* wave is not given (it is a blank cell in Table 10.5) for this energy, our phase shift analysis based on real scattering phase shifts makes it possible to determine this phase shift, which is presented in Table 10.5 with χ^2 = 0.31 and 10% errors of determination of experimental data from the figure in [200].

The energy 5.799 MeV exactly corresponds to a level 5.809 ± 18 MeV, and the tables in [200] do not contain the values of scattering phase shifts for some partial waves (blank cells in Table 10.7). In our phase shift analysis, it is possible to describe the differential scattering cross sections with the average χ^2 = 0.37 and find all partial phase shifts.

Table 10.5. Results of phase shift analysis of $^4He^{12}C$ elastic scattering and their comparison with data [200] at 3.371 MeV

E_{lab} = 3.371 MeV (χ^2 = 0.31)		
L	δ° (our)	δ° [200]
0	169.4	–
1	103.4	103.7±1.7
2	–1.7	0.0±0.7
3	0.2	0.8±0.6

Table 10.6. Results of phase shift analysis of $^4He^{12}C$ elastic scattering and their comparison with data [200] at 4.851 MeV

E_{lab} = 4.851 MeV (χ^2 = 0.26)		
L	δ° (our)	δ° [200]
0	164.2	164±1.1
1	128.4	129.5±0.9
2	177.1	178.8±0.9
3	15.5	16.4±0.8
4	176.9	177.2±0.8
5	–0.3	0.5±0.5

Table 10.7. Results of phase shift analysis of ^{4}He^{12}C elastic scattering and their comparison with data [200] at 5.799 MeV

E_{lab} = 5.799 MeV (χ^2 = 0.37)		
L	Reδ° (our)	Reδ° [200]
0	162.2	–
1	128.2	–
2	83.2	82.3±0.6
3	86.0	–
4	173.8	175.3±0.7
5	–1.0	0.2±0.4

Table 10.8. Results of phase shift analysis of ^{4}He^{12}C elastic scattering and their comparison with data [200] at 6.458 MeV

E_{lab} = 6.458 MeV (χ^2 = 0.41)		
L	δ° (our)	δ° [200]
0	151.2	153±2.5
1	115.8	119.4±2.1
2	172.2	172.2±1.9
3	120.8	122.0±2.4
4	176.4	179.1±1.2
5	0.8	2.2±0.8
6	0.1	0.4±0.4

Table 10.9. Spectrum of ^{16}O nucleus levels in elastic ^{4}He^{12}C scattering with the isospin *T* = 0 [127]. Here, J^π is the total angular moment and parity, E_{lab} is the energy of incident α-particle, and Γ_{cm} is the level width

E_{lab} (MeV)	**J^π**	**Γ_{cm} (keV)**
3.324	1^-	480±20
3.5770±0.5	2^+	0.625±0.1
4.259	4^+	27±3
5.245±8	4^+	0.28±0.05
5.47	0^+	2500
5.809±18	2^+	73±5
5.92±20	3^-	800±100
6.518±10	0^+	1.5±0.5
7.043±4	1^-	99±7

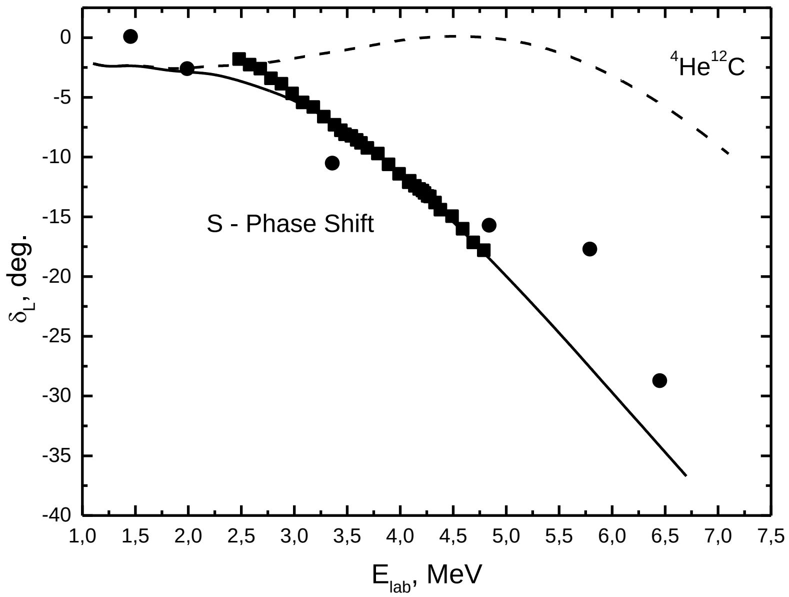

Figure 10.6. *S* phase shift of elastic $^4He^{12}C$ scattering. Squares show data [198]. Points show our results [202] obtained by using data from [200]. Curves show results of calculations with found potentials.

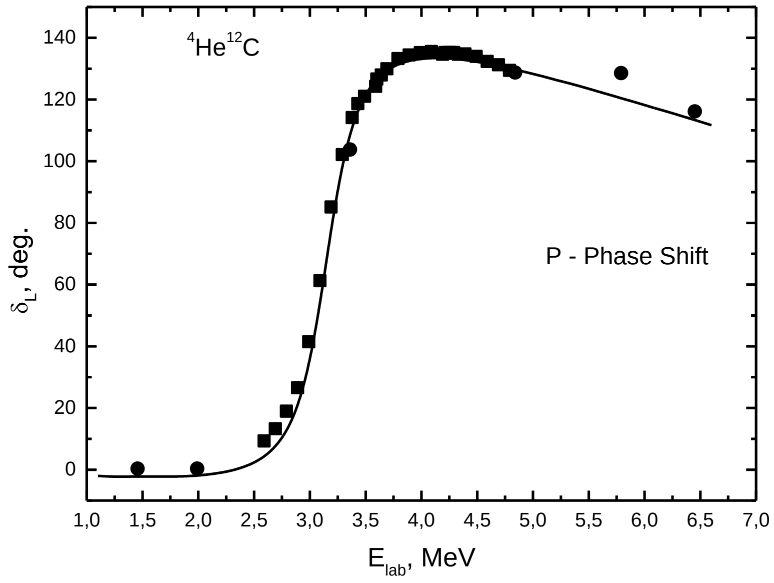

Figure 10.7. *P* phase shift of elastic $^4He^{12}C$ scattering. Conventional signs are the same as in Figure 10.6.

Other non-resonance energies (2.870, 4.851, and 6.458 MeV) are described by phase shifts that coincide with data from [200] within phase shift errors given in [200] and with account of possible 10% errors of our determination of experimental data from figures in [200]. The last three energy values 1.466, 1.973 and 2.073 MeV, in essence, are compatible with zero values of nuclear phase shifts and correspond to pure Coulomb, i.e., Rutherford, scattering.

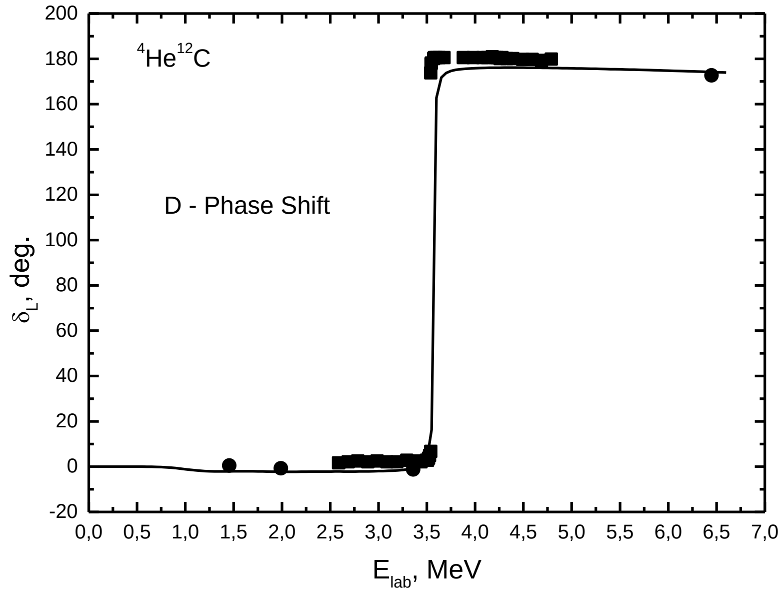

Figure 10.8. *D* phase shift of elastic $^4He^{12}C$ scattering. Conventional signs are the same as in Figure 10.6.

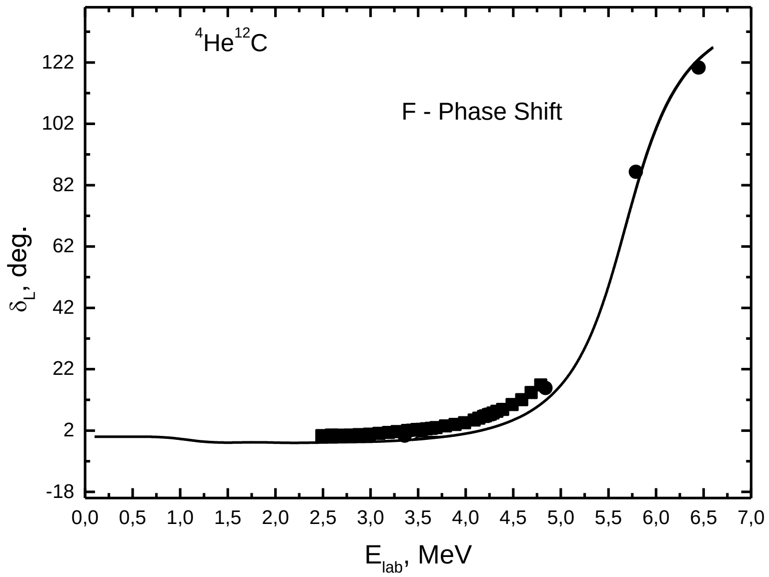

Figure 10.9. *F* phase shift of elastic $^4He^{12}C$ scattering. Conventional signs are the same as in Figure 10.6

The slight differences in scattering phase shifts may be due to the different values of constants and particle masses that are used in such an analysis. For example, exact values of particle masses [35] or their integer values can be used and the constant $\hbar^2/m$ can be taken equal, for example, to 41.47 or, more accurately, 41.4686 MeV fm^2. We estimate the accuracy of phase shift determination in the performed phase shift analysis based on data from [200] to be on a level 1°÷2°.

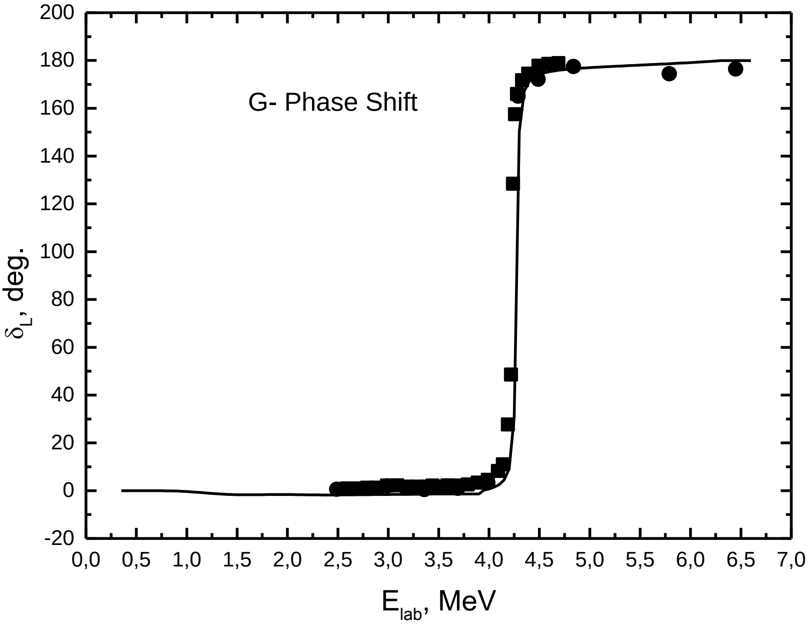

Figure 10.10. *G* phase shift of elastic ^{4}He^{12}C scattering. Conventional signs are the same as in Figure 10.6.

Figures 10.6÷10.10 show the comparison of results of our phase shift analysis [202] carried out by using experimental data from [200] (points) and phase shift analysis from [198] (squares). It can be seen from Tables 10.1÷10.8 and Figs. 10.6÷10.10 that the obtained phase shifts practically coincide with the results [200] but somewhat differ from the data of [198], especially as regards *S* wave.

10.3. DESCRIPTION OF SCATTERING PHASE SHIFTS IN POTENTIAL MODEL

Before going to construction of the potentials, let us first consider the classification of orbital states of ^{4}He^{12}C system which makes it possible to determine the total number of forbidden states in the potential of *S* wave interaction. The potentials obtained as a result can be used further for calculation of astrophysical *S*-factors, for example, capture reaction ^{12}C(^{4}He,γ)^{16}O [33].

Possible orbital Young schemes of the ^{4}He^{12}C system are defined by Littlewood's theorem [119], which in this case yields {444} × {4} = {844} + {754} + {7441} + {664} + {655} + {6442} + {6541} + {5551} + {5542} + {5443} + {4444} [199]. In the shell model, Young schemes {4} and {444} correspond to ^{4}He and ^{12}C nuclei in the ground state. According to rules [119], the conclusion can be drawn that only the Young scheme {4444} is Pauli-allowed for ^{16}O nucleus, all other orbital configurations being forbidden. In particular, all possible configurations in which the first row contains a number larger than four cells cannot exist, since the *s*-shell cannot contain more than four nucleons.

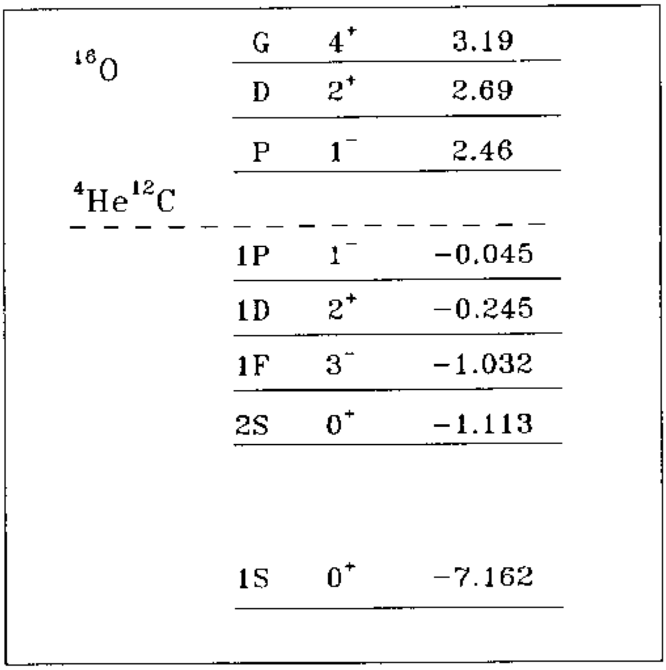

Figure 10.11. Spectrum of ^{16}O nucleus levels.

Orbital angular moments corresponding to different Young schemes can be determined using Elliott's rule [119]. As a result, we find that the states of ^{16}O nucleus with the angular moment $L = 0$ in the $^4He^{12}C$ system correspond to the following orbital schemes: {4444}, {5551}, {664}, {844}, and {6442}. This result can be used for determination of the number of bound forbidden states in the potential of the ground state. Since in the ground state only symmetry {4444} is allowed, and the other four Young schemes are forbidden, the potential of $^4He^{12}C$ interaction should have four bound forbidden states and one allowed bound state [199].

Earlier in [199] the parameters of potential of form (2.8) with spherical Coulomb interaction [45] and $R_{\text{Coul}} = 3.55$ fm for the ground state of the $^4He^{12}C$ system in ^{16}O nucleus have been obtained. This potential was constructed based on the requirement of description of such characteristics as binding energy, charge radius, Coulomb form factor at small transferred moments and probabilities of electromagnetic transitions between bound levels.

Then in [203] the parameters of potential of the ground 1*S* state [201] were specified (see Figure 10.11) for ^{16}O in the $^4He^{12}C$ channel and, for the same Coulomb radius, it was obtained that

$$V_{1S} = -256.845472 \text{ MeV}, \alpha = 0.189 \text{ fm}^{-2}. \tag{10.2}$$

The finite-difference method [24] was used for obtaining a binding energy –7.161950 MeV for this potential compared to an experimental value –7.16195 MeV [201] and a charge radius 2.705 fm for ^4He radius 1.671(14) fm [71] and ^{12}C radius 2.4829(19) fm [156] compared to that measured at the experiment value of ^{16}O radius is equal to 2.710(15) fm [201]. This potential has forbidden states at four energies –37.6, –80.8, –134.5, and –197.2 MeV according to the classification of forbidden and allowed states.

For the potential of the first excited 2*S* level with an experimental energy –1.113 MeV [201] that is correctly reproduced by this potential, more accurate parameters were obtained:

$V_{2S} = -143.1092$ MeV, $\alpha = 0.111$ fm^{-2}.

This results in forbidden states at –16.9, –40.5, –70.6 and –106.1 MeV. Upon refinement of parameters of the bound state potential in the 1*P* wave (Figure 10.11), the following values were obtained [203]:

$V_{1P} = -161.2665$ MeV, $\alpha = 0.16$ fm^{-2}.

This potential exactly reproduces the energy of the bound state –0.045 MeV and has three forbidden states at –20.4, –52.0, and –92.5 MeV.

For the parameters of the bound state potential in the 1*D* wave shown in Figure 10.11, the following was obtained:

$V_{1D} = -90.3803$ MeV, $\alpha = 0.1$ fm^{-2}.

This results in energy of the bound level –0.245 MeV, in complete agreement with data of [201] and contains two forbidden bound states at –14.0 and –34.3 MeV.

For the 1*F* state of ^{16}O nucleus in the ^{4}He^{12}C channel, the following parameters have been obtained:

$V_{1F} = -191.4447$ MeV, $\alpha = 0.277$ fm^{-2}.

The potential yields energy of the bound state –1.032 MeV, which agrees with data [201] and contains one forbidden bound state at the energy –38.3 MeV.

The following energy was obtained using the variational method with expansion of the wave function over the non-orthogonal Gaussian basis with the basis dimensionality $N = 8$ for the ground 1*S* state of ^{16}O nucleus with potential parameters (10.2): –7.16194 MeV, i.e., lower by approximately 10 eV than the experimental value. The parameters of the variational wave function of relative cluster motion in the ground state of ^{16}O nucleus of form (2.9) are given in Table 10.10.

A value 2.697 fm was obtained for the charge radius; this value is just slightly smaller than the result of finite-difference calculation. However, it should be noted that it is as of yet impossible to construct a wave function with large basis dimensionality *N*, as was usually done for lighter cluster systems (see, e.g., [45]); therefore, the values of this wave function already for R>7.5 fm decrease more rapidly than it follows from asymptotics (2.10). If this wave function is used, it should be matched with the asymptotic expression at distances of an order 7.0÷7.5 fm. Only a basis dimensionality 10 or higher can provide correct asymptotics of the variational wave function at distances of the order 10÷15 fm [59].

Table 10.10. Variational parameters and expansion coefficients of the radial wave function of the bound state of the $^4He^{12}C$ system for potential (10.2). Normalization of the wave function with these coefficients in an interval 0÷25 fm is N = 1.00000000000735

i	β_i	C_i
1	8.763690790288099E–002	–1.911450719348557E–001
2	1.866025286442256E–001	–2.207934474863762
3	4.827753981321283E–001	28.389690447396200
4	8.199789461942612E–001	–96.796133806414110
5	1.201089178851195	117.191836404848400
6	1.811929119752430	–48.033080106666700
7	2.549438805955688	–8.312967983049469E–001
8	6.019066491886866	2.748007062675085E–003

The potential of the ground 1*S* state does not result in the correct *S* scattering phase shift, as shown in Figure 10.6 by the dashed line. In order to describe phase shifts obtained from phase shift analysis, it is necessary to change its depth and take

$V_0 = -155$ MeV, $\alpha = 0.189$ fm^{-2}

with the same Coulomb radius. The results of calculation of *S* phase shift with this potential are shown in Figure 10.6 by solid line. The potential also contains four bound forbidden states at energies –1.3, –25.1, –61.5, and –107.7 MeV; it can be seen from Figure 10.6 that this potential reasonably describes *S* phase shift obtained in [198].

For *P*, *D*, *F* and *G* scattering waves the interaction potentials different from potentials of bound states were obtained. The parameters of these potentials and energies of forbidden states (in units of MeV) ($R_{Coul} = 3.55$ fm) are as follows:

$V_P = -145.0$ MeV, $\alpha_P = 0.160$ fm^{-2}, FS: –13.6, –42.1, –79.7;
$V_D = -435.25$ MeV, $\alpha_D = 0.592$ fm^{-2}, FS: –61.9; –167.0;
$V_F = -73.4$ MeV, $\alpha_F = 0.125$ fm^{-2}, FS: –7.5;
$V_G = -55.55$ MeV, $\alpha_G = 0.1$ fm^{-2}, FS: no.

The results of phase shift calculation for these potentials are shown in Figs. 10.7÷10.10 by solid lines, and, evidently, they give a correct general behavior of the experimental phase shifts of scattering.

Thus, the potentials of $^4He^{12}C$ interaction for scattering states and discrete levels have been obtained that correctly describe elastic scattering phase shifts and channel state energies. The difference of potentials describing scattering phase shifts from potentials describing characteristics of bound states can be explained by the small contribution of the considered channel in bound states of ^{16}O nucleus. It is possible that the simple cluster $^4He^{12}C$ model of ^{16}O nucleus, unlike lighter nuclei [87], is incapable of complete description of different characteristics of ^{16}O nucleus and $^4He^{12}C$ scattering channel based on unified potentials.

10.4. ASTROPHYSICAL S-FACTOR

Let us consider the astrophysical *S*-factor of the radiative capture reaction $^{12}C(^4He,\gamma)^{16}O$ at energies from 0.3 to 4.0 MeV based on the potential cluster model and compare it with the results of new experimental data from [196].

It is assumed that experimental data obtained below 2.5 MeV are due to the *E*1 transition [196]. However, in the considered model, this transition is possible only due to the difference of particle masses from corresponding integer values. The results of calculation of the *S*-factor of this transition turned out to be lower by two to three orders of magnitude than the experimental data, although the obtained *S*-factor has a correct form due to the resonance behavior of the *P* scattering phase shift [199].

Thus, the model under consideration cannot correctly describe experimental data based on the *E*1 process. However, in the framework of the applied potential cluster model with forbidden states, this data is reasonably described based on *E*2 transitions from different partial scattering waves to the ground bound state and some excited bound levels of ^{16}O nucleus shown in Figure 10.11. These results can be of particular interest from the point of view of demonstration of the general capabilities of the potential cluster model if the presence of *E*2 processes in the considered radiative capture at low energies is assumed.

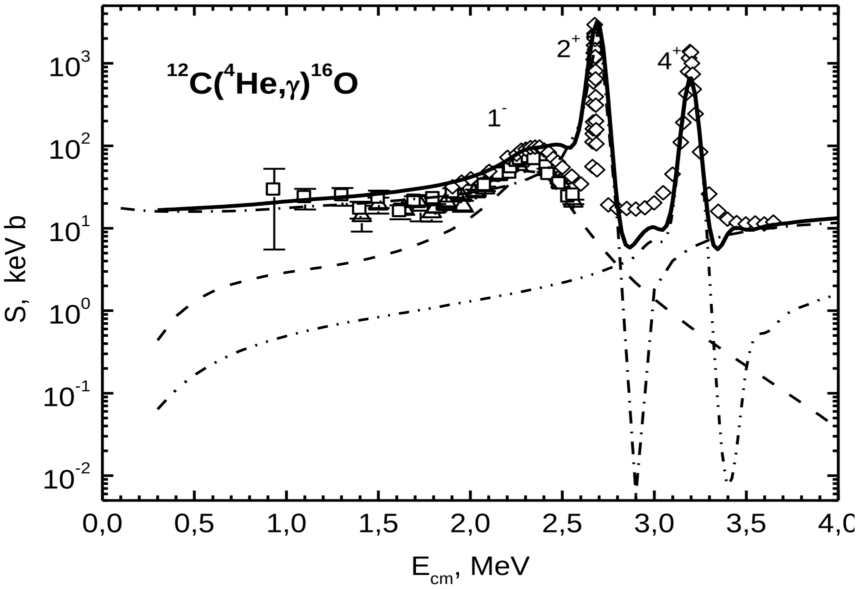

Figure 10.12. Astrophysical *S*-factor of radiative $^4He^{12}C$ capture. Squares show experimental data from survey [33], downward triangles from [204], upward triangles [205], and rhombs [196]. Curves show calculations of the *S*-factor for different *E*2 transitions.

Therefore, below we consider *E*2 transitions only; the first of these transitions is the transition from the *D* scattering wave to the ground bound 1*S* state of ^{16}O nucleus. This process results in the *S*-factor shown in Figure 10.12 by the dash-dotted line. The obtained *S*-factor reasonably explains the experiment at energies from 0.9 to 3.0 MeV but does not describe the resonance at 2.46 MeV, since this resonance is due to the behavior of the *P* scattering phase shift in this energy region.

At energies from 2.5 to 3.0 MeV, the calculated *S*-factor on the whole represents the position and height of the peak due to the resonance in the *D* scattering wave at an energy 2.69 MeV, but the level width is somewhat larger than the experimental one. This indicates insufficiently high growth of the calculated *D* scattering phase shift in the resonance region at 2.69 MeV.

If it is assumed that the experiment includes transitions to the 1*P* level, then the *E*2 process from the *P* scattering wave to the bound 1*P* state of ^{16}O nucleus at energy –0.045 MeV (Figure 10.11) can be considered. The results of this calculation shown in Figure 10.12 by a dashed line quite well reproduce the form of the resonance at 2.46 MeV.

The double-dash-dotted line shows the results of calculation of possible *E*2 transition from *G* scattering wave to the 1*D* bound state, which correctly reproduces the position and width of maximum 4^+ resonance but its value turns out to be lower by approximately a factor 2 than the experimental value. It should be noted that we did not succeed in finding the parameters of the potential for the *G* wave such that the value of the *S*-factor at 4^+ resonance energy was described correctly. If we will use potentials with another number of forbidden states, then, for *G* wave at one FS

$V_G = -110.7$ MeV, $\alpha_G = 0.127$ fm^{-2}, FS: –13.6 MeV

or two FS

$V_G = -222.4$ MeV, $\alpha_G = 0.127$ fm^{-2}, FS: –42,8; –14.6 MeV,

the calculated peak magnitude 4^+ resonance appreciably noticeably decreases, and, then reduction of the number of forbidden states in the bound 1*D* state to one

$V_D = -254.8$ MeV, $\alpha_D = 0.592$ fm^{-2}, FS: –57.0 MeV

or without FS

$V_D = -57.7833$ MeV, $\alpha_D = 0.1$ fm^{-2}

does not lead to the essential rising of the *S*-factor in the range 4^+ resonance.

The solid line in Figure 10.12 shows the sum of all three *E*2 transitions, which, on the whole, describes the experimental behavior of the astrophysical *S*-factor at energies from 0.9 to 4.0 MeV.

Our calculated *S*-factor at 300 keV due to *E*2 process with transition from *D* wave to the ground state of the nucleus turns out to be equal to 16.0 keV b, and at 100 keV its value is somewhat higher: 17.5 keV b. However, these results are noticeably lower than the known data for 300 keV, which result, for example, in $S_{E1} = 101(17)$ keV b and $S_{E2} = 42(^{+16}_{-23})$ keV b [175], $S_{E1} = 79(21)$ keV b or 82(26) keV b [206] and $S_{E2} = 120(60)$ keV b [33]. In the method of generator coordinates [207] taking into account different cluster configurations, the following values were obtained for 300 keV: $S_{E1} = 160$ and $S_{E2} = 70$ keV b. It can be seen that all of these results and our calculations strongly differ between each other.

However, it does not directly follow from the experimental data shown in Figure 10.12 that, at energies below 1 MeV, the *S*-factor experiences sharp growth and at 300 keV it has a value of the order of 100 keV b. In a range 1.1÷1.8 MeV, the *S*-factor is in an interval 16÷25 keV b with errors from 3 to 7 keV b, and at 0.9 MeV it has a value 29 ± 23 keV b [33].

CONCLUSION

Thus, the qualitative analysis of the number of forbidden and allowed states in intercluster interactions of the $^4He^{12}C$ system and partial potentials matched with elastic scattering phase shifts and bound state energies of ^{16}O nucleus obtained based on this analysis makes it possible to obtain an acceptable description of the available data on the astrophysical *S*-factor of radiative $^4He^{12}C$ capture at energies from 0.9 to 4.0 MeV based on the contribution of $E2$ transitions only under particular assumptions.

CONCLUSION

> A certain nuclear model, which can describe the available experimental data, for example astrophysical *S*-factors of a thermonuclear reaction within the energy range for which they are obtained, may also claim to predict correctly the behavior of the *S*-factor at ultralow energies – the range for which the experimental measurements are absent now [30].

Thus, on the basis of the potential cluster model there have been considered astrophysical *S*-factors of radiative capture reactions in nine cluster systems p^2H, p^3H, p^6Li, p^7Li, p^9Be, $p^{12}C$, $^2H^4He$, $^3H^4He$, $^3He^4He$ and $^4He^{12}C$. For the construction of potentials of interactions between the clusters in some of the systems under consideration a phase shift analysis of the available experimental data on elastic scattering at astrophysical energies was performed. Then on the basis of the descriptions of obtained or available in literature phase shifts corresponding intercluster interaction potentials were constructed within the framework of forbidden states concept in multinucleon system consisting of two subsystems the interaction between which is described, as it is supposed, by a local potential. For each partial wave an individual Gaussian-type potential differing from the potentials for other partial waves was obtained.

For the cluster systems pure in Young schemes the nuclear potential, which is obtained from the description of elastic scattering phase shifts, is then used for description of the properties of the ground bound states of nuclei. And it is assumed that the nucleus consists of two fragments the internal properties of which coincide with the properties of corresponding nuclei in a free state. Such a situation takes place in $p^{12}C$ system and with a high likelihood in $^2H^4He$, $^3H^4He$, $^3He^4He$ systems due to a strongly pronounced clusterization of ^6Li, ^7Li, and ^7Be nuclei in the channels under consideration.

In p^2H, p^3H, p^6Li and p^7Li systems the situation is more difficult due to mixing of orbital states in isospin or Young schemes. For the above systems, except p^7Li, two orbital symmetries with different Young schemes are allowed in the continuous spectrum in states with the minimum spin, while for the bound ground states of these systems only one of the two systems is allowed [28]. So, it is impossible to construct the potential for the bound states of clusters on the basis of experimental data description according to elastic scattering phases without the preliminary separation of phases in accordance with the Young schemes. The method of separation of orbital states and potentials of the scattering processes according to Young schemes is demonstrated on the example of p^2H and p^3H systems.

Classification of states according to Young schemes allows determining the presence and the number of Pauli forbidden states, allows fixing the number of wave function nodes of relative cluster motion and establishes a definite depth of the interaction potential. Thus the discrete ambiguity of the potential depth, characteristic of optical model, is avoided [45]. The form of each partial scattering phase as a function of energy is very sensitive to the width of the potential with the forbidden states, which is used to get rid of the continuous ambiguity of the potential, which is also characteristic of the usual optical model [45].

Therefore, all the parameters of scattering potentials in the cluster model under consideration are fixed quite unambiguously as compared to the common optical model. Furthermore, the obtained potentials of intercluster interactions pure in permutation symmetry and isospin or containing forbidden states allow describing correctly the main characteristics of the bound state of the nucleus as a system of two clusters.

The formalism worked out for obtaining intercluster potentials [20,25] is used here for the description of nuclear reactions of photocapture in the systems under consideration. The operator of electromagnetic transition for the processes of radiative capture, as opposed to other nuclear reactions mediated by strong interactions, is well-known. Moreover, in photocapture reaction there is no interaction in the final state, while the interaction in the initial state is described quite correctly on the basis of the well-developed potential approach. Therefore, one can expect the quantitative agreement between the theoretical description and experimental data.

And it is not surprising that within the considered cluster model it was possible to predict the energy dependence of the *S*-factor of radiative p^3H capture in the energy range from 50 to 700 keV by taking into account only E1 transition. On the basis of experimental data for energies beyond 700 keV we managed to calculate about 15 years ago the *S*-factor for the energies down to 10 keV [96]. As it was shown in chapter 4, the results of those calculations reproduce the new data on the *S*-factor [107] in the wide energy range from 50 keV to 5 MeV.

In addition, the predictions as to the behavior of *S*-factor of radiative p^2H capture at energies down to 10 keV [29] made within the potential cluster model under consideration at the times when we knew the experimental data for the energies beyond 150÷200 keV were in a good agreement with the results [66,67] which appeared much later for the energy range from 50 keV to 150÷200 keV.

The cluster interaction potentials given here may also be used for theoretical description of other nuclear processes at low energies involving the same particles. However, as it has been shown above, the reliable results for the intercluster potentials and, consequently, for the characteristics of nuclear processes calculated on their basis can be obtained only if the phase shifts of elastic scattering are accurately determined in the experiment. Unfortunately, at present time for the majority of lightest nuclear systems the elastic scattering phase shifts are found with significant errors reaching sometimes 20÷30%.

In this connection, it is very urgent to raise the accuracy of experimental measurements of elastic scattering of light nuclei at astrophysical energies and to perform a more accurate phase shift analysis. The increase in the accuracy will allow making more definite conclusions regarding the mechanisms and conditions of thermonuclear reactions, as well as understanding better their nature in general [30,219].

Appendix 1

CALCULATION METHODS FOR COULOMB AND WHITTAKER FUNCTIONS

THE COULOMB FUNCTIONS

Now we consider the calculation methods of Coulomb scattering wave functions, which regular $F_L(\eta,\rho)$ and irregular $G_L(\eta,\rho)$ parts are the linearly independent solutions of the radial Schrödinger equation with Coulomb potential for the scattering states having the form [78]

$$\chi_L''(\rho) + \left(1 - \frac{2\eta}{\rho} - \frac{L(L+1)}{\rho^2}\right)\chi_L(\rho) = 0 \quad ,$$

where $\chi_L = F_L(\eta,\rho)$ or $G_L(\eta,\rho)$, $\rho = kr$, and $\eta = (\mu Z_1 Z_2)/(\hbar^2 k)$ is Coulomb parameter. Wronskians of such functions have the forms [208]

$$W_1 = F_L' G_L - F_L G_L' = 1 ,$$
$$W_2 = F_{L-1} G_L - F_L G_{L-1} = \frac{L}{\sqrt{\eta^2 + L^2}} .$$

The recurrent relations between them write down as

$$L[(L+1)^2 + \eta^2]^{1/2} u_{L+1} = (2L+1)\left[\eta + \frac{L(L+1)}{\rho}\right] u_L - (L+1)[L^2 + \eta^2]^{1/2} u_{L-1} \quad ,$$
$$(L+1)u_L' = \left[\frac{(L+1)^2}{\rho} + \eta\right] u_L - [(L+1)^2 + \eta^2]^{1/2} u_{L+1} ,$$
$$L u_L' = [L^2 + \eta^2]^{1/2} u_{L-1} - \left[\frac{L^2}{\rho} + \eta\right] u_L ,$$

where $u_L = F_L(\eta,\rho)$ or $G_L(\eta,\rho)$.

The asymptotic of these functions at $\rho \to \infty$ may be represented as [209]

$$F_L = Sin(\rho - \eta \ln 2\rho - \pi L/2 + \sigma_L) ,$$

$$G_L = Cos(\rho - \eta \ln 2\rho - \pi L / 2 + \sigma_L) .$$

There are number of methods and approximations for calculation of Coulomb scattering wave functions [210-216]. However, only recently the quick convergent representation, that allowed get their values with high accuracy and in the wide diapason of variables, with the small computing time was appeared [42,43].

In this method the Coulomb functions are represented as infinite continued fractions [217]

$$f_L = F_L^{'} / F_L = b_0 + \cfrac{a_1}{b_1 + \cfrac{a_2}{b_2 + \cfrac{a_3}{b_3 + ...}}} \quad ,$$

where

$$b_0 = \left(L+1\right) / \rho + \eta / \left(L+1\right) \ ,$$

$$b_n = \left[2\left(L+n\right)+1\right][\left(L+n\right)\left(L+n+1\right)+\eta\rho] \ ,$$

$$a_1 = -\rho[\left(L+1\right)^2 + \eta^2]\left(L+2\right) / \left(L+1\right) \ ,$$

$$a_n = -\rho^2[\left(L+\mathrm{n}\right)^2 + \eta^2]\left[\left(L+n\right)^2 - 1\right]$$

and

$$P_L + iQ_L = \frac{G_L^{'} + iF_L^{'}}{G_L + iF_L} = \frac{i}{\rho}\left(b_0 + \cfrac{a_1}{b_1 + \cfrac{a_2}{b_2 + \cfrac{a_3}{b_3 + ...}}} \right) ,$$

where

$$b_0 = \rho - \eta, \qquad b_n = 2\left(b_0 + in\right) \ ,$$

$$a_n = -\eta^2 + n\left(n-1\right) - L\left(L+1\right) + i\eta\left(2n-1\right) \ .$$

By usage of given expressions we can find the relation between Coulomb functions and their derivatives [218]

$$F_L^{'} = f_L F_L \,,$$

$$G_L = (F_L^{'} - P_L F_L)/Q_L = (f_L - P_L)F_L/Q_L \,,$$

$$G_L^{'} = P_L G_L - Q_L F_L = [P_L(f_L - P_L)/Q_L - Q_L]F_L \,.$$

Such calculation method is applicable in region at $\rho \geq \eta + \sqrt{\eta^2 + L(L+1)}$, i.e. for $L = 0$ we have $\rho > 2\eta$, and it easy allowed get the high accuracy due to the quick convergence of continued fractions. As the Coulomb parameter η is of order to one and the moment L is always possible to set as zero, then this method gives the good results starting from $\rho > 2$. It is possible to get the values of Coulomb functions for any ρ and for $L > 0$ from the recurrent relations.

So, setting any magnitude of F_L at point ρ it is possible find all other functions and their derivatives accurate within constant factor, that determines from the Wronskians. Calculating the Coulomb functions by using of given formulas and comprising them with the table data [208] leads to the result that it is easy get the correct value with eight-nine accuracy of order if ρ satisfies the condition marked above.

The text of the computing program for the calculating of Coulomb functions is given below. This program has been written on the Fortran-90. Here Q – the Coulomb parameter, LM – the moment of a given partial wave, R – the distance from a centre where the Coulomb functions are calculating, F and G – the Coulomb functions, W – Wronskian, determining the accuracy of Coulomb functions calculation at the given distance.

```
SUBROUTINE CULFUN (LM,R,Q,F,G,W)

! ****Subprogram for the Coulomb functions calculating
IMPLICIT REAL(8) (A-Z)
INTEGER L,K,LL,LM
EP=1.0D-015; L=0; F0=1.0D-000
GK=Q*Q
GR=Q*R
RK=R*R
B01=(L+1)/R+Q/(L+1)
K=1
BK=(2*L+3)*((L+1)*(L+2)+GR)
AK=-R*((L+1)**2+GK)/(L+1)*(L+2)
DK=1.0D-000/BK
DEHK=AK*DK
S=B01+DEHK
15 K=K+1
AK=-RK*((L+K)**2-1.D-000)*((L+K)**2+GK)
BK=(2*L+2*K+1)*((L+K)*(L+K+1)+GR)
DK=1.D-000/(DK*AK+BK)
IF (DK>0.0D-000) GOTO 35
```

```
25 F0=-F0
35 DEHK=(BK*DK-1.0D-000)*DEHK
S=S+DEHK
IF (ABS(DEHK)>EP) GOTO 15
FL=S
K=1
RMG=R-Q
LL=L*(L+1)
CK=-GK-LL
DK=Q
GKK=2.0D-000*RMG
HK=2.0D-000
AA1=GKK*GKK+HK*HK
PBK=GKK/AA1
RBK=-HK/AA1
AOMEK=CK*PBK-DK*RBK
EPSK=CK*RBK+DK*PBK
PB=RMG+AOMEK
QB=EPSK
52 K=K+1
CK=-GK-LL+K*(K-1.)
DK=Q*(2.*K-1.)
HK=2.*K
FI=CK*PBK-DK*RBK+GKK
PSI=PBK*DK+RBK*CK+HK
AA2=FI*FI+PSI*PSI
PBK=FI/AA2
RBK=-PSI/AA2
VK=GKK*PBK-HK*RBK
WK=GKK*RBK+HK*PBK
OM=AOMEK
EPK=EPSK
AOMEK=VK*OM-WK*EPK-OM
EPSK=VK*EPK+WK*OM-EPK
PB=PB+AOMEK
QB=QB+EPSK
IF (( ABS(AOMEK)+ABS(EPSK) )>EP) GOTO 52
PL=-QB/R
QL=PB/R
G0=(FL-PL)*F0/QL
G0P=(PL*(FL-PL)/QL-QL)*F0
F0P=FL*F0
ALFA=1.0D-000/( (ABS(F0P*G0-F0*G0P))**0.5 )
G=ALFA*G0
GP=ALFA*G0P
F=ALFA*F0
```

```
FP=ALFA*F0P
W=1.0D-000-FP*G+F*GP
IF (LM==0) GOTO 123
AA=(1.0D-000+Q**2)**0.5
BB=1.0D-000/R+Q
F1=(BB*F-FP)/AA
G1=(BB*G-GP)/AA
WW1=F*G1-F1*G-1.0D-000/(Q**2+1.0D-000)**0.5
IF (LM==1) GOTO 234
DO L=1,LM-1
AA=((L+1)**2+Q**2)**0.5
BB=(L+1)**2/R+Q
CC=(2*L+1)*(Q+L*(L+1)/R)
DD=(L+1)*(L**2+Q**2)**0.5
F2=(CC*F1-DD*F)/L/AA
G2=(CC*G1-DD*G)/L/AA
WW2=F1*G2-F2*G1-(L+1)/(Q**2+(L+1)**2)**0.5
F=F1; G=G1; F1=F2; G1=G2
ENDDO
234 F=F1; G=G1
123 CONTINUE
END
```

The calculation results of Coulomb functions for $\eta = 1$ and $L = 0$ control and their compararison with the table data [208] are given in table A.1.1. We see that now the correct results are getting for $\rho = kr = 1$. The magnitude of Wronskian represented as $W_0 - 1$ is not larger $10^{-15} \div 10^{-16}$ for any $\rho \geq 1$.

Table A1.1 The Coulomb functions

ρ	**F_0 (Our calculation)**	**F_0 [208]**	**G_0 (Our calculation)**	**G_0 [208]**
1	2.275262105105590E–001	0.22753	2.043097162103547	2.0431
5	6.849374120059441E–001	0.68494	–8.98414359092021E–001	–0.89841
10	4.775608158625742E–001	0.47756	9.428742426537808E–001	0.94287
15	–9.787895837822600E–001	–0.97879	3.404637385301291E–001	0.34046
20	–3.292255362657541E–001	–0.32923	–9.72428398697120E–001	–0.97243

THE WHITTAKER FUNCTIONS

The Whittaker function is the solution of the Schrödinger equation without nuclear potential for forbidden states [208]

$$\frac{d^2W(\mu,\nu,z)}{dz^2}-\left(\frac{1}{4}-\frac{\nu}{z}-\frac{1/4-\mu^2}{z^2}\right)W(\mu,\nu,z)=0\,,$$

that is possible leads to the standard Schrödinger equation

$$\frac{d^2\chi(k,L,r)}{dr^2}-\left(k^2+\frac{g}{r}+\frac{L(L+1)}{r^2}\right)\chi(k,L,r)=0\,,$$

where $\mathrm{g}=\frac{2\mu Z_1Z_2}{\hbar^2}=2k\eta$, $\eta=\frac{\mu Z_1Z_2}{k\hbar^2}$ – Coulomb parameter, $z = 2kr$, $\nu=-\frac{g}{2k}=-\eta$ and $\mu = L + 1/2$.

For finding the numerical magnitudes of Whittaker function its integral representation is used frequently

$$W(\mu,\nu,z)=\frac{z^{\nu}e^{-z/2}}{\Gamma(1/2-\nu+\mu)}\int t^{\mu\text{-}\nu-1/2}(1+t/z)^{\mu+\nu-1/2}e^{-t}dt\,,$$

that may be transform to the form

$$W_{-\eta L+\frac{1}{2}}(z)=W(L+\frac{1}{2},-\eta,z)=\frac{z^{-\eta}e^{-z/2}}{\Gamma(L+\eta+1)}\int t^{L+\eta}(1+t/z)^{L\text{-}\eta}e^{-t}dt$$

It is easy to see that at $L = 1$ and $\eta = 1$ the integral marked above reduces into $\Gamma(3)$, that cancels with denominator. As the result we get the simple expression

$$W(1+\frac{1}{2},-1,z)=\frac{e^{-z/2}}{z}\,.$$

It possible use for the control of correctness the Whittaker function calculation at the arbitrary z, remembering that $L = 1$, $\eta = 1$ and $z = 2kr$.

The program for calculation of Whittaker function within its integral representation [208] is given below.

```
PROGRAM WHI
IMPLICIT REAL(8) (A-Z)
INTEGER L
L=1
```

```
SK=1.0D-000
GK=1.0D-000
DO X=1,20
CALL WW(SK,L,GK,X,WH)
W=DEXP(-X*SK)/2.0D-000/X/SK
PRINT*, X,WH,W
ENDDO
END
SUBROUTINE WW(SK,L,GK,RR,WH)
IMPLICIT REAL(8) (A-Z)
DIMENSION VV(0:100000)
INTEGER NN,L,NNN,I
SS=(ABS(SK))**0.5
AA=GK/SS
BB=L
ZZ=1.0D-000+AA+BB
AAA=1.0D-000/ZZ
NNN=1000000
DO I=1,NNN
AAA=AAA*I/(ZZ+I)
ENDDO
GAM=AAA*NNN**ZZ
CC=2.0D-000*RR*SS
NN=10000
HH=0.0050D-000
DO I=0,NN
TT=HH*I
VV(I)=TT**(AA+BB)*(1.0D-000+TT/CC)**(BB-AA)*EXP(-TT)
ENDDO
CALL SIMP(VV,HH,NN,SI)
WH=SI*EXP(-CC/2.0D-000)/(CC**AA*GAM)
END
SUBROUTINE SIMP(V,H,N,S)
IMPLICIT REAL(8) (A-Z)
DIMENSION V(0:10240000)
INTEGER N,II,JJ
A=0.0D-000; B=0.0D-000
A111: DO II=1,N-1,2
B=B+V(II)
ENDDO A111
B111: DO JJ=2,N-2,2
A=A+V(JJ)
END DO B111
S=H*(V(0)+V(N)+2.0D-000*A+4.0D-000*B)/3.0D-000
END
```

Here $A = \frac{\mu Z_1 Z_2}{k\hbar^2} = G/k$ is the Coulomb parameter, $G = \frac{\mu Z_1 Z_2}{\hbar^2}$, $k^2 = \frac{2\mu E}{\hbar^2} = \frac{2\mu E}{41.4686}$ – wave number in fm^{-2}, E – energy in MeV, X – distance from the center equals r in fm, $Z = 2kr$ – dimensionless variable, L – orbital moment.

Below the results of Whittaker function calculation at η = 1 and $k = 1$ for different orbital moments L and its exact magnitudes $W_{\exp}$ at $L = 1$ and η = 1 are given.

R	W(L = 0)
1.000000000000000	1.020290079327840E–001
2.000000000000000	2.363196623576423E–002
3.000000000000000	6.392391215042637E–003
4.000000000000000	1.863857863268692E–003
5.000000000000000	5.684597929937536E–004
6.000000000000000	1.786848627416934E–004
7.000000000000000	5.739835037958716E–005
8.000000000000000	1.874246806441706E–005
9.000000000000000	6.199016558901119E–006
10.000000000000000	2.071563699444139E–006
11.000000000000000	6.981628624614050E–007
12.000000000000000	2.369723360890071E–007
13.000000000000000	8.092018511054453E–008
14.000000000000000	2.777589770610260E–008
15.000000000000000	9.577168790058733E–009
16.000000000000000	3.315309238772864E–009
17.000000000000000	1.151676608740117E–009
18.000000000000000	4.013201009814541E–010
19.000000000000000	1.402378280368625E–010
20.000000000000000	4.912856187198094E–011

R	W(L = 1)	$W_{\exp}$(L = 1)
1.000000000000000	1.839408242280025E–001	1.839397205857212E-001
2.000000000000000	3.383402381280602E-002	3.383382080915318E-002
3.000000000000000	8.297894515224235E-003	8.297844727977325E-003
4.000000000000000	2.289468597870201E-003	2.289454861091772E-003
5.000000000000000	6.737987426912442E-004	6.737946999085467E-004
6.000000000000000	2.065639207693961E-004	2.065626813888632E-004
7.000000000000000	6.513481691899502E-005	6.513442611103688E-005
8.000000000000000	2.096654004284359E-005	2.096641424390699E-005
9.000000000000000	6.856141363786637E-006	6.856100227037754E-006
10.00000000000000	2.270010108152015E-006	2.269996488124243E-006
11.00000000000000	7.591727727640804E-007	7.591682177384391E-007
12.00000000000000	2.560103841139389E-007	2.560088480553421E-007
13.00000000000000	8.693626803869737E-008	8.693574642234824E-008
14.00000000000000	2.969763243906337E-008	2.969745425369885E-008
15.00000000000000	1.019680519741103E-008	1.019674401672753E-008

16.00000000000000	3.516745310397776E-009	3.516724209976847E-009
17.00000000000000	1.217636046617811E-009	1.217628740819167E-009
18.00000000000000	4.230575312477445E-010	4.230549929086842E-010
19.00000000000000	1.474428961693802E-010	1.474420115141386E-010
20.00000000000000	5.152914973511605E-011	5.152884056096395E-011

From this table we see the coincidence with exact function at $L = \eta = 1$ with the relative error of order 10^{-5}. Under usage of NNN = 1000 and NN = 1000 with HH = 0.015 this error is about 6 10^{-3} or 0.6%.

Appendix 2

BASIC ASTROPHYSICAL TERMS AND CONCEPTS (FOR BEGINNERS)

NUCLEAR ASTROPHYSICS

(http://en.wikipedia.org/wiki/Nuclear_astrophysics)

Nuclear astrophysics is an interdisciplinary branch of physics involving close collaboration among researchers in various subfields of nuclear physics and astrophysics, with significant emphasis in areas such as stellar modeling, measurement and theoretical estimation of nuclear reaction rates, cosmology, cosmochemistry, gamma ray, optical and X-ray astronomy, and extending our knowledge about nuclear lifetimes and masses. In general terms, nuclear astrophysics aims to understand the origin of the chemical elements and the energy generation in stars [8].

THERMONUCLEAR (FUSION) REACTION

(http://en.wikipedia.org/wiki/Fusion_reaction)

Fusion reactions power the stars and produce virtually all elements in a process called nucleosynthesis.

Generally, when dealing with elements lighter than iron, the lower the ratio of atomic mass to mass number. This is known as mass defect. Fusion of lighter nuclei into heavier nuclei leads to loss of mass when the energy of binding is removed (this energy carries away the lost mass), even though no nucleons are lost. This lost mass is present in the released energy in accordance with $E = mc^2$. Most of the excess binding energy is released as kinetic energy of the resulting particles. When these particles are slowed, this energy is available to do work or be converted to electromagnetic radiation or heat.

The fusion of lighter elements in stars releases energy (and the mass that always accompanies it). For example, in the fusion of four hydrogen nuclei to form helium, seven-tenths 1 percent of the mass is carried away from the system in the form of kinetic energy or other forms of energy (such as electromagnetic radiation). However, the production of elements heavier than iron absorbs energy.

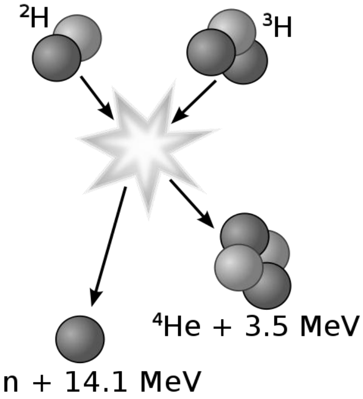

Fusion of deuterium with tritium creating helium-4, freeing a neutron, and releasing 17.59 MeV of energy, as an appropriate amount of mass changing forms to appear as the kinetic energy of the products, in agreement with kinetic $E = \Delta mc^2$, where Δm is the change in rest mass of particles.

PROTOSTAR

(http://en.wikipedia.org/wiki/Protostar)

A protostar, existence of which for the first time was proposed and postulated by the Soviet (Armenian) physicist Viktor Ambartsumian, is a large mass that forms by contraction out of the gas of a giant molecular cloud in the interstellar medium. The protostellar phase is an early stage in the process of star formation. This is a star formation stage before the moment of burning of thermonuclear reactions (proton-proton chain) in its core. After this the compression of the star brings to a stop and it becomes a stable star of the Main Sequence.

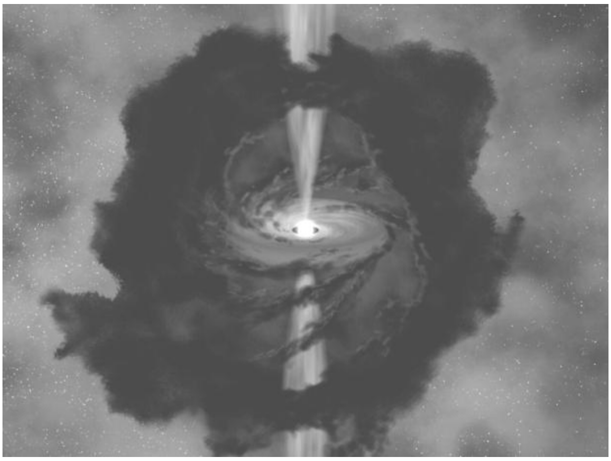

STAR

(http://en.wikipedia.org/wiki/Star).

For a one solar-mass star it lasts about 100,000 years. It starts with a core of increased density in a molecular cloud and ends with the formation of a T Tauri star, which then develops into a main sequence star. This is heralded by the T Tauri wind, a type of super solar wind that marks the change from the star accreting mass into radiating energy

A star is a massive, luminous ball of ionized gas and plasma heating at the expense of nuclear energy (fusion reactions) and held together by gravity. The nearest star to the Earth is the Sun, which is the source of most of the energy on the Earth. Other stars are visible from the Earth during the night when they are not outshone by the Sun or blocked by atmospheric phenomena. Binary and multi-star systems consist of two or more stars that are gravitationally bound, and generally move around each other in stable orbits. When two such stars have a relatively close orbit, their gravitational interaction can have a significant impact on their evolution. Stars can form part of a much larger gravitationally bound structure, such as a cluster or a galaxy [115].

SUN

(http://en.wikipedia.org/wiki/Sun)

The Sun is the star at the center of the Solar System. It is almost perfectly spherical and consists of hot plasma interwoven with magnetic fields. It has a diameter of about 1,392,000 km, about 109 times that of Earth, and its mass (about $2 \cdot 10^{30}$ kilograms, 330,000 times that of Earth) accounts for about 99.86% of the total mass of the Solar System. Chemically, about three quarters of the Sun's mass consists of hydrogen, while the rest is mostly helium. Less than 2% consists of heavier elements, including oxygen, carbon, neon, iron, and others.

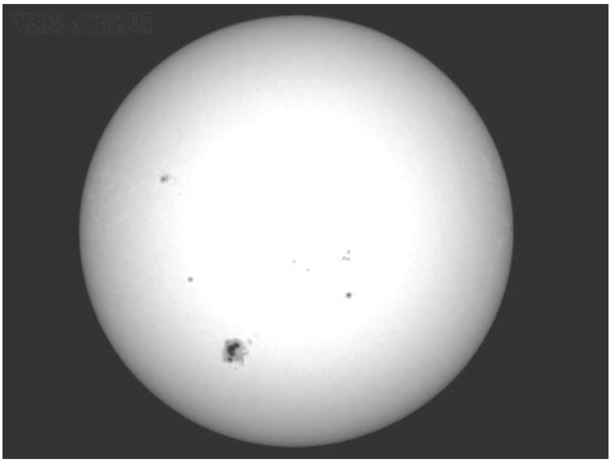

The Sun's stellar classification, based on spectral class, is G2V, and is informally designated as a Yellow Dwarf, because its visible radiation is most intense in the yellow-green portion of the spectrum and although its color is white, from the surface of the Earth it may appear yellow because of atmospheric scattering of blue light. In the spectral class label, G2 indicates its surface temperature of approximately 5778 K (5505° C), and V indicates that the Sun, like most stars, is a main sequence star, and thus generates its energy by nuclear fusion of hydrogen nuclei into helium. In its core, the Sun fuses 620 million metric tons of hydrogen each second [8].

MAIN SEQUENCE

(http://en.wikipedia.org/wiki/Main_sequence)

The main sequence is a continuous and distinctive band of stars that appears on plots of stellar color versus brightness. These color-magnitude plots are known as Hertzsprung–Russell diagrams after their co-developers, Ejnar Hertzsprung and Henry Norris Russell. Stars on this band are known as Main Sequence stars or "dwarf" stars. After a star has formed, it creates energy at the hot, dense core region through the nuclear fusion of hydrogen atoms into helium. During this stage of the star's lifetime, it is located along the main sequence at a position determined primarily by its mass, but also based upon its chemical composition and other factors. The main sequence is sometimes divided into upper and lower parts, based on the dominant process that a star uses to generate energy. Stars below about 1.5 times the mass of the Sun (or 1.5 solar masses) primarily fuse hydrogen atoms together in a series of stages to form helium, a sequence called the proton-proton chain. Above this mass, in the upper main sequence, the nuclear fusion process mainly uses atoms of carbon, nitrogen and oxygen as intermediaries in the CNO cycle that produces helium from hydrogen atoms [8].

HERTZSPRUNG-RUSSELL DIAGRAM

(http://en.wikipedia.org/wiki/Hertzsprung-Russell_diagram)

The Hertzsprung-Russell diagram is a scatter graph of stars showing the relationship between the stars' absolute magnitudes or luminosities versus their spectral types or classifications and effective temperatures. Hertzprung-Russell diagrams are not pictures or maps of the locations of the stars. Rather, they plot each star on a graph measuring the star's absolute magnitude or brightness against its temperature and color.

Another form of the diagram plots the effective surface temperature of the star on one axis and the luminosity of the star on the other. This is what theoreticians calculate using computer models that describe the evolution of stars. This type of diagram should probably be called temperature-luminosity diagram, but this term is hardly ever used, the term Hertzsprung-Russell diagram being preferred instead. One peculiar characteristic of this form of the H-R diagram is that the temperatures are plotted from high temperature to low temperature, which aids in comparing this form of the H-R diagram with the observational form.

Existence of the Main Sequence connected with the fact that hydrogen burning stage is equal to ~90% of evolution time of the majority of stars. The process of hydrogen burning in the central parts of star leads to the formation of isothermic helium core, transition to the Red Giant stage and to the leaving of the star from the Main Sequence. Relatively short evolution of Red Giants, in dependence of their masses, leads to the formation of White Dwarfs, neutron stars or black holes [6].

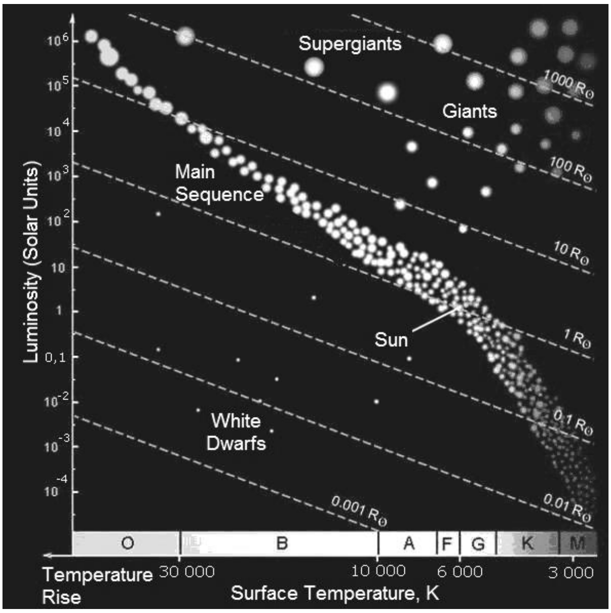

(from: http://zvezdi-galakt.narod.ru/diagr1.htm).

GALAXY

(http://en.wikipedia.org/wiki/Galaxy)

A Galaxy is a massive, gravitationally bound system that consists of stars and stellar remnants, an interstellar medium of gas dust, and an important but poorly understood component tentatively dubbed dark matter.

(from: http://astronet.ru/db/msg/1180523/pic01.html).

Typical Galaxies range from Dwarfs with as few as ten million (10^7) stars, up to giants with a hundred trillion (10^{14}) stars, all orbiting the galaxy's center of mass. Galaxies may contain many star systems, star clusters, and various interstellar clouds. The Sun is one of the stars in the Milky Way galaxy; the Solar System includes the Earth and all the other objects that orbit the Sun [8].

SOME ASTRONOMICAL DISTANCE UNITS

(http://en.wikipedia.org/wiki/Astronomical_unit)

Light-year

It is the distance unit using in astronomy and cosmology. A light-year is defined as the distance that light can travel in vacuum during 1 tropical year: 1 light-year (ly) = $9.46\ 10^{15}$ m = $9.46\ 10^{12}$ km = 0.307 pc [8].

Parsec

Another astronomical distance unit is parsec: 1 parsec (pc) = 3.26 ly = 206,265 AU = $3.086\ 10^{16}$ m [8].

Astronomical unit

An astronomical unit (abbreviated as AU, au or a.u.) is a unit of length equal to about 149,597,870.7 kilometers (92,955,807.27 miles) [8] or approximately the mean Earth-Sun distance. The AU was originally defined as the length of the semi-major axis of the Earth's elliptical orbit around the Sun. The AU is one of the most precisely defined astronomical constants. The best current (2009) estimate of the International Astronomical Union (IAU) for the value of the astronomical unit in meters is A = 149 597 870 700(3) m, based on a comparison of JPL and IAA–RAS ephemerides [8].

RED GIANT

(http://en.wikipedia.org/wiki/Red_Giant)

A red giant is a luminous giant star of low or intermediate mass (roughly 0.5÷10 solar masses) in a late phase of stellar evolution. The outer atmosphere is inflated and tenuous, making the radius immense and the surface temperature low, somewhere from 5,000 K and lower. The appearance of the red giant is from yellow orange to red, including the spectral types K and M, but also class S stars and most carbon stars.

The most common red giants are the so-called red giant branch stars (RGB stars) whose shells are still fusing hydrogen into helium, while the core is inactive helium. Another case of red giants are the asymptotic giant branch stars (AGB) that produces carbon from helium by the triple-alpha process [8].

WHITE DWARF

(http://en.wikipedia.org/wiki/White_Dwarf)

These are stars after evolution process with the mass not more than Chandrasekhar limit (it is an upper bound on the mass of a stable white dwarf star) and without sources of thermonuclear energy.

White Dwarfs are compact stars with masses comparable with solar mass, radiuses ~100 times and luminosities ~10,000 times less than the solar radius and luminosity correspondingly. The density of White Dwarfs are equal to $10^5 \div 10^9$ g/cm³, that is about one million times greater than the density of general stars of the Main Sequence. The number of White Dwarfs, from different estimation, equals 3÷10 % of stars of our Galaxy [8].

NEUTRON STAR

(http://en.wikipedia.org/wiki/Neutron_star)

A neutron star is a type of stellar remnant that can result from the gravitational collapse of a massive star during a Type II, Type Ib or Type Ic supernova event. Such stars are composed almost entirely of neutrons, which are subatomic particles without electrical charge and a slightly larger mass than protons.

Neutron star diameter is very small (about 20÷30 km); mean substance overall densities predicted by the APR EOS from $3.7 \cdot 10^{17}$ to $5.9 \cdot 10^{17}$ kg/m^3 ($2.6 \cdot 10^{14}$ to $4.1 \cdot 10^{14}$ times the density of the Sun) compares with the approximate density of an atomic nucleus of $3 \cdot 10^{17}$ kg/m^3.

In general, compact stars of less than 1.44 solar masses – the Chandrasekhar limit – are White Dwarfs, and above 2 to 3 solar masses (the Tolman-Oppenheimer-Volkoff limit), a quark star might be created; however, this is uncertain. Gravitational collapse will usually occur on any compact star between 10 and 25 solar masses and produce a black hole.

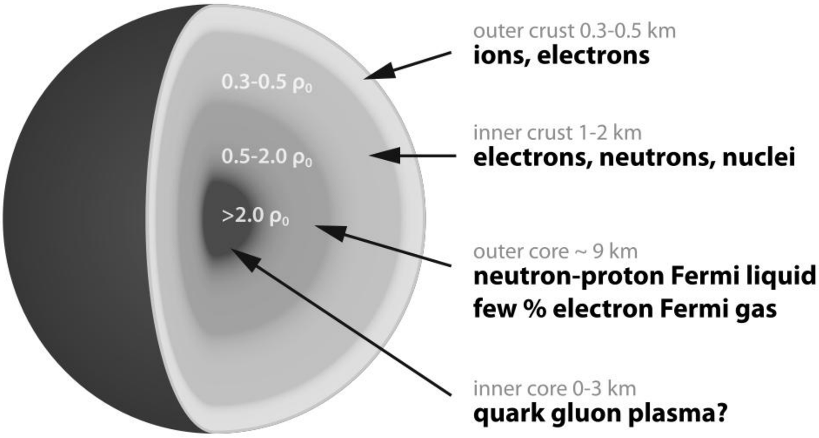

Cross section of neutron star.

Densities are in terms of ρ_0 the saturation nuclear matter density, where nucleons begin to touch

BLACK HOLE

(http://en.wikipedia.org/wiki/Black_hole)

A black hole is a region of space from which nothing, not even light, can escape. The theory of general relativity predicts that a sufficiently compact mass will deform space-time to form a black hole. Around a black hole there is an undetectable surface called an event horizon that marks the point of no return. It is called "black" because it absorbs all the light that hits the horizon, reflecting nothing, just like a perfect black body in thermodynamics. Quantum mechanics predicts that black holes emit radiation like a black body with a finite temperature. This temperature is inversely proportional to the mass of the black hole, making it difficult to observe this radiation for black holes of stellar mass or greater.

The event horizon is a theoretical boundary around a black hole beyond which no light or other radiation can escape. This horizon, in the simplest case of spherically symmetric black hole, is equal to the Schwarzschild radius $r_s = \frac{2GM}{c^2}$, where c is the speed of light, M – mass of a body, G – gravitation constant [6].

CHANDRASEKHAR LIMIT

(http://en.wikipedia.org/wiki/Chandrasekhar_limit)

The Chandrasekhar limit is an upper bound on the mass of a stable white dwarf star. It was named after Subrahmanyan Chandrasekhar, the Indian astrophysicist who predicted it in 1930. White dwarfs, unlike main sequence stars, resist gravitational collapse primarily through electron degeneracy pressure, rather than thermal pressure. The Chandrasekhar limit is the mass above which electron degeneracy pressure in the star's core is insufficient to balance the star's own gravitational self-attraction. Consequently, white dwarfs with masses greater than the limit undergo further gravitational collapse, evolving into a different type of stellar remnant, such as a neutron star or black hole. Those with masses under the limit remain stable as white dwarfs. The Chandrasekhar limit is analogous to the Tolman-Oppenheimer-Volkoff limit for neutron stars. The currently accepted numerical value of the limit is about 1.38÷1.44 $\mathfrak{M}_\odot$ [8].

OPPENHEIMER-VOLKOFF LIMIT

(http://en.wikipedia.org/wiki/Oppenheimer-Volkoff_limit)

The limit was computed by J. Robert Oppenheimer and Georges Volkoff in 1939, using the work of Richard Chace Tolman. Oppenheimer and Volkoff assumed that the neutrons in a neutron star formed a cold, degenerate Fermi gas. This leads to a limiting mass of approximately 0.7 solar masses. Modern estimates range from approximately 1.5 to 3.0 solar masses. The uncertainty in the value reflects the fact that the equations of state for extremely dense matter are not well-known [6].

In a neutron star less massive than the limit, the weight of the star is balanced by short-range repulsive neutron-neutron interactions mediated by the strong force and also by the quantum degeneracy pressure of neutrons, preventing collapse. If its mass is above the limit, the star will collapse to some denser form. It could form a black hole, or change composition and be supported in some other way (for example, by quark degeneracy pressure if it becomes a quark star).

SATELLITE

(http://en.wikipedia.org/wiki/Satellite)

It is celestial body circulating on the certain trajectory (orbit) around other object (for example planet) in outer space, under gravity. There are natural and non-natural satellites. Almost all planets of our Solar System have natural satellites [6].

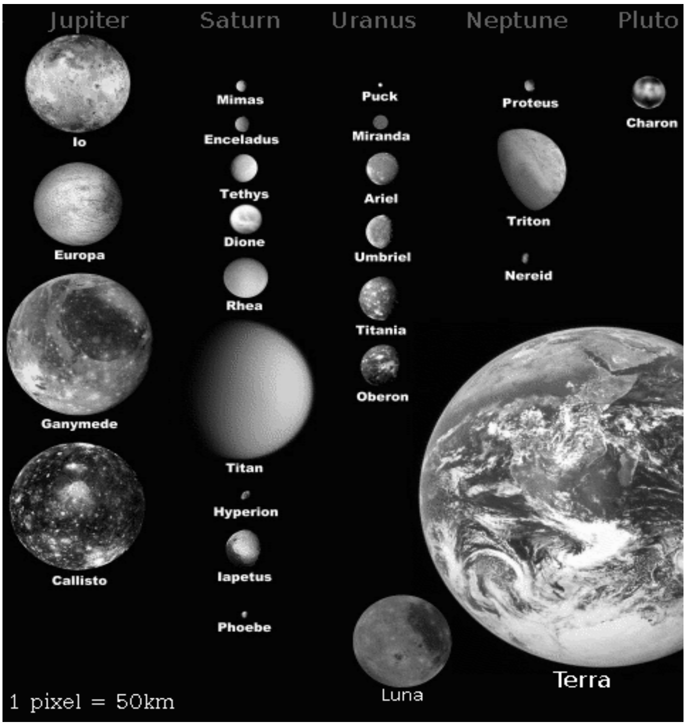

(from:http://ru.wikipedia.org/wiki/%D0%A4%D0%B0%D0%B9%D0%BB:Moons_of_solar_system _small.png).

PLANET

(http://en.wikipedia.org/wiki/Planet)

It is celestial body orbiting a star or stellar remnant in their gravitational field and shines by reflected light. The mass of such planet is not enough to cause thermonuclear fusion, such as the nuclear reaction can not be burned in interiors of planets with a mass less than 0.1 solar mass $\mathfrak{M}_{\odot}$ [8].

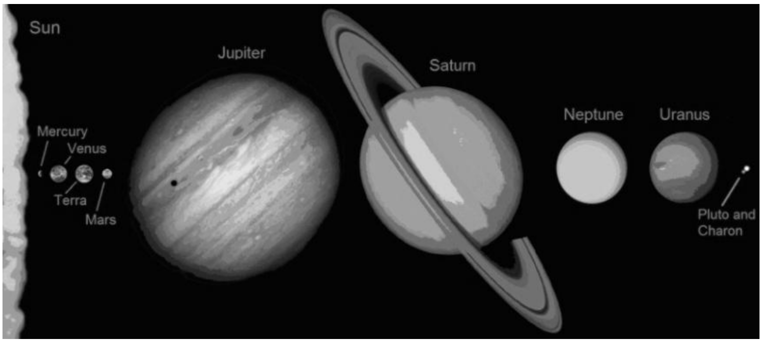

(from: http://astronet.ru/db/msg/1180522/pic01.html).

Table A2.1. Basic characteristics of the Universe and certain stages of its evolution [2] are shown below

t = 0		The Big Bang. Birth of the Universe $\rho(\text{g/cm}^3)=\frac{5\times10^5}{t^2(\text{sec})}$, $T(\text{K})=\frac{10^{10}}{\sqrt{t(\text{sec})}}$
t = 10^{-43} sec		Quantum gravitation era. Strings $\rho = 10^{90}$ g/cm^3, T = 10^{32} K
t = 10^{-35} sec		Quark-gluon medium $\rho = 10^{75}$ g/cm^3, T = 10^{28} K
t = 1 microsecond		Quarks are associated into neutrons and protons ρ = 1017 g/cm3, T = 6×1012 K
t = 100 sec		Formation of prestellar 4He ρ = 50 g/cm3, T = 109 K
t = 380,000 years		Formation of neutral atoms ρ = 0.5×10-20 g/cm3, T = 3×103 K
t = 108 years	EARLIEST STARS	Hydrogen burning in stars ρ = 102 g/cm3, T = 2×106 K Helium burning in stars ρ = 103 g/cm3, T = 2×108 K Carbon burning in stars ρ = 105 g/cm3, T = 8×108 K Oxygen burning in stars ρ = 105÷106 g/cm3, T = 2×109 K Silicon burning in stars ρ = 106 g/cm3, T = (3÷5)×109 K
t = 13.7 billions of years		Modern Universe ρ = 10-30 g/cm3, T = 2.73 K

REFERENCES

[1] Barnes, C. A.; Clayton, D. D.; Schramm, D. N.; *Essays in Nuclear Astrophysics* Presented to William A. Fowler; Publisher: Cambridge University Press, Cambridge, UK, 1982; pp 562.

[2] Kapitonov, I. M.; Ishkhanov, B. S.; Tutyn', I. A. *Nucleosynthesis in the Universe*; Publisher: Librokom, Moscow, 2009, (in Russian); http://nuclphys.sinp.msu.ru/lect/index.html; Peacock, J. A. *Cosmological Physics*; Publisher: Cambridge University Press, Cambridge, UK, 1999.

[3] Gorbunov, D. S.; Rubakov, V. A. *Introduction to theory of early Universe. Theory of hot Big Bang*; Publisher: Singapore, N.J. Hackensack, World Scientific, 2011.

[4] Zasov, A. V.; Postnov, K. A. *General astrophysics*; Publisher: Fryazino, Moscow, 2006, pp 496 (in Russian); Postnov, K. A. *Lectures on general astrophysics for physicists*; http://www.astronet.ru:8101/db/msg/1170612/index.html (in Russian).

[5] Shklovskii, I. S. *Stars: birth, life and death*; Publisher: San Francisco, W.H. Freeman, 1978.

[6] http://ru.wikipedia.org.

[7] Zel'dovich, Ya. B.; Novikov, I. D. *Structure and Evolution of the Universe*; Publisher: University of Chicago Press, L. Fishbone, 1983.

[8] http://astronet.ru.

[9] Gulyaev, S. A.; Zhukovski V. M.; Komov S. V. *World system*; http://detc.usu.ru/assets/ansci0011/general/index.html.

[10] Epelbaum, E.; Glockle, W.; Meissner, U. G. *Nucl. Phys.* 2005, vol. A 747, 362-424; Epelbaum, E. et al. *Phys. Rev.* 2002, vol. C 66, 064001-1-064001-17; Epelbaum, E. *Eur. Phys. J.* 2007, vol. A 34, 197-214.

[11] Fadeev, L. D. *Zh. Eksp. Teor. Fiz.* 1960, vol. 39, 1459-1467.

[12] Yakubovskii, O. A. *Yad. Fiz.* 1967, vol. 5, 1312-1320.

[13] Grassberger, P.; Sandhas, W. *Nucl. Phys.* 1967, vol. B2, 181-206; Alt, E. O.; Grassberger, P.; Sandhas W. *JINR Report* No. E4-6688, Dubna, 1972.

[14] Deltuva, A.; Fonseca, A. C. *Phys. Rev. Lett.* 2007, vol. 98, 162502-1-162502-4; Deltuva, A.; Fonseca, A. C. *Phys. Rev.* 2007, vol. C 76, 021001-1(R)-0211001-4(R).

[15] Lazauskas, R. *Phys. Rev.* 2009, vol. C 79, 054007-1-054007-5.

[16] Tang, Y. C.; Lemere, M.; Thompson, D. R. *Phys. Rep.* 1978, vol. 47, 167-223.

[17] Navratil, P.; Vary, J. P.; Barrett, B. R. *Phys. Rev. Lett.* 2000, vol. 84, 5728-5731.

[18] Quaglioni, S.; Navratil, P. *Phys. Rev. Lett.* 2008, vol. 101, 092501-1-092501-4.

[19] Kievsky, A.; Viviany, M.; Rosati, S. *Phys. Rev.* 2001, vol. C 64, 024002-1-024002-18.

[20] Dubovichenko, S. B. *Property of light atomic nuclei in potential cluster models*; Publisher: Daneker, Almaty, Kazakhstan, 2004; pp 248 (in Russian); http://xxx.lanl.gov/abs/1006.4944.

[21] Zaguskii, V. L. *Guide on numerical methods of solution of equations*; Publisher: Fiz. Mat. Lit, Moscow, 1960; pp 215.

[22] Melent'ev, P. V. *Approximate calculus*; Publisher: Fiz. Mat. Lit, Moscow, 1962; pp 387.

[23] Demidovich, B. P.; Maron, I. F. *Foundation of calculus mathematics*; Publisher: Nauka, Moscow, 1966; pp 664.

[24] Dubovichenko, S. B. *Calculation methods of the nuclear characteristics*; Publisher: Complex, Almaty, Kazakhstan, 2006; pp 311 (in Russian); http://xxx.lanl.gov/abs/1006.4947.

[25] Nemets, O. F.; Neudatchin, V. G.; Rudchik, A. T.; Smirnov, Y. F.; Tchuvil'sky, Yu. M. *Nucleon Association in Atomic Nuclei and the Nuclear Reactions of the Many Nucleons Transfers*; Publisher: Naukova dumka, Kiev, 1988, pp 488 (in Russian); Kukulin V.I., Neudatchin V.G., Obukhovsky I.T. and Smirnov Yu.F., *Clusters as subsystems in light nuclei,* in: *Clustering Phenomena in Nuclei.* Edited by K. Wildermuth and P. Kramer. Vieweg, Braunschweig, 1983. V.3, P.1.

[26] Baktybayev, M. K. et al. *The Fourth Eurasian Conference "Nuclear Science and its Application"*, October 31-November 3, Baku, Azerbaijan; 2006, p. 62; Burtebayev, N. et al. The new experimental data on the elastic scattering of protons from ^{6}Li, ^{7}Li, ^{16}O and ^{27}Al nuclei; *Book of Abstracts the Fifth Eurasian Conference on "Nuclear Science and its Application"*, October 14-17, Ankara, Turkey, 2008; p 40.

[27] Zazulin, D. M. et al. Scattering of protons from 12C; *The Sixth International conference "Modern Problems of Nuclear Physics"*, September 19-22, Tashkent, Uzbekistan, 2006; p 127; Baktybaev, M. K. et al. Elastic scattering of protons from ^{12}C, ^{16}O and ^{27}Al; *The 4th Eurasia Conf., "Nuclear Science and its Application"*, Baku, Azerbaijan, 2006; p 56.

[28] Neudatchin, V. G. et al. *Phys. Rev.* 1992, vol. C 45, 1512-1527.

[29] Dubovichenko, S. B. *Phys. Atom. Nucl.* 1995, vol. 58, 1174-1180.

[30] Dubovichenko, S. B.; Uzikov, Yu. N. *Phys. Part. Nucl.* 2011, vol. 42, 251-301.

[31] Fowler, W. A.; Caughlan, G. R.; Zimmerman, B. A. *Annu. Rev. Astron. Astrophys.* 1975, vol. 13, 69-112.

[32] Mohr, P. J.; Taylor, B. N. *Rev. Mod. Phys.* 2005, vol. 77(1), 1-107.

[33] Angulo, C. et al. *Nucl. Phys.* 1999, vol. A 656, 3-183.

[34] Varshalovich, D. A.; Moskalev, A. N.; Khersonskii, V. K. *Quantum Theory of Angular Momentum*; Publisher: World Scientific, Singapore, 1989.

[35] http://physics.nist.gov/cgi-bin/cuu/Value?mud|search_ for=atomnuc!

[36] Eisenberg, J. M.; Greiner, W. *Excitation mechanisms of the nucleus*; Publisher: North Holland, Amsterdam, 1976, pp 421.

[37] Plattner, G. R.; Viollier, R. D. *Nucl. Phys.* 1981, vol. A 365, 8-12.

[38] Mukhamedzhanov, A. M.; Tribble, R. E. *Phys. Rev.* 1999, vol. C 59, 3418-3424.

[39] Blokhintsev, L. D.; Borbey, I.; Dolinskii, E. I. *Fiz. Elem. Chastits Atom. Yadra* 1977, vol. 8, 1189-1254 [*Sov. J. Part. Nucl.* 1977, vol. 8, 485].

[40] Marchuk, G. I.; Kolesov, V. E. *Application of Numerical Methods to Neutron Cross-Section Calculations*; Publisher: Atomizdat, Moscow, 1970, pp 304 (in Russian).

[41] Abramowitz, I. G. et al. *Reference mathematical library. Mathematical analysis, Differentiation and integration*; Publisher: Fiz. Mat. Lit., Moscow, 1961, pp 350 (in Russian).

[42] Barnet, A. et al. *Comput. Phys. Comm.* 1974, vol. 8, 377-395.

[43] Dubovichenko, S. B.; Chechin, L. M. *Bulletin of KazNPU Phys.-Math.* (Kazakhstan) 2003, vol. 1(7), 115-122.

[44] Itzykson, C.; Nauenberg, M. *Rev. Mod. Phys.* 1966, vol. 38, 95-101.

[45] Hodgson, P. E. *The Optical Model of Elastic Scattering*; Publisher: Clarendon Press, Oxford, 1963, pp 211.

[46] Dubovichenko, S. B. *Phys. Atom. Nucl.* 2008, vol. 71, 65-74.

[47] Dubovichenko, S. B.; Takibaev, N. Zh.; Chechin, L. M. *Physical processes in deep and near space*; Publisher: Daik-Press, Almaty, 2008, pp 228; http://xxx.lanl.gov/abs/1012.1705.

[48] Kukulin, V. I. et al. *Nucl. Phys.* 1984, vol. A 417, 128-156.

[49] Skornyakov, L. A. *Reference mathematical library. General algebra*; Publisher: Nauka, Moscow, 1990, pp 591 (in Russian).

[50] Popov, B. A.; Tesler, G. S. *Computer calculation of functions*; Publisher: Naukova Dumka, Kiev, 1984, pp 598 (in Russian).

[51] Korn, G.; Korn, T. *Reference book on mathematics*; Publisher: Mir, Moscow, 1974, pp 832 (in Russian).

[52] Dubovichenko, S. B.; Chechin, L. M. *Bulletin of KazNPU Phys.-Math.* (Kazakhstan) 2003, vol. 1(7), 110-115; Dubovichenko, S. *B. Bulletin of KazNU Ser. Phys.* (Kazakhstan) 2008, vol. 1, 49-58.

[53] Dubovichenko, S. B. *Izv. NAN RK Ser. Fiz.-Math.* (Kazakhstan) 2007, vol. 4, 52-55.

[54] Mikhlin, S. G.; Smolitskii, Kh. L. *Approximate methods of solution of differential and integral equations*; Publisher: Nauka, Moscow, 1965, pp 383 (in Russian).

[55] Dubovichenko, S. B.; Chechin, L. M. *Materials of the Conference "Modern problems and tasks of Informatization in the Kazakhstan"*, October 6-10, Almaty, Kazakhstan; 2004, p. 358-390.

[56] Blatt, J. M.; Weisskopf, V. F. *Theoretical nuclear physics*; Publisher: John Wiley and Sons Inc., New York, 1952, pp 864 [Publisher: IL, Moscow, 1954, pp 658 (in Russian)].

[57] Fowler, W. A. *Experimental and Theoretical Nuclear Astrophysics: the Quest for the Original of the Elements*; Nobel Lecture, Stockholm, 8 Dec. 1983; Fowler, W. A. Uspehi Fiz. Nauk 1985, vol. 145, 441-488.

[58] Snover, K. A. *Solar p-p chain and the* $^{7}Be(p,\gamma)^{8}B$ *S-factor*; Publisher: University of Washington, CEPRA, NDM03, 1/6/2008.

[59] Dubovichenko, S. B.; Dzhazairov-Kakhramanov, A. V. *Euro. Phys. Jour.* 2009, vol. A 39, 139-143.

[60] Schiavilla, R.; Pandaripande, V. R.; Wiringa, R. B. *Nucl. Phys.* 1986, vol. A 449, 219-242.

[61] Uzikov, Yu. N. *Phys. Rev.* 1998, vol. C 58, 36-39.

[62] Uzikov, Yu. N.; Haidenbauer, J. *Phys. Rev.* 2003, vol. C 68, 014001-1-014001-6.

[63] Schmelzbach, P. et al. *Nucl. Phys.* 1972, vol. A 197, 273-289; Arvieux, J. *Nucl. Phys.* 1967, vol. A 102, 513-528; Chauvin, J.; Arvieux, J. *Nucl. Phys.* 1975, vol. A 247, 347-358; Huttel, E. et al. *Nucl. Phys.* 1983, vol. A 406, 443-455.

[64] Dubovichenko, S. B.; Dzhazairov-Kakhramanov, A. V. *Sov. J. Nucl. Phys.* 1990, vol. 51, 971-980.

[65] Griffiths, G. M.; Larson, E. A.; Robertson, L. P. *Can. J. Phys.* 1962, vol. 40, 402-411.

[66] Ma, L. et al. *Phys. Rev.* 1997, vol. C 55, 588-596.

[67] Schimd, G. J. et al. *Phys. Rev.* 1997, vol. C 56, 2565-2681.

[68] LUNA Collaboration; Casella, C.; Costantini, H. et al. *Nucl. Phys.* 2002, vol. A 706, 203-216.

[69] Dubovichenko, S. B. *Rep. Nat. Acad. Sci. RK* (Kazakhstan) 2008, vol. 3, 33-38.

[70] Tilley, D. R.; Weller, H. R.; Hasan, H. H. *Nucl. Phys.* 1987, vol. A 474, 1-60.

[71] Tilley, D. R.; Weller, H. R.; Hale, G. M. *Nucl. Phys.* 1992, vol. A 541, 1-157.

[72] Kirzhnits, D. A. *Pis'ma Zh. Eksp. Teor. Fiz.* 1978, vol. 28, 479-481 [*JETP Letters* 1978, vol. 28, 444-446].

[73] Bornard, M. et al. *Nucl. Phys.* 1978, vol. A 294, 492-512.

[74] Platner, G. R.; Bornard, M.; Viollier, R. D. *Phys. Rev.* Lett. 1977, vol. 39, 127-130.

[75] Lim, T. K. *Phys. Rev. Lett.* 1973, vol. 30, 709-710.

[76] Kievsky, A. et al. *Phys. Lett.* 1997, vol. B 406, 292-296.

[77] Ayer, Z. et al. *Phys. Rev.* 1995, vol. C 52, 2851-2858.

[78] Mott, N. F.; Massey, H. S. W. *The theory of atomic collisions*; Publisher: Oxford Univ. Press, London, 1965, pp 858 [Publisher: Mir, Moscow, 1969, pp 756 (in Russian)].

[79] Schimd, G. J. et al., *Phys. Rev. Lett.* 1996, vol. 76, 3088-3091.

[80] Schimd, G. J. et al. *Phys. Rev.* 1995, vol. 52, R1732-R1733.

[81] Viviani, M.; Schiavilla, R.; Kievsky, A. *Phys. Rev.* 1996, vol. C 54, 534-553.

[82] Warren, J. B. et al. *Phys. Rev.* 1963, vol. 132, 1691-1692; http://prola.aps.org/search/field/author/Warren_J_B

[83] Berman, B. L.; Koester, L. J.; Smith, J. H. *Phys. Rev.* 1964, vol. 133, B117-B129.

[84] Fetisov, V. N.; Gorbunov, A. N.; Varfolomeev, A. T. *Nucl. Phys.* 1965, vol. 71, 305-342.

[85] Ticcioni, G. et al. *Phys. Lett.* 1973, vol. B 46, 369-371.

[86] Geller, K. N.; Muirhead, E. G.; Cohen, L. D. *Nucl. Phys.* 1967, vol. A 96, 397-400.

[87] Dubovichenko, S. B.; Dzhazairov-Kakhramanov, A. V. *Phys. Part. Nucl.* 1997, vol. 28, 615-641.

[88] Dubovichenko, S. B. *Rus. Phys. J.* 2011, vol. 54, 157-164.

[89] Dubovichenko, S. B. *Rus. Phys. J.* 2008, vol. 51, 1136-1143.

[90] Dubovichenko, S. B.; Neudatchin, V. G.; Sakharuk, A. A.; Smirnov, Yu. F. *Izv. Akad. Nauk SSSR Ser. Fiz.* 1990, vol. 54, 911-916; Neudatchin, V. G.; Sakharuk, A. A.; Dubovichenko, S. B. *Few Body Systems* 1995, vol. 18, 159-172.

[91] Berg H., et al. *Nucl. Phys.* 1980, vol. A 334, 21-34; Kavanagh, R. W.; Parker, P. D. *Phys. Rev.* 1966, vol. 143, 779-782; Morrow, L.; Haeberli, W. *Nucl. Phys.* 1969, vol. A 126, 225-232.

[92] Dubovichenko, S. B. *Phys. Atom. Nucl.* 1995, vol. 58, 1295-1302.

[93] Tombrello, T. A. *Phys. Rev.* 1965, vol. 138, B40-B47.

[94] Yoshino, Y. et al. *Prog. Theor. Phys.* 2000, vol. 103, 107-125.

[95] McSherry, D. H.; Baker, S. D. *Phys. Rev.* 1970, vol. C 1, 888-892.

[96] Drigo, L.; Pisent, G. *Nuovo Cimento* 1967, vol. BLI, 419-436.

[97] Szaloky, G.; Seiler, F. *Nucl. Phys.* 1978, vol. A 303, 57-66.

[98] Tombrello, T. A. et al. *Nucl. Phys.* 1962, vol. 39, 541-550.

[99] McIntosh, J. S.; Gluckstern, R. L.; Sack, S. *Phys. Rev.* 1952, vol. 88, 752-759.

[100] Frank, R. M.; Gammel, J. L. *Phys. Rev.* 1955, vol. 99, 1406-1410.

[101] Kankowsky, R. et al. *Nucl. Phys.* 1976, vol. A 263, 29-46.

[102] Arkatov, Yu. M. et al. *Yad. Fiz.* 1970, vol. 12, 227-233 [*Sov. J. Nucl. Phys.* 1971, vol. 12, 123].

[103] Hahn, K. et al. *Phys. Rev.* 1995, vol. C 51, 1624-1632.

[104] Canon, R. et al. *Phys. Rev.* 2002, vol. C 65, 044008-044014.

[105] Dubovichenko, S. B. *Izv. NAN RK Ser. Fiz.-Mat.* (Kazakhstan) 2008, vol. 4, 89-92; Dubovichenko, S. B.; Dzhazairov-Kakhramanov, A. V. *Uz. J. Phys.* (Uzbekistan) 2008, vol. 10, 364-370.

[106] Lim, T. K. *Phys. Lett.* 1975, vol. B 55, 252-254; Lim, T. K. *Phys. Lett.* 1973, vol. B 44, 341-342.

[107] Gibson, B. F. *Nucl. Phys.* 1981, vol. A 353, 85-98.

[108] Dubovichenko, S. B. *Rus. Phys. J.* 2009, vol. 52, 294-300.

[109] Perry, J. E.; Bame, S. J. *Phys. Rev.* 1955, vol. 99, 1368-1375.

[110] Balestra, F. et al. *Nuovo Cimento* 1977, vol. 38A, 145-166.

[111] Meyerhof, W. et al. *Nucl. Phys.* 1970, vol. A 148, 211-224.

[112] Feldman, G. et al. *Phys. Rev.* 1990, vol. C 42, R1167-R1170.

[113] Dubovichenko, S. B. et. al. *Rus. Phys. J.* 2010, vol. 53, 743-749; Dubovichenko, S. B.; Burtebayev, N.; Zazulin, D. M.; Kerimkulov, Zh. K.; Amar, A. C. A. *Phys. Atom. Nucl.* 2011, vol. 74, 984-1000.

[114] Skill, M. et al. *Nucl. Phys.* 1995, vol. A 581, 93-106.

[115] http://nuclphys.sinp.msu.ru/nuclsynt.

[116] Dubovichenko, S. B.; Dzhazairov-Kakhramanov, A. V.; Sakharuk, A. A. *Phys. Atom. Nucl.* 1993, vol. 56, 1044-1053.

[117] Neudatchin, V. G.; Sakharuk, A. A.; Smirnov, Yu. F. *Sov. J. Part. Nucl.* 1992, vol. 23, 210; Neudatchin, V. G.; Struzhko, B. G.; Lebedev, V. M. *Phys. Part. Nucl.* 2005, vol. 36, 468-497.

[118] Petitjean, C.; Brown, L.; Seyler, R. *Nucl. Phys.* 1969, vol. A 129, 209-219.

[119] Neudatchin, V. G.; Smirnov, Yu. F. *Nucleon associations in light nuclei*; Publisher: Nauka, Moscow, RU, 1969; pp 414 (in Russian).

[120] Tilley, D. R. et al. *Nucl. Phys.* 2002, vol. A 708, 3-163.

[121] Switkowski, Z. E. et al. *Nucl. Phys.* 1979, vol. A 331, 50-60; Bruss, R. et al. Astrophysical S-Factors for the Radiative Capture Reaction ^{6}Li(p,γ)^{7}Be at Low Energies; *Proc. 2-nd Intern. Symposium on Nuclear Astrophysics, Nuclei in the Cosmos*; Karlsruhe, Germany, 6-10 July, 1992, in: F. Kappeler, K. Wisshak (Eds.); Publisher: IOP Publishing Ltd., Bristol, UK, 1992; vol. 1093, p 169.

[122] Arai, K.; Baye, D. *Nucl. Phys.* 2002, vol. A 699, 963-975.

[123] Prior, R. M. et al. *Phys. Rev.* 2004, vol. C 70, 055801-055808.

[124] Burker, F. C. *Austr. J. Phys.* 1980, vol. 33, 159-176.

[125] Cecil, F. E. et al. *Nucl. Phys.* 1992, vol. A 539, 75-96.

[126] Dubovichenko, S. B.; Dzhazairov-Kakhramanov, A. V. *Rep. Nat. Acad. Sci. RK* (Kazakhstan) 2009, vol. 6, 41-45.

[127] Dubovichenko, S. B.; Zazulin, D. M. *Rus. Phys. J.* 2010, vol. 53, 458-464.

[128] Dubovichenko, S. B.; Dzhazairov-Kakhramanov, A. V. *Rus. Phys. J.* 2009, vol. 52, 833-840.

[129] Dubovichenko, S. B. *Phys. Atom. Nucl.* 2010, vol. 73, 1526-1538.

[130] Dubovichenko, S. B. *Rus. Phys. J.* 2010, vol. 53, 1254-1263; Dubovichenko, S. B. *Phys. Atom. Nucl.* 2011, vol. 74, 358-370; Dubovichenko, S. B. et al. *Izv. NAN RK Ser. Fiz.-Mat.* (Kazakhstan) 2010, No 4, 32-36.

[131] Tilley, D. R. et al. *Nucl. Phys.* 2004, vol. A 745, 155-363.

[132] http://cdfe.sinp.msu.ru.

[133] Warters, W. D.; Fowler, W. A.; Lauritsen C. C. *Phys. Rev.* 1953, vol. 91, 917-921.

[134] Brown, L. et al. *Nucl. Phys.* 1973, vol. A 206, 353-373.

[135] Zahnow, D. et al. *Z. Phys.* 1995, vol. A 351, 229-236.

[136] Avotina, M. P.; Zolotavin, A. V. *Moments of ground and excited states of nuclei*; Publisher: Atomizdat, Moscow, 1979, pp 522 (in Russian).

[137] Godwin, M. A. et al. *Phys. Rev.* 1997, vol. C 56, 1605-1612.

[138] Spraker, M. et al. *Phys. Rev.* 1999, vol. C 61, 015802-015808.

[139] Zahnow, D. et al. *Nucl. Phys.* 1996, vol. A 589, 95-105.

[140] Bohr, A.; Mottelson, B. R. *Nuclear structure Vol. I Single particle motion*; Publisher: World Scientific Pub Co Inc, Singapore, 1998 [Publisher: Mir, Moscow, 1971, pp 456 (in Russian)].

[141] Ajzenberg-Selove, F. *Nucl. Phys.* 1988, vol. A 490, 1-225.

[142] Wulf, E. A. et al. *Phys. Rev.* 1998, vol. C 58, 517-523.

[143] Sattarov, A. et al. *Phys. Rev.* 1999, vol. C 60, 035801-035808.

[144] Mukhamedzhanov, A. M. et al. *Phys. Rev.* 1999, vol. C 56, 1302-1312.

[145] Dubovichenko, S. B. *Rus. Phys. J.*, 2011, vol. 54, № 7.

[146] Dubovichenko, S. B. *Bulletin of KazNTU* (Kazakhstan) 2004, vol. 3, 137-144.

[147] Dubovichenko, S. B. et al. *Izv. NAN RK Ser. Fiz.-Math.* (Kazakhstan) 2007, vol. 6, 58-67.

[148] Jahns, M. F.; Bernstein, E. M. *Phys. Rev.* 1967, vol. 162, 871-877.

[149] Barnard, A.; Jones, C.; Well, J. *Nucl. Phys.* 1964, vol. 50, 604-620.

[150] Brown, R. I.; Haeberli, W.; Saladin, J. X. *Nucl. Phys.* 1963, vol. 47, 212-213.

[151] Jackson, H. L. et al. *Phys. Rev.* 1953, vol. 89, 365-369.

[152] Jackson, H. L. et al. *Phys. Rev.* 1953, vol. 89, 370-374.

[153] Moss, S. J.; Haeberli, W. *Nucl. Phys.* 1965, vol. 72, 417-435.

[154] Barnard, A. C. L. et al. *Nucl. Phys.* 1966, vol. 86, 130-144.

[155] Ajzenberg-Selove, F. *Nucl. Phys.* 1991, vol. A 523, 1-101.

[156] Ajzenberg-Selove, F. *Nucl. Phys.* 1990, vol. A 506, 1-186.

[157] Burtebaev, N.; Igamov, S. B.; Peterson, R. J.; Yarmukhamedov, R.; Zazulin, D. M. *Phys. Rev.* 2008, vol. C 78, 035802-1-035802-11.

[158] Kukulin, V. I.; Neudatchin; V. G. Smirnov, Yu. F. *Sov. J. Part. Nucl.* 1979, vol. 10, 1006.

[159] Imbriani, D. Underground laboratory studies of pp and CNO some astrophysical consequences LUNA; *Third European Summer School on Experimental Nuclear Astrophysics*, October 2-9, S. Tecla (Catania), Sicily, Italy, 2005.

[160] Caciolli, A. et al. Eur. Phys. J. 2009, vol. A 39, 179-186.

[161] Dubovichenko, S. B.; Dzhazairov-Kakhramanov, A. V. *Phys. Atom. Nucl.* 1995, vol. 58, 579-585; Dubovichenko, S. B.; Dzhazairov-Kakhramanov, A. V. *Phys. Atom. Nucl.* 1995, vol. 58, 788-795.

[162] Dubovichenko, S. B.; Dzhazairov-Kakhramanov, A. V. *Phys. Atom. Nucl.* 1993, vol. 56, 195-202; *Phys. Atom. Nucl.* 1994, vol. 57, 733-740.

[163] Barnard, A. C.; Jones, C. M.; Phillips, G. C. *Nucl. Phys.* 1964, vol. 50, 629-640.

[164] Spiger, R.; Tombrello, T. A. *Phys. Rev.* 1967, vol. 163, 964-984.

[165] Ivanovich, M.; Young, P. G.; Ohlsen, G. G. *Nucl. Phys.* 1968, vol. A 110, 441-462.

[166] McIntyre, L. C.; Haeberli, W. *Nucl. Phys.* 1967, vol. A 91, 382-398.

[167] Keller, L. G.; Haeberli, W. *Nucl. Phys.* 1979, vol. A 156, 465-476.

[168] Gruebler, W. et al. *Nucl. Phys.* 1975, vol. A 242, 265-284.

[169] Schmelzbach, P. A. et al. *Nucl. Phys.* 1972, vol. A 184. 193-213.

[170] Dubovichenko, S. B. *Phys. Atom. Nucl.* 1998, vol. 61, 162-168.

[171] Blokhintsev, L. D. et al. *Phys. Rev.* 1993, vol. C 48, 2390-2394.

[172] Blokhintsev, L. D. et al. *Yad. Fiz.* 2006, vol. 69, 456-466.

[173] Lim, T. K. *Phys. Lett.* 1975, vol. B 56, 321-324.

[174] Igamov, S. B.; Yarmukhamedov, R. *Nucl. Phys.* 2007, vol. A 781, 247-276.

[175] Brune, C. R. et al. *Phys. Rev. Lett.* 1999, vol. 83, 4025-4028.

[176] Igamov, S. B.; Tursunmakhatov, K. I.; Yarmukhamedov, R. arXiv:0905.2026v4 [nucl-th] 6 Jan. 2010.

[177] Blokhintsev, L. D. et al. *Izv. Ros. Acad. Nauk, Ser. Fiz.* 2008, vol. 72, 321-326.

[178] Langanke, K. *Nucl. Phys.* 1986, vol. A 457, 351-366.

[179] Kajino, T. *Nucl. Phys.* 1986, vol. A 460, 559-580.

[180] Burkova, N. A. et al. *Phys. Lett.* 1990, vol. B 248, 15-20.

[181] Brune, C. R.; Kavanagh, R. W.; Rolf, C. *Phys. Rev.* 1994, vol. C 50, 2205-2218.

[182] Griffiths, G. M. et al. *Can. J. Phys.* 1961, vol. 39, 1397-1403.

[183] Schroder, U. et al. *Phys. Lett.* 1987, vol. B 192, 55-58.

[184] Brown, T. A. D. et al. *Phys. Rev.* 2007, vol. C 76, 055801.1-055801.12; arXiv:0710.1279v4 [nucl-ex] 5 Nov. 2007.

[185] Confortola, F. et al. *Phys. Rev.* 2007, vol. C 75, 065803; arXiv:0705.2151v1 [nucl-ex] 15 May 2007.

[186] Gyurky, G. et al. *Phys. Rev.* 2007, vol. C 75, 035805-035813.

[187] Singh N. et al. *Phys. Rev. Lett.* 2004, vol. 93, 262503-262507.

[188] Osborn, J. L. et al. *Nucl. Phys.* 1984, vol. A 419, 115-132.

[189] Bemmerer, D. et al. *Phys. Rev. Lett.* 2006, vol. 97, 122502-122507; arXiv:nucl-ex/0609013v1 11 Sep. 2006.

[190] Costantini, H. arXiv:0809.5269v1 [nucl-ex] 30 Sep. 2008.

[191] Robertson, R. C. et al. *Phys. Rev. Lett.* 1981, vol. 47, 1867-1870.

[192] Mohr, P. et al. *Phys. Rev.* 1994, vol. C 50, 1543-1549.

[193] Kiener, J. et al. *Phys. Rev.* 1991, vol. C 44, 2195-2208.

[194] Igamov, S. B.; Yarmukhamedov, R. *Nucl. Phys.* 2000, vol. A 673, 509-525.

[195] Salpeter, E. E. *Phys. Rev.* 1957, vol. 107, 516-525; Salpeter, E. E. *Astrophys. Jour.* 1952, vol. 115, 326; Rolfs, C. *Progress in Particle and Nuclear Physics* 2007, vol. 59, 43.

[196] Schurmann, D. et al. arXiv:nucl-ex/0511050v1. 29 Nov. 2005.

[197] Dubovichenko, S. B. *Rus. Phys. J.* 2007, vol. 50, 605-611.

[198] Jones, C. M. et al. *Nucl. Phys.* 1962, vol. 37, 1-9.

[199] Dubovichenko, S. B. *Phys. Atom. Nucl.* 1996, vol. 59, 421-427.

[200] Plaga, R. et al. *Nucl. Phys.* 1987, vol. A 465, 291-316.

[201] Tilley, D. R.; Weller, H. R.; Cheves, C. M. *Nucl. Phys.* 1993, vol. A 564, 1-183.

[202] Dubovichenko, S. B. et al. *Rus. Phys. J.* 2009, vol. 52, 715-724; Dubovichenko, S. B. et al. *Rep. Nat. Acad. Sci. RK* (Kazakhstan) 2008, vol. 6, 24-32.

[203] Dubovichenko, S. B.; Dzhazairov-Kakhramanov, A. V. *Rep. Nat. Acad. Sci. RK* (Kazakhstan) 2009, vol. 3, 30-36.

[204] Kettner, K. U. et al. *Z. Phys.* 1982, vol. A 308, 73-94.

[205] Dyer, P.; Barnes, C. A. *Nucl. Phys.* 1974, vol. A 233, 495-520.

[206] Asuma, R. E. et al. *Phys. Rev.* 1994, vol. C 50, 1194-1215.

[207] Descouvemont, P.; Baye, D. *Phys. Rev.* 1987, vol. C 36, 1249-1255.

[208] Abramowitz, M. *Reference book on special functions*; Publisher: Nauka, Moscow, 1979, pp 830 (in Russian).

[209] Luke, Yu. L. *Mathematical functions and their approximations*; Publisher: Academic Press, New York, 1975 [Mir, Moscow, 1980, pp 608 (in Russian)].

[210] Melkanoff, M. A. *Fortran program for elastic scattering analysis with nuclear optical model*; Publisher: Univ. California Pres. Berkley, Los Angeles, 1961, pp 116.

[211] Lutz, H. F.; Karvelis; M. D. *Nucl. Phys.* 1963, vol. 43, 31-44.

[212] Melkanoff, M. *Meth. in Comput.* Phys. Acad. Press. N-Y 1966, vol. 6, 1-80.

[213] Gody, W. J.; Hillstrom, K. E. *Meth. Comput.* 1970, vol. 111, 671-677.

[214] Smith, W. R. *Usics Communs.* 1969, vol. 1, 106-112.

[215] Froberg, C. E. *Rev. Mod. Phys.* 1955, vol. 27, 399-411.

[216] Abramowitz, M. *Tables of Coulomb wave function V. I*; Publisher: N.B.S., Washington, 1952, pp 141.

[217] Danilov, V. L. et al. *Reference mathematical library. Mathematical analysis. Functions, limits and continued fractions*; Publisher: Fiz. Mat. Lit., Moscow, 1961, pp 439 (in Russian).

[218] Kuznetsov, D. S. *Special functions*; Publisher: Vysshaya Shkola, Moscow, 1965, pp 272 (in Russian).

[219] Dubovichenko, S. B. *Thermonuclear processes of the Universe.* Publisher: A-tri, Almaty, 2011, pp 402 (in Russian), http://arxiv.org/abs/1012.0877 .

REVIEWERS AND SCIENTIFIC EDITORS OF THE BOOK

REVIEWERS

Professor Bagrov V.G. (TSU, Tomsk, Russia)
Professor Blokhintsev L.D. (MSU, Moscow, Russia)
Professor Danaev N.T. (KazNU, Almaty, RK)
Professor Duisebaev A.D. (INP, Almaty, RK)
Professor Ishkhanov B.S. (MSU, Moscow, Russia)
Professor Strakovsky I.I. (GWU, Washington, USA)

SCIENTIFIC EDITORS

Professor N.A. Burkova, Professor L.M. Chechin,
Assistant Professor A.V. Dzhazairov-Kakhramanov

INDEX

A

algorithm, 39
amplitude, 96, 128
astrophysical energies, xiii, 20, 21, 26, 80, 88, 95, 103, 104, 143, 144
asymptotics, 43, 44, 105, 118, 138
atmosphere, 160
atomic nucleus, 8, 9, 11, 27, 161
atoms, 2, 6, 158, 164
Azerbaijan, 166

B

base, 62, 70, 76, 80, 84, 118
beryllium, 11
Big Bang, 111, 164, 165
binding energy, 16, 17, 26, 29, 32, 34, 43, 44, 45, 57, 58, 71, 72, 76, 82, 105, 107, 108, 116, 118, 119, 120, 122, 124, 137, 155
black hole, 18, 19, 158, 161, 162, 163

C

calculus, 166
candidates, viii
carbon, 11, 14, 15, 16, 18, 157, 158, 160
chemical, xi, 1, 16, 20, 155, 158
Chicago, 165
classification, vii, xv, 21, 23, 29, 34, 51, 54, 58, 62, 63, 69, 70, 77, 78, 79, 81, 82, 87, 88, 89, 90, 104, 111, 125, 136, 138, 157
cluster model, vii, xiii, xv, 21, 22, 23, 27, 28, 29, 30, 31, 33, 42, 43, 44, 50, 53, 54, 57, 59, 62, 63, 76, 77, 85, 87, 93, 95, 104, 111, 112, 121, 122, 125, 127, 140, 143, 144, 166
clusters, 27, 28, 29, 31, 33, 83, 114, 143, 144, 160
collaboration, 155
collisions, 26, 168
color, 18, 157, 158
complexity, 25
composition, xi, 158, 163
compression, 1, 2, 3, 5, 7, 14, 16, 18, 19, 156
computer, viii, 34, 37, 38, 39, 43, 45, 58, 82, 92, 97, 129, 158
computing, 34, 146, 147
conference, 166
configuration, 29, 42, 69, 77, 78, 88, 127
construction, 27, 35, 50, 70, 80, 104, 136, 143
convergence, 147
cooling, 18
Coulomb interaction, 25, 33, 137
cycles, viii, xiii, xiv, 4, 11, 13, 20

D

dark matter, xi, 159
decay, 2, 11, 78
deformation, 117
degenerate, 162
dense matter, 162
depth, 75, 76, 77, 139, 144
derivatives, 146, 147
deuteron, 8, 42, 43, 82, 117
deviation, 25, 39, 129
dichotomy, 38
dimensionality, 45, 58, 107, 108, 118, 119, 138
direct measure, vii, 21, 25
distribution, 6, 7, 27
distribution function, 6

E

electric charge, 6
electromagnetic, xiii, xiv, 31, 41, 42, 83, 84, 92, 93, 114, 116, 137, 144, 155

electromagnetic interactions, xiii, 41
electron, 6, 8, 41, 162
elementary particle, xiii
elucidation, 103
emission, 12
equilibrium, 18
Eurasia, 166
evolution, viii, xi, xiii, xiv, 1, 3, 4, 5, 19, 20, 21, 53, 95, 157, 158, 160, 161, 164
excitation, 22, 28, 32, 64, 70, 79, 80, 99, 103, 129
exclusion, 54
extraction, 58

F

force, 1, 6, 8, 11, 14, 27, 162
formation, xi, xiii, 1, 2, 3, 4, 8, 12, 15, 16, 19, 20, 21, 27, 29, 77, 78, 127, 156, 158
formula, 100
fragments, 25, 143
fusion, 3, 5, 6, 8, 13, 15, 16, 18, 25, 41, 42, 53, 103, 111, 127, 155, 157, 158, 163

G

Galaxy, 2, 159, 161
Germany, 169
graph, 158
gravitation, 8, 162, 164
gravitational collapse, 18, 161, 162
gravitational field, 163
gravitational force, 5, 14, 18
gravity, 1, 2, 3, 5, 11, 14, 16, 19, 157, 163
growth, 65, 105, 141, 142

H

half-life, 13, 15
Hamiltonian, 37
height, 7, 141
helium, 1, 3, 4, 8, 11, 13, 14, 15, 16, 18, 127, 155, 156, 157, 158, 160
hydrogen, xi, 1, 3, 5, 6, 7, 8, 11, 13, 14, 15, 16, 18, 95, 155, 157, 158, 160
hydrogen atoms, 158

I

initial state, 144
initiation, 1, 5, 6
integration, 34, 167
interaction process, 5
intermediaries, 158
ionization, 6
ions, 93
iron, 16, 18, 21, 155, 157
isolation, 1, 28
isospin, 34, 35, 36, 53, 54, 55, 58, 59, 69, 70, 78, 79, 80, 81, 84, 88, 133, 143, 144
Italy, 170

J

justification, 22, 23, 26

K

K^+, 147, 148
Kazakhstan, ix, 166, 167, 168, 169, 170, 172

L

laboratory studies, 170
lead, xiii, xiv, 91, 107, 141
lifetime, 4, 158
light, xi, xiii, xiv, xv, 1, 6, 8, 21, 23, 27, 34, 38, 44, 87, 116, 144, 157, 160, 162, 163, 166, 169
low temperatures, 6
luminosity, 5, 20, 158, 161

M

magnesium, 16
magnetic field, 157
magnetic moment, 31, 83
magnitude, 36, 42, 69, 104, 108, 109, 121, 124, 140, 141, 147, 149, 158
mass, xi, 2, 3, 4, 5, 7, 8, 11, 13, 14, 15, 16, 17, 18, 19, 20, 28, 30, 31, 33, 53, 59, 83, 95, 96, 99, 104, 108, 155, 156, 157, 158, 160, 161, 162, 163
materials, viii, ix
mathematics, 166, 167
matrix, 26, 33, 34, 37, 38, 39, 64, 82, 87, 91, 96
matter, vii, xi, 1, 2, 3, 4, 19, 20, 25, 31, 159, 161, 162
measurement, vii, 63, 65, 87, 95, 129, 155
measurements, 21, 22, 25, 36, 50, 51, 60, 63, 83, 85, 95, 103, 122, 143, 144
Mercury, 11
MES, ix
Milky Way, xi, 160
Ministry of Education, ix
mixing, 54, 79, 125, 143

models, vii, 21, 22, 23, 26, 27, 47, 111, 121, 158, 166
momentum, 42
Moscow, viii, ix, 165, 166, 167, 168, 169, 170, 172, 173

N

National Academy of Sciences, ix
neglect, 11, 28
neon, 16, 157
neutral, 164
neutrinos, 11
neutron stars, 158, 162
neutrons, xi, 21, 53, 54, 161, 162, 163, 164
nitrogen, 15, 158
nodes, 28, 29, 144
NSA, ix, x
nuclear charge, 6
nuclear matter, 161
nuclei, xi, xiii, xiv, xv, 3, 4, 5, 6, 7, 8, 9, 11, 12, 13, 14, 15, 16, 18, 21, 23, 25, 26, 27, 28, 29, 32, 33, 34, 38, 41, 42, 44, 53, 54, 69, 76, 111, 112, 114, 116, 117, 120, 121, 125, 136, 139, 143, 144, 155, 158, 166, 169, 170
nucleons, vii, 26, 27, 28, 29, 35, 78, 104, 136, 155, 161
nuclides, xi

O

operations, 39
orbit, 11, 157, 160, 163
oxygen, 14, 15, 16, 157, 158

P

parity, 133
particle mass, 34, 43, 57, 72, 135, 140
particle physics, xiii
PCM, 22, 23, 27, 42, 51, 78, 87, 94
permission, 43, 45, 46, 47, 48
phase shifts, 22, 23, 26, 27, 29, 32, 35, 36, 42, 50, 51, 54, 55, 62, 63, 64, 65, 66, 68, 69, 70, 71, 73, 74, 76, 77, 79, 80, 81, 83, 88, 90, 95, 97, 98, 99, 103, 104, 112, 114, 115, 116, 121, 125, 127, 128, 129, 132, 134, 135, 136, 139, 142, 143, 144
physics, 1, 5, 7, 20, 22, 26, 37, 41, 155, 166, 167
planets, 163
polarization, 96, 97
positron, 8
potential cluster model (PCM), xiii
principles, 22
probability, 5, 6, 7, 11, 14, 21, 27, 53, 71, 111, 112, 127
project, 41, 48, 50
protons, 8, 53, 161, 164, 166

Q

qualitative concept, 93
quanta, 21, 22, 28
quantum mechanics, 22

R

radiation, xi, 1, 18, 31, 155, 157, 162
radiative capture processes, xiii, xiv, 111
radius, 11, 26, 28, 32, 33, 43, 44, 49, 50, 57, 58, 71, 72, 74, 82, 88, 90, 91, 105, 107, 108, 109, 112, 116, 117, 137, 138, 139, 160, 161, 162
reaction rate, 10, 16, 127, 155
reaction time, 10, 12, 13
reactions, vii, xiii, xiv, 1, 3, 4, 5, 7, 8, 10, 11, 12, 13, 14, 15, 16, 18, 19, 20, 21, 22, 23, 25, 26, 27, 29, 30, 41, 42, 53, 77, 87, 103, 127, 143, 144, 155, 156, 157
recall, 108
reconstruction, 29
relativity, 162
reliability, viii
reproduction, 29, 129
repulsion, vii, 5, 6, 42
researchers, viii, 155
reserves, 13, 34
residuals, 26, 39, 92
resistance, 19
restructuring, 77, 85
root, 34, 83
rules, 53, 136
Russia, ix, 173

S

saturation, 161
scatter, 44, 158
Schrödinger equation, 26, 28, 32, 33, 37, 39, 145, 149, 150
science, vii, ix, xi
shade, 6
showing, 158
signs, 96, 129, 130, 131, 134, 135, 136
silicon, 16, 19
Singapore, 165, 166, 170

sodium, 16
solution, 25, 26, 27, 28, 32, 33, 36, 37, 38, 39, 149, 166, 167
space-time, 162
speed of light, 162
spin, 31, 34, 35, 36, 42, 50, 54, 63, 64, 69, 70, 74, 75, 78, 79, 80, 81, 83, 95, 97, 104, 128, 143
stability, 16, 39, 117
stars, vii, viii, xi, xiii, 1, 3, 4, 5, 6, 8, 11, 13, 14, 15, 16, 18, 19, 20, 21, 25, 41, 42, 103, 155, 157, 158, 159, 160, 161, 162, 164
stellar CNO cycle, xiii
strong force, 162
strong interaction, 6, 8, 31, 127, 144
structure, vii, xi, 1, 12, 20, 25, 27, 51, 62, 157, 170
sulfur, 16
Sun, vii, xi, 2, 4, 6, 11, 41, 42, 157, 158, 160, 161
symmetry, 28, 35, 50, 70, 78, 137, 144
synthesis, 16

T

temperature, 1, 2, 3, 5, 6, 11, 13, 14, 15, 16, 18, 53, 95, 111, 127, 157, 158, 160, 162
thermodynamic equilibrium, 18
thermodynamics, 162
thermonuclear reactions, xiii, xiv, 1, 3, 4, 7, 8, 14, 16, 18, 19, 21, 27, 41, 144, 156
threshold level, 81, 88
total energy, 127
trajectory, 163
transformation, 3, 18
transformations, 18, 19, 37
transparency, 3
triggers, 95
tunneling, 7
tunneling effect, 7
Turkey, 166

U

UK, 165, 169
uranium, xi
USA, ix, 173
Uzbekistan, 166, 169

V

vacuum, 160
variables, 34, 36, 146
velocity, 6, 7
Venus, 11

W

Washington, ix, 167, 172, 173
wave number, 30, 32, 33, 34, 96, 151
weak interaction, xiii, 11, 21, 41

Y

yield, 35, 41, 44, 46, 58, 76, 105, 122, 124